# A Computational Model of the Human Head and Cervical Spine for Dynamic Impact Simulation

By

David van Lopik



A Doctoral Thesis.

Submitted in partial fulfilment of the requirements for the award of Doctor of Philosophy at Loughborough University

# Acknowledgements

I wish to express my thanks to my supervisor Dr Memis Acar for his guidance, kind words, and continued advice throughout the completion of this thesis. To my partner Kate for her encouragement and patience without whom I would have spent many long evenings hungry! Thanks also to my family for listening and for their everlasting support.

The financial support from the Engineering and Physical Sciences Research Council (EPSRC) is gratefully acknowledged.

# Abstract

Injury to the human neck is a frequent consequence of automobile accidents and has been a significant public health problem for many years. The term 'whiplash' has been used to describe these injuries in which the sudden differential movement between the head and torso leads to abnormal motions within the neck causing damage to its soft tissue components. Although many different theories have been proposed, no definitive answer on the cause of 'whiplash' injury has yet been established and the exact mechanisms of injury remain unclear.

Biomechanical research is ongoing in the field of impact analysis with many different experimental and computational methods being used to try and determine the mechanisms of injury. Experimental research and mathematically based computer modelling are continually used to study the behaviour of the head and neck, particularly its response to trauma during automobile impacts.

The rationale behind the research described in this thesis is that a computational model of the human head and neck, capable of simulating the dynamic response to automobile impacts, could help explain neck injury mechanisms. The objective of the research has been to develop a model that can accurately predict the resulting head-neck motion in response to acceleration impacts of various directions and severities.

This thesis presents the development and validation of a three-dimensional computational model of the human head and cervical spine. The novelty of the work is in the detailed representation of the various components of the neck. The model comprises nine rigid bodies with detailed geometry representing the head, seven vertebrae of the neck and the first thoracic vertebra. The rigid bodies are interconnected by spring and damper constraints representing the soft-tissues of the neck. 19 muscle groups are included in the model with the ability to curve around the cervical vertebrae during neck bending. Muscle mechanics are handled by an external application providing both passive and active muscle behaviour.

The major findings of the research are:

From the analysis of frontal and lateral impacts it is shown that the inclusion of active muscle behaviour is essential in predicting the head-neck

response to impact. With passive properties the response of the head-neck model is analogous to the response of cadaveric specimens where the influence of active musculature is absent.

Analysis of the local loads in the soft-tissue components of the model during the frontal impact with active musculature revealed a clear peak in force in the majority of ligaments and in the intervertebral discs very early in the impact before any forward rotation of the head had occurred.

For the case of rear-end impact simulations it has been shown for the first time that the inclusion of active musculature has little effect on the rotation of the head and neck but significantly alters the internal loading of the soft-tissue components of the neck.

**Keywords:** cervical, spine, head, neck, whiplash, biomechanics, crash, injury, multi-body dynamics.

# Table of Contents

# Table of Figures

# Table of Tables

# Glossary of Terms

**Anterior** – Situated toward the front of the human body.

**Aponeurosis** - A sheetlike fibrous membrane, resembling a flattened tendon, connecting muscle to bone.

**Atlanto-axial** - relating to or being structures (as a joint or ligament) joining the atlas and the axial vertebrae.

**Atlanto-occipital** - relating to or being structures (as a joint or ligament) joining the atlas and the occipital bone.

**Atlanto-odontoid** - relating to or being structures (as a joint or ligament) joining the atlas and the odontoid process.

**Atlas** – Uppermost or first vertebra of the cervical spine; C1.

**Axis** – Second vertebrae of the cervical spine; C2.

**Biofidelity** – The degree to which a model accurately reproduces the human like response.

**Cervical Spine** – Upper section of the spinal column located in the neck, made up of 7 vertebrae; C1-C7.

**Dens Process** – A process projecting upward from the vertebral body of the Axis around which the Atlas rotates.

**Dorsal** - Being or located near, on, or toward the back or posterior part of the human body.

**Extension** – Rearward bending of the neck.

**Fascicle** – A small bundle of muscle fibres.

**Facet** - a smooth flat or nearly flat circumscribed anatomical surface.

**Flexion** – Forward bending of the neck.

**Hyperextension** – Extension of a joint beyond its normal range of motion.

**Hyperflexion** – Flexion of a joint beyond its normal range of motion.

**Hypertranslation** – Translation of a joint beyond its normal range of motion.

**Inferior** - Situated towards the feet or further away from the head than another similar part on the human body.

**In-vivo** – Within a living body.

**Lordosis** – The natural forward curvature of the cervical spine.

**Lumbar Spine** – Lower section of the spinal column made up of 5 vertebrae; L1-L5.

**Mid-Sagittal Plane** - The median vertical longitudinal plane that divides the human body into right and left halves.

**Muscle Morphometry** – A quantitative measurement of the properties of muscle.

**Nociceptors** - A sensory receptor that responds to pain.

**Nuchal Line** – Any of several ridges on the outside of the skull.

**Occiput** – The base of the skull.

**Odontoid Process** – See *Dens Process*

**Occipital Condyles** – Rounded prominences on the occipital bone for articulation with the superior articular facets of the Atlas.

**Pedicles** – Bony stalk connecting the articular process of a vertebra to the vertebral body.

**Posterior** – Situated toward the back of the human body.

**Spinous Process** – Rearward pointing process of a vertebra.

**Superior** – Situated towards the head or further away from the feet than another similar part on the human body.

**Tetanic** - A condition of muscle; a fusion of a number of simple spasms into an apparently smooth, continuous effort, is known as a tetanic contraction.

**Thoracic Spine**- Middle section of the spinal column located in the thorax made up of 12 vertebrae; T1-T12.

**Tomography** - a method of producing a three-dimensional image of the internal structures of the human body.

**Vertebra** – One of twenty-four bony segments that make up the human spinal column.

# Nomenclature

$F_i$ - Force in i-axis (i = x, y, z).

$M_i$ - Moment about i-axis (i = x, y, z)

$t_i$ - Translation in the i-axis (i = x, y, z)

$\theta_i$ - Rotation about the i-axis (i = x, y, z)

$v_i$ - Velocity in the i-axis (i = x, y, z)

$\omega_i$ - Angular velocity about the i-axis (i = x, y, z)

$k$ - Stiffness coefficient.

$b$ - Damping coefficient.

$F_{CE}$ - Contractile element force of muscle fascicles.

$F_{PE}$ - Passive element force of muscle fascicles.

Af - Isometric, activation-frequency relationship of muscle.

$F_0$ - Maximum isometric active muscle force.

$L_0$ - Optimum length of muscle fascicles for peak isometric muscle force.

$f_{0.5}$ - Frequency at which half of maximal tetanic force of muscle fibres is obtained

$V_{0.5}$ - Shortening velocity required to produce half the maximum tetanic force of muscle.

$L_0^T$ - Length of muscle tendon at maximal tetanic isometric muscle force.

$L_S^T$ - Tendon slack length.

$L_{max}$ - Length of the muscle fascicles at the maximal anatomical length of the muscle.

# CHAPTER 1

# Introduction

Injury to the human neck is a frequent consequence of automobile accidents and has been a significant public health problem for many years. The term 'whiplash' has been used to describe these injuries in which the sudden differential movement between the head and torso leads to abnormal motions in the neck causing damage to its soft tissue components. 'Whiplash' can occur in all vehicle impact directions as well as a result of other mishaps but is most commonly reported as a consequence of rear-end impacts. Very little is actually known about the precise mechanisms of 'whiplash' injury and although in most cases the injuries are relatively minor, resulting symptoms can continue months and even years after an accident.

This thesis outlines the development of a computational model that is capable of simulating the dynamic behaviour of the human head and neck in response to automobile impacts. The model is able to predict the resulting head motion and the loads and deformations in the various components of the neck providing a better understanding of the possible causes of injury.

This introductory chapter provides background information on injuries to the neck and on the need for computational models. The research aims and objectives are discussed together with an overview of the contents of this thesis.

# 1.1 Soft-Tissue/ 'Whiplash' Injuries of the Neck

Of the many disabling injuries that occur in automobile accidents, trauma to the neck has become the most common. By the end of the 1970's they represented around 30% of all injuries sustained in automobile collisions in Sweden (Nygren, 1984). A British emergency department reported that in 1986 65% of all automobile accident victims sustained some form of neck injury (Olney and Marsen, 1986) and Morris and Thomas (1996a, 1996b) report that the incidence of neck injuries in England has doubled over a ten year period. Similar findings have been reported for Japan by Ono and Kanno (1993) who state that 50% of all car-to-car collisions resulted in whiplash injuries and Japenese researchers Tsuchisashi et al. (1981) found that 29% of 167,721 motor vehicle crashes resulted in neck injury. The cost to society as a result of 'whiplash' injuries is enormous. It has been estimated that 80% of personal injury claims made against British Insurers are related to Whiplash injury, costing around £1 billion annually with this figure rising yearly (Thatcham, 2001).

Soft tissue injuries or minor injuries to the cervical spine are basically defined as an injury in which bone fracture does not occur or is not readily apparent. A minor injury is therefore an injury to one or more of the many ligaments, intervertebral discs, facet joints or muscles of the neck i.e. a soft tissue injury. 'Whiplash' is the typical and most common soft tissue injury to the neck, rarely are fractures present and yet patients persistently complain of symptoms and in many cases develop chronic symptoms lasting way beyond the expected healing times for typical soft tissue injuries analogous to other regions of the body. Soft tissue injuries are essentially invisible to modern imaging techniques, X-ray and computerised tomography (CT) scans are capable of detecting fractures and dislocation but are unable to define any soft tissues. Magnetic resonance imaging (MRI) is able to determine certain soft-tissue injuries but to date no link has been found between neck pain and any feature evident on MRI (Bogduk and Yoganandan, 2001).

The mechanism of injury is not fully understood but there have been a number of different hypotheses offering explanations for the source of neck pain following 'whiplash' motion. An early study by MacNab et al. (1964) identified neck hyperextension, severe rearward bending of the neck, as the primary injury mechanism. However, after the advent of head restraints failed to alleviate the problem of whiplash, further hypotheses have been proposed. Hypertranslation of the head with respect to the torso was first proposed as a possible injury mechanism by Penning (1992a, 1992b). In a rear-end collision the head effectively remains still while the torso accelerates forwards, the lower cervical spine is forced into hyperextension and the upper into hyperflexion producing a characteristic 'S' shaped curvature of the neck. The heads inertia leads to a situation of high shear in the top of the neck causing overstretching of the ligaments and joint capsules. Grauer et al. (1997) further supported the theory that the development of the 'S' shaped curvature was injurious by using isolated spine specimens to simulate 'whiplash' motion, but identified potentially damaging non-physiological levels of extension in the lower cervical spine as the primary source of injury.

Aldman (1986) and Svensson et al. (1993) found that a pressure increase in the spinal canal due to the rapid formation of combined flexion and extension in the neck can create pressure on the dorsal root ganglion causing it to send pain signals to the brain.

Injury to the neck muscles is another possible source of pain following 'whiplash' motion. During hyperextension of the head and neck the anterior muscle groups are stretched as they try and contract resulting in tearing of the muscle fibres. However muscle damage is unlikely to lead to chronic neck pain problems as in most cases the muscles heal within a few days following an accident.

Ono et al., (1997) and Yoganandan et al., (1998) have both proposed 'pinching' of the facet joints capsules as a possible injury mechanism. The theory being that a portion of the facet capsule can be trapped between the

articulating facet surfaces resulting in damage to the joint, causing pain. As stated by Deng (2000) there is no biomechanical evidence that the capsule is loose enough to be able to be trapped between the facet surfaces and that there are any pain sensitive nocicepters in the area of the facet capsules themselves. Although many different theories have been proposed no definitive answer on the cause of 'whiplash' injury has yet been established. Biomechanical research is ongoing in the field of impact analysis with many different experimental and computational methods being used to try and determine the mechanisms of injury and ultimately to improve vehicle safety.

## 1.2 The Need for Computational Models

The structure of the human cervical spine is mechanically and geometrically complex; vertebrae of the neck interconnected by soft tissues such as intervertebral discs, ligaments, and muscles interact to provide mobility to the head and protection to the spinal cord. Experimental research and mathematically based computer modeling are continually used to study the behavior of the head and neck, particularly its response to trauma during automobile impacts. To gain insight into injury mechanisms of the cervical spine during motor vehicle collisions studies have been completed using human volunteers, whole cadavers, isolated cervical spine specimens and impact dummies. Testing on human volunteers is limited to situations that are not traumatic and hence only low acceleration impacts can be studied. Cadaver and dummy testing, where realistic impact conditions can be simulated, does not reflect the true human response due to lacking live anatomical structure. Computational modeling offers a cost effective and useful alternative to experimental methods being able to provide information on simulated situations that could not otherwise be obtained. Mechanical engineering software packages that are most commonly used to develop automotive and aeronautical parts along with many other mechanically complex structures lend themselves to biomechanical applications such as the movement and interactions of the human body and in particular the human cervical spine.

## 1.3 Research Outline

The rationale behind this research is that a fully validated detailed computational model of the human head and neck can help explain the mechanisms of 'whiplash' and increase our understanding of neck injury during automobile impacts. Whether the mechanism of injury be due to the development of angular motions beyond physiological limits or to shear forces leading to local failure of the soft-tissue structures, investigation into the local kinematics of the intervertebral joints and into the loads and deformations of the soft-tissue components will lead to a better understanding of its mechanics.

## 1.4 Research Objective

The objective of this research is to develop and validate a detailed three-dimensional model of the human head and cervical spine that can accurately predict the dynamic response of the head and neck to various automobile impact situations. As well as being able to define the motion of the head with respect to the torso the model must also be able to predict the local kinematics of the individual vertebrae as well as the loads and deformations of the surrounding soft tissues.

## 1.5 Thesis Overview

Chapter 2 describes the biomechanics of the cervical spine. A review of the anatomy, kinematics, physical and mechanical properties of the cervical spine and its components thought relevant to the computational modelling of the cervical spine is given.

Chapter 3 presents a summary of existing spine models concentrating on the cervical spine. Early continuum models, simple two-pivot models, and more complex discrete parameter and finite element models are reviewed.

The development of a computational model of the human head and neck is described in Chapter 4. The model comprises detailed three-dimensional solid models of the skull and vertebrae interconnected by mechanical constraints representing the soft-tissue components and musculature of the human head and neck.

In Chapter 5 the response of the individual segments of the neck model to small and large external static loads are investigated and compared against experimental data. The main and coupled motions between vertebrae and the loads developed in the soft-tissue components in response to external loading are studied. Also in this chapter the moment generating capacity of the neck muscle elements are investigated and validated against experimental findings before the complete head-neck model is used for dynamic analysis of impacts in Chapter 6.

The model response to frontal and lateral impact is validated against sled acceleration test results using human volunteers and the role of muscle behaviour is studied. A detailed analysis of the local loads and deformations of the vertebrae and soft-tissues of the neck is presented. The final part of Chapter 6 investigates the effects of muscle parameters on the head-neck response to frontal impacts.

Chapter 7 implements the head-neck model without musculature to the study of 'whiplash' motion. Experimental bench-top sled results using isolated cadaveric cervical spine specimens are used to validate the models response before the muscles are added back to the model to determine their role in 'whiplash'. The effect of muscle tensioning on the head neck response and on the internal tissue loads to rear-end impacts is examined.

The final chapter concludes this thesis bringing together the findings of this research and outlining the limitations of the model. Further possible enhancements to the model are described as well as future applications and developments that may aid in a better understanding of the head and neck response to automobile impacts.

# CHAPTER 2

# Biomechanics of the Human Cervical Spine

The cervical region of the human spine provides mobility to the head and neck and is the most mobile region of the spine. The four basic motions are flexion (forward bending), extension (rearward bending), lateral bending and axial rotation. Along with the rest of the spine the cervical region protects the spinal cord and directly supports the head. All of these primary functions of the spine can only be achieved by integration of the mechanical forces contributed by the bony architecture and ligaments of the spine together with the structures of the intervertebral discs and complex extrinsic forces provided by skeletal muscles adjacent to the axial skeleton. Figure 2.1 depicts the whole spinal column showing the different anatomical regions and all the vertebrae of the spine.

The cervical spine as a unit consists of seven vertebrae labelled C1-C7, interconnected by a variety of structures that collectively are known as the soft tissues of the cervical spine. Ligaments of various types connect vertebral bodies and the posterior elements of the cervical vertebrae and span one or more segments depending on type and vertebral level. Facet capsules connect the articular processes of the vertebrae and adjacent vertebral bodies are bound by intervertebral discs. These soft tissues allow for movement between the cervical vertebrae and, together with muscles, control the overall motion of the neck.

This chapter describes the biomechanics of the cervical spine. Section 2.1 summarizes the bony anatomy of the cervical spine and how the shape and structure of the vertebrae dictate the movements of the neck. Section 2.2

presents the in-vivo kinematics of the cervical spine. Section 2.3 reviews the available data on the mechanical characteristics of the functional spinal units that make up the cervical spine and section 2.4 details the soft tissues that interconnect the cervical vertebrae. A brief description of the inertial properties of the cervical spine is given in section 2.5 and finally in section 2.6 the mechanisms of injury to the cervical spine and its components are discussed.

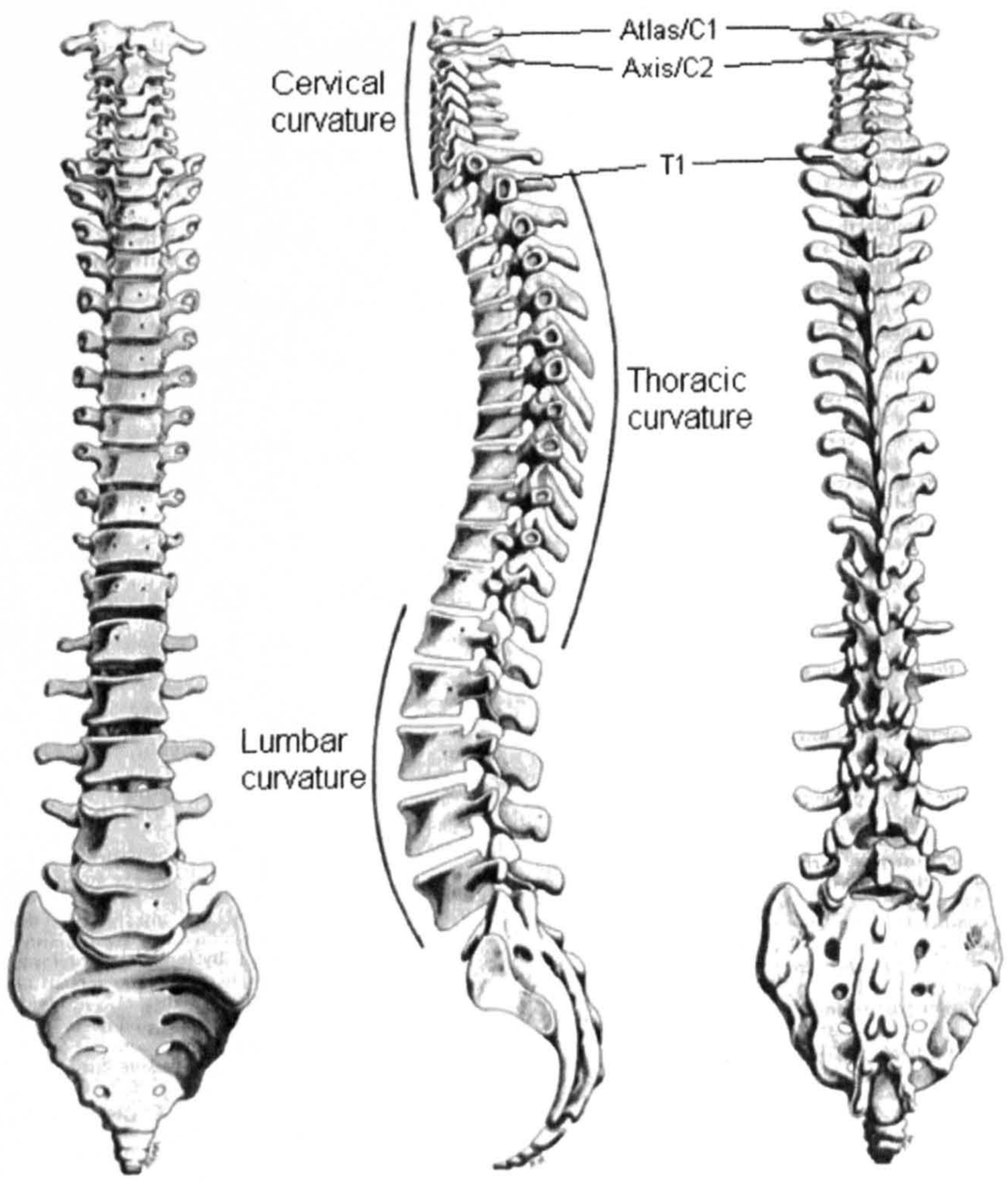


**FIGURE 2.1:** The vertebral column. Anterior aspect (left), lateral aspect (centre) and dorsal aspect (right).

# 2.1 Bony Anatomy

Due to unique regional differences the neck can be divided into two main segments, the upper and lower cervical spine. These can be further sub-divided into four distinct units, each with a unique morphology that determines its kinematics and its contribution to the functions of the complete cervical spine. These units are: the atlas (C1) and axis (C2), comprising the upper cervical spine then the C2-C3 junction and the remaining (C4-C7) typical cervical vertebrae comprising the lower cervical spine.

## 2.1.1 The Upper Cervical Spine

The upper cervical spine, also known as the occipital-atlanto-axial joint, consists of the occiput (base of the skull, labelled C0), and the atlas (C1) and axis (C2) vertebrae. An anatomical drawing of the C1 and C2 vertebrae is shown in figure 2.2. The atlas has no vertebral body and is essentially a bony ring with two oval shaped lateral masses bearing superior and inferior articular surfaces and the transverse processes onto which muscle attachments are made. It has no pedicles, laminae or spinous process as are common to the other cervical vertebrae. The atlanto-occipital (C0-C1) joint is very strong allowing only nodding movements between the head and atlas. This strong interaction is achieved through the concave superior articular sockets of the atlas and the convex condyles of the occiput. The sidewalls of the concave sockets limit side-to-side movement and the front and back walls prevent anterior and posterior gliding of the head (Bogduk and Mercer, 2000). Axial rotation and lateral bending are not physiological movements of the C0-C1 joint and can only be induced artificially by forcing the head while keeping the atlas fixed; they are not producible by the action of the muscles. A combination of rolling and sliding of the occipital condyles across the superior articular surfaces of the atlas produces the flexion and extension motions. The inferior articular surfaces of the atlas correspond to the superior facets of the axis, additionally there is a small oval shaped articular facet on the posterior surface of the anterior ring of the atlas which has interactions with the odontoid process of the axis.

The axis or C2 vertebra is the largest cervical vertebra and is similar to the lower vertebrae in that it comprises a body and an arch, but in addition there is also the odontoid process or dens. Laterally there are two articular surfaces and transverse processes. The posterior arch of the axis consists of two narrow laminae that run obliquely and medially joining to form the spinous process, which has two tubercles like every other cervical vertebra beneath it (Kapandji, 1974). After weight bearing, the main function of the atlanto-axial joint (C1-C2) is to allow a large range of axial rotation, for this movement the anterior arch of the atlas pivots and slides around the odontoid process of the axis and the inferior facet surfaces of the atlas slide across the large superior facet surfaces of the axis. Due to the biconvex joint structure of the atlantial and axial facets the atlas nestles into the axis on rotation as the atlantial facets slide down the slope of the axial facets in opposites directions on either side of the vertebrae (Bogduk and Mercer, 2000). The inferior articular surfaces of the axis correspond to the superior articular surfaces of C3 and are the commencement of the lower cervical spine.

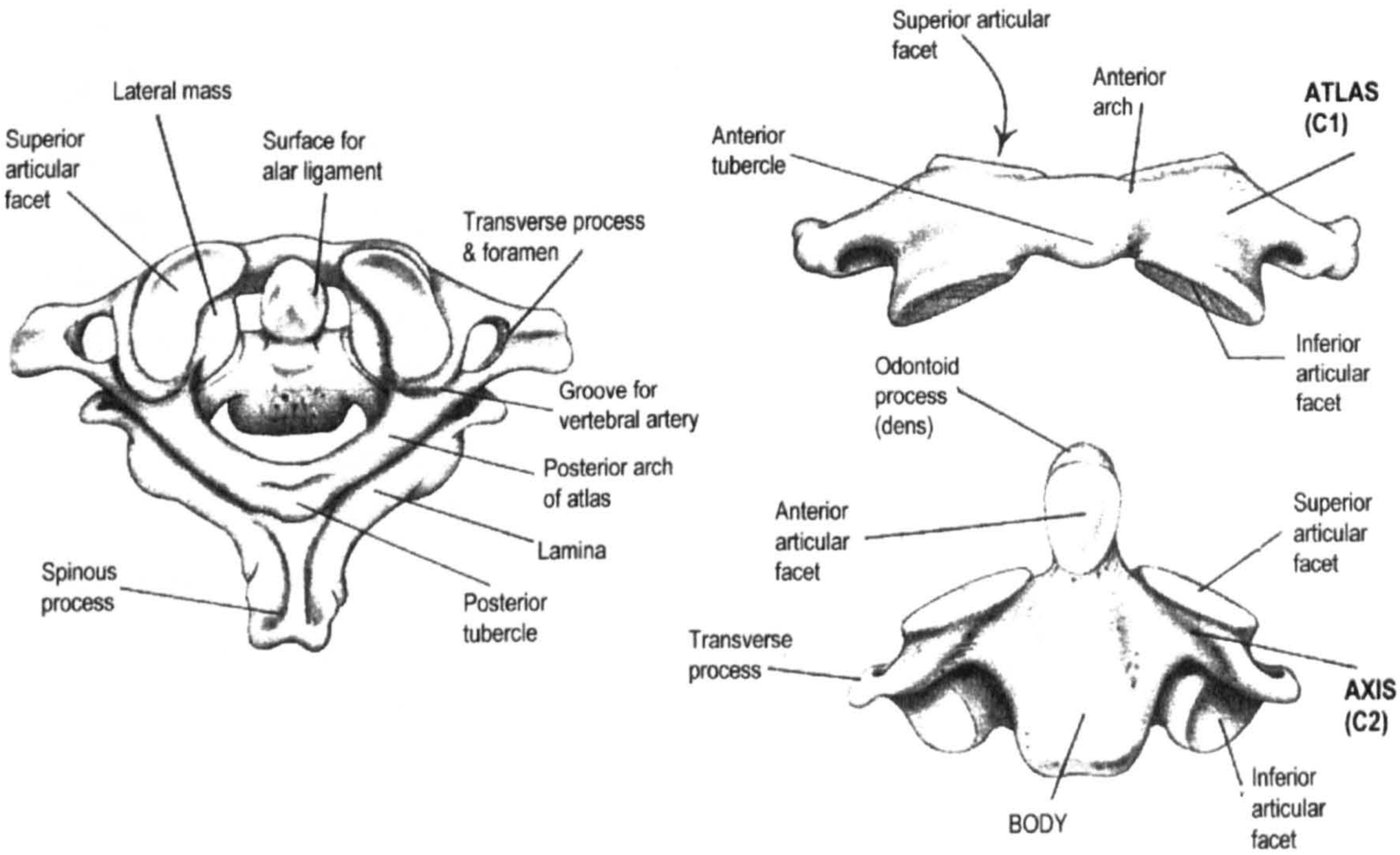


**FIGURE 2.2:** The atlas and axis vertebrae of the upper cervical spine (adapted from Adam and Rouilly, Anatomical Chart Co., 1992)

## 2.1.2 The Lower Cervical Spine

The lower cervical spine comprises vertebrae C3 though to C7 which are irregular shaped bony elements with common geometrical features. They each consist of a vertebral body and an arch that includes two pairs of articular facets, a spinous process and two transverse processes. The main bodies of the vertebrae are separated by intervertebral discs and are approximately cylindrical in shape with a large cross sectional area to withstand applied loads. The opposing surfaces of each body are gently curved in the sagittal plane and are also curved from side to side. The inferior anterior edge of the vertebral body forms a lip that hangs down towards the superior anterior edge of the vertebra below. The superior surface of each vertebral body slopes downwards and forwards resulting in the intervertebral disc sitting obliquely to the long axis of the vertebral bodies. This structure reflects flexion-extension being the predominant movement of typical cervical segments and because the discs are thicker anteriorly than posteriorly, the cervical spine has a natural anterior convex curve known as cervical lordosis. A recent paper by Bogduk and Mercer (2000) describes the cervical intervertebral joints as 'saddle' joints: consisting of two concavities facing one another and set at right angles to one another. This then allows the vertebral body to rock forward in the sagittal plane, around a transverse axis and from side to side in the plane of the facets around an axis perpendicular to the facets.

The articular facets of the lower cervical spine are almost flat and are covered with a thin layer of cartilage, they are orientated at about 45° to the transverse plane of the vertebrae. The facet joints are synovial joints formed by the corresponding articular facets of adjacent vertebrae. They guide and constrain the motion between vertebrae.

The geometry of the vertebral bodies and orientation of the facet joints stipulates that horizontal rotation is coupled with lateral flexion and vice-versa, meaning that the vertebrae tilt to the side of rotation or, rotates to the side of lateral flexion.

The posterior region consists of pedicles, facets, laminae and other processes that allow muscle attachment. The spinal cord passes through each vertebra through a hole called the neural canal, which is made up by the vertebral body,

pedicles and lamina. Figure 2.3 shows the 5th cervical Vertebrae, typical of C3-C7 of the cervical region, all significant body anatomy are labelled.

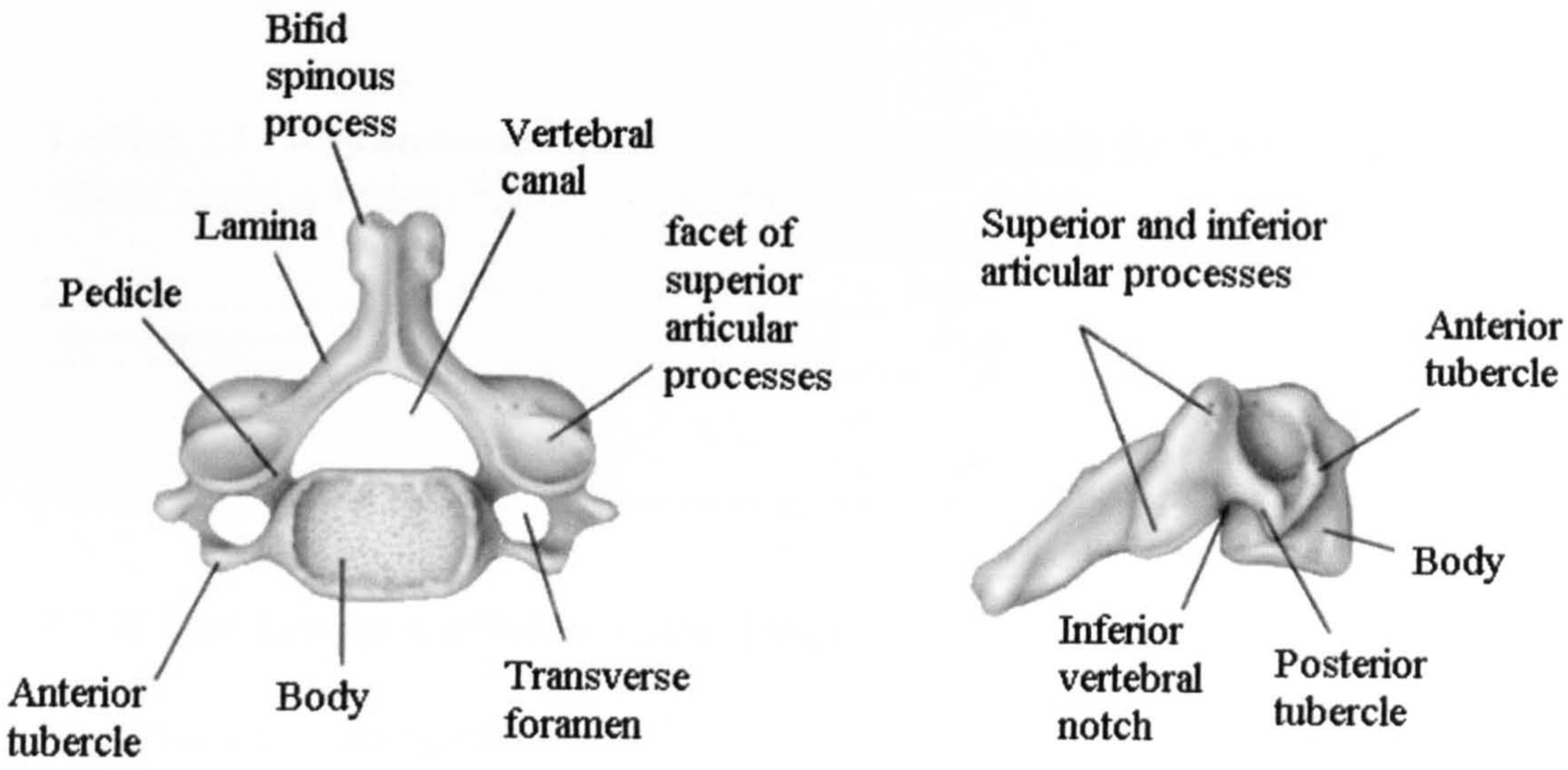


**FIGURE 2.3:** A typical vertebrae of the lower cervical spine, superior and lateral view (adapted from Adam and Rouilly, Anatomical Chart Co., 1992).

## 2.2 Kinematics of the Cervical Spine

The upper region of the cervical spine is different in structure and behaviour to the lower cervical spine. Special anatomical differences of the joint structure result in different kinematic characteristics that have been reported by a number of authors.

### 2.2.1 The Upper Cervical Spine Joints

White and Panjabi (1990) have presented the range of motion for the atlanto-occipital and atlanto-axial joints, these values are shown in table 2.1. It can be seen that both joints exhibit fairly even amounts of flexion/extension motion and also of lateral bending. Very little axial rotation is observed between C0 and C1, the major rotation of the upper cervical spine region is between C1-C2 where as much as 47° to one side has been reported (Werne, 1957). Axial rotation of the C1-C2 unit is accompanied by a certain degree of extension

(~14°) and contralateral lateral bending (~24°). Translation motion of the upper cervical spine has been found to be insignificant in almost all directions. In the sagittal plane around 2-3mm translation between the dens and the anterior ring of the atlas has been observed.

**TABLE 2.1:** Representative values of in-vivo range of motion for the Occipital-Atlanto -Axial complex (White and Panjabi, 1990).

| | Combined Flexion/Extension | One Side Axial Rotation | One Side Lateral Bending |
|---|---|---|---|
| Spinal Segment | | (deg) | |
| C0-C1 | 25 | 5 | 5 |
| C1-C2 | 20 | 40 | 5 |

## 2.2.2 The Lower Cervical Spine Joints

Studies of cadavers give an idea on the range of motion of individual vertebral segments however these studies do not accurately reflect the in-vivo response due to the lack of active muscles. White and Panjabi (1990) present representative values for in vivo ranges of motion of the lower cervical spine based on a number of studies but mainly on the work of Lysell (1969) (table 2.2). Most of the flexion/extension motion takes place in the central region with the C5-C6 segment having the largest range. The range of motion for lateral bending and axial rotation is generally smaller in the more caudal segments of the lower cervical spine.

**TABLE 2.2:** Representative values of in-vivo range of motion for the lower cervical spine motion segments (White and Panjabi, 1990).

| | Combined Flexion/Extension | One Side Axial Rotation | One Side Lateral Bending |
|---|---|---|---|
| Spinal Segment | | (deg) | |
| C2-C3 | 10 | 3 | 10 |
| C3-C4 | 15 | 7 | 11 |
| C4-C5 | 20 | 7 | 11 |
| C5-C6 | 20 | 7 | 8 |
| C6-C7 | 17 | 7 | 6 |
| C7-T1 | 9 | 2 | 4 |

### 2.2.3 Coupling

No range of motion for axial rotation in the plane of the facet joints has been determined and so when measured in the horizontal plane axial rotation is coupled with lateral flexion. A study by Mimura et al. (1989) has provided data on coupled movements for axial rotation for all segments of the cervical spine (table 2.3). These data were found from trigonometric reconstructions of movements studied by biplanar radiography. From this data it can be seen that this method yields slightly different ranges of axial rotation than shown previously, noticeably a more generous range for the C2-3 segment. A second characteristic coupling of the lower cervical spine is translation with flexion/extension motion. Flexion is coupled with anterior translation and extension with posterior translation.

**TABLE 2.3:** Range of motion of cervical spine in axial rotation with ranges of coupled motions (Mimura et al., 1989).

| | Main Motion | Coupled Motion | |
|---|---|---|---|
| | Axial Rotation | Combined Flexion/Extension | Lateral Flexion |
| Spinal Segment | | (deg). (SD) | |
| Occ-C2 | 75 (12) | -14 (6) | -2 (6) |
| C2-C3 | 7 (6) | 0 (3) | -2 (8) |
| C3-C4 | 6 (5) | -3 (5) | 6 (7) |
| C4-C5 | 4 (6) | -2 (4) | 6 (7) |
| C5-C6 | 5 (4) | 2 (3) | 4 (8) |
| C6-C7 | 6 (3) | 3 (3) | 3 (7) |

## 2.3 Mechanical Characteristics of the Cervical Spine

The mechanical behaviour of the human cervical spine is quantified by its physical properties. This section deals with the mechanical properties of intact functional spinal units of the cervical spine. First an outline of the general testing procedure used to determine the mechanical response of motion segments is presented. Following this there is a review of studies that have defined the mechanical characteristics of the upper and lower cervical spine segments. This data is useful in understanding the mechanical response at each

level of the cervical spine and for the validation of computational models. The mechanical characteristics of the individual soft tissues of the cervical spine are dealt with in section 2.4 and finally the inertial characteristics of the neck are discussed in section 2.5.

## 2.3.1 Loads and Displacements of Motion Segments.

A motion segment, functional spinal unit or intervertebral joint comprises of two adjacent vertebrae with all soft tissues attached. The entire spinal column can be thought of as being composed of a number of functional spinal units connected in series. The general experimental set-up for determining the mechanical response of a motion segment is shown in figure 2.4. The lower vertebra is fixed with the upper vertebra being free to move in all six degrees of freedom in response to a load applied to the centre of the upper vertebral body. All soft tissues such as intervertebral disc, facet joints and ligaments between the vertebrae are left intact. Load/displacement curves are used to describe the complete mechanical behaviour of a motion segment. Due to differing response in the positive and negative directions, the load components are split up into a total of twelve loading conditions; six moments about, and six forces along, the three axes of a coordinate system applied at the geometric centre of the upper vertebral body. These twelve load components are: anterior/posterior shear, left/right lateral shear, tension/compression, left/right lateral bending, flexion/extension and left/right (or sometimes CW and CCW) axial rotation. Mid-sagittal symmetry is assumed, resulting in the left and right responses to lateral bending, lateral shear or axial rotation being identical.

It should be noted that the set-up for determining the mechanical response of motion segments varies widely between studies; different fixation devices are used along with different loading techniques. Therefore a large variation in the reported responses is seen across studies, highlighting not only the difficulty in accurately performing these tests but also the natural variation in response of a biological structure such as the human spine.

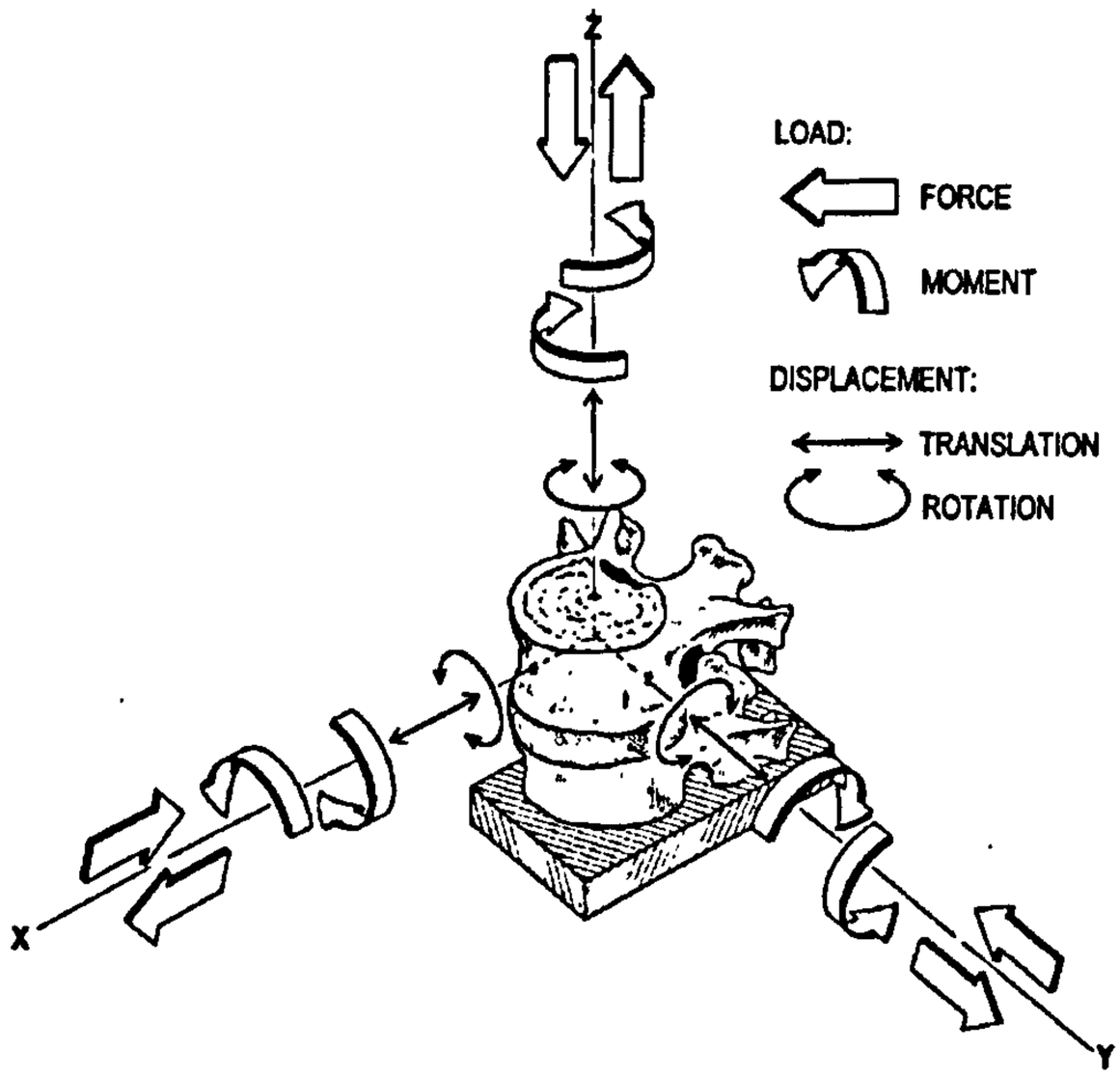


**FIGURE 2.4**: A typical spinal motion segment. (Adapted from White and Panjabi, 1990)

## 2.3.2 The Upper Cervical Spine

In studies on the biomechanics of the upper cervical spine the occipito-atlanto-axial joint is usually treated as a single unit due to its unique functional arrangement.

Panjabi et al. (1988) studied the three-dimensional movements of the C0-C1 and C1-C2 joints. Whole cervical spine segments were used, fixed at C7 with loads being applied at the occiput in flexion, extension, lateral bending and axial rotation. Pure moment was used to ensure uniform loading along the specimen with a maximum applied moment of 1.5Nm. Each moment was applied in a three-load-unload cycle, the maximum moment being reached in three equal steps. On the third load cycle the vertebral motions were measured for each load step. Viscoelastic effects were minimised by the use of this load-unload technique and in addition after each load step the specimen was held for 30 seconds to allow creep to occur before the measurements were taken. Therefore the characteristics reported here are static behaviours of the two joints. Mean and standard deviation of neutral zone and range of motion for all six movements of both joints are reported. Further static characteristics have

been reported by Panjabi and co-workers (Panjabi et al., 1991a; Panjabi et al., 1991b; Oda et al., 1992) studying the effects of alar ligament transection and the role of the tectorial membrane on the upper cervical spine. In these studies similar experimental techniques were used on smaller spine specimens of C0-C3. Goel et al. (1988b) used C0-C5 specimens to study the static characteristics of the occipito-atlanto-axial complex. Reported ROM's with standard deviations for both joints for flexion, extension, left lateral bending and left axial rotation are reported in response to a 0.3Nm applied moment. Panjabi et al. (1988, 1991a) state that 1.5 Nm is sufficient to produce the maximum physiologic range of motion and so the small 0.3Nm moment used by Goel et al. does not represent the physiologic ROM for the upper cervical spine segments. Vishteh et al. (1999) studied the effect of unilateral occipital condyle resection on the craniovertebral junction and reports load-deformation curves for flexion-extension, lateral bending and axial rotation as well as axial translation from tension-compression. Spine specimens from the skull to C3 were used, rigidly fixing the skull and applying loads to C3. Loads were applied quasi-statically in 0.25Nm increments to a maximum of 1.5Nm and so represent the physiologic ranges. For the compression to tension displacements of the C0-C2 unit, loading was again applied quasi-statically in 10N increments to a maximum of 70 N. Graphs showing the load/deformation response of the two joints for each of the rotations tested are given but the supporting data are not. The range of motion and neutral zone at maximum load are presented for axial translation across C0-C2 in tension and compression.

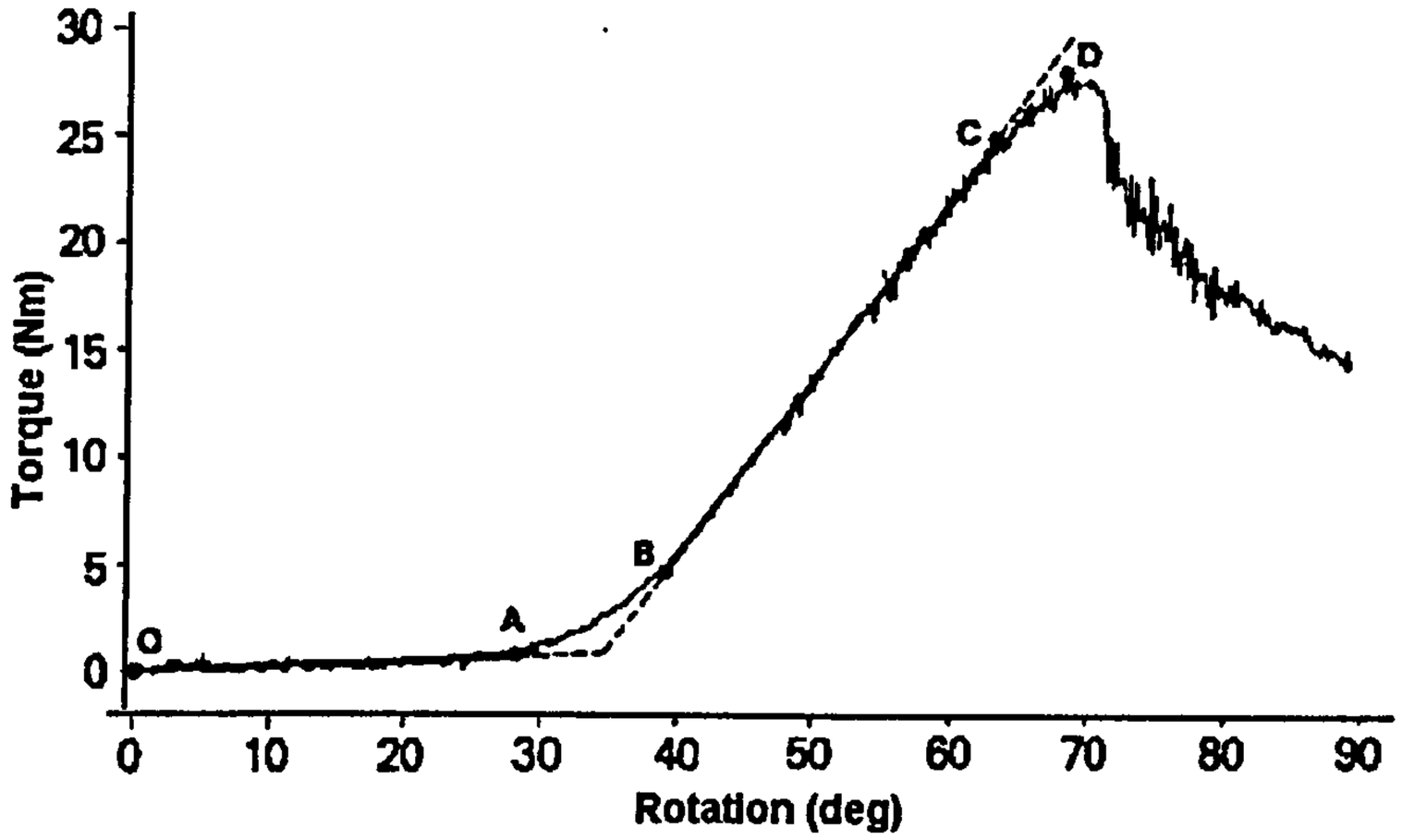


**FIGURE 2.5:** Torque rotation curve for a typical C0-C2 specimen in response to right axial rotation (Chang et al., 1992).

Chang et al. (1992) report quasi-static and dynamic characteristics of the upper cervical spine in response to right axial rotation. C0-C2 specimens were tested to failure at loading rates of 4, 50, 100, and 400°/s. Load was applied at C2 simulating right axial rotation and the resulting moment was measured at C0, only axial rotation was constrained, leaving the unit free to move in all other coupling directions. The motion of C1 was not measured. The weight of the loading apparatus contributed an axial compressive pre-load of approx. 3.5N. A torque-right angular rotation curve was obtained for each specimen (figure 2.5). Points A, B, and C were determined by fitting straight lines to the sections OA and BC on the curve representing the least and steadily increasing resistance respectively. Stiffnesses for regions OA and BC are reported along with the value for the point of maximum resistance, D. Table 2.4 summarises the results obtained for all specimens at each loading rate tested. The authors conclude that at higher loading rates the C0-C2 region becomes stiffer with an increase in torque required to produce failure of the specimen. Also the degree of right axial rotation does not increase significantly with increased loading rates.

**TABLE 2.4:** Reported values for quasi-static and dynamic loading rates, points A-D to define moment rotation curves and stiffness of sections OA and BC (taken from Chang et al., 1992).

| Loading Rates | Points on curve | | | | | | | | Stiffness | |
|---|---|---|---|---|---|---|---|---|---|---|
| | A | | B | | C | | D | | OA | BC |
| deg/s | (deg) | Nm | (deg) | Nm | (deg) | Nm | (deg) | Nm | Nm/deg | |
| 4 | 20.7 | 0.5 | 29.9 | 2.0 | 57.8 | 11.9 | 68.1 | 13.6 | 0.028 | 0.383 |
| 50 | 27.7 | 0.6 | 37.4 | 3.0 | 56.5 | 13.0 | 67.8 | 14.3 | 0.027 | 0.528 |
| 00 | 29.2 | 1.0 | 40.1 | 4.6 | 65.9 | 23.7 | 77.7 | 27.8 | 0.035 | 0.733 |
| 400 | 30.0 | 1.5 | 30.0 | 1.5 | 57.8 | 20.3 | 64.7 | 23.2 | 0.053 | 0.669 |

## 2.3.3 The Lower Cervical Spine

There have been many studies characterising the response of the lower cervical spine segments. The following section details the most important of these and compares their findings. Large variations between studies are found, mainly due to the difficulty in obtaining the mechanical characteristics, performing the relevant experiments and to the natural variation typically found for biological structures.

Panjabi et al. (1986) provides load-displacement curves for 6 of the possible 12 types of pure loading force of the cervical spine. A method for applying the forces was used to allow the testing of all functional spinal units as opposed to the previous method of testing isolated motion segments. The main coupled motions are given along with each of the major load-displacement curves.

The testing method keeps the cervical spine specimen intact, isolating each joint being studied in turn by clamping the bodies of adjacent vertebrae. A special loading jig is attached to the upper vertebra of the joint being tested with a second fixation jig being attached to the inferior adjacent vertebra. This method optimises the information gathered from each specimen by testing the joint at each cervical level. Each intervertebral joint was loaded with six different types of force: right shear ($-F_x$), left shear ($+F_x$), axial compression ($+F_y$), axial tension ($-F_y$), posterior shear ($-F_z$), and anterior shear ($+F_z$).

The apparatus did not produce any asymmetry when applying loads in the various directions and so any asymmetry in the results is due to the spinal configuration itself. All forces were applied, and displacements were

measured, at the geometric centre of the body of the loading vertebra, the geometric centre being at the intersection of the diagonals of a quadrangle whose sides are tangent to the sides of the vertebral body. Each force increased over four equally incremented steps up to a maximum of 50N. No pre-load was applied to the specimen, but there was a total apparatus weight of 985g acting on the spine (resulting in 10N equivalent preload). It should be noted that the weight of the head is approximately 6kg and was not included in the test; the muscles of the neck were also not incorporated.

There was no systematic variation of the load-displacement curves for vertebral level and so the results are given as averaged load-displacement curves for each load and motion type. From these curves, the total ranges of motion (ROM), neutral zones and neutral zone ratios were determined for both coupled and main motions. Neutral zone ratio is the ratio of the neutral zone to the corresponding ROM. The neutral zones reported in the paper represent the range of motion for each direction for which the spine is easily displaced without any significant external load application. Flexibility coefficients are also given and defined as the gradient of the curve between the first and third load steps.

The main motion associated with lateral shear was lateral translation and the mean total ROM was found to be 3.0 ±0.3mm, divided approximately equally between left and right. The flexibility coefficient was 19.0 ±11.4mm/kN in left shear and 19.0 ±11.3mm/kN for right shear. The major coupled rotation to this loading was axial rotation with a mean total range of 3.8° ±0.6°. Right axial rotation coupled left shear and left axial rotation coupled right shear. There was a small amount of lateral bending experienced with a mean total of 1.6° ±0.2°.

For the compression-distraction loading the mean ROM was found to be 0.7mm compression and 1.1mm in tension giving a mean total ROM of 3.5 ±0.3mm. The flexibility coefficient was 7.1 ±8.4mm/kN for a negative load (compression) and 19.0 ±12.4mm/kN for a positive load (distraction). There were two major coupled rotations, flexion/extension (4.8° ±1.0°) and lateral bending (3.3° ±1.0°). Extension and right lateral bending coupled compression and flexion and left lateral bending coupled distraction.

The main response to anterior/posterior loading was translation in the direction of the applied load. The mean total ROM was 3.5 ±0.3mm divided unequally: 1.9mm for anterior shear and 1.6mm for posterior shear. The flexibility coefficient was 29.6 ±10.9mm/kN for anterior shear and 19.0 ±11.1mm/kN for posterior shear. The major coupled motion to this was flexion/extension with a mean total ROM 9.9° ±1.2°. 6.3° of flexion with anterior shear and 3.6° of extension with posterior shear. There was also a small amount of axial rotation experienced.

The fact that head weight and muscle contraction were not included in these in vitro tests and that only small forces were used should be taken into account if comparisons are to be made with in-vivo situations.

Moroney et al. (1988) reports load –displacement behaviour for 35 cadaveric cervical spine motion segments in compression, shear, bending, and axial torsion. Segments were tested as intact specimens or as disc segments comprising two vertebral bodies, the intervertebral disc, and both longitudinal ligaments. Average principle and coupled motions are presented along with the corresponding stiffnesses. C2-C3 down to C7-T1 segments were tested, the lower vertebra of each segment was rigidly fixed while the upper vertebra was free to move in response to the applied loads. Loads where applied at the centre of the disc, a 49N preload was used to simulate the in vivo loading due to the weight of the head. The moments applied to produce the rotation responses were typically in the range 1.2-2.2 Nm, for translational responses loads ranged from 10 to 39 N in shear. Disc segment responses were achieved using load ranges from 0.39-1.57Nm in bending and from 4-16N in shear.

A paper by Goel at al. (1984) describes the three-dimensional motion behaviour of the multi-level spinal segments of the cervical spine. They used segments comprising vertebrae C2-T1 to enable them to study the stabilizing effects of fixation devices on artificially injured specimens.

Six defect free specimens (C2-T1) were taken from fresh cadavers keeping ligaments and joint capsules intact but removing muscles and extra soft tissue. The test sample consisted of specimens from two females and four males with an average age of 76 yrs. The specimen for testing was rigidly attached via the inferior vertebra to the test apparatus while moments were applied to the upper vertebra. Flexion, extension, right lateral bending and right axial rotation loads

were applied sequentially to the upper vertebra (C2). A maximum of 0.3Nm moment was found to be sufficient to produce motions within the physiological limits.

The paper describes the study of the effect of artificially produced injuries at the C5-C6 level. Various ligaments were severed in order and the test protocol repeated after each injury. Then the effects of stabilizing techniques were studied. Of interest are the results obtained for the intact specimens only. The results reported were restricted to major rotations only, ignoring any coupled motions experienced. Table 2.5 shows the mean relative rotations between C5-C6 and C4-C5 vertebrae for the intact specimens tested. Only the results corresponding to the maximum moment magnitude of 0.3Nm are presented in this paper.

**TABLE 2.5:** The relative rotations between vertebrae for intact specimens tested. Values given for 0.3Nm moment (Geol et al., 1984). All rotations in degrees.

| Spinal Level | Flexion Mean (SD) | Extension Mean (SD) | R. Lateral Bending Mean (SD) | Axial Rotation Mean (SD) |
|---|---|---|---|---|
| C5-C6 | 8.7 (3.2) | -1.4 (0.3) | 2.3 (1.4) | -1.4 (0.8) |
| C4-C5 | 5.9 (4.5) | -1.4 (0.9) | 2.7 (1.1) | -1.8 (1.3) |
| C4-C6 (averaged) | 7.3 (3.9) | -1.4 (0.6) | 2.5 (1.3) | -1.6 (1.1) |

The results show significant standard deviations, being as large as 75% of the reported mean rotations. As stated by the authors this is quite common in biological studies. This interspecimen variation can be attributed to a number of factors such as age and degree of degeneration of the original specimens, experimental errors in measuring and applying the loads and the duration of the test. These in-vitro tests also lack muscular stability, which would likely decrease the ROM's reported.

A further study by Goel et al. (1988b) studying the effect of total laminectomoies and facet wiring provides data on motion segments of the lower cervical spine using a similar technique to that described above. Flexion, extension, right lateral bending and right axial rotation ranges are reported

along with the respective coupled rotations for each load type (table 2.6). A maximum moment of 0.3Nm was used to induce each rotation response.
The authors state that the values for the left lateral bending and left axial rotations were of similar magnitudes and it can be therefore assumed that the corresponding coupled motions be the same but in the opposite direction.

**TABLE 2.6:** The relative rotations between vertebrae for intact specimens tested. Values given for 0.3Nm moment (Geol et al., 1988). All rotations in degrees.

| Spinal Level | Flexion Mean (SD) | | Extension Mean (SD) | | Right Lateral Bending Mean (SD) | | Right Axial Rotation Mean (SD) | |
|---|---|---|---|---|---|---|---|---|
| | | Coupled Rotations | | Coupled Rotations | | Coupled Rotations | | Coupled Rotations |
| C3-C4 | 3.5 (1.6) | -0.2 AR 0.2LB | -2.9 (0.7 | -0.2 LB | 3.2 (1.8) | 0.5 FLX -1.7 AR | -2.3 (1.8) | -0.3 EXT 2.3 LB |
| C4-C5 | 3.5 (1.6) | -0.1 AR -0.5 LB | -2.7 (0.6) | -0.1 AR 0.2 LB | 3.6 (2.4) | 0.1 FLX -1.4 AR | -2.3 (1.3) | -0.4 EXT 1.7 LB |
| C5-C6 | 2.6 (1.0) | 0.4 AR -0.1 LB | -2.6 (1.1) | -0.1 AR 0.1 LB | 2.4 (1.3) | 0.2 FLX -1.2 AR | -2.3 (1.0) | -0.1 EXT 1.5 LB |
| C6-C7 | 2.9 (1.3) | - | -2.8 (1.2) | -0.2 AR 0.2 LB | 1.8 (1.1) | -0.2 EXT -0.7 AR | -1.7 (1.4) | 0.7 LB |
| C7-T1 | 1.2 (0.6) | 0.2 LB | -1.1 (0.7) | -0.2 LB | 1.5 (0.9) | -0.2 EXT -0.4 AR | -1.4 (0.8) | -0.3 EXT 0.5 LB |

Panjabi (1994) used a similar experimental set up to Geol et al., (1984 & 1988a) using a slightly shorter specimen consisting of the C4-C7 vertebrae. 10 specimens were tested; C7 was fixed while pure moments were applied to C4. Six moments of flexion, extension, right and left lateral bending and right and left axial torque were applied to a maximum value of 1.5 Nm. Only main rotations are presented for each of the six moments and the results for lateral bending and axial rotation are the average of left and right motions. Neutral zone (NZ) and range of motion (ROM) are reported (table 2.7) describing the non-linear behaviour of the segments. The neutral zone provides a quantitative measure of intervertebral laxity, i.e. the range of motion for which a small increase in load causes large rotation.

**TABLE 2.7:** Neutral zones (NZ) and range of motion (ROM) for intact specimens (Panjabi. 1994).

| Motion Segment | Flexion (deg) | | Extension (deg) | | Lateral Bending (deg) | | Axial Rotation (deg) | |
|---|---|---|---|---|---|---|---|---|
| | NZ (SD) | ROM (SD) | NZ (SD) | ROM (SD) | NZ (SD) | ROM (SD) | NZ (SD) | ROM (SD) |
| C4-C5 | 3.4 (0.6) | 16.2(2.8) | 3.4 (0.6) | 15.6(2.4) | 3.3 (0.6) | 11.2(1.6) | 2.2 (0.5) | 10.6 1.8) |
| C5-C6 | 3.4 (0.8) | 16.8(2.9) | 3.4 (0.8) | 13.0(1.8) | 2.6 (0.5) | 9.8(1.4) | 1.7 (0.4) | 10.2(1.8) |
| C6-C7 | 2.9 (0.7) | 17.0(2.7) | 2.9 (0.7) | 11.8(2.2) | 2.3 (0.4) | 9.6(1.2) | 1.2 (0.2) | 6.2(1.0) |

A study by Shea et al. (1991) was conducted to determine the biomechanical properties along the mid (C2-C5) and lower (C5-T1) cervical spine and to investigate the mechanisms of injury for sagittal plane loading. They hypothesise that the stiffness and strength of the mid and lower sections of the cervical spine are different and that the initial position of the spine affects the threshold of injury for flexion compression loading. Their objectives were to determine the *in vitro* load-displacement response of the two segments for combinations of sagittal motions and to measure possible variations in the load-displacement and failure properties for each level.

A different set up was used; the spine segments tested consisted of three adjacent vertebrae with their interconnecting soft tissues intact including ligaments and discs. 18 individual cadavers with a mean age of 74 yr were used to obtain segments for the mid and lower cervical spine, resulting in defect free test segments (C2-C4), (C3-C5) for the mid level and (C5-C7), (C6-T1) for the lower level.

The specimens were tested using a planar testing apparatus. The lowest of the three vertebrae in each segment was fixed to a movable test stage which was able to produce the three components of displacement describing sagittal motion; axial translation, anterior-posterior shear, and flexion-extension rotation. The upper most of the three vertebrae was fixed to a load cell. Using this apparatus it was possible to rotate and displace the specimen about the geometric centre of the middle vertebrae.

Displacements rates were 5mm/s for translation and 5 deg/s for rotation. The authors state that the results obtained at these rates are not significantly

different to results obtained at rates as slow as 0.5mm/s and 0.05 deg/s. The displacements prescribed were 2mm in compression/tension, 1.5mm in anterior/posterior shear, 17° in flexion and 5° in extension.

The sagittal load-displacement curves for the tested segments were highly non-linear for even small applied loads. The curves clearly displayed a neutral zone near zero displacement where a small increase of load results in large deformations. They found that for 300N axial force all specimens were stiffer in compression than in tension. They found no significant difference between stiffness in anterior or posterior shear at 150N or in flexion extension at 5Nm.

Mean cervical stiffness values were calculated at 500N of compression and 100N of tension, 100N of anterior-posterior shear, 3.5Nm of extension and 5Nm of flexion for comparisons of mid and lower spine segments. The results showed that the mid cervical region was stiffer in compression and extension than specimens from the lower region.

The strength of the mid cervical specimens was found to be 7Nm with a mean flexion angle of 26°at failure. The strength of the lower cervical spine specimen was found to be 12.1Nm with a compressive force of 2158N. It was found that a combination of flexion and axial compression was required to produce failure in the majority of the tested lower segments.

All modes of failure of the specimens were similar, displaying soft tissue failure before bony fracture in flexion. Disc injuries were noted more frequently then any other injury.

The effects of pre-torsion on the specimens was investigated and it was found that all specimens tested were stiffer in tension and anterior shear after the axial pre-torque and less stiff in extension. It was noted that the presence of pre-torque diminished the zone of low slope (neutral zone) in all three sagittal motions by taking up the slack in the ligaments. The average flexion angle at failure was 17.7°, lower than the 25°mean failure of specimens that were not pre-torqued. Greater ligamentous and annular damage was observed for the pre-torqued specimens than for those that were not. This indicates that there is an increased injury risk for cervical spines that are pre-torqued prior to load application.

In conclusion the authors found that the mid region of the cervical spine is stiffer in compression and extension than the lower region. They found that

specimens from the mid section generally failed in flexion (<33°), while specimens from the lower region generally sustained 33° of flexion rotation and failed with a combination of flexion rotation and compression motion indicating that the lower cervical spine is more mobile than the mid. The limitations of this study are the low rate of displacement and the absence of surrounding muscles and tissues.

A more recent study by Richter et al. (2000) reports on in-vitro load-displacement properties of the lower cervical spine, investigating the stabilizing effects of the disco-ligamentous structures. Six human cadaver spine segments C4-C7 were tested in flexion/extension, axial rotation and lateral bending using a pure bending moment of 2.5Nm applied at a constant rate of 2°/s. The range of motion and neutral zone of the segment C5-C6 are presented for each direction of loading, no axial preload was applied to the test segments.

**Comparison of the Studies:**

Table 2.8 shows a summary of the neutral zones and range of motion from the various studies outlined in the previous section. Table 2.9 shows the average reported stiffnesses for various spinal levels. All of the studies differ from one another in terms of experimental set-up and method of load application used making it difficult to directly compare the results obtained.

Panjabi et al and Moroney et al. (1988) performed tests for low levels of loading and hence concluded that there was no variation in stiffness along the lower cervical spine. Shea et al. (1991) proved that for higher level loading there is a variation in both stiffness and strength along the spine.

**TABLE 2.8**: Neutral zone and range of motion for motion segments of the lower cervical spine.

Neutral Zone (NZ)

| Author et al | Spinal level | TNS | CMP | AS | PS | LS | | FLX | EXT | LB | AR |
|---|---|---|---|---|---|---|---|---|---|---|---|
| | | mm | | | | | | deg | | | |
| Panjabi(1986) | C2-T1 | 0.3 | 0.3 | 0.8 | 0.8 | 0.7 | | | | | |
| Panjabi(1994) | C4-C5 | | | | | | | 3.4 | 3.4 | 3.3 | 2.2 |
| | C5-C6 | | | | | | | 3.4 | 3.4 | 2.6 | 1.7 |
| | C6-C7 | | | | | | | 2.9 | 2.9 | 2.3 | 1.2 |
| Richter (2000) | C5-C6 | | | | | | | 5.2 | 5.2 | 2.7 | 0.8 |

Range of Motion (RoM)

| | mm | | | | | | deg | | | |
|---|---|---|---|---|---|---|---|---|---|---|
| Panjabi (1986) | 1.1 | 0.7 | 1.9 | 1.6 | 1.5 | | | | | |
| Moroney (1988) | | 0.1 | 0.2 | 0.1 | 0.4 | | 5.6 | 3.5 | 4.7 | 1.9 |
| Panjabi (1994) | | | | | | | 10.2 | 16.7 | 13.5 | 9.0 |
| Goel (1988b) | | | | | | | 2.5 | 2.7 | 2.4 | 2.0 |
| Goel (1984) | | | | | | | 2.5 | 7.3 | 1.4 | 1.6 |
| Richter (2000) | | | | | | | 6.7 | 6.7 | 4.3 | 5.0 |

**TABLE 2.9:** Stiffness for motion segments of the lower cervical spine.

| Author et al | Spinal level | TNS | CMP | AS | PS | LS | | FLX | EXT | LB | AR |
|---|---|---|---|---|---|---|---|---|---|---|---|
| | | N/mm | | | | | | Nm/deg | | | |
| *Static Stiffness:* | | | | | | | | | | | |
| Panjabi (1986) | C2-T1 | 52.6 | 140.8 | 52.6 | 33.8 | 52.6 | | | | | |
| Moroney (1988) | C2-T1 | | 1318 | 131 | 49 | 119 | | 0.43 | 0.73 | 0.68 | 1.16 |
| Panjabi (1994) | C4-C5 | | | | | | | 0.12 | 0.12 | 0.19 | 0.12 |
| | C5-C6 | | | | | | | 0.11 | 0.16 | 0.21 | 0.18 |
| | C6-C7 | | | | | | | 0.11 | 0.17 | 0.21 | 0.30 |
| Goel (1988b) | C3-T1 | | | | | | | 0.11 | 0.12 | 0.12 | 0.15 |
| Goel (1984) | C4-C6 | | | | | | | 0.04 | 0.22 | 0.12 | 0.19 |
| Richter (2000) | C5-C6 | | | | | | | 1.61 | 1.61 | 0.56 | 0.35 |
| *Quasi-static stiffness:* | | | | | | | | | | | |
| Shea (1991) | | | | | | | | | | | |
| | C2-T1a | 433 | 718 | 183 | 162 | | | 1.13 | 1.88 | | |
| | C2-T1b | 193 | 957 | 123 | 114 | | | 1.13 | 1.74 | | |
| | C2-C5b | 229 | 1114 | 110 | 115 | | | 1.44 | 2.29 | | |
| | C5-T1b | 157 | 800 | 136 | 112 | | | 0.83 | 1.19 | | |

Panjabi [1986]: calculated as the reciprocal of the reported flexibility coefficient at 25N.
Moroney [1988]: as reported
Panjabi [1994]: calculated from reported NZ and ROM at 1.5Nm: (1.5Nm/ROM-NZ)
Goel [1988b], [1984]: calculated from averaged reported ROM at 0.3Nm: (0.3Nm/average ROM)
Richter [2000]: calculated from reported NZ and ROM at 2.5Nm: (2.5Nm/ROM-NZ)
Shea [1991] C2-T1a: reported average stiffness at 300NCMP/TNS, 150N AS/PS, and 5Nm FLX/EXT.
C2-T1b: reported average stiffness at 500N CMP, 100N TNS, 100N AS/PS, 3.5Nm EXT, and 5Nm FLX.

**Coupling:**

Moroney et al. (1988), Panjabi et al. (1986) and Goel et al. (1988a) report coupled displacements with the major motions measured. Between studies there is a large variation in the magnitude of the coupled motions and their direction, in many cases the standard deviations are of the same magnitude as the coupled displacement. Table 2.10 shows a summary of the most significant coupled motions reported.

**TABLE 2.10:** Significant reported coupled motions.

| | R. LS | L.LS | CMP | TNS | AS | PS | FLX | EXT | R.LB | L.AR | R.AR |
|---|---|---|---|---|---|---|---|---|---|---|---|
| | | | mm | | | | | | deg | | |
| Panjabi (1986) C2-T1 | 1.4 Coupled: 1.3°FLX 1.5°LAR | 1.6 Coupled 0.9°FLX 2.3°RAR | 0.7 Coupled: 2.4°EXT 1.4°RLB | 1.1 Coupled: 2.8°FLX 1.9°LLB | 1.9 Coupled: 6.3°FLX 1.7°LAR | 1.6 Coupled: 3.6°EXT 1.0°RAR | | | | | |
| Moroney (1988) C2-T1 | | | | | | | 5.5 Coupled: 1.5mm AS | 3.5 Coupled: 1.2mm PS | 4.7 Coupled: 1.5°RAR | 1.85 Coupled: 1.0°LLB | |
| Goel (1988) C3-C7 | | | | | | | | | 2.8 Coupled: 1.3RAR | | 2.15 Coupled: 1.6RLB |

*Panjabi: reported RoM at 50N with most significant coupled rotation .*
*Moroney: reported main rotations at 1.8Nm with most significant coupled motions.*
*Goel: RoM for rotations with significant coupled motions for load step of 0.3Nm*

## 2.4 The Soft-Tissue Components of the Cervical Spine

The vertebrae of the cervical spine are interconnected by a variety of biological structures that collectively are known as the soft tissues of the neck. At each vertebral level there is an intervertebral disc joining adjacent vertebral bodies. Ligaments bridge vertebral pairs connecting vertebral bodies and spinous processes while surrounding the articular facet joints to form the synovial capsules. A complex system of muscles surrounds the neck, spanning more than one vertebra and connecting the cervical spine to the skull and thorax. These soft tissues provide stability to the head and neck complex while allowing movements within physiological limits. They are also essential in protecting the spinal cord in case of trauma. The following sections detail the various soft tissues of the neck with respect to function and physical properties.

### 2.4.1 Intervertebral Discs

The intervertebral disc is a fibrocartilaginous joint between the endplates of two adjacent vertebral bodies. Intervertebral discs are found between each pair of vertebrae down the whole of the spinal column, there are no discs between the axis, atlas and occiput. A complex structure of layered collagen fibres make up the disc enclosing a nucleus, which is a fluid filled sac, called the nucleus pulposus. There are 8-12 layers to each disc arranged at approximately 30° to each other with the fibres in each layer lying roughly parallel. The outer surface contains more concentrated fibres to enable this area to withstand greater load. Figure 2.6 shows a typical inter-vertebral disc.

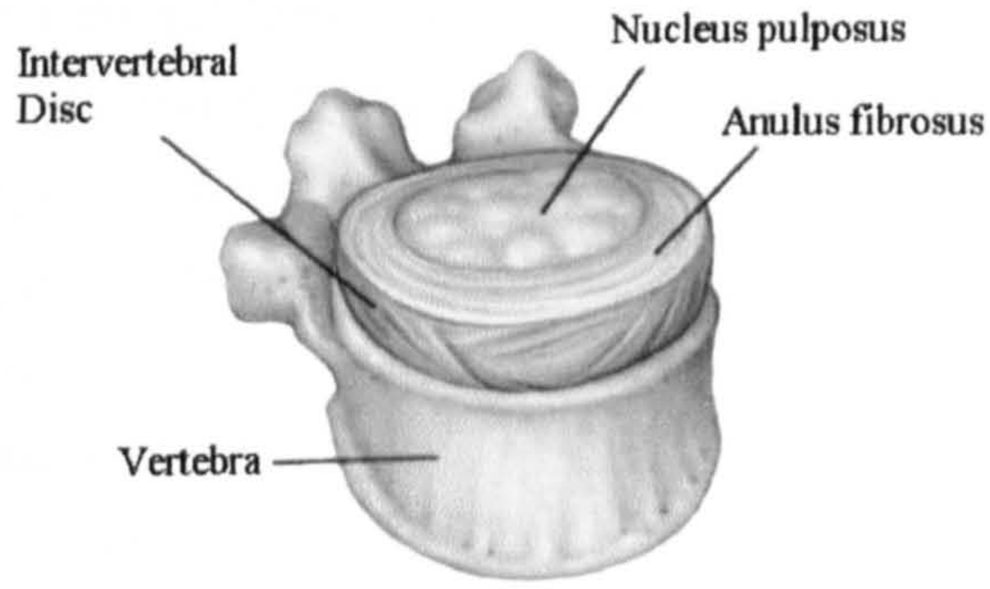


**FIGURE 2.6:** Vertebrae and intervertebral disc.

### 2.4.1.1 Function

The intervertebral discs play an important role in resisting a variety of forces and moments experienced by the spinal column. The discs resist load in all directions but together with the facet joints carry predominantly compressive loads under any external loading except for direct uniaxial tension. During everyday tasks the weight of the head places the cervical column and hence the C2-T1 discs in some degree of compression. Due to the eccentric placement of the head with respect to the neck the compression in the discs is also associated with moment. During traumatic load applications the intervertebral discs are able to resist and respond to a wide variety of load vectors including compression, bending and tension (Yoganandan et al., 2001).

### 2.4.1.2 Geometrical Characteristics

In order to model the intervertebral discs or to determine the relative position of the cervical vertebrae it is important to quantify the disc dimensions. Nissan and Gilad (1984) reported the anterior and posterior disc height in the sagittal plane for all the cervical discs measured from lateral x-rays of normal healthy men. Frobin et al. (2002) have also measured the sagittal plane discs dimensions of the cervical spine. If required, disc area can be approximated from the measurements of Panjabi et al. (1992) on the cervical vertebrae using the dimensions of the superior and inferior endplates of the vertebral bodies.

### 2.4.1.3 Mechanical Characteristics

Intervertebral disc responses are obtained by subjecting a body-disc-body segment to an external load. Disc stiffness has been reported by Pintar et al. (1986) and Yoganandan et al. (1996) in tension and by Yoganandan et al. (2001) in compression.

Pinter et al. (1986) measured force deflection curves for quasi-static direct axial tension at a rate of 1cm/s to failure. Stiffness is reported for each lower cervical disc and was measured as the slope of the most linear part of the force deflection curve. Yoganandan et al. (1996) appear to have reported averaged values of the same results obtained by Pintar et al. (1986) for spinal levels C2-

C3 down to C7-T1. Yoganandan et al [2001] report stiffness for intervertebral discs under compression for spinal levels C2-T1. Moroney et al. (1988) reports disc segment stiffness in all directions except in tension. Longitudinal ligaments and uncovertebral joints were left in place on the disc segments tested and also an axial preload was applied to represent the weight of the head and so may have increased the stiffness of the units. Table 2.11 summarises the reported cervical disc stiffness.

**TABLE 2.11:** Summary of reported intervertebral disc stiffness.

| | No.of speci-mens | Stiffness | | | | | | | | |
|---|---|---|---|---|---|---|---|---|---|---|
| | | TNS | CMP | AS | PS | RLS | FLX | EXT | RLB | RAR |
| | | N/mm | | | | | Nm/deg | | | |
| Pintar (1986) | | | | | | | | | | |
| C2-C3 | 5 | 63.5 | | | | | | | | |
| C3-C4 | 5 | 69.8 | | | | | | | | |
| C4-C5 | 3 | 66.8 | | | | | | | | |
| C5-C6 | 1 | 22.0 | | | | | | | | |
| C6-C7 | 2 | 69.0 | | | | | | | | |
| C7-T1 | 4 | 82.2 | | | | | | | | |
| Yoganandan(2001) | | | | | | | | | | |
| C2-C3 | | | 637.5 | | | | | | | |
| C3-C4 | | | 765.3 | | | | | | | |
| C4-C5 | | | 784.6 | | | | | | | |
| C5-C6 | | | 800.2 | | | | | | | |
| C6-C7 | | | 829.7 | | | | | | | |
| C7-T1 | | | 973.6 | | | | | | | |
| Moroney (1988) | | | | | | | | | | |
| Averaged C2-T1 | 28 | | 492 | 62 | 50 | 73 | 0.21 | 0.32 | 0.33 | 0.42 |

## 2.4.2 Uncovertebral Clefts

The uncovertebral clefts are located between adjacent vertebral bodies between the uncinate processes of the lower vertebra and the lower endplate of the upper vertebra extending to meet in the middle forming a transverse fissure along the back of the intervertebral disc. Previously these clefts have been described as joints (uncovertebral joints or joints of Luschka). However as stated by Yoganandan et al (2001) these clefts are not formed at birth, they arise in late childhood and become more evident with advancing age, and so do not constitute joints.

#### 2.4.2.1 Function

The uncovertebral clefts aid in allowing the large degree of movement that is possible between vertebrae and through the intervertebral disc. The clefts allow the disc to be able to accommodate the coupled motion of lateral bending and axial rotation that is produced through the interaction of the facet joints.

#### 2.4.2.2 Geometrical and Mechanical Properties

No specific data on the mechanical properties of the uncovertebral clefts could be found. However, as the clefts are an intrinsic part of the intervertebral disc, their mechanical influence on the behaviour of motion segments is already included in experiments that have characterised disc response. If the mechanical properties are to be lumped in with those of the disc the geometrical properties are not required. However, for finite element modelling, three-dimensional characteristics have been determined from a cadaveric specimen using cryomicrotomy (Kumaresan et al., 1997).

### 2.4.3 Ligaments

Ligaments differ from the other soft tissues of the cervical spine in that they require to be stretched before they will produce a force and they will buckle under compression (White and Panjabi, 1990). Some ligaments are capable of resisting tensile force in a range of directions due to their fibre arrangement and orientation. The anatomy of the upper cervical spine ligaments differ significantly to those of the lower cervical spine joints whose structure and position are similar at each level up to C2. More than one ligament spans each vertebral pair arranged in such a way that when a spinal motion segment is subjected to complex forces and moments the individual ligaments will develop tension in resistance to the external loading.

#### 2.4.3.1 Function

The main function of the ligaments is to provide stability to the spinal joints while allowing a range of physiological motion. They also provide some

degree of protection for the spinal cord in traumatic situations by restricting vertebral displacement and absorbing impact energy. Figure 2.7 shows the ligaments of the lower cervical spine, in this region the ligaments vary in size, orientation, and attachment points but are similar in structure.

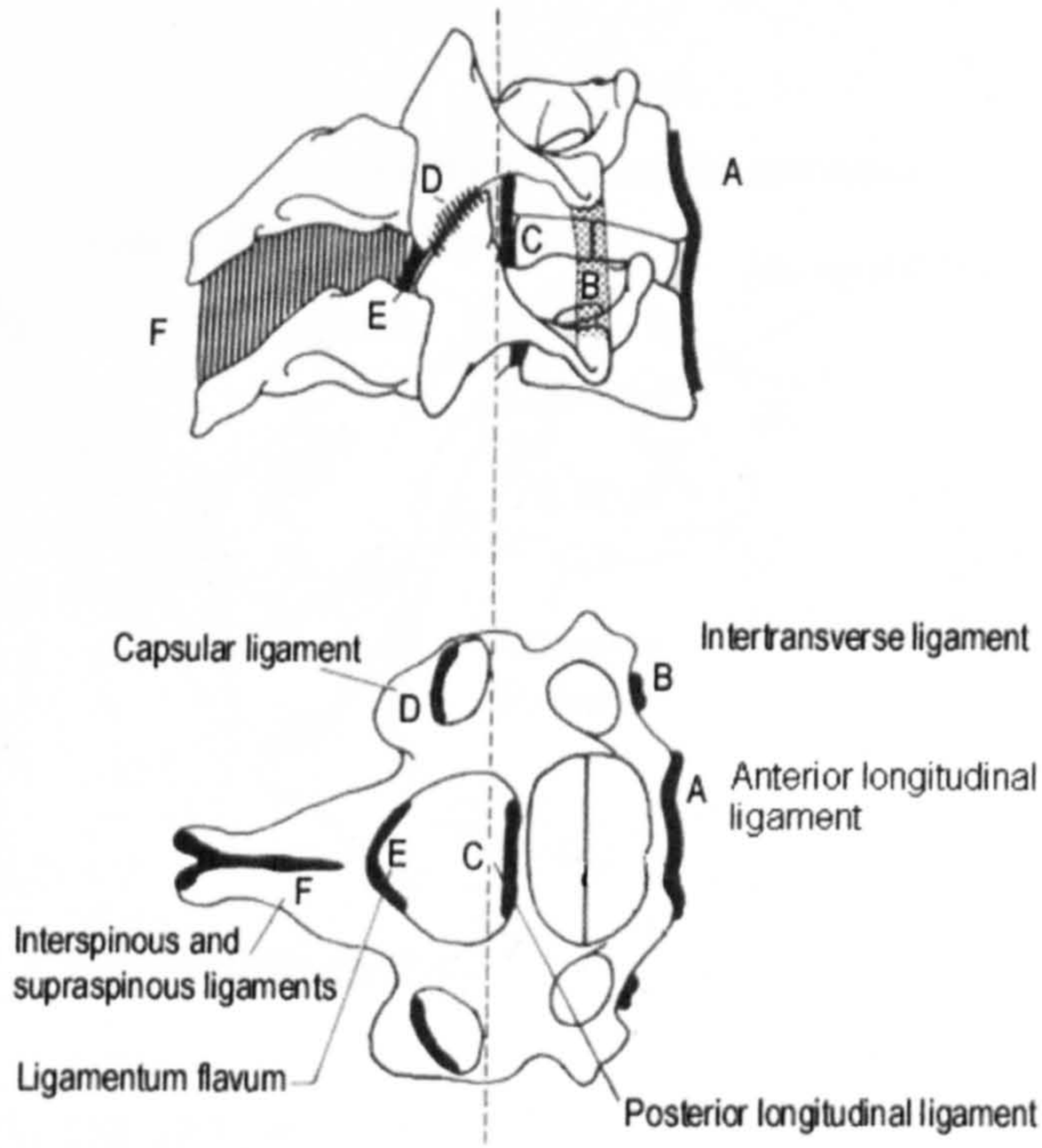


**FIGURE 2.7:** Lower cervical spine ligaments (adapted from White and Panjabi, 1990).

The anterior longitudinal ligament is attached to the anterior surfaces of all vertebrae starting at the basioccipital down to the sacrum including light fixation to the intervertebral discs. The anterior longitudinal ligament is most effective under an extension bending moment (Myklebust et al., 1988). The posterior longitudinal ligament runs down the posterior surface of all the vertebral bodies down to the coccyx. The capsular ligaments, enclosing the facet joints, are orientated perpendicular to the plane of the articular processes. The ligamenta flava connect the borders of adjacent laminae and represent the most pure elastic tissue in the human body (White and Panjabi, 1990). The interspinous ligament is a tough membrane between adjacent spinous processes and its attachments extend from the root to the apex of each process.

The nuchal ligament, runs from the occiput to C7 down the posterior edge of the spinous processes. All ligaments posterior to the anterior longitudinal ligament limit flexion of the cervical spine. Figure 2.8 shows a schematic of the major ligaments involved in the stability of the upper cervical spine.

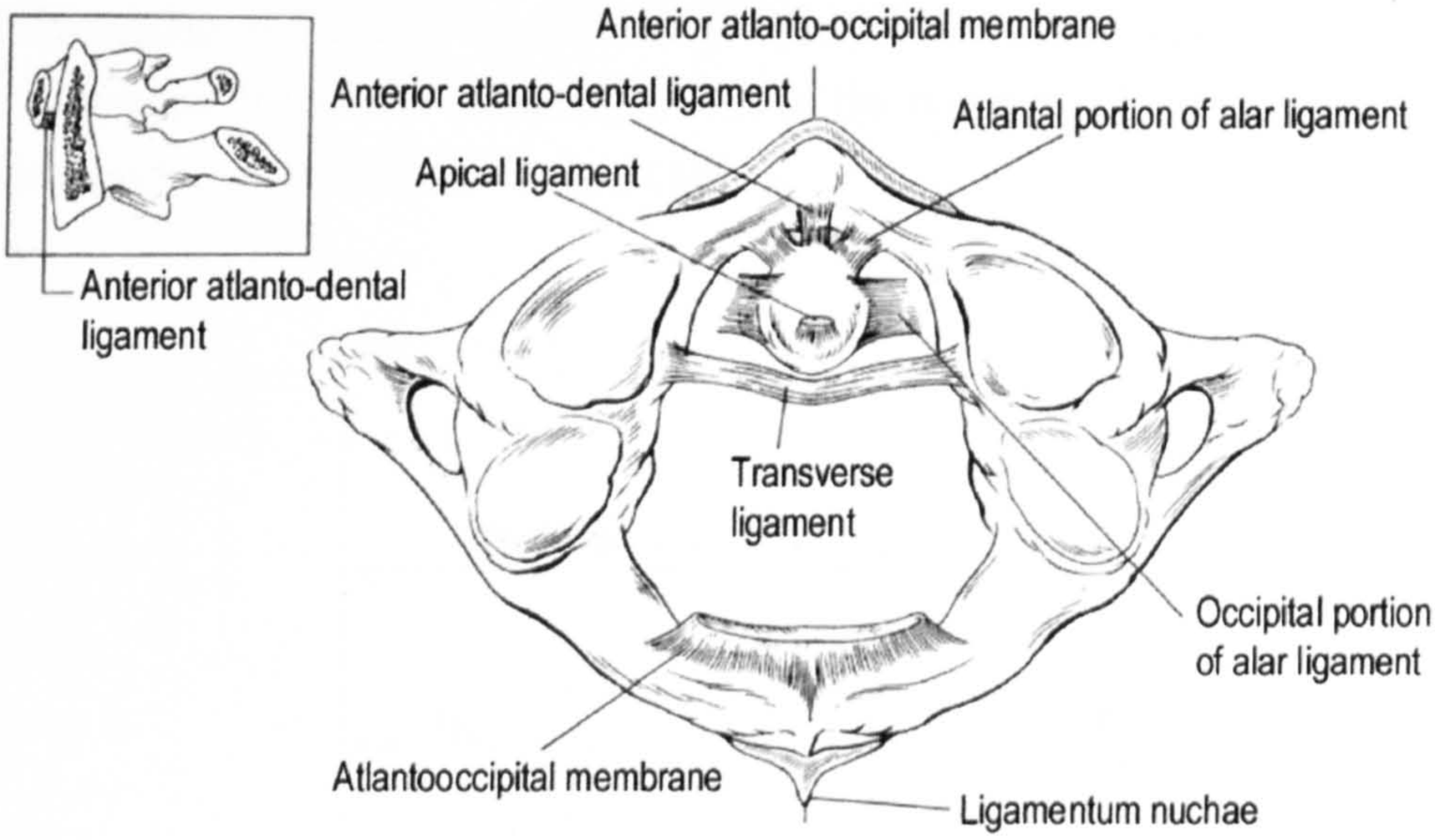


**FIGURE 2.8:** Upper cervical spine ligaments (Adapted from White and Panjabi, 1990).

The anterior and posterior occipito-atlantal and atlanto-axial membranes are continuations of the anterior longitudinal ligament and the ligamenta flava respectively. The atlanto-dens ligament runs between the dens and the anterior ring of C1 and the transverse ligament holds the dens against the anterior arch of the atlas. The dens is further held by the apical ligaments connecting to the occiput and by the alar ligament to each side of the occipital condyles and the atlas, thus limiting rotation of this region. The tectorial membrane is a continuation of the posterior longitudinal ligament joining the axis to the occiput. The posterior atlanto-occipital membrane connects the posterior ring of the atlas to the occiput.

### 2.4.3.2 Geometrical and Mechanical Characteristics

In order to accurately model the ligaments of the cervical spine, fundamental properties such as insertion points, length, cross sectional area, stiffness or elastic modulus, stress and strain, are generally required. Figure 2.9 shows a typical force-displacement curve of a ligament. Each ligament of the cervical spine can be characterised by its unique combination of stiffness, maximum deformation and failure load. Average failure loads along with corresponding deformation for all the major ligaments of the upper and lower cervical spine are reported in White and Panjabi (1990).

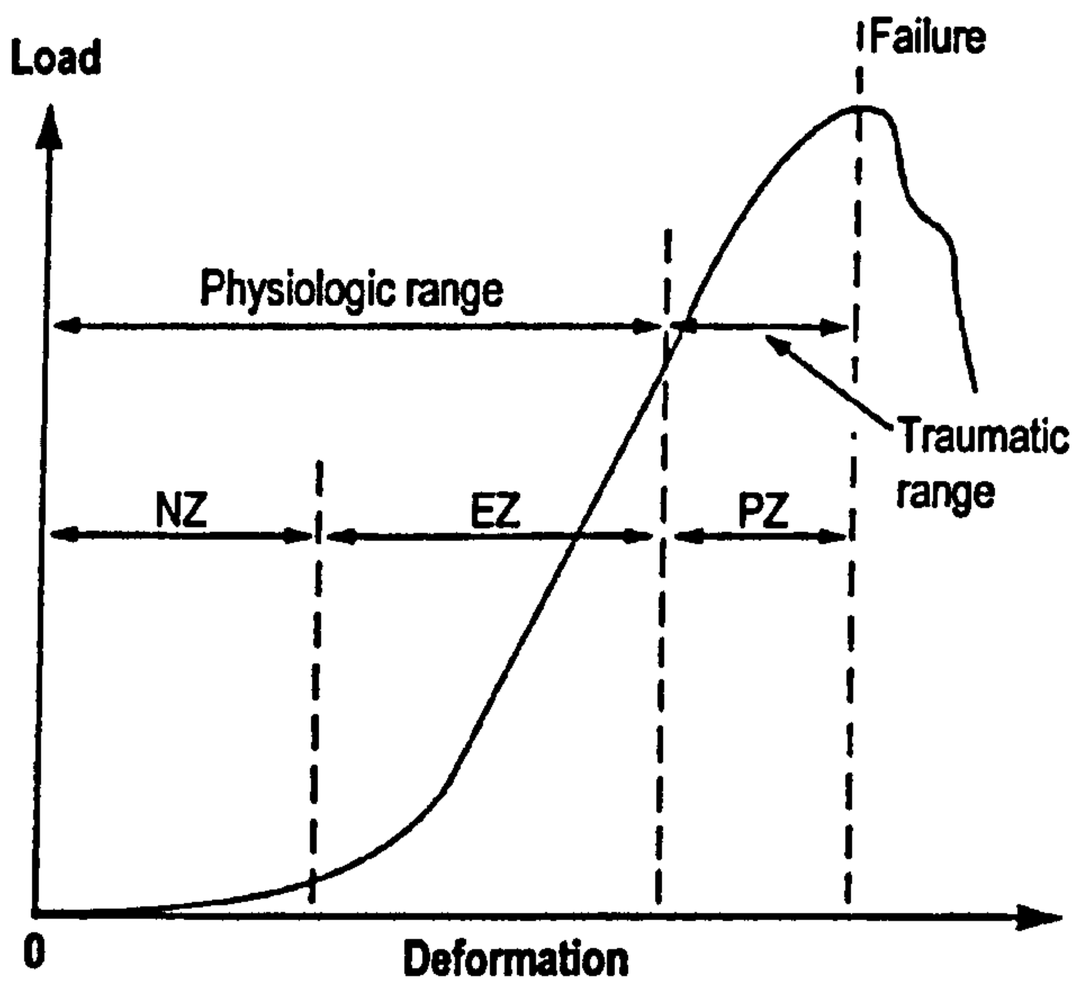


**FIGURE 2.9:** Typical load-deformation curve of a ligament. The physiologic range can be divided into the neutral zone (NZ), the part of the curve where little load results in deformation, and the elastic zone (EZ), where greater load is required to deform the ligament. The plastic zone (PZ) represents the traumatic range of the ligament were microtrauma is occurring until failure at maximum load (adapted from White and Panjabi, 1990).

Chazal et al. (1985) reported the load and deformation at the start and end of the elastic zone and at failure of one cervical anterior longitudinal ligament and three cervical posterior longitudinal ligaments in response to tensile loading at a rate of 1/60mm/s. For the anterior longitudinal ligament the failure force and displacement were 140N and 2.4mm respectively with elastic zone

stiffness calculated to be 71N/mm. For the three posterior longitudinal ligaments average force and displacement at failure were 185N and 2.4mm with elastic zone stiffness of 100N/mm.

Dvorak et al. (1988) documented the dimensions and tensile strengths of the alar and transverse ligaments of the upper cervical spine. Load was applied to bone-ligament-bone specimens of 11 alar (6 left, 5 right) and 7 transverse ligaments at a rate of 1.5mm/s. Average failure forces reported are 212N and 216N for left and right alar ligaments respectively, and 354N for the transverse ligament. Myklebust et al. (1988) reported the force and deformation at failure of all spinal ligaments at all levels. Each ligament was isolated by sectioning all other elements and loaded at a rate of 10mm/s.

Yoganandan et al. (1989) tested the dynamic response of the anterior longitudinal ligament and ligamentum flavum of the cervical spine at loading rates of 9, 25, 250 and 2500mm/s. The tensile strength and stiffness were both found to increase with loading rate for both ligaments whereas the deformation at failure varied little. Stiffness was calculated from the most linear part of the force-deformation curve.

Recently Yoganandan et al. (2000) have determined the geometrical and mechanical properties of the cervical spine ligaments. Cryomicrotomy images were used to determine the lengths and cross sectional areas of longitudinal ligaments, capsular ligaments, ligamentum flavum and interspinous ligament for the C2-T1 region of the cervical spine. The lengths of the ligaments were defined as follows: anterior and posterior longitudinal ligaments were taken from the mid vertebral body height of the lower vertebra to the mid height of its upper adjacent vertebral body (figure 2.10 ALL&PLL); the joint capsules were defined from the superior tip of the cephalad facet to the inferior tip of the caudal facet articulation (figure 2.10 JC); the ligamentum flavum and interspinous ligaments were defined from the superior points of attachments to their corresponding inferior points of attachments on the lower vertebra (figure 2.10 FL&ISL). Cross-sectional areas of the anterior, posterior longitudinal ligaments and the ligamentum flavum were taken approximately at the level of the mid height of the intervertebral discs. For the capsular ligaments the area was measured at the mid height of the joint capsule and for the interspinous ligament the cross-sectional area was measured mid way between adjacent

spinous processes. Average lengths and cross sectional areas with standard deviations are presented for the ligaments described in the region C2-C5 and C5-T1.

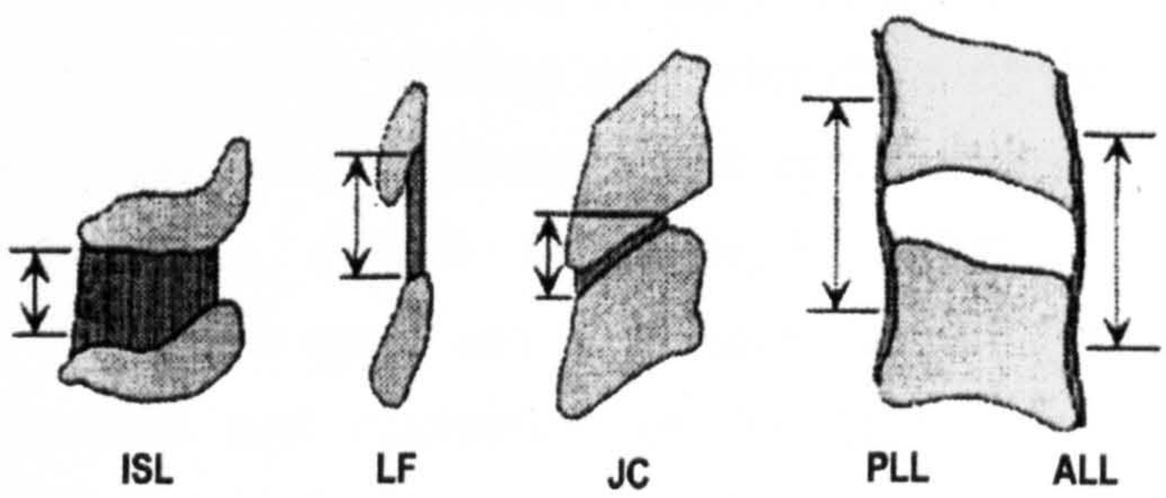


**FIGURE 2.10:** Schematic showing the length definitions for the various ligaments of the lower cervical spine (taken from Yoganandan et al., 2000).

Due to the destructive nature of the cryomicrotomy for determining the geometrical properties a new set of cadavers were used to determine the mechanical properties of the ligaments. Force-deflection curves, stiffness, stress, strain and energy data were determined using in-situ quasi-static (10mm/s) axial tensile tests. The data was grouped into middle, C2-C5, and lower, C5-T1 cervical spine categories.

## 2.4.4 Facet Joints

The articular processes of the lower cervical spine carry superior and inferior facet surfaces and are rigidly attached posteriorly to, and on either side of each vertebral body via the pedicles. The superior facet surfaces correspond to the inferior facet surfaces of the overlying vertebrae and are enclosed by the capsular ligament to form the facet joints. These articular joints are covered with a thin layer of hyaline cartilage and kept lubricated with synovial fluid allowing for an almost frictionless sliding motion between adjacent facet surfaces.

### 2.4.4.1 Function

Together with the intervertebral disc the facet joints resist compressive forces in the cervical spine. The amount of compressive load resisted at any cervical level is dependent on the orientation of the joint and the eccentricity of the external force. It is also the position and orientation of the facet joints that determines the pattern of movement of the cervical spine and hence their mechanical importance (White and Panjabi, 1990). The coupling characteristics of both the upper and lower cervical spine are governed by the size, shape, position and orientation of the facet joints and so a true representation of the joints in a mathematical or computational model is crucial to being able to reproduce accurate vertebral motion.

### 2.4.4.2 Geometrical Characteristics

A detailed study by Panjabi et al. (1993) on the articular facets of the entire spinal column has documented the three-dimensional geometry of the articular facets of the cervical vertebrae. The results were obtained from 12 cadaveric spine specimens both male and female with an average age of 46.3 years, weight of 67.8 kg and height 167.8cm. The dimensions presented were the facet surface height and width, the vertical distance between the superior and inferior facet surfaces and the lateral distance to the centre of each facet surface from the mid-sagittal plane. In addition the orientation of each facet surface is given in terms of two rotations about the X and Y-axis. It was assumed that the facet angles would be equal and opposite due to sagittal plane symmetry of the spine. Ebraheim et al. (1997a) have also reported the facet height, width and orientation based on measurements from 41 cervical spine specimens. The angulations of the facet surfaces were defined relative to the slope of the anterior surface of the vertebral body, but the dimensions of the vertebral bodies of the vertebrae measured are not given making reproduction of these facet angles difficult.

#### 2.4.4.3 Mechanical Characteristics

There appear to be no data in the literature for the mechanical properties of the facet joints of the cervical spine

Little deformation of the facet joints is expected in compression due to only a very thin layer of cartilage covering the stiff vertebral articular pillar. Frictionless contact between the facets can be assumed due to the lubricating properties of the synovial fluid filling the gap between them. Resistance to movement between the facets comes from the capsular ligaments, which resist tension and shear.

### 2.4.5 Muscles of the Head and Neck

Muscles of the neck form a multi-layered structure that can generate force and initiate movements of the head and cervical spine. Together with the mechanical forces provided by the bony anatomy, ligaments and intervertebral discs the muscles help to support the head and protect the neural elements. Muscles are able to generate force without relying on stretching because they contain contractile elements which allow them to provide the amount of force required dependent on neural activation. An inactivated or passive muscle has physical properties similar to those of other non-contractile soft tissues. Due to midsagittal symmetry, muscles appear twice, one on either side of the cervical spine. When contracted simultaneously or unilaterally they are able to flex, extend, bend, or rotate the spine. There is an immense number of muscle groups acting on the cervical region of the spine and it is therefore necessary to simplify these, group them, and consider only those that contribute most to the stability of the head and control of the neck.

#### 2.4.5.1 Identification of Functionally Relevant Muscle Groups:

The muscles of the neck can be divided into three groups: deep, intermediate and superficial. Deep muscles lie close to the cervical vertebrae spanning one or more spinal units with attachment points to the spinous and transverse processes. The intermediate muscles bridge the cervical vertebrae and the

thorax or link the skull with the spine. Finally the superficial muscles link the skull to the thoracic region.

- Deep muscles of the neck:

  Longissimus Cervicis
  Longus Colli
  Multifidus
  Obliquus Capitis Inferior
  Obliquus Capitis Superior
  Rectus Capitis Posterior Major
  Rectus Capitis Posterior Minor
  Semispinalis Cervicis
  Splenius Cervicis

- Intermediate muscles of the neck:

  Levator Scapulae
  Longissimus Capitis
  Longus Capitis
  Scalenus Anterior
  Scalenus Medius
  Scalenus Posterior
  Semispinalis Capitis
  Splenius Capitis

- Superficial muscles of the neck:

  Sternocleidomastoid
  Trapezius

The function of each of these muscle groups along with a detailed description of their attachment sites and morphometric properties is given in Chapter 4.

## 2.5 Inertial Characteristics of the Head and Neck

Inertial characteristics of the head-neck complex include mass, location of centre of gravity, and principle moments of inertia of the head, neck and vertebrae. The values assigned to the individual vertebrae should represent those of the complete neck at that level i.e. including all surrounding soft tissues.

Walker et al. (1973) report values of mass, volume, centre of mass, and mass moment of inertia for the head and for the head and neck determined from a sample of human cadavers.

Liu et al. (1971) determined the inertial properties of horizontal segments of a cadaver trunk. Cuts were made at the level of each intervertebral disc, determined from x-rays, and so each segment contained roughly one vertebra. The authors report that the cervical segments were poorly cut as they were the first cuts made and were generally uneven. Also the upper-cervical segments contained parts of the lower jaw as can be seen in figure 2.11, and the lower segments contained sections of the right shoulder. Due to these errors the results reported for the inertial characteristics of the cervical levels should be interpreted with care for use in a computer model.

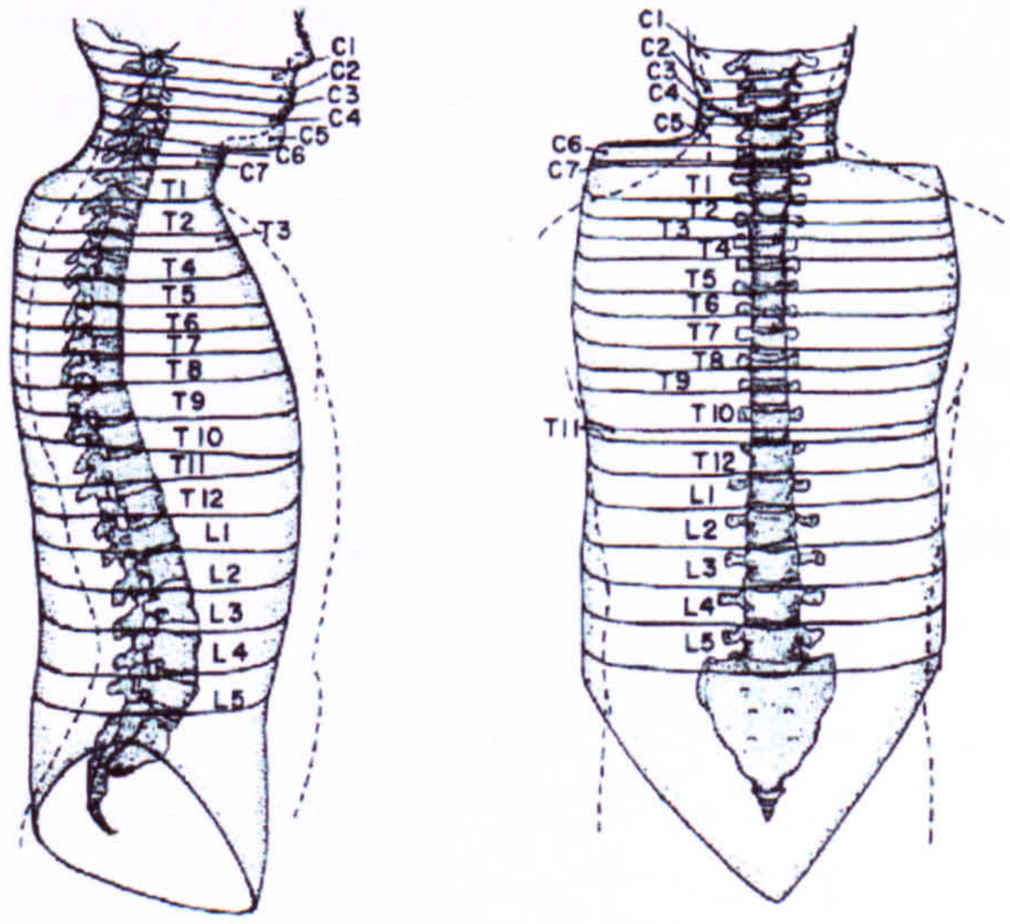


**FIGURE 2.11:** Side and front view of the cut positions used in determining the inertial properties, note how the upper-cervical levels contain sections of the jaw. (taken from Liu et al., 1971)

## 2.6 Mechanisms of Injury to the Cervical Spine and its Components

The mechanism of injury to the cervical spine during automobile impacts is of great significance in understanding head and neck trauma. Injury may occur as the result of direct impact to the head and neck or from the inertial loading of the head with respect to the torso. The injury mechanism is the process by which an external applied load leads to deformation of the neck and its soft tissues beyond their physiological limits resulting in permanent deformation or injury. To determine the biomechanics of injuries to the cervical spine it is necessary to determine how the external loads experienced during an automobile impact are transferred to the soft tissue components of the head and neck and how these local loads and deformations lead to injury. Mathematical models, finite-element models, physical models and experiments using animals, human volunteers or human cadavers have been used in continuing efforts to determine the mechanisms of injury during head-neck trauma. In experimental studies it is impracticable and often impossible to determine the local strains and stresses in the soft tissues However, a sufficiently detailed and accurate computational model may be able to predict them.

Computational modelling involves mathematically describing the cervical vertebrae and the forces exerted on them by the discs and surrounding ligaments and muscles with the objective being to faithfully reproduce the kinematic motions of the head and neck and to predict their response under abnormal loading conditions. Provided a high degree of biofidelity can be achieved the model can be used to predict the loads and deformations in the individual soft tissue components which can then be compared with the experimentally defined tissue failure characteristics to determine if injury has occurred.

### 2.6.1 Soft Tissue Failure Criteria

There have been many different hypotheses on the mechanisms responsible for injuries to the soft tissues of the cervical spine and although the suggested anatomical location and nature of the injury differs between studies they all

agree that injury occurs due to the movements between the cervical vertebrae resulting from the relative motion developed between the head and thorax during impact. The most common injuries caused by this relative motion between vertebrae are over-stretching of the soft tissues. It is therefore necessary to define the limits of these soft tissues.

**Intervertebral Discs:**

Due to the relative motions between vertebrae the intervertebral discs could in theory be damaged in any loading configuration if forced beyond physiological limits. Moroney et al. (1988) tested isolated vertebral body-disc- vertebral body segments to failure in flexion and extension under static loading conditions. 16 disc segments where tested in extension with a mean failure moment of 3.2Nm (1.8 SD), 8 segments were tested in flexion failing at 3.5Nm (1.4 SD). Only one disc segment was tested in right lateral bending, which failed at 8.2 Nm. Yoganandan et al. (2001) have presented failure forces for discs under quasi-static loading in tension and compression with mean values of 577N in tension and 718N in compression. Yamada (1970) reports static failure forces of 3139N in compression, 863N in tension and 5.0Nm in axial rotation. No data could be found for shear or dynamic failure loads of intervertebral discs.

**Ligaments:**

Injury to ligaments could occur when they are tensioned beyond their physiological limits. Myklebust et al. (1988) have reported the quasi-static failure forces for the ligaments of both the upper and lower cervical spine. Yoganandan et al. (2000) has also reported quasi-static failure forces for lower cervical spine ligaments. The results from these two studies are shown on table 2.12. No complete study of the dynamic properties of all the cervical spine ligaments is available. However Yoganandan et al. (1989) performed dynamic testing on cervical anterior longitudinal ligaments (ALL) and on the ligamentum flavum (LF). They found that the mean tensile strength of the ligaments increased by a factor of 2.7 when the loading rate of the ligament was increased from the quasi-static rate of 8.89 mm/sec to the dynamic 2500mm/sec.

**TABLE 2.12:** Quasi-static and dynamic failure forces of the upper (UCS) and lower (LCS) cervical spine ligaments.

| LCS Ligaments | Static Failure Force (N) | | Dynamic Failure Force (N) | UCS Ligaments | Static Failure Force (N) | Dynamic Failure Force (N) |
|---|---|---|---|---|---|---|
| | a | b | c | | a | c |
| ALL - | | | | AM – | | |
| C2-C5 | 100 | 90 | 257 | C0-C1 | 233 | 629 |
| C5-T1 | 120 | 155 | 371 | C1-C2 | 281 | 759 |
| PLL - | | | | PM - | | |
| C2-C5 | 71 | 88 | 215 | C0-C1 | 83 | 224 |
| C5-T1 | 94 | 181 | 371 | C1-C2 | 113 | 305 |
| CL - | | | | CL – | | |
| C2-C5 | 201 | 254 | 614 | C0-C1 | 315 | 851 |
| C5-T1 | 228 | 350 | 780 | C1-C2 | 315 | 851 |
| LF - | | | | APICAL | 214 | 578 |
| C2-C5 | 72 | 115 | 252 | ALAR | 357 | 964 |
| C5-T1 | 156 | 126 | 381 | TL | 354 | 956 |
| ISL - | | | | TM | 76 | 205 |
| C2-C5 | 32 | 38 | 95 | | | |
| C5-T1 | 36 | 39 | 101 | | | |

a. Myklebust et al. (1988)
b. Yoganandan et al. (2000)
c. Average static failure force times dynamic stiffening factor of 2.7.

## Facet Joints:

The cervical facet joints have been identified as possible areas of injury during automobile impacts, specifically in rear-end impact or 'whiplash' motion (Winkelstein, 1997, Winkelstein et al., 1997, 2000a, Siegmund et al., 2001). Biomechanical studies have demonstrated that the lower cervical facet joints are impacted during whiplash movement (Yoganandan et al., 1997, 1998b). Kaneoka et al. (1999), who studied human volunteers subjected to simulated rear end impacts, found that the relative motion between vertebrae caused the inferior articular facet to collide with the superior facet of the lower vertebrae causing impingement and inflammation of the synovial folds between the facet joints. Winkelstein and Myers (2000b) have studied the stresses and strains in the cervical facet capsule but failure forces for the joint have not yet been reported. Yamada (1970) has reported a compressive failure load of 3100N for cervical vertebrae, this figure could be used with caution as an estimate of the failure force for the bony articular facets but it is likely that damage to the softer cartilage covering would occur at lower loads.

**Muscles:**

Skeletal muscle can be injured under its own contraction and is likely to be damaged during a single lengthening contraction. Since a large proportion of the human neck is made up of skeletal muscle it is very likely that injury to these structures will occur during head and neck trauma. Brault et al. (2000) have established that muscle response is an integral part of an occupant's response to whiplash and that the potential for injury due to rapid lengthening contractions exist. It has been shown that as little as 5% elongation of maximally activated muscle can produce injury. Brault et al. (2000) observed increased muscle activation with increased vehicle speed change, suggesting the potential for muscle damage is proportional to impact severity.

Gurumoorthy and Twomey (2000) state that the sternocleidomastoid muscle is frequently injured due to sudden hyperextension of the neck with the tendinous insertion on the mastoid process being the primary source of pain. Hyperflexion is likely to injure the semispinalis capitis at origin and insertion and the upper sections of the trapezius and levator scapulae are also susceptible to injury in situations where the head is thrown forward. The deep multifidus muscle, which is thought to help control translatory movements in the facet joints, is vulnerable to injury during sudden forward flexion of the neck. Sudden acceleration of the head is most likely to affect the sub-occipital muscles i.e. the rectus capitis posterior major and minor and the obliquus capitis superior and inferior.

## 2.6 Discussion

In this chapter the anatomy of the complex human cervical spine has been discussed. The skull and 7 cervical vertebrae make up the bony anatomy of the head and neck. Articular facets, intervertebral discs and ligaments guide and constrain the cervical spine allowing movement between vertebrae and ultimately movement of the head relative to the torso. The complex musculature of the neck provides stability to the system and generates the intricate movements of the head.

The geometrical differences between vertebrae have been identified and it has been shown how these differences affect the overall kinematics of the cervical spine. Important coupling characteristics of both the upper and lower cervical spine have been discussed highlighting the importance of the cervical facet joints in depicting the complex motions of the neck. The in-vivo kinematic range of motion in all rotational directions is complete for all motion segments of the neck and this information can be used at a later stage for validation of a computational model.

The mechanical characteristics of complete motion segments and for the individual soft tissues have been identified. Numerous studies have tested isolated cadaveric motion segments to determine the load-displacement response in all loading directions. No data for the translational response of the upper cervical spine segments could be found. However little displacement in these directions has been seen in in-vivo studies of the occipital-atlanto-axial joints. Static properties of cervical intervertebral discs have been determined for all loading directions and it should be noted that these properties include the contribution of the uncovertebral clefts as they are an integral part of the disc. The facet joints can be assumed to be very stiff in compression with almost frictionless contact between facet surfaces, resistance to load of the facet capsule in other directions than compression comes from the surrounding capsular ligaments. Static properties of the cervical spine ligaments are complete with load-deformation characteristics defined. Generally dynamic data for the response of the soft tissues and motion segments as a whole are lacking in the literature.

19 functionally important muscle groups have been identified with further information on their morphometry and attachment points being detailed in Chapter 4.

Investigators have used a variety of means in an effort to determine the biomechanics of injuries that might occur during an automobile impact. Physical, animal and human experiments have given insight into the mechanisms of injury however no well-established neck injury criteria exist. Information on the failure characteristics of the various soft tissues of the neck has been presented. Failure loads for the ligaments have been established and for the disc in most loading directions. Although the stresses and strains have been studied in the facet joints no failure forces have been reported.

A successfully validated computational model of the head and neck with sufficient detail to be able to describe the local loads and deformations of the soft tissues should be able to predict injury and give insight into the injury mechanism during cervical spine impact trauma. The geometrical, mechanical and inertial properties of the cervical spine and its components described in this chapter can be utilized in the construction of a computational model of the human head and neck. The following chapter reviews previous attempts at mathematically modelling the cervical spine.

CHAPTER 3

# Computational Models of the Human Head and Neck – A review of the literature

If a computational model of the human head and neck is to be used for injury analysis the mechanical behaviour of the cervical spine and its components must be represented in detail. A successful model must be able to reproduce the normal kinematics of the cervical spine and predict its behaviour when subjected to abnormal loads.

There are four main types of head-neck models found in the literature and of these multi body/discrete parameter models and finite element models appear most suitable for the representation of the complex anatomical structure and mechanical behaviour of the cervical spine. The others, continuum and two pivot models, can only represent the spine in a much-simplified form. Continuum rod models represented the whole spine as a curved homogeneous beam-column reducing the geometrical complexity and had strongly simplified mechanical behaviour. Two-pivot models have been shown to be capable of describing the global motion of the head and neck relative to the torso but cannot describe the local kinematics between vertebrae.

The following section reviews existing spine models and outlines the progress of cervical spine modelling to date. First a brief overview of continuum rod and 2-pivot models is presented followed by a review of multi-body and finite elements models of the head and cervical spine.

## 3.1 Continuum and 2-Pivot Models

Early models of the human spine mainly attempted to investigate the overall behaviour of the spine. Due to the complexity of the human spine as a whole these models were limited and, due to lack of experimental data and computational power, were difficult to validate.

Cramer et al. (1976) produced a one dimensional continuous rod model that represented the whole spine as a curved homogeneous beam-column with infinite degrees of freedom. It reduced the geometric complexity of the model concentrating on dynamic situations such as those associated with pilot ejection. A 10g acceleration applied to the pelvis was used to simulate the ejection motion and also the weight of the trunk was applied as a distributed force over the entire length of the spine. The data for the model was obtained from cadaver specimens. The results of the model showed the position of the spine at various time intervals and the axial force, shear force and bending moments for the impact situation. The model predictions are said to agree well with pilot ejection injury data, although viscoelastic properties of the spine and external constraints were omitted.

It has been shown that a simple 3-body model of the head and neck can accurately simulate the sagittal plane motion of the head relative to the torso in automobile collisions. These two-pivot models consist of 3 rigid bodies, the head, neck and torso, the neck link representing the lumped properties of the 7 cervical vertebrae. Torso motion obtained from sled experiments on human volunteers or cadavers is used as an input to the model to predict head motion which can then be used to validate the model against the measured experimental head motion. Tien and Huston (1987) showed that their relatively simple two-pivot model successfully simulated the gross motion of the head and neck just as accurately as a more detailed 9-body model developed by Huston et al. (1976). The 3-body model has just 18 degrees of freedom as opposed to the 54 for the 9-body model. Springs and dampers between the rigid bodies were used to simulate the combined properties of the soft tissues, disks, ligaments and muscles. The model was validated against sled experiment results obtained by Ewing et al. (1977) and the authors conclude that the 3-body model is capable of efficiently predicting the global

head/neck dynamics of accidents but is not able to describe the mechanics of the neck in detail and is therefore of no use for injury analysis.

Further two-pivot models have been developed and validated, Bosio and Bowman (1986) used Naval Biodynamics Laboratory (NBDL) data to simulate, using a 3-link model, the dynamic head response to frontal and lateral acceleration impacts. A slightly altered neck link location gave improved model biofidelity for the g-levels simulated but the authors state that the optimal lower pivot point location varies for different g-level loadings.

Wismans et al. (1986,1987) presented a simple two-pivot analogue system for analysis of omni-directional head-neck response. The model was validated for frontal, lateral and oblique impacts again using NBDL data on human volunteer experiments, and then later (1987) using data from post-mortem human subject (PMHS) experiments. It was concluded that the two-pivot linkage model is capable of quite accurately simulating the relative head-neck motions of both human volunteers and PMHSs. Thunnissen et al. (1995) extended this work correcting previous errors in T1 rotations, and developed a new head-neck linkage mechanism. An extensible neck link was used instead of the constant length link used earlier and the lower pivot was now located in the T1 anatomical origin (figure 3.1). A set of performance requirements have been presented that can be used for validation of mechanical and mathematical models for frontal impact situations.

From these findings it has been shown that two-pivot models are indeed capable of simulating the general global head behaviour for various impact directions of varying severity. However, a single two-pivot model suited for all impact directions and impact levels has not been obtained to date.

## 3.2 Multibody Models

Multibody or discrete parameter models allow for a more detailed representation of the spine, in which rigid bodies with corresponding mass and inertial properties applied idealise the head and vertebrae. Mass-less spring and damper elements connected between adjacent rigid bodies represent the lumped characteristics of the intervertebral discs and surrounding soft tissues, such as ligaments, facet joints and sometimes muscles. Geometric detail is kept simple with many components and parameters being lumped together resulting in high computational efficiency and making validation of these models more straight forward. Multibody models are suitable to describe the global and local behaviour of the head-neck complex in detail.

An early two-dimensional discrete parameter model by Orne and Liu (1971) was the first to allow for shear and bending moments as well as compression. It included viscoelastic properties of the disks and effects of rotational inertia on the vertebrae. The model was limited by lack of data but contributed to the explanation of the occurrence of anterior lip fractures in the vertebrae experienced by pilots ejecting from high performance aircraft.

Early three-dimensional discrete parameter models of the spine were limited by the lack of experimental data. Panjabi (1972) developed a general method for producing a discrete parameter model and for determining the governing equations using the human spine as one possible application. Rigid bodies represent bony elements of the spine, namely the head and vertebrae, while connecting tissues are represented by connections of springs and dampers. Belytschko et al. (1972) describes a similar method as Panjabi for producing a discrete parameter model of the human spine. Used here were rigid bodies to represent the bony elements of the spine with deformable elements representing the intervertebral discs and connective tissues. Seven spring elements with axial stiffness between each vertebral pair were used to simulate ligaments and other soft tissues. The intervertebral disc element joining the end plates of each vertebral pair possessed stiffness in flexion/extension, lateral bending and axial rotation, shear and torsion.

Belytschko et al. (1976) produced a detailed three-dimensional model of the entire spine again to investigate the pilot ejection situation. The head, vertebrae, pelvis and ribcage were represented as rigid bodies as shown in figure 3.1. Beam elements represented the inter-vertebral disks, spring elements represented spinal ligaments and hydrodynamic elements governed by fluid-Pressure laws were used to represent the articular facets of the spine.

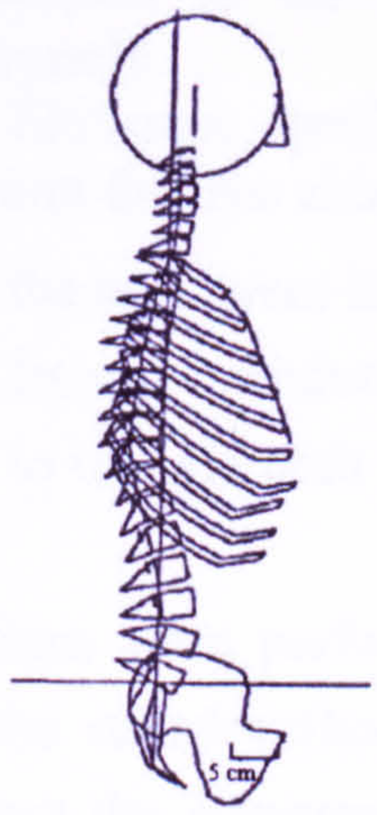


**Figure 3.1:** Lateral view of Belytscho et al's complex model showing just the rigid bodies.

The ejection system model included the pilot's chair represented by a vertical and horizontal plane surface and a constraint system consisting of three springs connecting T1, T2 and T3 with the seat back and a single spring connecting to the pelvis. Effects of a helmet were simulated assuming the helmet moved with the head and then changing the mass and eccentricity of the head. The model simulated vertical ejection situations of varying force and the model predictions show a history of axial force and flexion moment of the spine and head.

Williams and Belytschko (1983) developed a three-dimensional model of the head and neck The vertebrae C1-C7 are modelled as rigid bodies interconnected by deformable elements representing the intervertebral disks, facet joints, ligaments and muscles. They speculate that spring models of the facet constraint do not correctly model both lateral and frontal plane motions. The facets in the cervical spine act to stabilise the spine as the intervertebral

disks have a very low stiffness. Hence a new facet element that allows the model to simulate both lateral and frontal plane motions and prevents unrealistic displacements between adjacent vertebrae was developed.

The model consisted of four different types of deformable elements

1. Spring Elements; with stiffness along the axis joining the two elements they connect.
2. Beam Elements; with axial bending and torsional stiffness.
3. Muscle Elements; similar to spring elements but with the axial force being independent to the neck elongation to mimic the contraction of the muscle.
4. Pentahedral Facet Elements; special element developed to model the articular facet joint that has axial and shear stiffness.

Twenty-two muscle groups of the neck were included with the force from each muscle group being estimated from the product of its stress and cross-sectional area. The model was the first to include both passive and active properties of muscles.

Simulations for impact situations were performed with and without muscle activity to see the effects of the stretch-reflex response during impact. They showed that with frontal impact the compression, shear forces and bending moments in the disk were reduced with muscle activity but under lateral loading the stretch-reflex response increased compressive and shear force in the disk. This difference in response under lateral and frontal impact emphasises the importance of modelling the head and neck in three-dimensions for impact studies.

**Table 3.1:** Model details for Merrill, Goldsmith and Deng (1984)

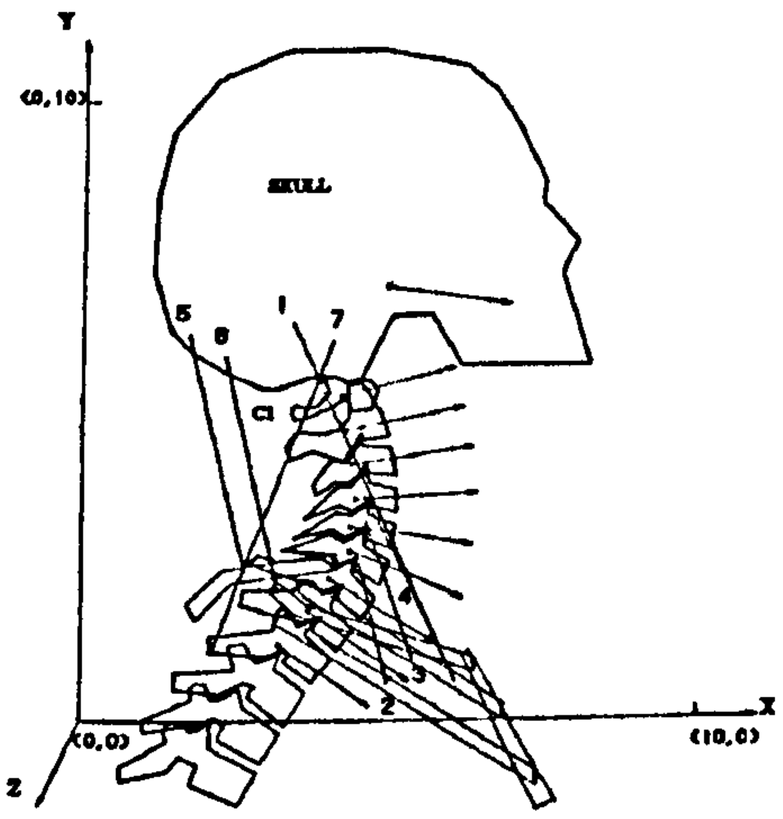


| | |
|---|---|
| **AUTHOR:** | Merill, Goldsmith & Deng (1984) |
| **SOFTWARE:** | UNKNOWN |
| **HEAD:** | Rigid |
| **VERTEBRAE:** | Rigid |
| **OCCIPIUT-ATLAS-AXIS:** | C1-C2 2D ball and socket joint |
| **DISCS:** | Lumped into intervertebral joint |
| **LIGAMENTS:** | Lumped into intervertebral joint |
| **FACET JOINTS:** | Frictionless ball on plane |
| **MUSCLES:** | 7 passive linear elements |
| **VALIDATION:** | Volunteer and physical model tests |
| **APPLICATION:** | 2D flexion whiplash, 3D lateral impact |

An interesting series of studies charting the development of a three-dimensional multi-body model of the head and neck has shown that discrete parameter models are capable of describing global motions of the head and neck and also the local kinematics of the individual vertebrae. The two-dimensional lumped parameter model developed by Reber and Goldsmith (1979) was extended to three dimensions by Merril et al. (1984), shown in table 3.1. The model was further improved by Deng and Goldsmith (1987). The resulting model consisted of head, neck and upper torso (C1 down to T2) with fifteen pairs of passive neck muscles. The mechanical behaviour of each individual spinal unit was lumped into a single intervertebral joint with a linear stiffness matrix characterising the segmental response. Following the work of Deng and Goldsmith, de Jager (1996) implemented their model in the multibody software package Madymo developing a sophisticated model of the head and cervical spine. The new model consisted of head, neck (C1-C7) and the first thoracic vertebrae (T1). Intervertebral discs, facets joints, and various cervical ligaments were included in the model along with 14 pairs of the cervical spines most significant muscle groups capable of simulating both passive and active muscle behaviour. A summary of the model can be seen in table 3.2.

Recently van der Horst (1997, 2002) has made further improvements to the de Jager model by increasing the geometric detail of the vertebrae, updating the material properties of the soft tissues and modelling the neck muscles in greater detail. The 3D shape of the vertebrae and skull were constructed from anatomic slices through a 78 year old post mortem human subject that had been seated and frozen in an automobile seat before been sliced into 5mm sections. The initial configuration of the vertebrae was adjusted similar to that used by de Jager to represent a head-neck complex of an average young human. The mass, moments of inertia and positions of centre of gravities of the rigid bodies are as used by de Jager. The representation of the intervertebral discs is the same as that of de Jager but with improved material properties for flexion, extension and compression; which now have nonlinear characteristics based on more recent literature. Facet joints are modelled as three-dimensional non-linear springs, with stiffness in compression only, allowing minimal deformation of the facet joints. New in this model is the

inclusion of contact between spinous processes, which has been modelled in the same way as facet joint contact. Ligaments in the model are represented by 2D non-linear viscoelastic spring-damper elements producing force in tension only. 16 cervical muscle groups sub-divided into 68 muscle elements are modelled with improved geometry and lines of action curving around the cervical vertebrae. The Hill type muscle model, as used by De Jager and available in the Madymo software package is used to describe active and passive muscle behaviour.

**Table 3.2:** Model details for De Jager (1996)

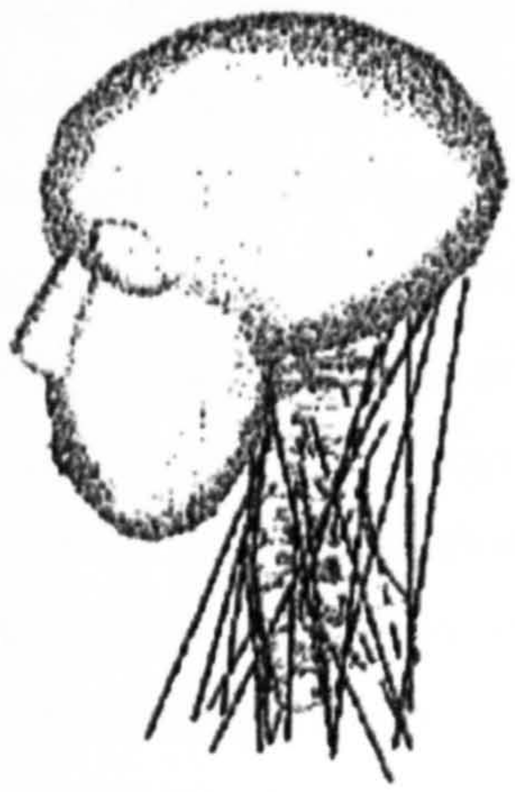

| | |
|---|---|
| **AUTHOR:** | De Jager (1996) |
| **SOFTWARE:** | MADYMO |
| **HEAD:** | Rigid |
| **VERTEBRAE:** | Rigid |
| **OCCIPIUT-ATLAS-AXIS:** | Hyper-ellipsoid frictionless contact |
| **DISCS:** | Linear viscoelastic Kelvin elements |
| **LIGAMENTS:** | Non-linear viscoleastic |
| **FACET JOINTS:** | Hyper-ellipsoid frictionless contact |
| **MUSCLES:** | 14 Hill type muscle elements (active and passive) |
| **VALIDATION:** | 15g frontal impact, 7g lateral impact (NBDL volunteer data*) |
| **APPLICATION:** | Frontal and lateral impacts |

## 3.3 Finite Element Models

Finite element models are able to model the spine in its entirety, each anatomical component is now broken down into a large number of deformable elements with respective biological properties defined. The model can be used to study the internal stresses sustained and the response of the soft tissues and structures to an applied load. In principle a finite element model is capable of simulating any type of geometry, material behaviour, loading and boundary condition data. However in reality finite element methods are limited by computational power and complex validation requirements. Although there are a greater number of FE models available in the literature compared to multi-body models the differences in detail are small. The bony geometry of the models varies widely between studies but the material properties are mostly

based on the same literature. None of the current FE models available have included active muscle behaviour; those that have modelled the muscles of the neck have only looked at passive properties.

There have been several finite element models reported in the literature but to date only a few have been developed to study the effects of whiplash on the whole cervical spine. Kleinberger (1993) developed a three-dimensional model of the head –neck complex (C0-T1) to study the mechanics of cervical injuries related to automobile crashes. The model consists of all cervical vertebrae, intervertebral discs, and biomechanically relevant ligaments. A summary of the model can be seen in table 3.3. Numerous assumptions and simplifications were employed in the model. Vertebrae were modelled as rigid, linear elastic material properties were used for the intervertebral discs, facet joints and ligaments and no muscular structure was included. Facet angles were kept at a constant 45° for all levels of the cervical spine with the atlanto-occipital joint represented by a simplified pin joint, allowing rotation in the y-axis only. Ligamentous attachments between the cervical spine and the skull were also omitted. Despite these simplifications the model did show reasonable results in terms of response to axial compression and frontal flexion demonstrating the potential of finite element methods for investigating head-neck response to impact.

**Table 3.3:** Model details for Kleinberger (1993)

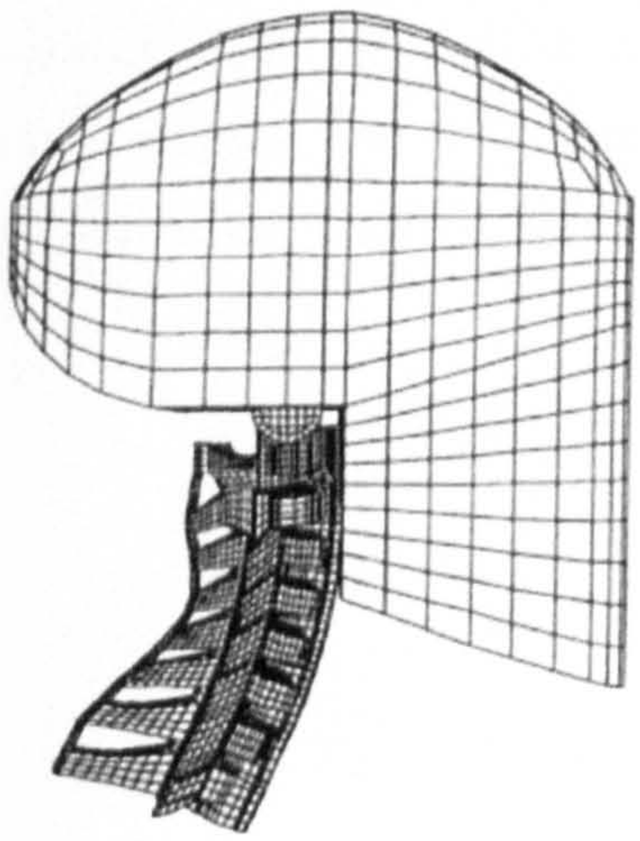

| | |
|---|---|
| **AUTHOR:** | Kleinberger (1993) |
| **SOFTWARE:** | LS-Dyna |
| **HEAD:** | Rigid |
| **VERTEBRAE:** | Rigid |
| **OCCIPIUT-ATLAS-AXIS:** | Pivot joint for C0-C1 allowing FLX/Ext only. |
| **DISCS:** | Linear Elastic |
| **LIGAMENTS:** | Linear Elastic |
| **FACET JOINTS:** | Linear Elastic |
| **MUSCLES:** | Absent |
| **VALIDATION:** | Axial Compression, McElhaney et al. (1983), Yoganandan et al. (1989) |
| **APPLICATION:** | Axial Compression, 8g frontal impact |

Dauvilliers et al. (1994) constructed a finite element model of the cervical spine based on cadaver x-rays. To keep the number of solid elements at a minimum only the major geometrical features of the vertebrae were defined. These included vertebral body, spinous processes and articular facets. The positions and orientations of the facet surfaces were based on measurements reported in the literature. The vertebrae and head were modelled as rigid bodies. Intervertebral discs were represented by solid elements along with spring-dampers for the disc fibres. All major ligaments of the lower neck are included and represented by spring-damper elements. The link between the atlas, axis, and head were represented by spherical joints and therefore no odontoid process or occipital condyles were included. Contact between articular surfaces was simulated by contact interfaces between shell elements. No muscles were included in the model although the stiffness of the posterior and lateral ligaments at all levels was increased to account for the passive stiffening effect of muscles. A brief summary of the model is shown is table 3.4. Initially material properties reported in the literature were used which were at this time scarce and incomplete. The model elements material properties were then calibrated to produce a response similar to that of NBDL volunteers for frontal and lateral impact. A reasonable response was achieved for frontal impact simulation but the vertical displacement of the head failed to meet the response corridors by a significant degree. The authors suggest this might be due to failing to prescribe the rotation of T1 during the loading phase. Satisfactory agreement was seen between the model response and the volunteer data for lateral impacts but acceleration spikes are present that greatly exceed the volunteer corridors; this is likely due to insufficient damping of the model's elements.

**Table 3.4:** Model details for Dauvilliers (1994)

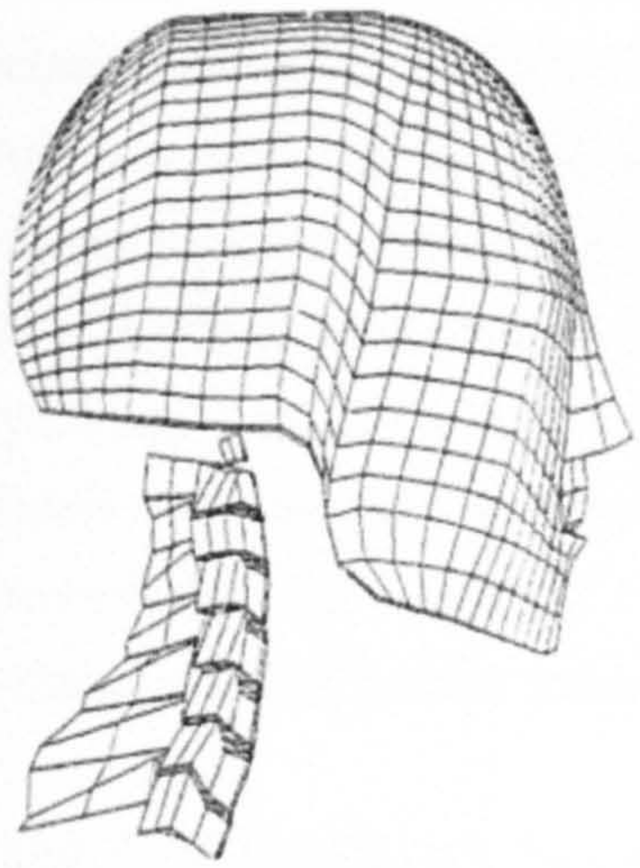

| | |
|---|---|
| **AUTHOR:** | Dauvilliers (1994) |
| **SOFTWARE:** | RADIOSS |
| **HEAD:** | Rigid |
| **VERTEBRAE:** | Rigid |
| **OCCIPIUT-ATLAS-AXIS:** | C0-C1Flx/Ext only, C1-C2 AR only. |
| **DISCS:** | Linear elastic: 8 solid elements, 32 crossed spring-damper elements |
| **LIGAMENTS:** | Linear viscoelastic spring-damper elements |
| **FACET JOINTS:** | Frictionless contact between shell elements. |
| **MUSCLES:** | Absent |
| **VALIDATION:** | 15g frontal impact, 7g lateral impact (NBDL volunteer data*) |
| **APPLICATION:** | Frontal and Lateral impact acceleration |

Camacho et al. (1997) developed a head neck model to study the dynamic response of the head and cervical spine to near vertex head impact. Geometric and inertial characteristics were derived from three-dimensional reconstructions of skull and vertebral CT scans from the Visible Human Data Set. Detailed FE meshes of the cervical vertebrae were constructed to calculate mass, centre of gravity and moments of inertia, which were then applied to less detailed rigid body representations of the vertebrae in the final model. A deformable finite element head consisting of skull and maxillofacial structures was constructed to enable accurate transmission of loads from the contact surface through to the cervical spine. Flexion-extension flexibility measurements were taken on human head and cervical spine preparations to define model parameters. The mechanical properties of the soft tissues were lumped into a single intervertebral joint between each pair of adjacent vertebrae. The head-neck model was used to reproduce the buckling kinematics of cadaveric specimens in near-vertex head impacts. It was shown that the computational spine model accurately portrayed the buckling behaviour of the spine specimens in terms of resultant head and neck forces with time and resultant head acceleration. A visual comparison is also presented showing the model and specimens over a series of time steps throughout the impact. Camacho's model has been extended by Van Ee et al.

(2000) to include neck musculature and revised tensile properties of the intervertebral joints (table 3.5). Muscles were modelled as non-linear spring elements with lines of action defined from origin to insertion. 24 muscle pairs were modelled; muscles with broad areas of attachment were divided into sub-volumes each represented by a discrete non-linear spring. Muscle force was estimated from the physiologic cross-sectional area of the muscle, initial muscle length and change in muscle origin to insertion length, no activation dynamics were simulated. The new version of the model was validated against tensile loading tests on ligamentous cervical spine specimens. The results showed that the inclusion of muscular forces increased the tolerance of the cervical spine to tensile loading by a factor of 2.3.

**Table 3.5:** Model details for Camacho (1997) / Van Ee (2000)

| | |
|---|---|
| **AUTHOR:** | Camacho (1997) / Van Ee (2000) |
| **SOFTWARE:** | LS-DYNA |
| **HEAD:** | Elastic |
| **VERTEBRAE:** | Rigid |
| **OCCIPIUT-ATLAS-AXIS:** | Lumped into intervertebral joint |
| **DISCS:** | Lumped into intervertebral joint; non-linear springs and linear dampers (sagittal plane motion only). |
| **LIGAMENTS:** | Lumped into intervertebral joint |
| **FACET JOINTS:** | Lumped into intervertebral joint |
| **MUSCLES:** | Non-linear spring elements (passive). |
| **VALIDATION:** | Head and neck drop test, Nightingale et al. (1997). |
| **APPLICATION:** | Axial impact at 3.2m/s |

Halidin et al. (2000) produced a detailed finite element model of the isolated head and neck complex again to investigate the effect of axial impacts. The vertebral geometry for the model was constructed from CT scans of a 27-year-old male then scaled to represent a $50^{th}$-percentile male. Facet joint contact as well as contact between spinous processes were included and thought important due to the nature of loading the model was designed to simulate. Muscles were not included in the model due to the theory that they have little importance in compression impacts. All elements of the intervertebral disc were modelled consisting of nucleus pulposus, annulus fibrosus and ground

substance. Linear springs were used to represent the ligaments of the neck. The transverse ligament was modelled as a membrane element to enable contact definitions with the dens. The stiffness of the ligaments of the upper cervical segments (C0-C3) were optimised to allow the upper joints to meet the range of motions reported by Panjabi et al. (1988). A detailed FE model of the head was included in the model to allow accurate transfer of loads to the neck during near vertex head impact simulation. A summary of the model can be seen in table 3.6. Motion segment validation was done for compression, shear and rotational loading on the C4-C5 segment compared against experimental data. The model agreed well with the results of Nightingale et al. (1996, 1997) for axial impact loading in terms of resultant neck and head forces. Following validation the model was used to assess automobile roof designs designed to prevent injuries to the head and neck during head impacts.

**Table 3.6:** Model details for Halidin (2000)

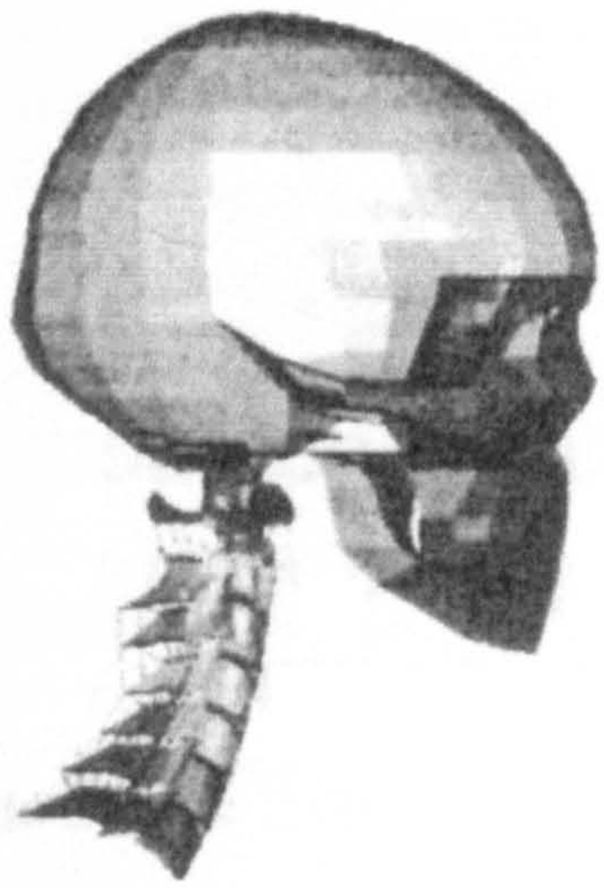

| | |
|---|---|
| **AUTHOR:** | Halidin (2000) |
| **SOFTWARE:** | DYNA 3D/ LS-DYNA |
| **HEAD:** | Hyperviscoelastic |
| **VERTEBRAE:** | Linear Elastic |
| **OCCIPIUT-ATLAS-AXIS:** | Sliding contact with friction |
| **DISCS:** | Linear Elastic |
| **LIGAMENTS:** | Linear Elastic |
| **FACET JOINTS:** | Sliding contact with friction |
| **MUSCLES:** | Absent |
| **VALIDATION:** | C4-C5 segment loading. C0-C3 segment loading. Head and neck drop test, Nightingale et al. (1996,1997). |
| **APPLICATION:** | Analysis of roof design. |

Yang et al.(1998) developed a detailed FE model of the cervical spine in an effort to study the mechanics of the head and neck when subjected to acceleration impacts. MRI scans of a 50$^{th}$ percentile male volunteer were used to construct the geometry of the cervical vertebrae, C1-C7 and the first thoracic vertebra, T1. A summary of the model can be seen in table 3.7. The vertebrae were constructed using 8-node brick elements with linear elastic-plastic material properties. The curvature of the constructed neck was adjusted to give a cervical lordosis of 34° with a height (superior end of C1 to inferior

end of C7) of 120 mm. Intervertebral discs were modelled using linear viscoelastic materials with the nucleus pulposus and annulus fibrosus represented by solid elements. Non-linear tension-only membrane and bar elements were used to represent the ligaments of the neck with their geometry based on anatomic descriptions and the modelled bony geometry of the vertebrae as a reference for attachment points. Sixty tension-only spring elements were used to represent the cervical muscles with origin and insertions based on those described by Deng and Goldsmith (1987). Only the passive properties of the muscle were considered in the model simulations. A previously developed FE head model was utilized to complete the model of the head and neck.

The model was validated with reasonable success against the head and neck drop tests performed at Duke University as also used by Camacho et al. (1997). To further validate the model a rear end impact was simulated and compared to results from 24 km/hr cadaveric sled tests. Model validation was only carried out on the global response of the head and neck; no validation of the local kinematics of the vertebrae or loads in the soft tissues was presented. Following validation the head and neck model was used together with a previously developed model of the upper torso and used to simulate head and neck interaction with a pre-deployed air bag. The model was used to study head and neck kinematics, load histories and ligament forces.

**Table 3.7:** Model details for Yang (1998)

| | |
|---|---|
| **AUTHOR:** | Yang (1998) |
| **SOFTWARE:** | PAM-CRASH |
| **HEAD:** | Rigid or Elastic |
| **VERTEBRAE:** | Elastic |
| **OCCIPIUT-ATLAS-AXIS:** | Frictionless contact. |
| **DISCS:** | Linear viscoelastic |
| **LIGAMENTS:** | Non-linear tension-only membrane and bar elements |
| **FACET JOINTS:** | Frictionless contact. |
| **MUSCLES:** | Sixty tension only spring elements (Passive) |
| **VALIDATION:** | Head and neck drop test, Winkelstein et al. (1996) and Nightingale et al.(1997). 8g rear-end impact |
| **APPLICATION:** | Axial impact at 3.2m/s. Interactions with pre-deployed airbag |

Nitsche et al. (1996) developed a FE model of the human spine (C1-C7) consisting of deformable vertebral bones, intervertebral discs, facets, and ligaments (table 3.8). The geometric construction is approximated from the literature. All material properties in the model are linear elastic, the intervertebral discs are isotropic and the cartilages and ligaments anisotropic. The model is validated against NBDL data for frontal and lateral impacts as used by De Jager (1996). The model shows reasonable agreement with the volunteer data. No cervical muscles were included in the original model but Wittek et al. (2000) have added muscles to Nitsche's model to study their effect in low speed rear-end impacts. The model was modified further by representing the intervertebral discs as visco-elastic elements with an incompressible nucleus and by improving the anatomical representation of the articular facets and their orientation. Contact was defined between facet surfaces and between spinous processes and the force-tension properties of the longitudinal and flava ligaments were redefined as non-linear. The cervical muscles were modelled as Hill Type muscle elements, their geometry and attachment points being based on the literature. The curving of long muscles around vertebrae was modelled by sub-dividing each muscle in three series connected muscle elements. The model was validated using volunteer data for angular displacements of the head, its resultant accelerations and for the relative angles of the vertebrae from C2-C6 for low speed rear-end impacts. Expected and unexpected impacts were simulated by varying the muscle response time to study the effects of muscle tension on the kinematics of the head-neck complex. For the case of unexpected impact the model agrees very closely with the experimental results. However, when the impacts were anticipated the model predicts too low head accelerations compared to those experienced by volunteers. This is thought to be due to the level of muscle activation being the same for all muscles belonging to each functional group, flexors or extensors.

**Table 3.8:** Model details for Nitsche (1996)

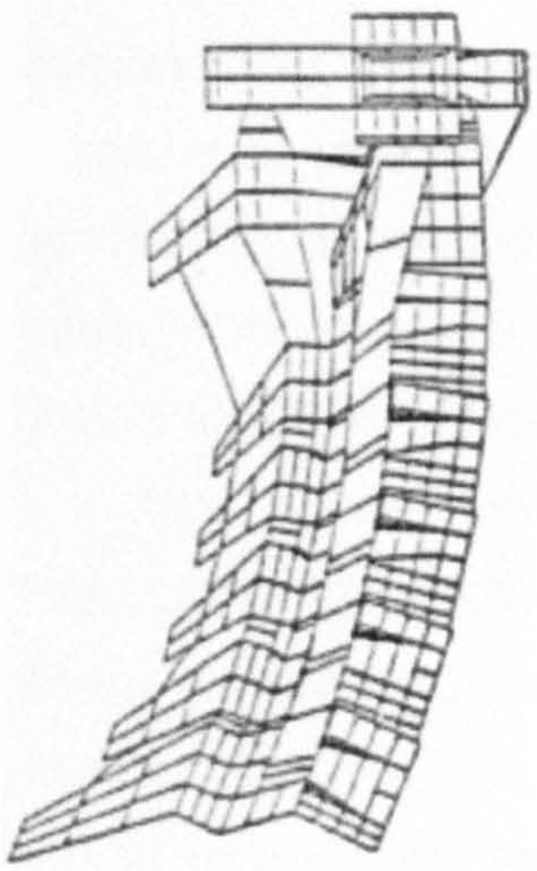

| | |
|---|---|
| **AUTHOR:** | Nitsche (1996) |
| **SOFTWARE:** | PAM-CRASH |
| **HEAD:** | No head modelled |
| **VERTEBRAE:** | Elastic |
| **OCCIPIUT-ATLAS-AXIS:** | No C0-C1 joint. C1-C2 frictionless facets. |
| **DISCS:** | Elastic |
| **LIGAMENTS:** | Linear anisotropic |
| **FACET JOINTS:** | Frictionless contact. |
| **MUSCLES:** | Absent |
| **VALIDATION:** | 15g frontal impact, 7g lateral impact (NBDL volunteer data*). Compression loading, Pintar et al.(1989), Pintar et al. (1995) |
| **APPLICATION:** | Frontal and Lateral impact acceleration. Compression loading |

* Wismans et al. (1986), Wismans et al. (1987), Thunnissen et al. (1995)

A recent paper by Gentle et al. (2001) outlines the development of a finite element model of the head and cervical spine to study whiplash injuries. The topological information for the skull and vertebrae was extracted from pictures obtained by the Visible Human Project (1994) for the male data set. The topology was simplified to keep the overall computational time down but detailed contact surfaces were defined to give realistic motion characteristic. All bony structures have been modelled as rigid bodies. All biomechanically relevant soft tissues are incorporated into the model, including intervertebral discs, facet joints and a wide range of cervical ligaments and muscles. Alar and transverse ligaments are modelled as three-dimensional structures using solid elements; the remaining ligaments were represented by non-linear discrete tension-only elements. A mixture of non-linear spring elements and shell elements has been used to simulate the ligamentum flavum and the nuchal ligament. Nine muscles of the neck are modelled as non-linear springs with attachment points based on anatomical description. The intervertebral disc is modelled as a single component with Blatz-Ko rubber material properties defined, proven to give realistic deformation response to bending load cases (the main load associated with the disc during rear end impact). No active muscle response is defined due to the short simulation period studied,

being less than human reaction time. A summary of the model can be seen in table 3.9.

Volunteer experiments have been used to validate the model for rear end impact using the original acceleration history as an input to the torso. A head restraint is included in the simulation based on the Mercedes W124 head restraint with material properties of Blatz-Ko foam. Good agreement can be seen between model and volunteer response for relative head rotation and acceleration. However, further validation of the model response in terms of vertebral rotation, neck length, neck rotation, occipital condyles and head CG trajectories appears to be lacking. The model has then been used to predict the forces developed in all the relevant neck ligaments resulting from twice the impact speed of the volunteer experiments used in model validation. The model successfully reproduces the characteristic 'S' shaped curvature of the neck seen in rear impact experiments.

**Table 3.9:** Model details for Gentle (2001)

| | |
|---|---|
| **AUTHOR:** | Gentle (2001) |
| **SOFTWARE:** | LS-DYNA |
| **HEAD:** | Rigid |
| **VERTEBRAE:** | Rigid |
| **OCCIPIUT-ATLAS-AXIS:** | Occipital condyles omitted. |
| **DISCS:** | Elastic |
| **LIGAMENTS:** | Non-linear springs. |
| **FACET JOINTS:** | Frictionless contact between shell elements. |
| **MUSCLES:** | 9 non-linear springs (passive). |
| **VALIDATION:** | 10.5km/h rear-end impact, Geigl et al. (1994) |
| **APPLICATION:** | 21km/h rear-end impact with head restraint. |

## 3.4 Discussion

A relatively large number of computational models of the human head and neck have been developed over the last 30 years with each generation having greater anatomical detail as modelling techniques have improved and computers have advanced.

Early models were two-pivot lumped parameter models where the mechanical behaviour of the neck is represented by a single neck link with neck-torso and neck-head pivots. These simple two-pivot models have been used for analysis of head-neck global kinematics in volunteer and cadaver experiments. Multibody models are an extension of these simple lumped parameter models with a greater amount of detail. Rigid bodies are used to represent the head and cervical vertebrae interconnected with massless spring and damper elements to represent the disc, ligaments and muscles. Finally finite-element modelling allows the complete reconstruction of the bones, joints, ligaments, discs and muscles of the cervical spine in terms of one-, two- or three-dimensional geometric elements. Each element is then given its respective material properties so the internal stresses and strains can be calculated and the response of the various structures and tissues can be studied when subjected to external loads. A brief review and summary of the most important of these head-neck models has been presented in this chapter.

Although in theory finite element models are able to represent the cervical spine and its soft tissues in their entirety and the development of this type of model has clearly dominated in the last 10 years, the level of detail actually included is not significantly greater than that seen in the multibody model of De Jager. The geometries of the models are mostly based on different data, obtained from a specific subject then scaled to represent a $50^{th}$ percentile male while the mechanical characteristics and validation of both finite element and multibody models are mostly based on the same experimental data. For most models large simplifications and assumptions have been made to allow for more efficient simulations or to fill in missing material properties. The soft tissue properties have been lumped into single intervertebral joints (Camacho,

1997, van Ee, 2000), the representation of the upper cervical joints has been by simple pin joints (Kleinberger, 1993, Dauvilliers, 1994) and very few models have included muscle properties and studied the effects of muscle activation. Another major disadvantage of detailed finite-element models is the exceptionally large run times they require, for example the head-neck model of Halidin et al. (2000) took around 45hrs for a 25ms simulation, compared against de Jagers model that could run a 200ms simulation in just under 20 minutes. For evaluation of new safety systems, where small improvements and modifications are to be made based on simulation results, short, reliable run times are advantageous if not essential.

All models are limited by the available material properties and as more experiments are completed on the response of the soft tissues of the cervical spine they are readily used to define more detail in head-neck models and to validate their response. One area where material properties are lacking is the intervertebral discs, dynamic response of which are still largely uncharacterised, with most modellers choosing linear properties based on quasi-static experimental data. Although complex finite-element representations of the intervertebral discs have been included in some head-neck models it is believed, due to the lacking material properties, that they offer no greater accuracy then the simple six-degree of freedom spring damper arrangement used by de Jager.

Models are continually been developed for specific loading purposes and no single model is yet suitable for all applications. Validation of models has been in the form of segment loading, axial compression tests and frontal, lateral and rear-end impact. Most of the models are validated in terms of the global response of the head and neck with respect to the torso and all types of model have been shown to be successful at reproducing this motion. Validation of the local kinematics of the individual vertebrae is less common. For the purpose of injury prediction it is important that a model be able to predict local tissue deformations and loads and validation of these loads is critical.

It was decided that the multibody approach to modelling the head-neck be used for this study based on the reasons highlighted above with the view of improving on the model developed by de Jager in terms of geometrical detail of the vertebrae, representation of the facet joints and improved material

properties of the soft tissues with the main area of improvement being in the detail of the cervical muscles. It is believed that sufficient detail can be achieved for predicting the head-neck response to impacts, with accurate local kinematics and the ability to predict tissue loads and deformations while keeping runs times to a minimum. The development of this new multibody model of the head and cervical spine is described in full in the following chapter.

# CHAPTER 4

# Development of a Computational Model of the Human Head and Neck

The following chapter presents the three-dimensional multibody model of the human head and cervical spine developed to simulate the dynamic behaviour of the head and neck to acceleration impacts. Detailed representations of the cervical vertebrae and surrounding soft tissues are described along with the complex array of muscles of the neck.

## Software

The three-dimensional geometry of the vertebrae and skull were defined using Solid-Edge, version 9, CAD software from EDS (Electronic Data Systems Corporation). The body geometries were then imported into, and the model constructed, using rigid-body dynamics package visualNastran 4D 2001 R2, version 6.4, from MSC Software. VisualNastran uses numerical methods to allow the solution of the motion of mechanical systems, which are governed by differential equations arising from mechanics principles. The Kutta-Merson integration method with variable time-step is used to calculate bodies' positions and velocities. VisualNastran also provides an extensive analytical toolset for easy evaluation of designs and models.

## 4.1 Rigid Head and Vertebrae

Nine rigid bodies represent the head (C0), the seven cervical vertebrae (C1-C7) of the neck and the first thoracic vertebrae (T1). T1 serves as the base of the head-neck model and is located at the origin of the world coordinate system. The local coordinate system of T1 is aligned with the world coordinate system with the x-axis pointing forward, the y-axis to the left and the z-axis pointing upward. Figure 4.1 shows the basic configuration of the rigid bodies of the model from the occiput to T1. Figure 4.2 shows the model of the skull. The base of the skull, or occiput, is shown in both figures together with the occipital condyles showing how it is positioned with respect to the neck in figure 4.1 and how it forms part of the skull, figure 4.2. The configuration of the upper and lower cervical spine models were developed separately due to distinct anatomical differences before being brought together to form the complete head-neck model.

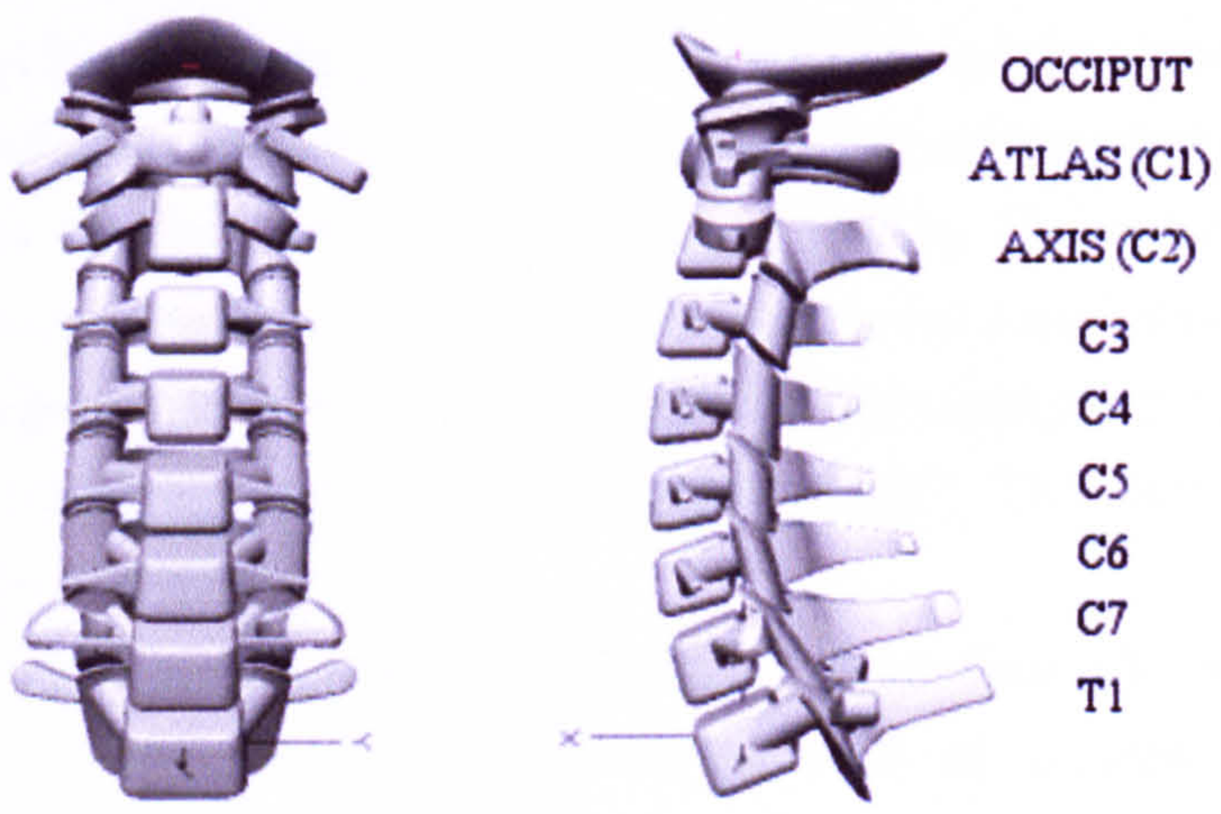


**Figure 4.1**: Frontal and left lateral view of the configuration of the rigid bodies representing the cervical vertebrae and base of the skull (occiput) of the multibody neck model.

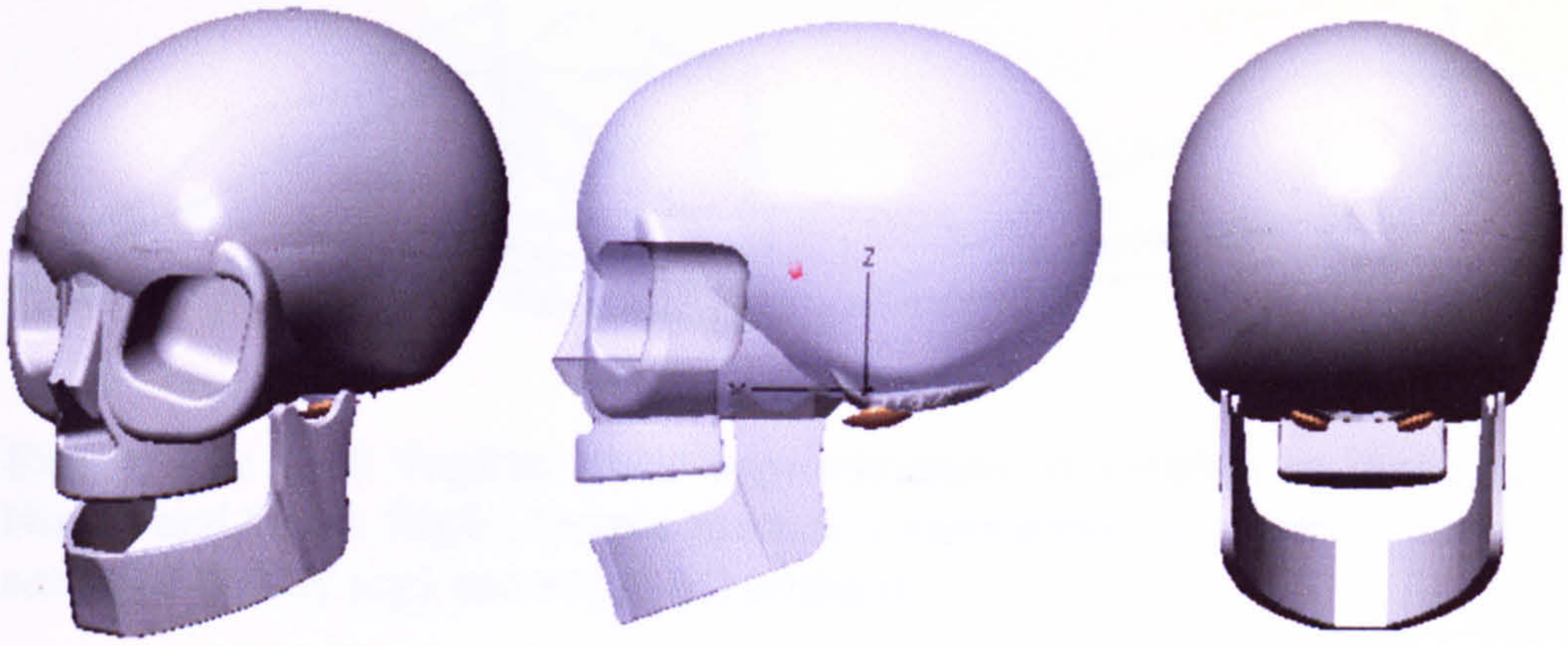


**Figure 4.2:** Three-dimensional representation of the human skull and occiput, occipital condyles are shown in orange. Centre image shows the position of the local coordinate system and the centre of gravity of the head (red).

## 4.1.1 Configuration of the Lower Cervical Spine.

The initial configuration of the vertebrae (C2-T1) was based on a number of studies quantifying the three-dimensional anatomy of the cervical spine as well as on decisions made by other researchers. The mid-sagittal configuration of C2-C7 was derived from Nissan and Gilad (1984). The vertebral body and transverse process widths, pedicle angles, and spinal canal dimensions were based on Panjabi et al. (1992) and the position and orientation of the articular facets for C2-T1 were derived from Panjabi (1993). The dimensions of T1 were taken from Panjabi (1991).

Nissan and Gilad used lateral radiograms of more than 130 erect standing volunteers to determine mid-sagittal dimensions of cervical and lumbar vertebrae and intervertebral discs. The vertebral body is approximated by a quadrangle with corners at the four extremes of the body's outline; a fifth point represents the most dorsal aspect of the spinous process (figure 4.3). The heights of the intervertebral discs were measured between the superior corners of the lower vertebrae and the inferior corners of the superior adjacent vertebrae.

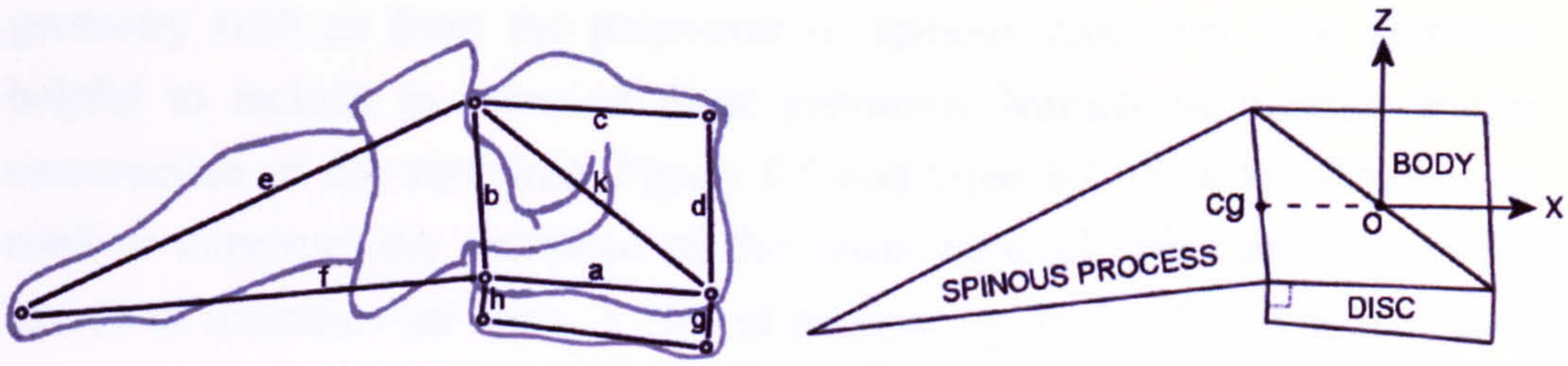


**Figure 4.3:** Left: Sagittal plane approximation of vertebra as presented by Nissan and Gilad. Right: Simple geometric representation of vertebra showing centre of gravity (cg) and origin (o) position.

The following assumptions as described by de Jager (1996) were employed in the construction of the model:

- The posterior height *h* of the intervertebral disk was measured perpendicular to the inferior edge *a* of the upper vertebral body.
- The geometric centre of each vertebra lies at the centre of the diagonal *k* connecting opposite corners of the vertebral body.
- The origin of the local coordinate system of each vertebra was positioned at the geometric centre of the body thus having the x-axis parallel to the lower end plate *a*.
- The centre of gravity of each vertebra lies on the posterior side *d* of the body in line with the body's geometric centre along the x-axis.

The above assumptions allow for the positions and orientations of vertebrae C2-C7 to be determined for the initial position of the model. Figure 4.4 shows the mid-sagittal configuration of C2-C7. The mid-sagittal dimensions of T1 were derived from the C7-T1 disc dimensions reported by Nissan and Gilad and from quantitative three-dimensional data presented by Panjabi et al. (1991c). The origin and local coordinate system of T1 is positioned at (0,0,0) of the world coordinate system for the model. The position and orientation of each of the vertebrae are described relative to T1.

Attachment points of ligaments and muscles on to the cervical vertebrae are described in the literature with respect to anatomical landmarks of the bony

geometry such as from the transverse or spinous processes. It is therefore helpful to include as many of these geometric features as possible in the construction of the vertebrae. Figure 4.5 and table 4.1 show the dimensions used to construct the vertebrae of the lower cervical spine along with the source of reference for each. A typical motion segment (C5-C6) of the lower cervical spine model is shown in figure 4.6.

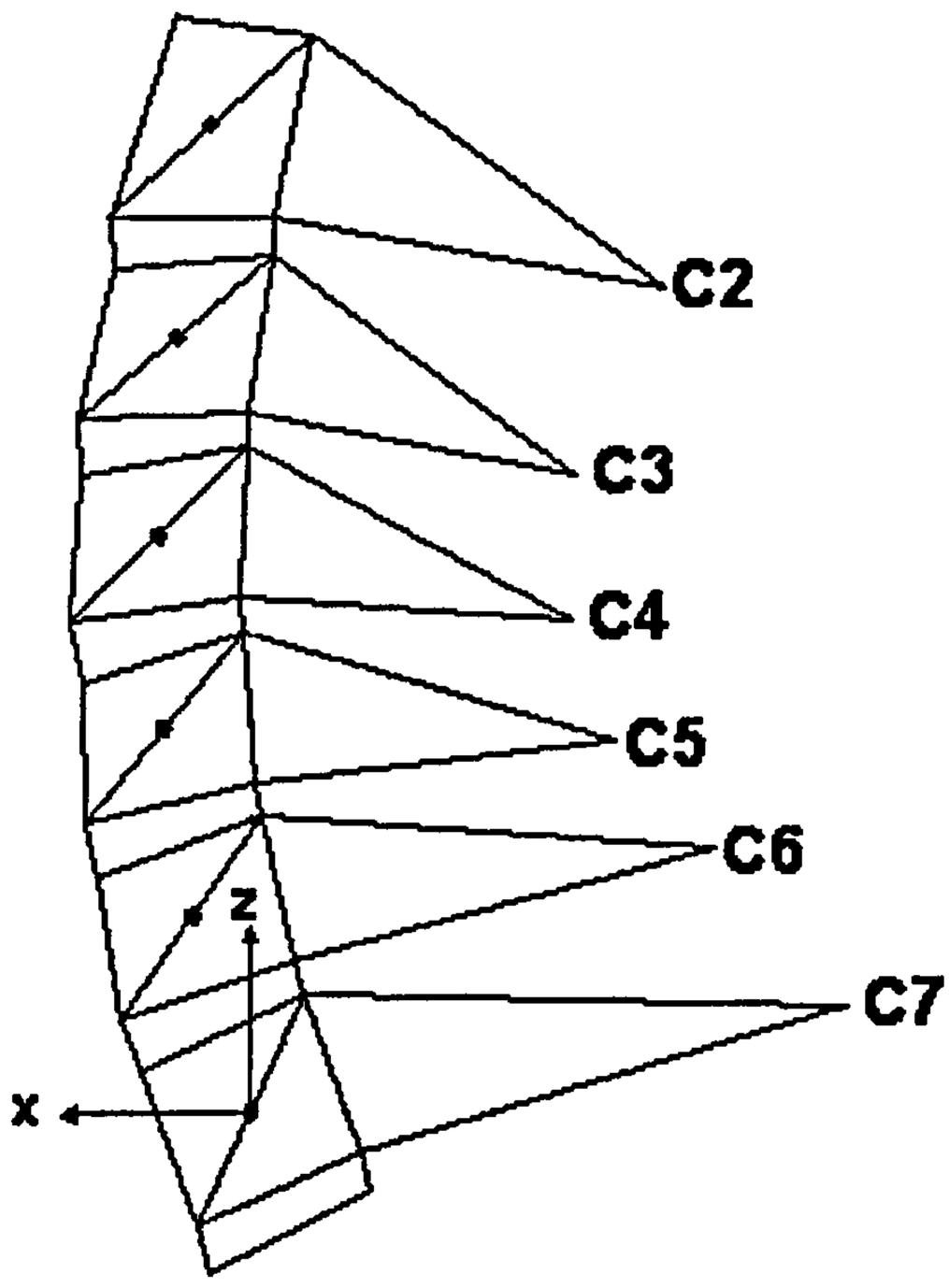


**Figure 4.4:** Mid-sagittal configuration of C2-C7 based on the geometric approximations reported by Nissan and Gilad (1984).

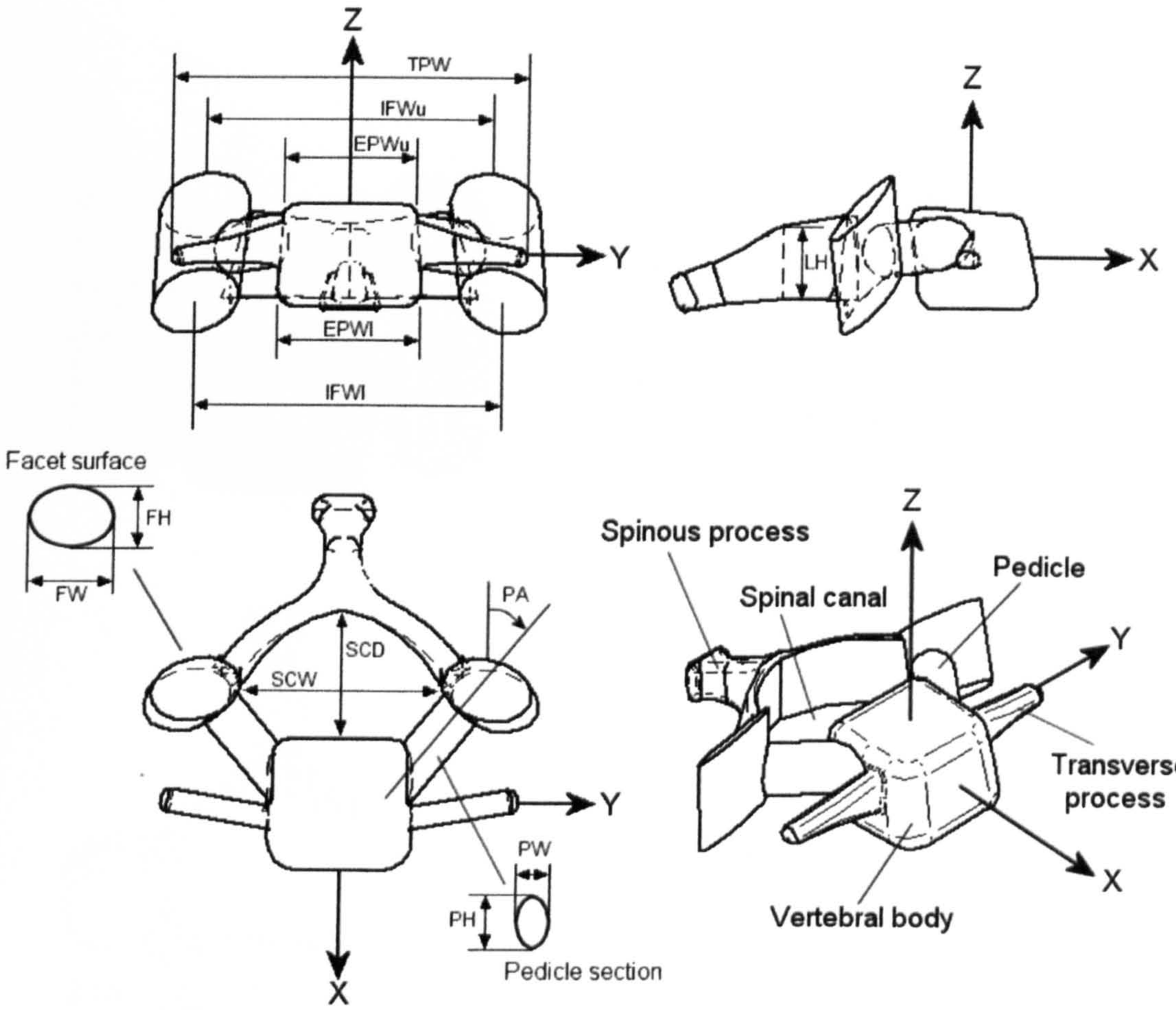


**Figure 4.5:** Three orthogonal views (front, side and top) of the C5 vertebra. Various dimensions used in construction are shown and explained further in Table 3.1. The fourth isometric view shows the local body coordinate system and has various anatomical features labelled.

**Table 4.1:** Nomenclature and references, lower cervical vertebrae (Refer to Fig. 4.5)

| *Mnemonics* | *Dimension* | *Reference* |
|---|---|---|
| EPWu | End-Plate Width, Upper | Panjabi et al. (1992) |
| EPWl | End-Plate Width, Lower | |
| TPW | Transverse Process Width | |
| SCW | Spinal Canal Width | |
| SCD | Spinal Canal Depth | |
| PA | Pedicle Angle | |
| PW | Pedicle Width | |
| PH | Pedicle Height | |
| IFWu | Interfacet Width, Upper | Panjabi et al. (1993) |
| IFWl | Interfacet Width, Lower | |
| FW | Facet Width | |
| FH | Facet Height | |
| LH | Laminar Height | Xu et al. (1999) |

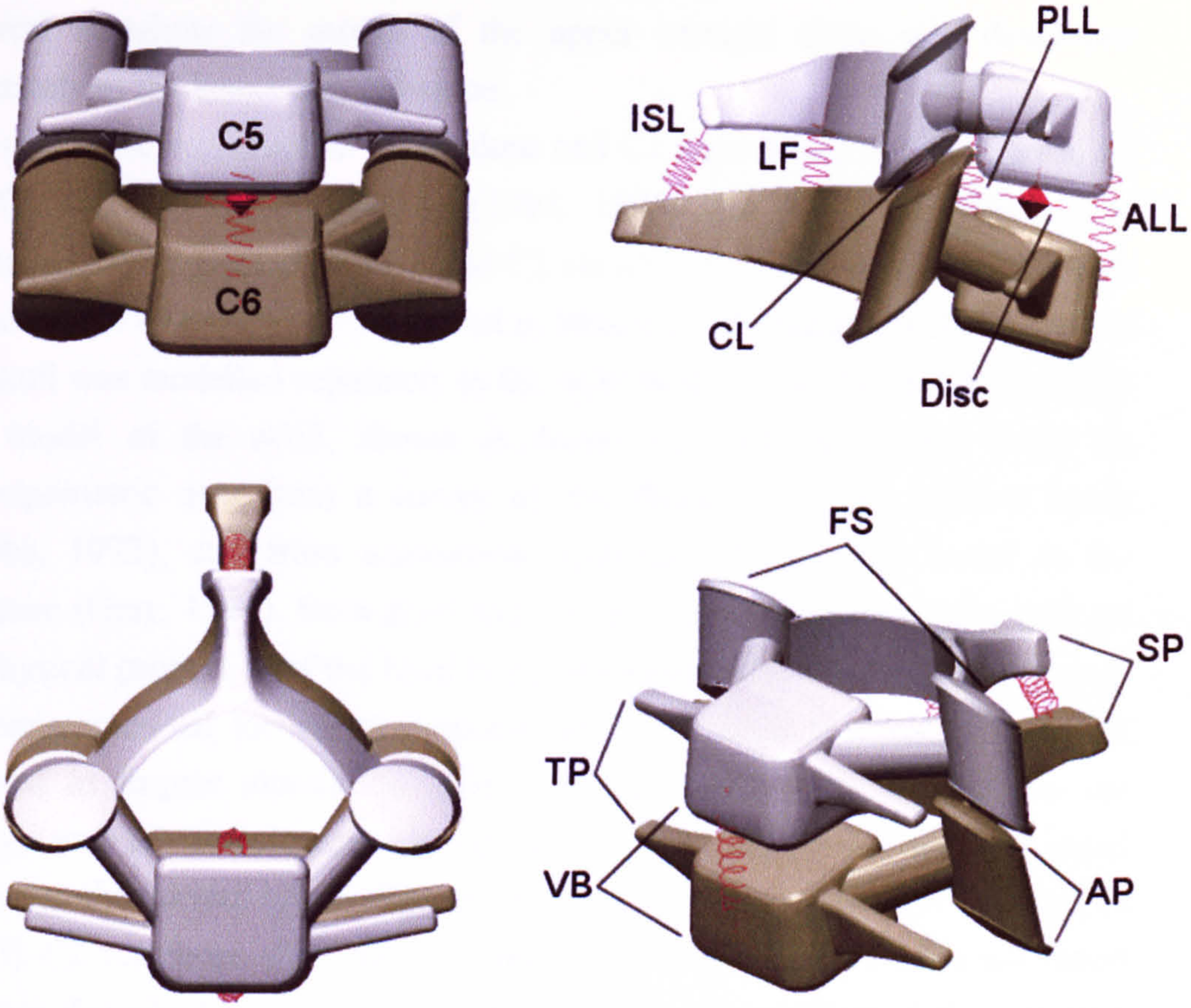


**Figure 4.6:** C5-C6 motion segment model. Shown are the solid bodies representing the **C5** and **C6** vertebrae consisting of; vertebral body (**VB**), transverse processes (**TP**), articular processes (**AP**), facet surfaces (**FS**) and spinous process (**SP**). Also shown are the ligaments of the C5-C6 motion segment: anterior and posterior longitudinal ligament (**ALL** and **PLL**), capsular ligaments (**CL**), ligamentum flavum (**LF**), and interspinous ligament (**ISL**). The intervertebral **Disc** is also shown.

### 4.1.2 Configuration of the Upper Cervical Spine

Due to the anatomical differences of the atlas and axis vertebrae to the other cervical vertebrae the model of the upper cervical spine was developed separately to the lower cervical spine.

The geometric construction of the dens and C1 were based on Schaffler et al. (1990), Doherty and Heggeness (1994, 1995) and Xu et al (1995). The dimensions used to construct C1 and C2 are shown in figures 4.7 and 4.8 with the source of reference for each listed in table 4.2. The occiput (C0), or base of the skull was modelled separately to the skull with the two being rigidly fixed. The model of the skull, shown in figure 4.2, was developed based on anthropometric data from a survey of 500 Royal Air Force aircrew heads (Hobbs, 1972), and from anatomical drawings of the skull found in the literature (Gray, 1980). Both skull and occiput share the same origin, with all the physical properties of the head being associated with the occiput, the skull is merely included for visual purposes and for contact to external bodies if required in impact simulation. The occipital condyles are attached to the occiput and all muscle attachments to the skull are positioned and fixed relative to the occiput origin. Figure 4.9 shows the configuration of the occiput and C1-C2 vertebrae, the centre of gravity and origin of the bodies are based on those described by de Jager (1996) including the position of the occipital condyles. The origin of C1 lies 16.5mm directly above the origin of C2 positioned at the upper half of the dens. The centre of gravity of C1 is positioned 7.7mm posterior to the origin. The origin of C0 is positioned at the apparent centre of rotation of C0 relative to C1 as described by Kapandji (1974) and de Jager (1996). The centre of gravity of the skull is positioned relative to the origin of C0 as reported by Thunnissen et al. (1995).

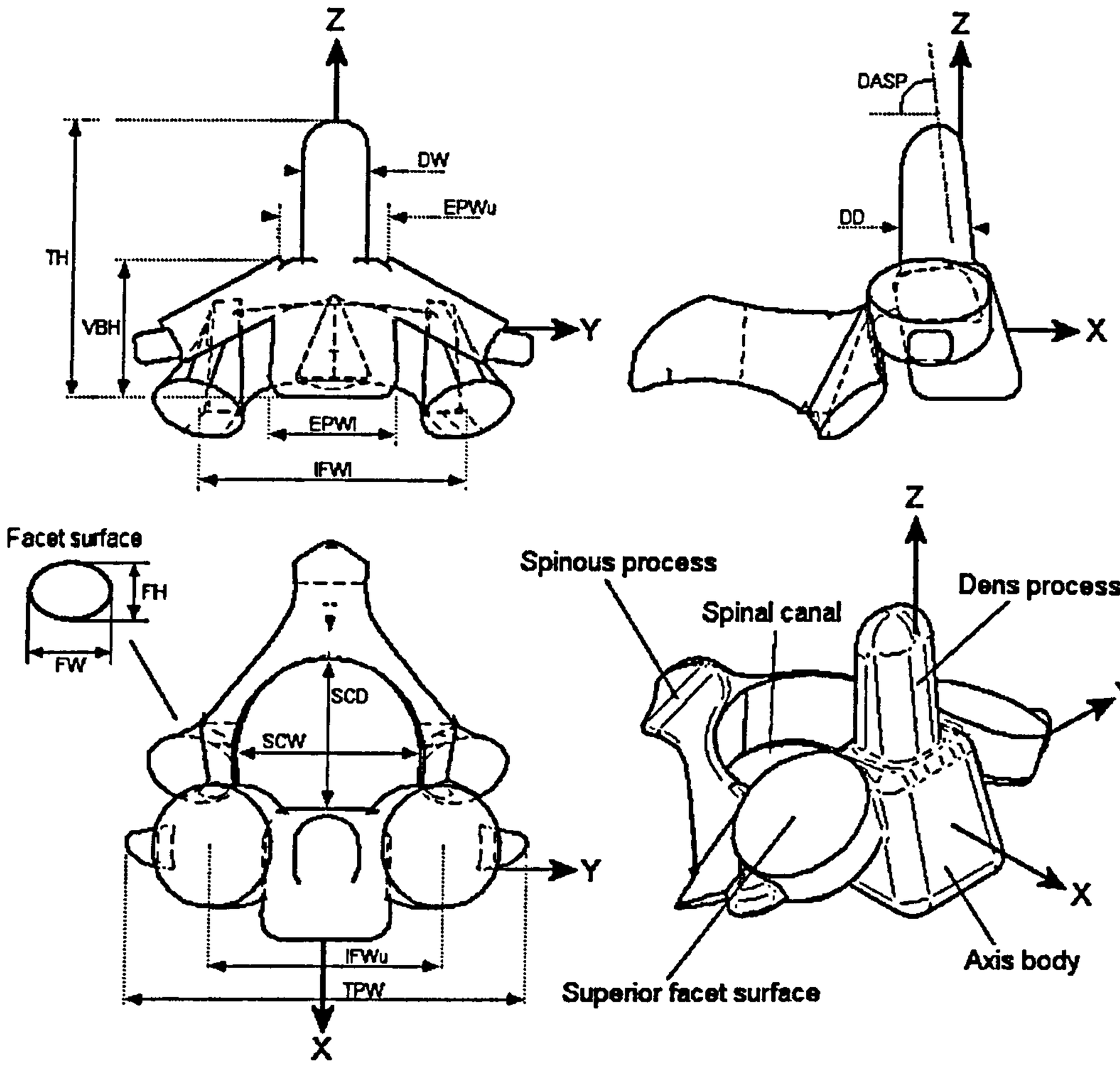


**Figure 4.7:** Three orthogonal views (front, side and top) of C2 vertebra. Various dimensions used in construction are shown and explained further in Table 4.2. The fourth isometric view shows the local body coordinate system and has various anatomical features labelled.

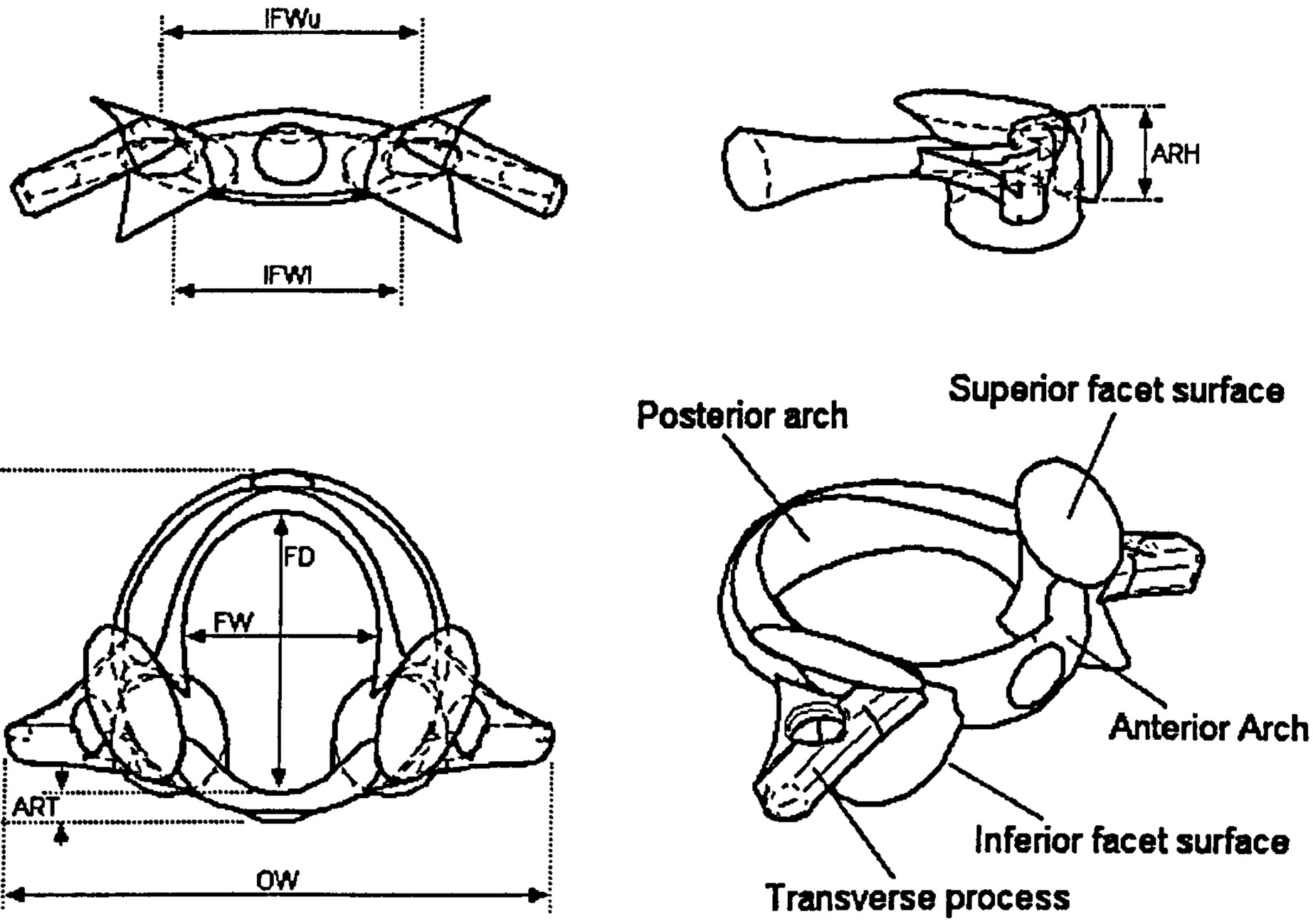


**Figure 4.8:** Three orthogonal views (front, side and top) of C1 vertebra. Various dimensions used in construction are shown and explained further in table 4.2. The various anatomical features are labelled in the isometric view.

**Table 4.2:** Nomenclature and references for upper cervical vertebrae (Refer to Figures 4.7 and 4.8).

| *Mnemonics* | *Dimension* | *Reference* |
|---|---|---|
| EPWu | End-Plate Width, Upper | Panjabi et al. (1992) & Xu et al. (1995) |
| EPWl | End-Plate Width, Lower | |
| TPW | Transverse Process Width | |
| SCW | Spinal Canal Width | |
| SCD | Spinal Canal Depth | |
| IFWu | Interfacet Width, Upper | Panjabi et al. (1993) |
| IFWl | Interfacet Width, Lower | |
| FW | Facet Width | |
| FH | Facet Height | |
| DW | Dens Width | Doherty et al. (1995) & Schaffler et al. (1992) |
| DD | Dens Depth | |
| DASP | Dens Angle (Sag Plane) | |
| TH | Total Height | |
| VBH | Vertebral Body Height | |
| ARH | Anterior Ring Height | Doherty et al. (1994) |
| ART | Anterior Ring Thickness | |
| OD | Overall Depth | |
| OW | Overall Width | |
| FW | Foramen Width | |
| FD | Foramen Depth | |

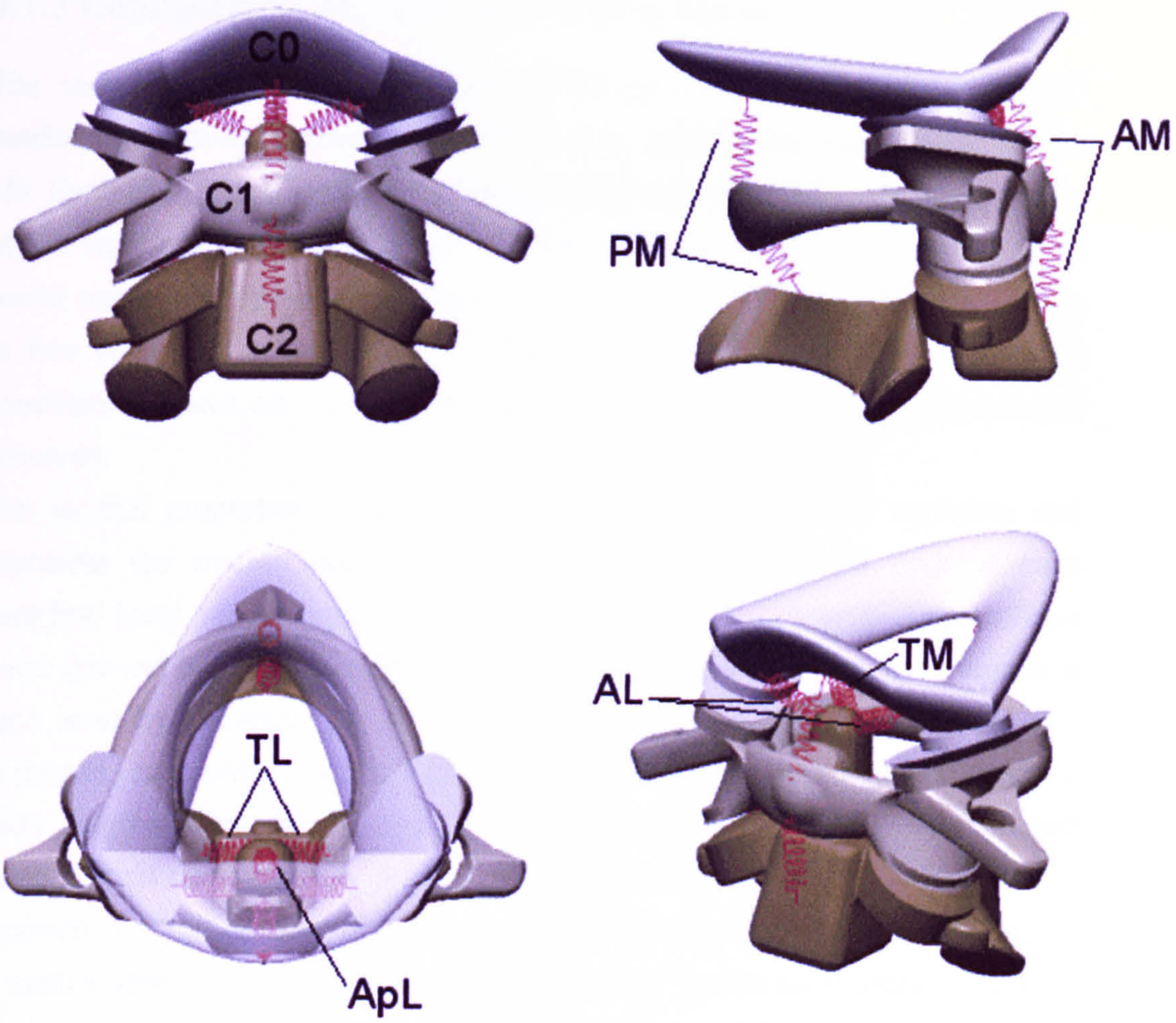


**Figure 4.9:** Upper cervical spine model **C0-C1-C2**. Shown are the solid bodies of the occiput and occipital condyles, atlas and axis with dens process and facet surfaces. Also shown are the ligaments of the upper cervical spine: anterior and posterior membranes (**AM** and **PM**), transverse ligament (**TL**), apical ligament (**ApL**), left and right alar ligaments (**AL**), and the tectorial membrane (**TM**).

### 4.1.3 Configuration of the Entire Cervical Spine.

The individual vertebrae were constructed as described in Solid Edge 3D modelling software before being imported as solid bodies into VisualNastran 4D. Each body has a local right-handed coordinate system located at the centre of the vertebral body. The vertebrae were each positioned with respect to the world coordinate system with the T1 origin and local coordinate system being in line with, and at the origin of, the world coordinate system. The world coordinate system was set up with x, y, z-axes pointing forward, to the left and upwards.

The inertial properties of the neck are lumped into the rigid vertebrae and represent the inertial characteristics of a slice through the neck at each vertebral level containing all surrounding soft tissues. The properties used are those derived by de Jager (1996). De Jager calculated the moment of inertia at each level by assuming the straightened neck to be a cylinder made up of 7 segments, each with a height equal to the distance between adjacent vertebral body origins. The volume and radius of the cylinder were then calculated using a total neck mass of 1.63kg with an average density of 1170kg/m$^3$ as reported by Walker et al. (1973) and used to determine the moments of inertia at each vertebral level. The principal moments of inertia are defined parallel to the local body coordinate system of each vertebra originating at the centre of gravity. As described earlier the centre of gravity of each vertebra lies on the posterior edge of the vertebral body in line with the x-axis of the local body coordinate system (see figure 4.10).

**Table 4.3:** Inertial and geometric data for the rigid bodies of the cervical spine (adapted from de Jager, 1996).

| Name | Mass (kg) | Moments of Inertia ($Kg.cm^2$) | | | | Origin of local body coordinate system expressed in global coordinates. (mm) | | Position of c.g. w.r.t. local body coordinates system. (mm) | | Initial orientation. (deg) |
|---|---|---|---|---|---|---|---|---|---|---|
| | | $I_{xx}$ | $I_{yy}$ | $I_{zz}$ | $I_{xz}$ | X | Z | $cg_x$ | $cg_z$ | $\alpha_y$ |
| T1 | | | | | | 0.0 | 0.0 | | | 0.0 |
| C7 | 0.22 | 2.2 | 2.2 | 4.3 | - | 6.4 | 16.8 | -8.2 | 0.0 | 20.8 |
| C6 | 0.24 | 2.4 | 2.4 | 4.7 | - | 11.1 | 34.7 | -8.3 | 0.0 | 15.2 |
| C5 | 0.23 | 2.3 | 2.3 | 4.5 | - | 12.9 | 52.2 | -8.1 | 0.0 | 10 |
| C4 | 0.23 | 2.3 | 2.3 | 4.4 | - | 12.7 | 69.8 | -7.9 | 0.0 | 5.3 |
| C3 | 0.24 | 2.4 | 2.4 | 4.6 | - | 10.3 | 87.5 | -7.8 | 0.0 | 0.0 |
| C2 | 0.25 | 2.5 | 2.5 | 4.8 | - | 7.02 | 106.5 | -7.7 | 0.0 | 0.0 |
| C1 | 0.22 | 2.2 | 2.2 | 4.2 | - | 7.02 | 123.0 | -7.7 | 0.0 | 0.0 |
| C0 | 4.69 | 181 | 236 | 173 | 71.0 | 3.02 | 143.0 | 37.0 | 43.0 | 0.0 |

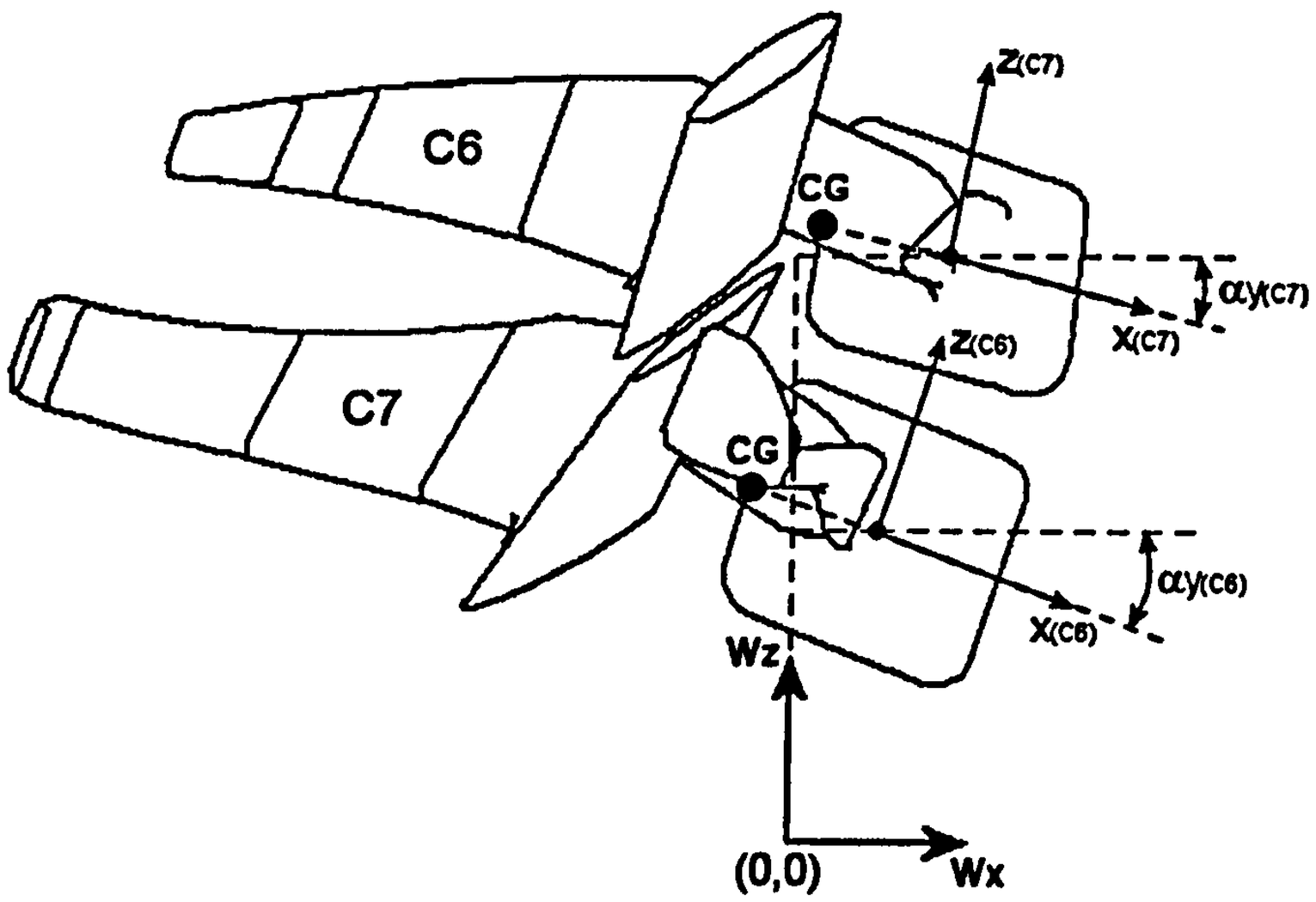


**Figure 4.10:** Schematic showing origin position and local body coordinate system used in the head-neck model. The origin of each vertebra is expressed in World coordinates (Wx, Wy, Wz) with rotation about the world y-axis ($\alpha y$). The local coordinate system of each vertebra lies at the centre of the vertebral body with the x-axis parallel to the lower endplate of the body. The position of the body's centre of gravity is also shown (CG).

## 4.2 Facet Joints

Together with the intervertebral disc, the facet joints resist compressive forces in the cervical spine. The amount of compressive force resisted by the facet joint pair at any cervical level depends on their orientation and on the eccentricity of the external load applied (Nowitzke et al., 1994). The coupling motion of the lower cervical spine in lateral bending and axial rotation is also determined by the oblique orientation of the facet joints. The facet surfaces are rigidly attached to the articular processes or their parent vertebrae. The articular facets are covered with a thin layer of cartilage and lubricated with synovial fluid allowing for almost frictionless sliding motion between adjacent facet surfaces (White and Panjabi, 1990).

In the model the articular facet surfaces are approximated by a slice off a sphere at a diameter equal to the average of the ellipse diameters reported by Panjabi et al. (1993) as an approximation of measured facets surfaces. The height of curvature was taken to be 1mm to give a slight curve to the surface of the almost flat facets. Panjabi also presents vertical and lateral distance between the centres of the facet surfaces and the orientation of the facets for vertebrae C2-C7. No position of the facets with respect to the vertebral bodies is given so the method of facet positioning used by de Jager (1996) has been adopted. To position the facets with respect to the vertebra it is assumed that the middle of the vertical distance (h) between facet surfaces lies at the same height as the origin of the vertebral body. The facet surfaces are at an equal distance on either side of the vertebra (due to mid-sagittal symmetry) and are positioned posteriorly, at a distance equal to the anterior-posterior radius of the facet surface (a), to the cg of the vertebra. Figure 4.11 shows the construction of an articular facet (A) and the positioning of the facets with respect to the vertebrae (B). The orientations of the facets have been adjusted slightly so adjacent facets are parallel in their initial configuration. Also once positioned in visualNastran, the facet positions have been slightly adjusted so that adjacent facets are just touching. No data on the contact between facet joints could be found. Contact between facets is defined and modelled as frictionless rigid body contact allowing the facets to slide relative to each other without friction approximating the synovial joint behaviour of real facet joints.

VisualNastran detects collisions geometrically by finding intersections between bodies. All body-to-body collisions are reduced to one or more point-to-point contacts. If a vertex of a body collides with a face of another body, the contact point can be defined on the face with a simple geometric calculation. When bodies collide, visualNastran computes the forces and/or impulses necessary to prevent interpenetration and applies these responses at the contact points. The individual facet surfaces were modelled separately to the vertebrae, positioned relative to the vertebrae within visualNastran then attached rigidly to their relevant parent vertebrae.

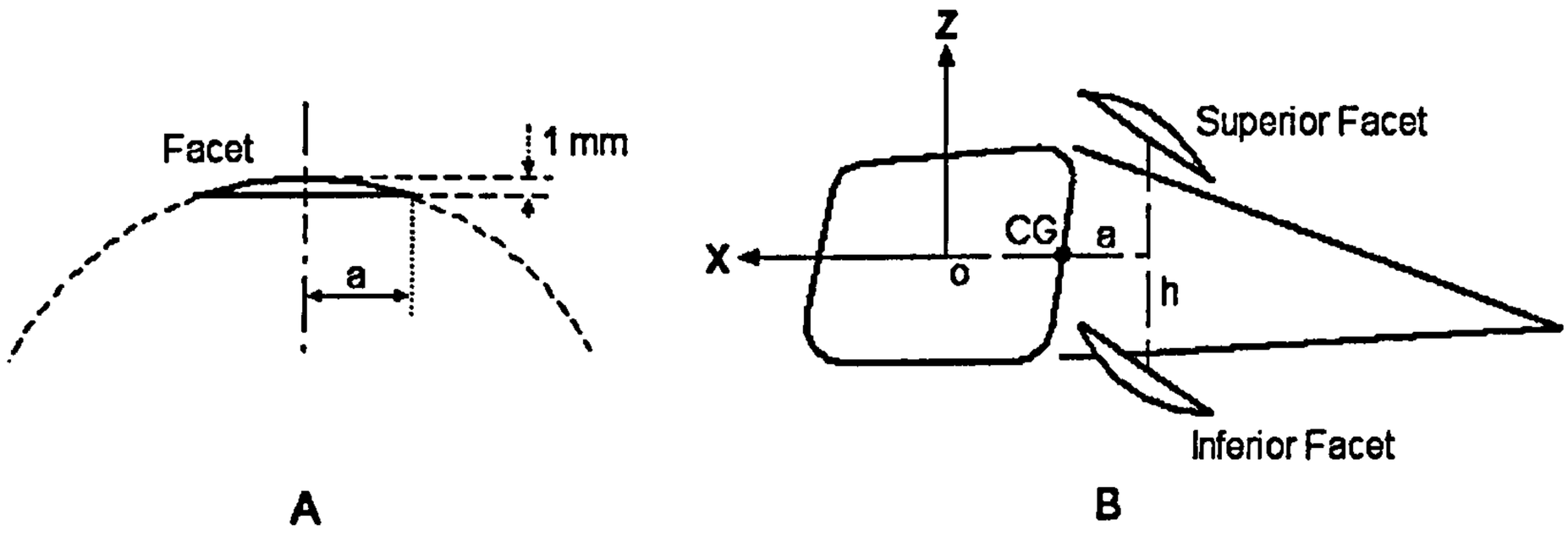


**Figure 4.11:** Articular facet construction. A: construction of facet surface. B: position of facet surfaces with respect to the vertebrae.

### 4.2.1 Atlanto-occiptal, Atlanto-axial and Atlanto-odontoid Joints

The occipital condyles of the skull are received by the superior articular sockets of the atlas allowing for predominantly nodding movements between the two bodies (see figure 4.12). This atlanto-occipital joint creates a large degree of stability due to the concave-convex interaction. The sidewalls of the sockets prevent the occiput form sliding sideways while the front to back walls prevent anterior and posterior gliding of the head. This concave-convex interaction is included in the model.

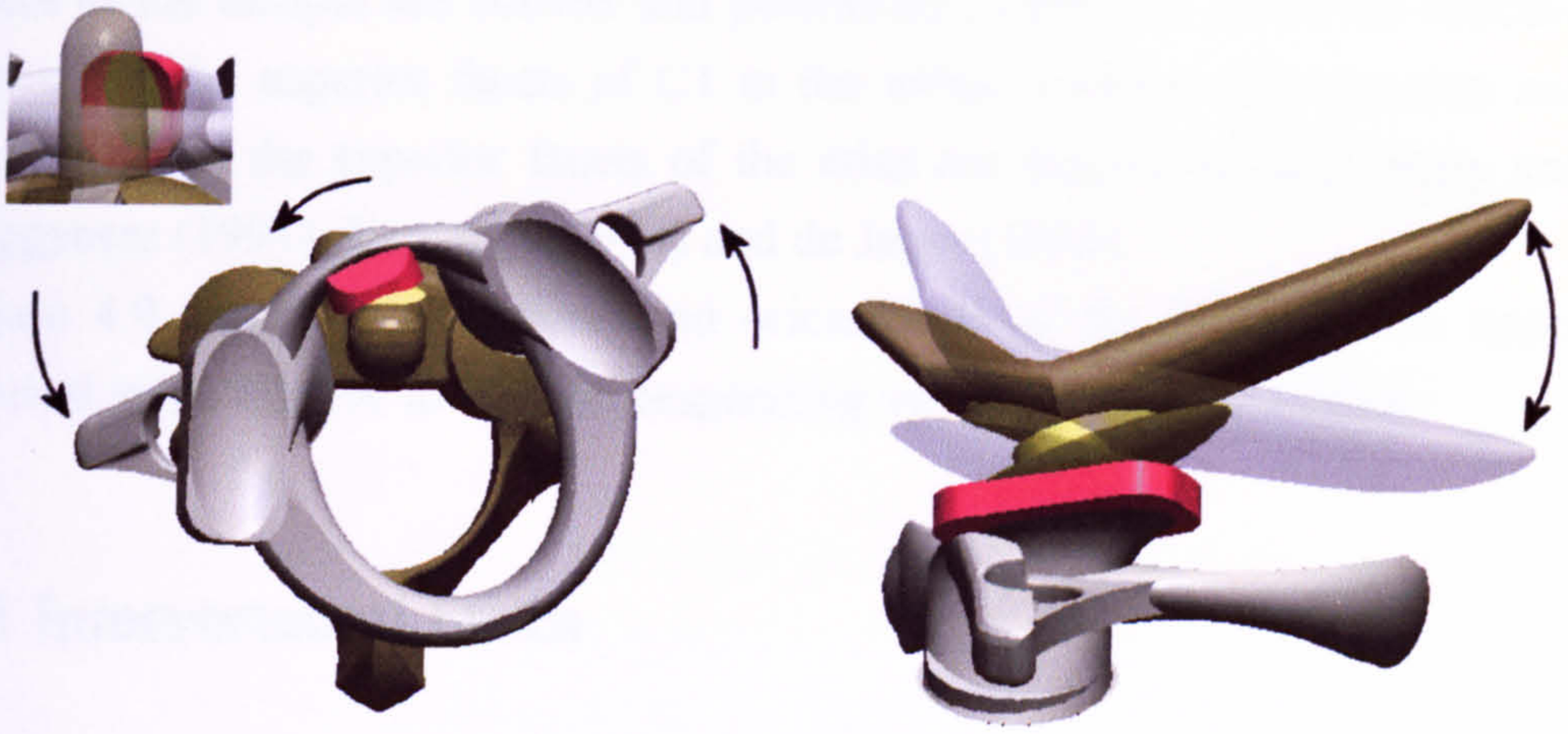

**Figure 4.12:** Upper cervical spine motion. Left: atlanto-axial rotation showing how the anterior arch of the atlas (red) slides around the facet of the dens process (yellow). Right: flexion and extension of the atlanto-occipital joint showing how the convex occipital condyles (yellow) move in the concave sockets of the superior facets of the atlas (red).

The odontoid process of the axis acts as a pivot for the atlanto-axial joint with its convex facet articulating with the concave facet on the anterior arch of the atlas. The two joints work together allowing for a large degree of axial rotation (see figure 4.12), moderate flexion and extension and only a small amount of lateral bending.

The facets of the upper cervical spine joints are modelled in a similar manner to those of the lower cervical spine, the atlanto-axial joints being two articulating convex surfaces with dimensions approximated from Panjabi et al. (1993) and Tominaga et al. (1995). The height of curvature of the C2 superior facets (1.8mm) is slightly larger than the inferior facets of C1 (1mm). The C2 superior facets are rotated about the x-axis orientated according to Panjabi et al. (1993). The centre of the dens facet is positioned on the anterior surface of the dens 18.4 mm above the vertebral origin at an angle of -13° to the vertical (Doherty and Heggeness, 1995). The height and width of the facet is approximated from Doherty and Heggeness (1995) and Xu et al (1995). The facet is convex with a curvature height of 1mm, the anterior facet of the atlas has a corresponding concave curvature with a depth of 1mm and is positioned in line with the dens facet and with the same orientation in the initial position. A similar arrangements is used for the atlanto-occipital joints, the inferior

facets of the occiput are convex and positioned so they are sat in the concave sockets of the superior facets of C1 in the initial position. The position and orientation of the superior facets of the atlas are derived from Doherty and Heggeness (1994), Kapandji (1974) and de Jager (1996).
Figure 4.9 shows the positions and orientations of the facets of the upper cervical spine relative to their corresponding vertebrae and the occiput.

## 4.3 Intervertebral Discs

The intervertebral discs located between the vertebrae of the lower cervical spine resist loads in multiple directions. Under any external loading with the exception of direct uniaxial tension, discs carry compressive forces in association with other components and along with the facets joints are responsible for carrying all the compressive forces the neck is subjected to (White and Panjabi, 1990). The discs are held in some degree of compression during normal physiological motion due to the weight of the head.
The intervertebral discs are modelled as linear viscoelastic 'bushing' constraints in visualNastran 4D and are located at the disc centre located approximately at the centre of the space between the upper and lower end plates of adjacent vertebrae at a fixed distance relative to the centre of the upper vertebrae. There are no discs between the axis, atlas and occiput. A 'bushing' constraint allows all translational and rotational degrees of freedom restricted by spring and damper relationships.
The direction and magnitude of a spring force is determined by the distance between its two end points for a translational spring or by the relative angle between its two end points for a rotational spring. Similarly the direction and magnitude of a damper force is determined by the relative velocity between its two end points for a translational damper or by the relative angular velocity between its two end points for a rotational damper. The loads exerted by the bushing constraint on the vertebrae are therefore given by:

$$F_i = k_{ti} \cdot t_i + b_{ti} \cdot v_i$$
$$M_i = k_{\theta i} \cdot \theta_i + b_{\theta i} \cdot \omega_i \qquad (i = x, y, z)$$

where $F_i$ and $M_i$ are the components of the forces and moment relative to the $i$-axis of the lower vertebrae, $t_i$ and $\theta_i$ are the relative translations and rotations between the vertebrae measured from the geometric centre of the disc and $v_i$ and $\omega_i$ are the relative translational and rotational velocities of the disc centre. The stiffnesses $k_i$ and the damping coefficients $b_i$ represent the intervertebral disc behaviour.

Material properties of the intervertebral discs are required for multiple directions of loading i.e. flexion, extension, tension, compression, anterior and posterior shear, lateral shear, axial rotation and lateral bending. Due to the mid-sagittal symmetry of the cervical spine, disc response can be assumed to be the same for left and right lateral bending, lateral shear and axial rotation. Vertebral disc responses are obtained by subjecting a motion segment (vertebra-disc-vertebra) or a disc segment (body-disc-body) to external loading. Disc stiffnesses reported by Moroney et al. (1988) were used along with the tension and compression values presented in Yoganandan et al. (2001). Moroney states that disc stiffnesses were not independent to disc level. However, the stiffness coefficients reported by Yoganandan for compression of cervical discs gradually increase from 637.5N/mm at C2-C3 to 973.6 N/mm at C7-T1. As no other data on disc stiffnesses can be found Moroney's values have been used for axial rotation, lateral bending and all shear stiffness coefficients. A recent study on flexion and extension of the cervical spine presents non-linear load-displacement curves at various levels (Camacho et al., 1997). Although the stiffness curves reported represent the response of entire motion segments (two adjacent vertebrae with surrounding soft tissues; disc, ligaments and facet joints) theses values can still be used to define the flexion/extension response of the disc. From the results of Moroney on intact segments and disc segments it can be seen that approximately half the flexibility of the motion segment is caused by the ligaments and the other half by the disc in flexion and extension. From the intact segment tests it was found that the linear stiffness was 0.43 and 0.73 Nm/deg for flexion and extension respectively while for the isolated disc segments the stiffness was found to be 0.21 and 0.32Nm/deg. It is therefore reasonable to divide the flexion/extension stiffness functions, presented by Camacho et al. (1997), by 2 to give the approximate non-linear response of the intervertebral discs.

The translational damping coefficients of the discs are set to 1000kg/s and rotational coefficients to 1.5Nm/s as a preliminary estimation based on those used by de Jager as no actual disc damping coefficients have been reported in the literature. These damping coefficients were shown not to account for the dynamic stiffening of the disc but instead were used to attenuate vibration accelerations of the head (de Jager, 1996). In the model the dynamic stiffness of the disc is assumed to be twice the static stiffness.

**Table 4.4:** Biomechanical stiffness and damping data for the intervertebral discs.

| Loading Direction | Stiffness *k* [N/mm] | | | | | | Damping *b* C2-T1 [Ns/m] |
|---|---|---|---|---|---|---|---|
| | C2-C3 | C3-C4 | C4-C5 | C5-C6 | C6-C7 | C7-T1 | |
| Anterior Shear | 62 | 62 | 62 | 62 | 62 | 62 | 1000 |
| Posterior Shear | 50 | 50 | 50 | 50 | 50 | 50 | 1000 |
| Lateral Shear | 73 | 73 | 73 | 73 | 73 | 73 | 1000 |
| Tension | 63.5 | 69.8 | 66.8 | 68.0 | 69.0 | 82.2 | 1000 |
| Compression | 637.5 | 765.3 | 784.6 | 800.2 | 829.7 | 973.6 | 1000 |
| | [Nm/rad] | | | | | | [Nms/rad] |
| Flexion | Load Curve from Camacho et al., (1997) /2 | | | | | | 1.5 |
| Extension | Load Curve from Camacho et al., (1997) /2 | | | | | | 1.5 |
| Lateral Bending | 0.33 | 0.33 | 0.33 | 0.33 | 0.33 | 0.33 | 1.5 |
| Axial Rotation | 0.42 | 0.42 | 0.42 | 0.42 | 0.42 | 0.42 | 1.5 |

## 4.4 Ligaments

Ligaments of the neck provide stability to the motion segments allowing motion within physiological limits and absorbing energy during trauma. Ligaments are uniaxial structures that resist only tensile or distractive forces becoming slack in compression.

### 4.4.1 Lower Cervical Spine Ligaments

Six ligaments of the lower cervical spine are included at each level: anterior and posterior longitudinal ligament (ALL and PLL), flava ligament (FL), interspinous ligament (ISL), and the left and right capsular ligaments (see figure 4.6). The anterior longitudinal ligament spans adjacent vertebrae attaching at the mid-vertical height on the anterior surface of the two vertebral

bodies, the posterior longitudinal ligaments are defined from the mid-height of the inferior vertebral body on the posterior surface, at the same position as the centre of gravity, to the mid-height of the superior vertebral body. The ligamentum flavum attaches to the spinous process in line with the centre of gravity along the x-axis at a distance equal to the depth of the spinal canal as reported by Panjabi et al. (1992). The interspinous ligament spans the two adjacent vertebrae attaching at the very tip of the spinous processes. The capsular ligaments are positioned so they are perpendicular to the facet joints and pass through the centres of the facets surfaces attaching 2mm from the centres giving them a rest length of around 6mm (Yoganandan et al., 2000).

### 4.4.2 Upper Cervical Spine Ligaments

Seven ligaments of the upper cervical spine are included in the model: apical ligament, transverse ligament, left and right alar ligaments, tectorial membrane, anterior and posterior membranes and the left and right capsular ligaments (see figure 4.9).

The left and right alar ligaments attach to either side of the upper part of the dens process of C2 and pass obliquely upward and laterally to attach to the side of the occipital condyles of the occipital bone. The rest length of the alar ligaments is 10.9mm, which is in agreement with the measured length reported by Panjabi et al. (1991). The apical ligament extends from the tip of the dens between the alar ligaments to insert on the anterior wall of the foramen magnum and has a rest a length of 10.5mm. The transverse ligament is split into two sections, left and right, passing from the midline of the posterior boarder of the mid portion of the dens to attach to the left and right lateral masses of C1. The combined length of the two sides of the transverse ligament is 20.74mm, similar to the reported length of 21.9mm reported by Panjabi et al. (1991d). The tectorial membrane is a continuation of the posterior longitudinal ligament of the lower cervical spine. It attaches to the body of C2 at the mid-height of the posterior surface and inserts on to the anterior edge of the foramen magnum. The anterior membrane is a continuation of the anterior longitudinal ligament of the lower cervical spine and hence is positioned similarly between C2 and C1. Between C1 and the occiput the anterior

membrane extends from the tubercle of the anterior arch of the atlas to the anterior margin of the foramen magnum. The posterior membrane is anatomically analogous to the flava ligament of the lower cervical spine attaching to the posterior arch of the atlas and inserting on the posterior margin of the foramen magnum. Due to the large diameters of the facet surfaces of the atlanto-axial joint the capsular ligaments are represented by four spring elements positioned around the perimeter of the facet joints. Three spring elements represent the capsular ligaments of each atlanto-occipital facet joint, one positioned in the centre in a similar manner to the capsular ligaments of the lower cervical spine and one at either edge of the large diameter of the facet surfaces (see figure 4.13).

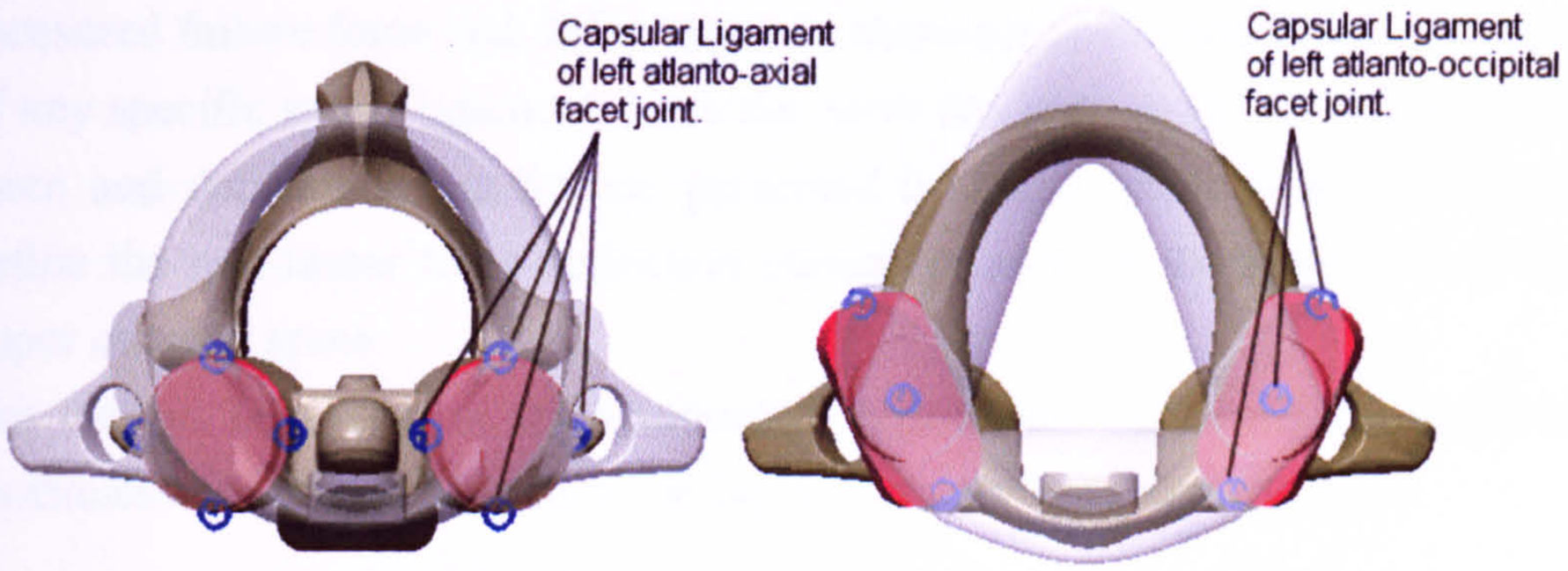


**Figure 4.13:** Arrangement of spring elements representing the capsular ligaments of the upper cervical spine.

## 4.4.3 Ligament Properties

The ligaments are modelled as non-linear viscoelastic spring elements in VisualNastran. The non-linear force-deflection curves presented by Yoganandan et al. (2000) for lower cervical spine ligaments (C2-T1) are used to define load curves for ligament response. The curves are described in look-up tables in visualNastran with the elements defined as being active for positive values of deflection only i.e. the ligament elements act similar to a rubber band, producing force in tension only. The ligaments' rest lengths are defined as the element lengths in the initial body position. The results reported by Yoganandan are from tests on in-situ cervical ligaments where the internal load balance due to initial ligament tension is maintained and so the force

deflection curves represent the ligament response starting from their initial pre-stress reducing the toe-region of the curves. This should give the motion segment greater stability in its initial configuration.

No force-deflection curves have been characterized for the ligaments of the upper cervical spine although Yoganandan et al. (2001) have presented failure force and deformation for each. Chazal et al (1985) defined the non-linear force-strain behaviour of ligaments from the thoracic and lumbar spine including a few from the lower cervical region. The average dimensionless force-strain curve, normalized relative to the failure force $F_{max}$ and failure strain $E_{max}$, for all ligaments tested by Chazal et al. is shown in figure 4.14. This curve demonstrates that spinal ligaments exhibit almost identical behaviour in dimensionless form, and so the curve can be used together with measured failure force and deformation to characterise the non-linear response of any specific spinal ligament. Here the curve has been used together with the force and deformation at failure, presented in Yoganandan et al. (2001), to define the non-linear force-deflection curves for each of the ligaments of the upper cervical spine.

The viscous behaviour of the ligaments is represented by a constant damping coefficient of 300kg/s as used by de Jager as an arbitrary starting value.

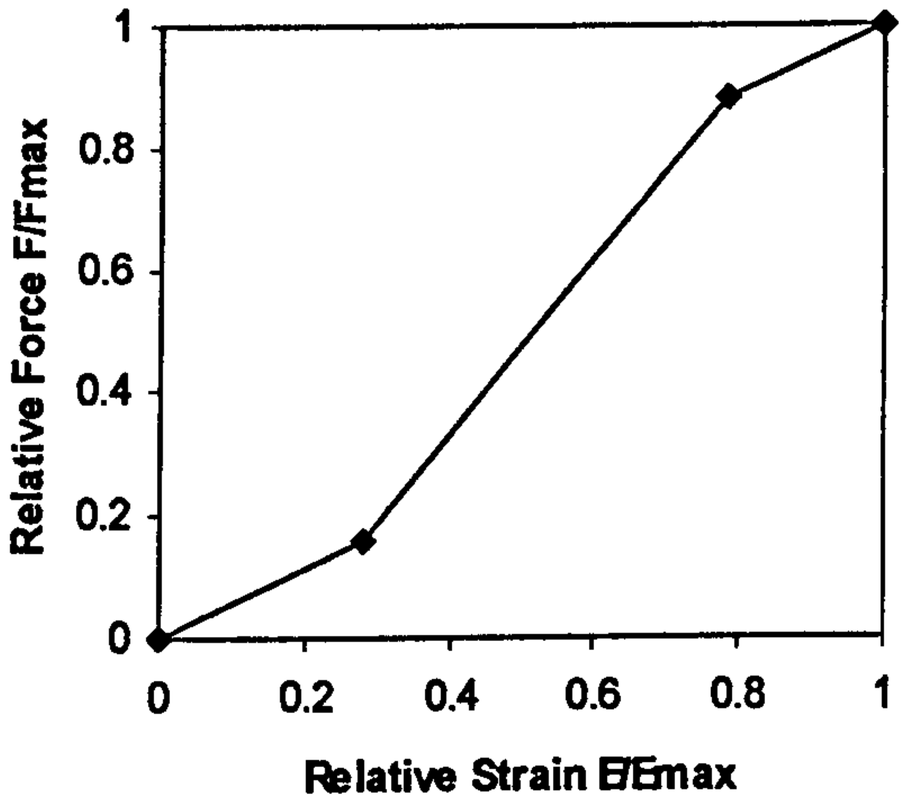


**Figure 4.14:** Average dimensionless force-strain curve used to define force-deflection curves for the upper cervical spine ligaments. The strain relative to the strain at failure ($E_{max}$) is given along the horizontal axis, and the force relative to the force at failure ($F_{max}$) is given along the vertical axis.

## 4.5 Muscles

The muscles of the human neck serve to make movements of the head, stabilize the head and neck and assist in the protection of the cervical spine. Humans make head movements by using more than 20 pairs of neck muscles. The movements they produce sub-serve sensory activities and the motor requirements of eating, gesture and speech. Neck muscles must stabilize the head, neck and thoracic segments relative to each other to maintain posture and resist unnatural movements (Kamibayashi and Richmond, 1998). In the head/neck model muscles are included to investigate the effect of muscle forces on the behaviour of the head and neck response to impact.

19 muscle groups of the head and neck are included in the model, as can be seen in the muscle map shown in figure 4.15. Many of these muscles cross two or more vertebral pairs as they span between multiple sites of attachment. For this reason muscles with broad areas of attachment are subdivided into a number of individual muscle elements resulting in 138 individual muscle segments. Muscle attachment sites were chosen based on other researchers decisions and on published anatomic descriptions. Due to T1 being the lowest vertebra included in the model, muscles whose attachment sites lie beneath T1 attaching to lower thoracic vertebrae or to other bony anatomy such as the clavicle or scapula are fixed with respect to T1, positioned at their appropriate anatomical locations. This ensures realistic muscles lengths and more accurate muscle lines of action.

In addition to the origins and insertions each muscle element passes through a series of predefined intermediate points to simulate the curving of the muscle around the vertebrae and soft tissues of the neck during neck bending. This curved musculature is modelled by a chain of connected actuators resulting in a more realistic representation of the change in muscle length during head-neck motion. The following section gives a more detailed description of the muscle model used, the muscle groups included in the model and of their various elements and attachment sites.

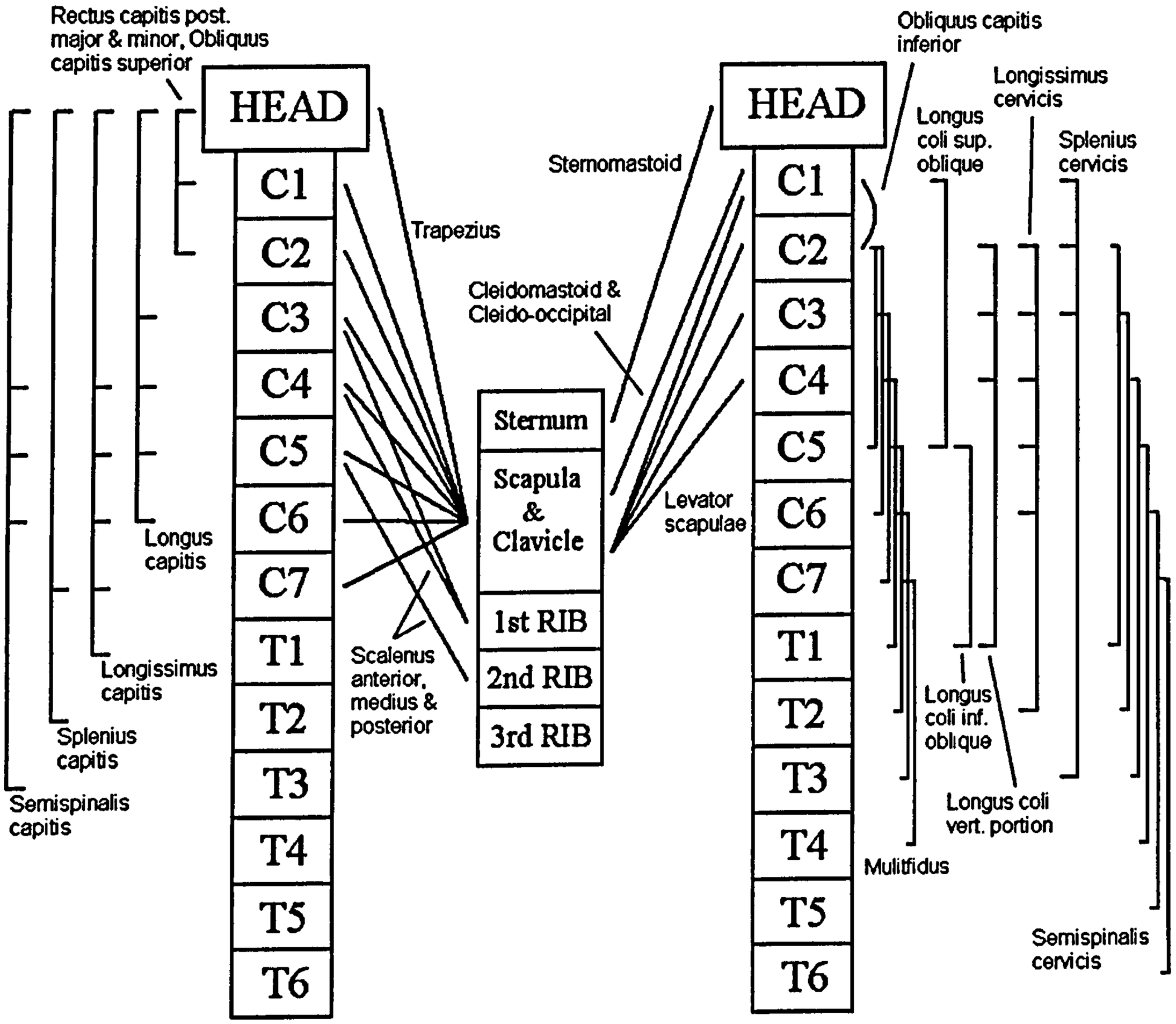


**Figure 4.15:** Muscle map of neck muscles included in the head-neck model, showing points of attachment origins and insertions.

### 4.5.1 Virtual Muscle

Muscle mechanics is handled by an external application called Virtual Muscle vs. 3.1.5, developed at the Alfred E. Mann Institute at the University of Southern California, that runs within Matlab and Simulink. Virtual Muscle has been created to be used in the context of a hierarchical model of motor control with itself occupying the middle layer (figure 4.16). Realistic muscle properties provided by Virtual Muscle drive the skeletal dynamics that are in turn handled by visualNastran comprising the lowest level of the system. At the top-level, muscle activation is controlled.

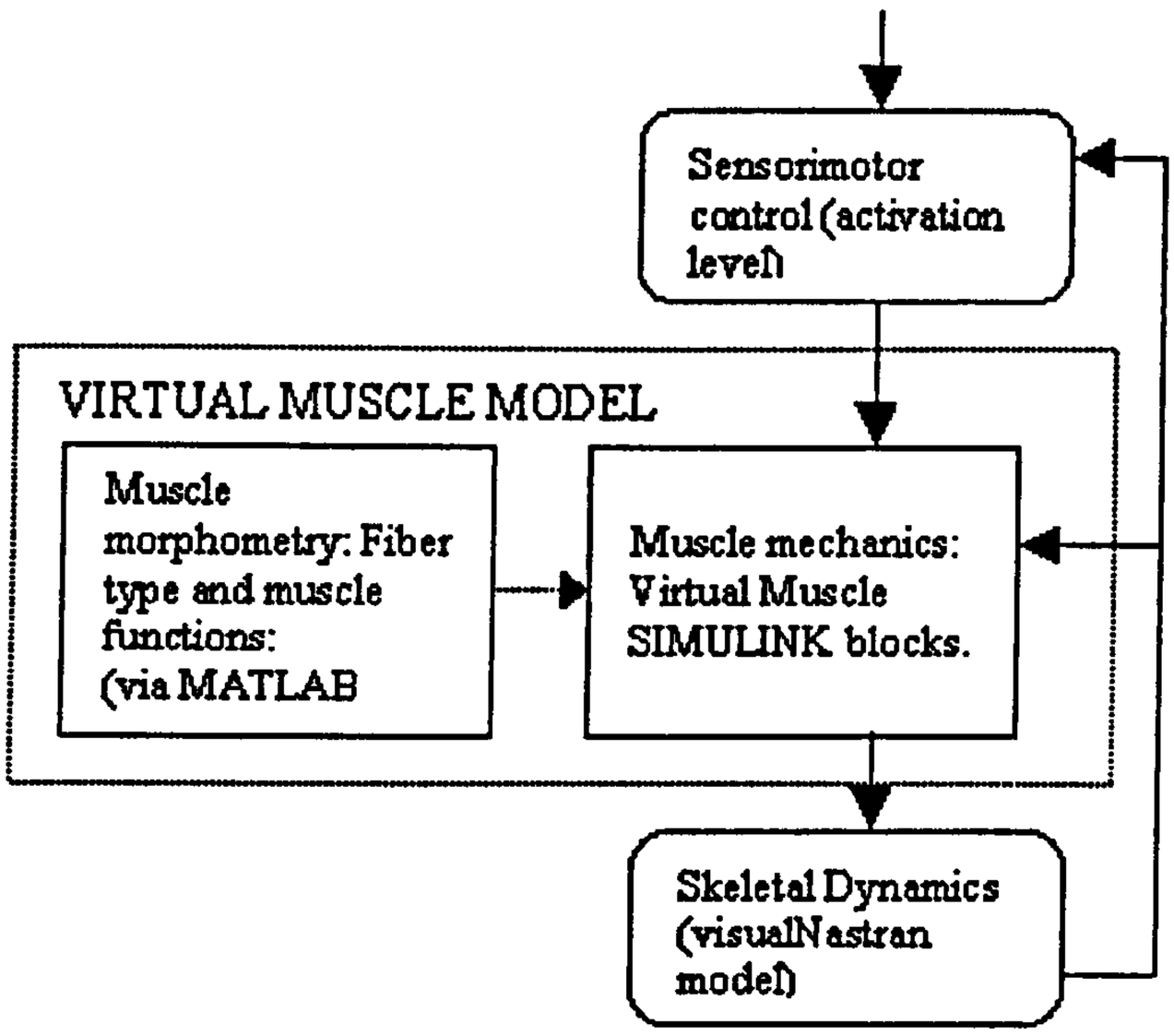


**Figure 4.16:** Flow diagram showing the order of muscle control.

The basic form of the muscle model is generally similar to those of Hill (1970) and Zajac (1990) and is shown schematically in figure 4.17. The model consists of an active contractile element (CE) describing active force $F_{CE}$ with activation, length and velocity dependencies in parallel with a viscoelastic element (PE) describing the passive properties of fascicles $F_{PE}$. The total fascicular force is applied in series to the inertial mass of the muscle and a series elastic element (SE) for tendon and aponeurosis. The mass plus a small amount of viscosity in the passive muscle provides realistic damping that prevents computational instability (Brown and Loeb, 2000).

A mathematical summary of the models fascicular force is shown in equations 1-3.

$$F = F_{CE} + F_{PE} \quad (1)$$

$$F_{CE} = Af \cdot FL \cdot FV \quad (2)$$

$$F_{PE} = F_{PE1} + Af \cdot F_{PE2} \quad (3)$$

A schematic description of these main elements of the model along with their associated sub-elements is provided in figure 4.18 with a description of the contribution of each constituent physiological component (see Appendix A for model equations). In equation 1, F is the total force produced by the muscle fascicles while $F_{CE}$ and $F_{PE}$ represent the forces produced by the CE and PE respectively. In equation 2 Af is defined as the activation-frequency relationship and is a unitless quantity ($0 \leq Af \leq 1$, Af=1 for tetanic stimulation). FL is defined as the titanic force-length relationship and has units of $F_0$ (maximal potentiated isometric force); FL is primarily dependent upon fascicle length. FV is defined as the titanic force-velocity relationship and is unitless (FV=1 for isometric condition); FV depends primarily upon fascicle velocity, which is defined as positive for lengthening velocities. In equation 3 $F_{PE1}$ and $F_{PE2}$ are spring-like components with units of $F_0$ and are non-linear functions of length (Brown et al., 1999).

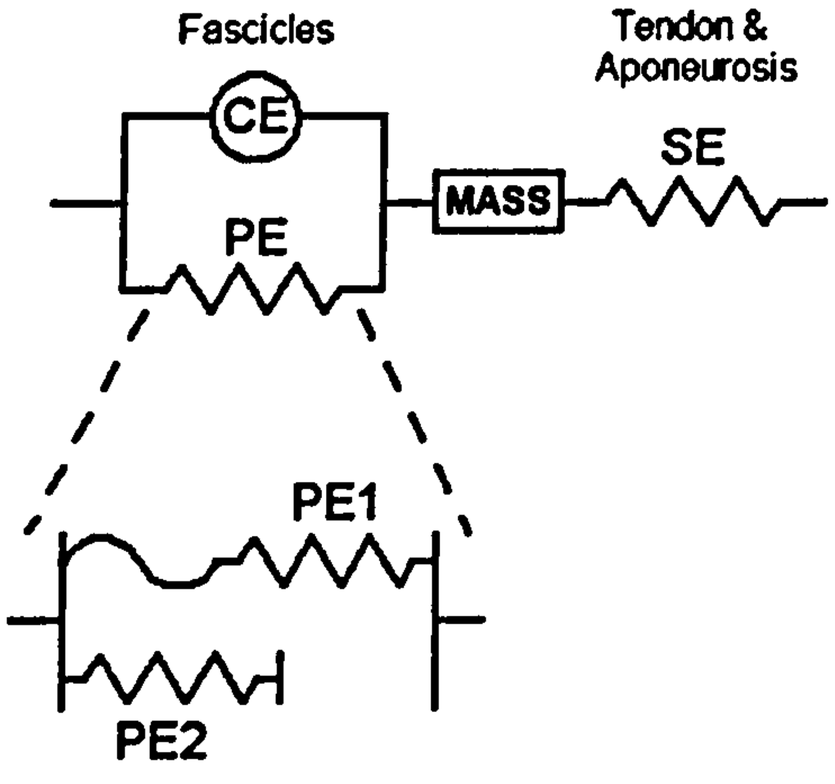


**Figure 4.17:** Schematic of basic muscle model elements. The muscle fascicles are represented by the contractile element (CE) in parallel with the passive elastic element (PE). The series elastic element (SE) represents the combined tendon and aponeurosis. The inertial mass of the muscle is also applied in series to the fascicles. PE1 is a non-linear spring that resists stretch in the passive muscle, while PE2 is non-linear spring resisting compression during active contraction at short lengths.

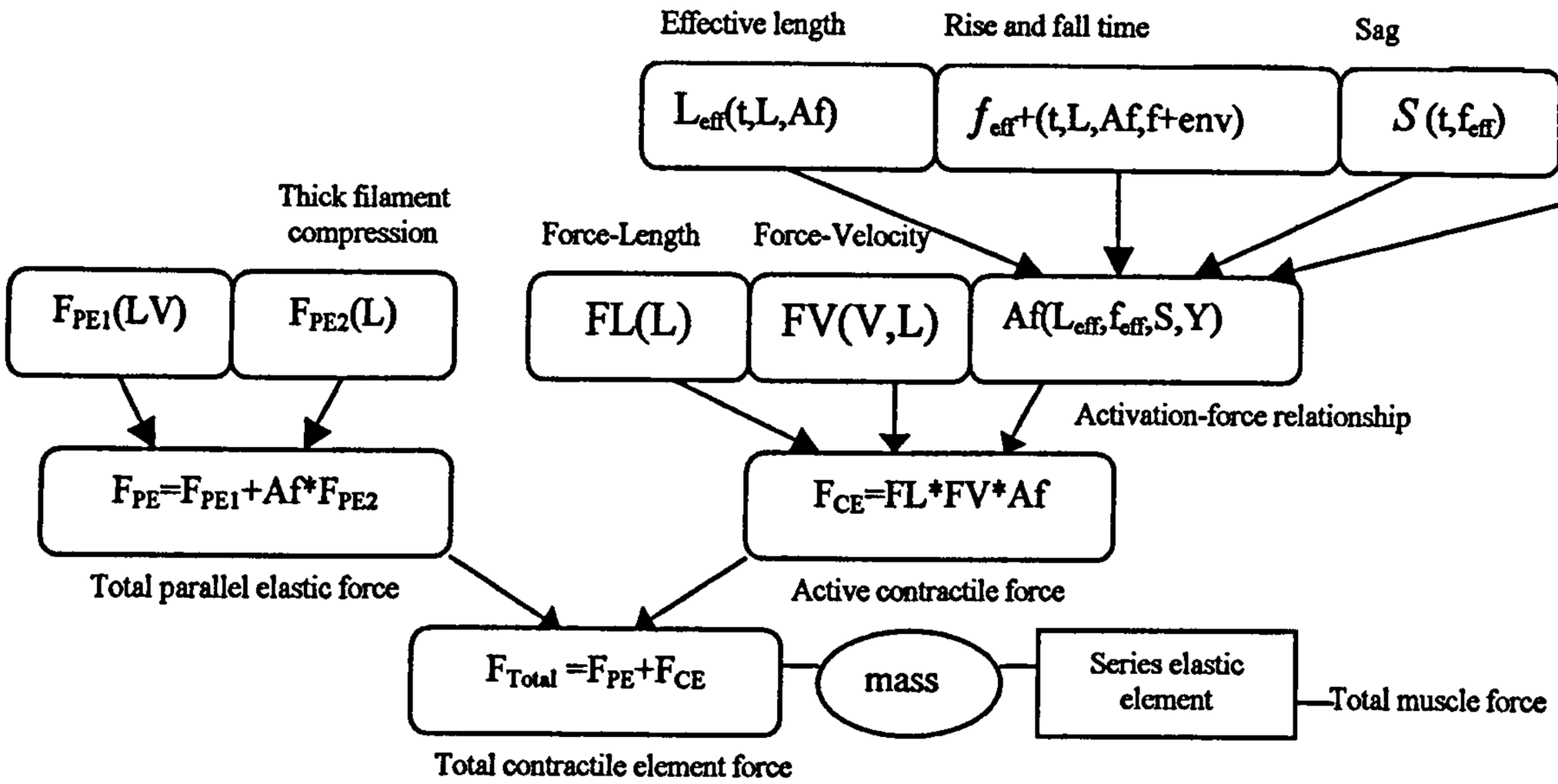


**Figure 4.18:** Schematic representation of Virtual Muscle's equations and terms. Complete descriptions of all elements shown can be found in Brown and Loeb (2000) and Brown et al. (1999). $F_{Total}$- total force produced by muscle fascicles. $F_{PE}$- total passive force produced by parallel elastic element PE. $F_{CE}$- total active force produced by contractile element CE. $F_{PE1}$- passive visco-elastic properties of stretching a muscle. $F_{PE2}$- passive resistance to compression of the thick filaments at short muscle lengths. FL- tetanic Force-Length relationship. FV- tetanic Force-Velocity relationship. Af- isometric, activation-frequency relationship. $F_{eff}$- time lag between changes in firing frequency and internal activation (i.e. rise and fall times). $L_{eff}$- time lag between changes in length and the effect of length on the Af relationship. S represents the effects of 'sag' on the activation during a constant stimulas frequency. Y represents the effects of yielding (on activation) following movement during sub-maximal activation.

### 4.5.1.1 Defining Muscle Fibre Types.

Zajac (1989) showed that the behaviour of the contractile element of muscle scales well from the sarcomere level up to the whole muscle fibre and again up to the level of an entire recruitment group of motor units. By defining the properties of each fibre type that will be used throughout the muscle model in a single database, allows the muscle model to reference these properties when fibre types are combined in varying percentages to form a typical mixed-fibre-type muscle. For the purpose of this study the generic fast twitch and typical

slow twitch fibre types derived for human muscles as presented in Cheng et al. (2000) are used (see Appendix A for specific fibre type best-fit constants and associated equations). The parameters used to define these fibre types are presented in table 4.5. The optimal sarcomere length of 2.7 μm was taken from Herzog et al. (1992), which is in close agreement with the value 2.8 μm reported in another study by Rack and Westbury (1969). This value is used to scale the active and passive force-length properties. The recruitment rank defines which fibre type is recruited first in a muscle composed of more than one fibre type. $V_{0.5}$ is the shortening velocity required to produce half the maximum tetanic force (0.5 $F_0$) at 1.0 $L_0$ (fascicle length at which $F_0$ is elicited). $f_{0.5}$, the frequency at which half of maximal tetanic force is obtained (isometric at 1.0 $L_0$), scales the rise and fall times. For details of how $V_{0.5}$ and $f_{0.5}$ were obtained the reader is referred to Cheng et al. (2000).

The specific tension is defined as the maximal isometric force produced at the optimal length per unit cross-sectional area. As a starting point the default value of 31.8N/cm$^2$ has been used based on Scott et al. (1996) and Brown el al. (1998). However the value has been estimated to be anywhere between 20 and 100 N/cm$^2$ by Winters and Stark (1988) and it is hypothesised that a higher value than 31.8 may be required to truly represent the maximum muscular forces that can be exerted by a human subject and that the value of specific tension is likely to vary between subjects due to gender differences and different levels of muscular development. For this reason a range of values of specific tension are explored in Chapter 6 to see the effect on head and neck response to impact conditions.

**Table 4.5:** Muscle model fibre type parameters.

| Fiber Type Parameter | 'typical' slow-twitch fibre type | generic fast-twitch fibre type |
|---|---|---|
| Optimal Sarcomere Length (μm) | 2.7 | 2.7 |
| Recruitment Rank | 1 | 2 |
| $V_{0.5}$ ($L_0$/s) | -1 | -1.67 |
| $f_{0.5}$ (pps) | 12 | 20 |
| Specific Tension (N/cm$^2$) | 31.8 | 31.8 |

### 4.5.1.2 Defining Muscle Morphometry

The parameters required for the muscle model that are independent of fiber type and are specific to individual muscles are $F_0$, $L_0$, $L_0^T$ and $L_{max.}$ $L_0$ is the muscle fibre length at peak isometric active muscle force ($F_0$) as mentioned previously ($L_0$ and $F_0$ are specific to the muscle fascicles). $L_0^T$ is the length of muscle tendon at maximal tetanic isometric force and differs from the more commonly used tendon slack length ($L_S^T$) Zajac (1989). $L_S^T$ is less well defined than $L_0^T$ and tends to be around 5% shorter (Cheng et al., 2000). $L_{max}$ is the length of the muscle fascicles at the maximal anatomical length of the muscle.

The morphometric values required for the model are muscle mass, optimal fascicle length, optimal tendon length and the maximal anatomical musculotendon path length. These measures are then used either directly or to calculate the required parameters of the models equations. Optimal fascicle length and optimal tendon length correspond directly to $L_0$ and $L_0^T$. Muscle mass and fascicle length are used to derive the physiological cross-sectional area (PCSA) of the muscle, which is proportional to $F_0$. $L_{max}$ is calculated from the difference of the maximum whole-muscle length and the tendon $L_0^T$, scaled by muscle fascicle length $L_0$.

Mass and optimal fascicle length of most neck muscles have been reported by Kamibatashi and Richmond (1998). The muscle fascicle lengths reported were used for each of the sub-elements of a given muscle. Muscle mass was either divided equally between the sub-volumes or proportionally so as to give the required PCSA of the individual elements and the overall muscle. Optimal tendon length was approximated by using 105% of tendon slack length Cheng (2001). Tendon slack length was calculated as the difference between the musculotendon length at the neutral head position of the model and the muscle fascicle length, Kamibatashi and Richmond state that the measured muscle fascicle length in the neutral posture are within 15% of their optimal length. Values of maximal musculotendon path length have been chosen based on the

path length of the muscle elements in the head-neck model at extreme positions of the head so as to give values of $L_{max}$ between 1.1 and 1.42 (Cheng, 2001).

Once the specific morphometry of an individual muscle has been established the muscle must be apportioned to the relevant muscle fibre types. The histochemical composition of most neck muscles has been reported in the literature, table 4.6 shows the fibre type distribution for the neck muscles included in the model along with the source of reference. Finally the number of motor units that is to be used to simulate each fibre type in the muscle is specified. Normally a muscle has about 100 or more motor units. While it is possible to create such a detailed muscle model with Virtual Muscle, for the head-neck model where a large amount of muscles are being simulated, this resolution would make the model run very slowly and is not necessary. Here a small number of motor units are used where each unit represents a group of 'real' motor units. For example the Splenius Capitis consists of 37% slow- and 63% fast-twitch muscle fibres, with three motor units allocated to the slow-twitch portion and 5 motor units to the fast-twitch portion of the muscle.

**Table 4.6:** Histochemical composition of muscle fibre types in the muscles of the head-neck model.

| Muscle Name | Fibre Type Distribution/ Number of Motor Units | | Reference |
|---|---|---|---|
| | Slow-twitch | Fast-twitch | |
| Suboccipital | | | |
| Rectus capitis post. Major | 60% / 4 | 40% / 3 | a |
| Rectus capitis post. Minor | 60% / 4 | 40% / 3 | a |
| Obliquus capitis superior | 50% / 3 | 50% / 3 | a |
| Obliquus capitis inferior | 30% / 2 | 70% / 4 | a |
| Longissimus capitis | 33% / 2 | 67% / 4 | b |
| Longissimus cervicis | 45% / 3 | 55% / 3 | b |
| Splenius capitis | 37% / 2 | 63% / 4 | b |
| Splenius cervicis | 50% / 3 | 50% / 3 | a |
| Semispinalis capitis | 35% / 2 | 35% / 4 | b |
| Semispinalis cervicis | 35% / 2 | 35% / 4 | b |
| Scalenus | | | |
| Scalenus anterior | 29% / 2 | 71% / 4 | b |
| Scalenus medius | 29% / 2 | 71% / 4 | b |
| Scalenus posterior | 29% / 2 | 71% / 4 | b |
| Sternocleidomastoid | | | |
| Sternomastoid | 23% / 2 | 77% / 4 | b |
| Cleidomastoid | 23% / 2 | 77% / 4 | b |
| Cleido-occipital | 28% / 2 | 72% / 4 | b |
| Trapezius | 26% / 2 | 74% / 4 | b |
| Longus colli | 54% / 3 | 46% / 3 | c |
| Longus capitis | 40% 3 | 60% / 4 | d |
| Levator scapulae | 26% / 2 | 74% / 4 | d |
| Multifidus | 77% / 4 | 23% / 2 | c |

a. Winters and Woo [1990]
b. Richmond et al. [2001]
c. Boyd-Clark et al. [2001]
d. Estimated. Not present in the literature.

### 4.5.1.3 Musculotendon Blocks

Once fibre types have been selected and the morphometry of the individual muscle volumes and sub-volumes defined the stand-alone Simulink muscle blocks can be created. In total for the head-neck model there are 69 unique muscle blocks each repeated for the left and right symmetrical muscle elements. Each musculotendon block requires inputs for activation and for musculotendon path length. The output from the musculotendon element is force in Newtons. A schematic of the Simulink model for the Splenius Capitis is shown in figure 4.19.

It is assumed here that the activation input of a muscle is determined by a single neural input where the level of activation lies between 0 and 1, 0 for passive muscle and 1 for maximally activated muscle. For muscle activation it is assumed that the level of activation changes instantaneously from 0 to 1 after a certain onset/reflex delay. Reflex time is defined as the time it takes to start activating a muscle in reaction to an external disturbance, which in the case of a motor vehicle collision may be a visual signal, a loud noise, or impact induced motion. Reported reflex times for neck muscles range from 25 to 90 ms (Snyder et al., 1975, Reid et al., 1981, Ono et al., 1997, Brault et al., 2000).

The total length of each chain of connected actuators representing the individual muscle elements is read from VisualNastran at each time step of simulation and passed to Simulink as the input for musculotendon path length. This along with level of activation is used to calculate the muscle force which in turn is passed back to the head-neck model.

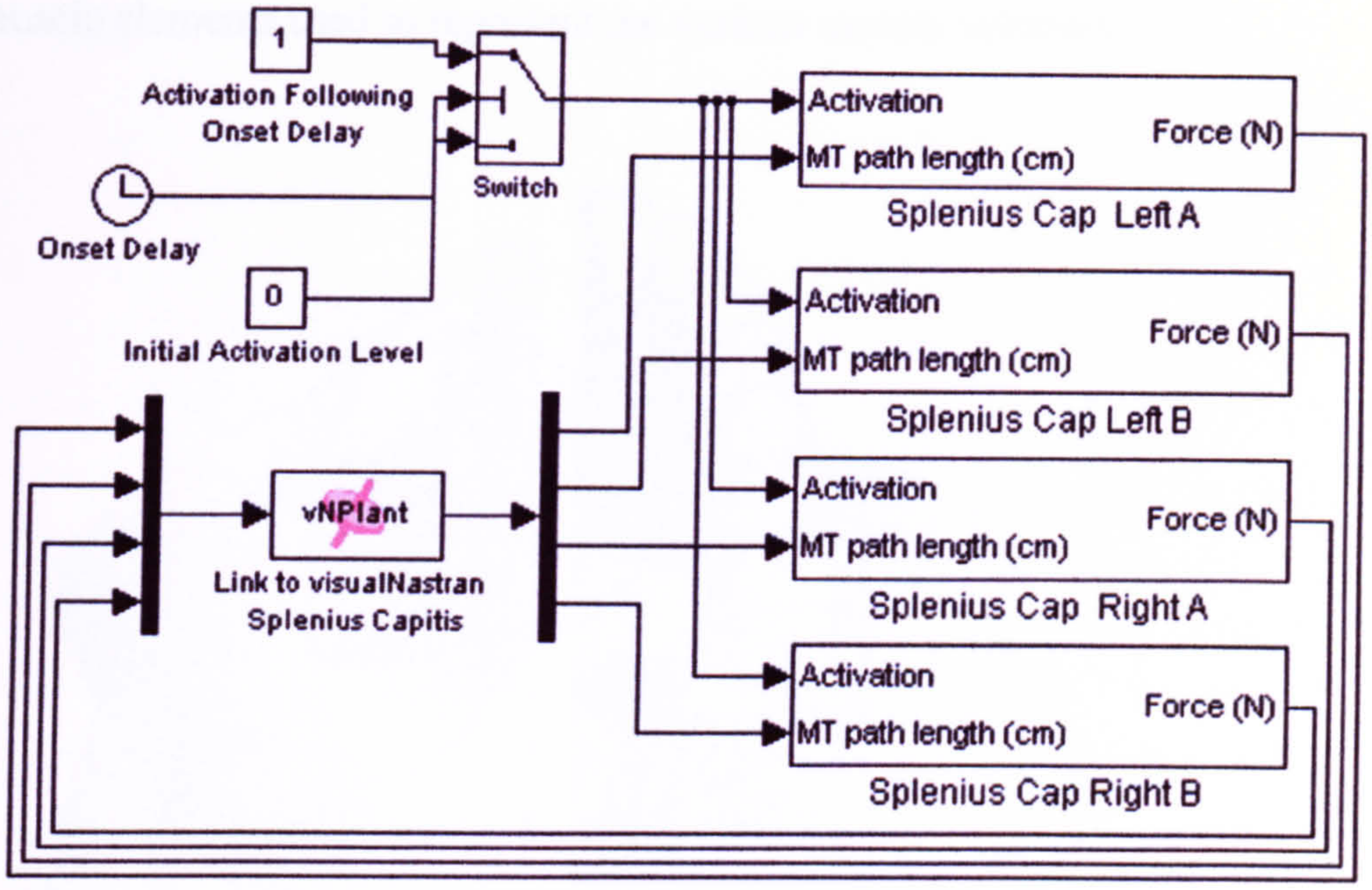


**Figure 4.19**: Simulink model for the Splenius Capitis muscle group. The switch is used to change the level of activation following a specified onset delay.

## 4.5.2 Muscle Descriptions and Sites of Attachment

The cervical vertebrae have been modelled in detail to include the bony anatomy that facilitates the location of attachment points of the muscle tendons. The three main areas of muscle attachment are to the tip of the spinous process, the tip of the transverse process and to the anterior tubercle of the transverse process. Muscles attaching to the anterior tubercle were positioned laterally at a distance of two thirds of the transverse process width in line with the anterior edge of the vertebral body.

A large number of the muscle groups of the neck make attachment to the skull. The positions of these attachments are important in controlling the movement of the head and neck. Figure 4.20 shows the positioning of the various muscle groups onto the skull along with an anatomical drawing of the same muscles and their attachment areas.

The following section describes each muscle group included in the head-neck model detailing the points of attachment and morphometric values of the muscle elements used to represent the various muscle volumes.

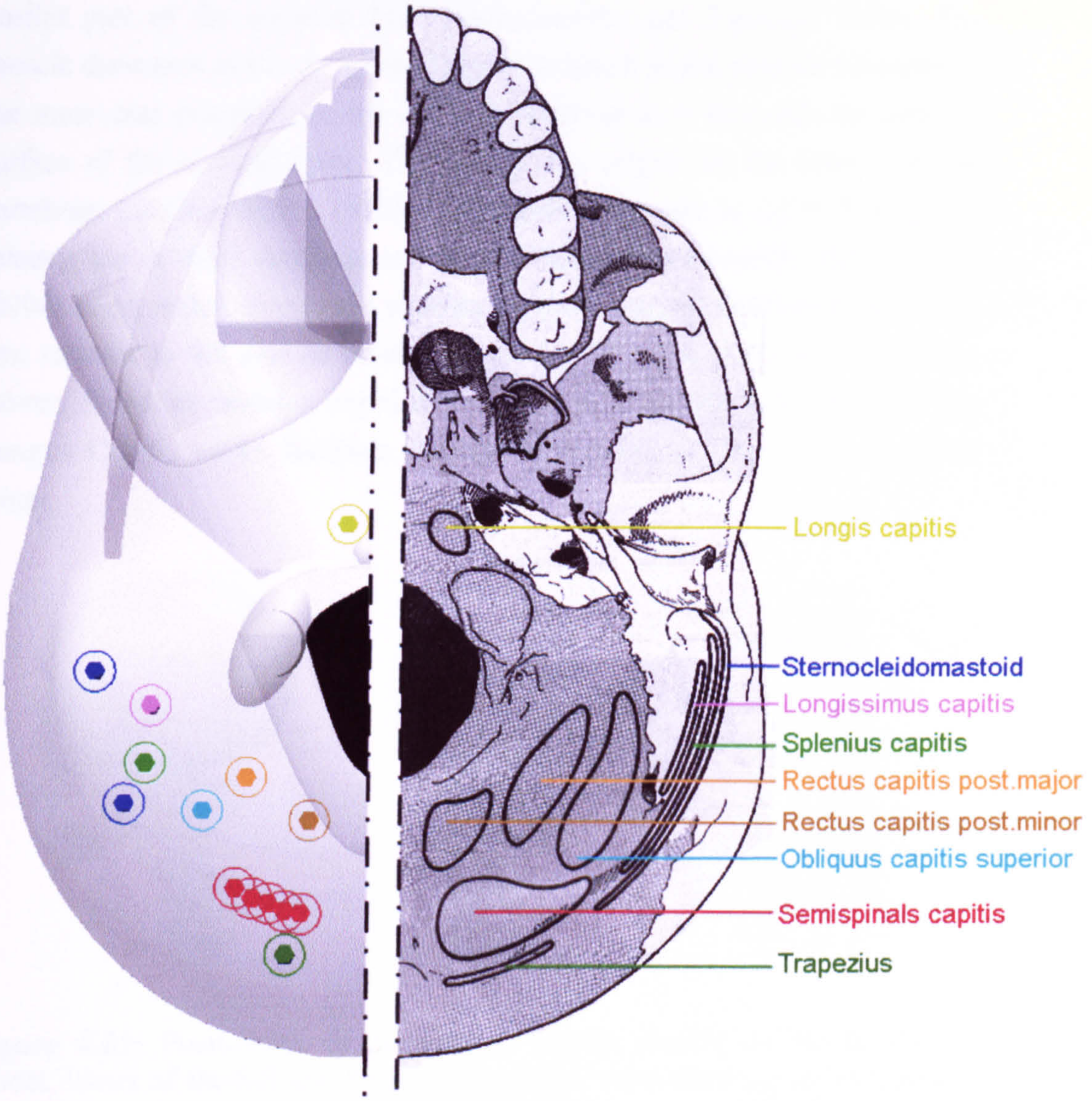


**Figure 4.20:** Muscle attachments to the skull. Left side: inferior surface of the right half of the base of the skull model showing points of attachment of muscle groups with insertions on the skull in the X-Y plane. Right side: outline drawing adapted from Gray (1980) showing attachments of muscle volumes.

### 4.5.2.1 Flexors

#### Longus Capitis

The longus capitis is a long fleshy muscle inserting on the inferior surface of basilar part of the occipital bone (Gurumoorthy and Twomey, 2000). The muscle decreases in size as it branches off to attach to the anterior tubercles of the transverse processes of the cervical vertebrae as it descends the anterior surface of the cervical spine. The muscle has origins on the lower cervical vertebrae, C3-C6 (Warfel, 1985). The muscle is thought to aid in flexing and rotating the cervical vertebrae and head although Gurumoorthy and Twomey (2000) suggest that, due to the muscles location, sites of attachment and lever arm relation to the axis of rotation of the C0-C1 joint, it cannot be a prime mover. However perhaps together with the other sub-occipital muscles the Longus Capitis could facilitate normal movements of the atlanto-occipital joints.

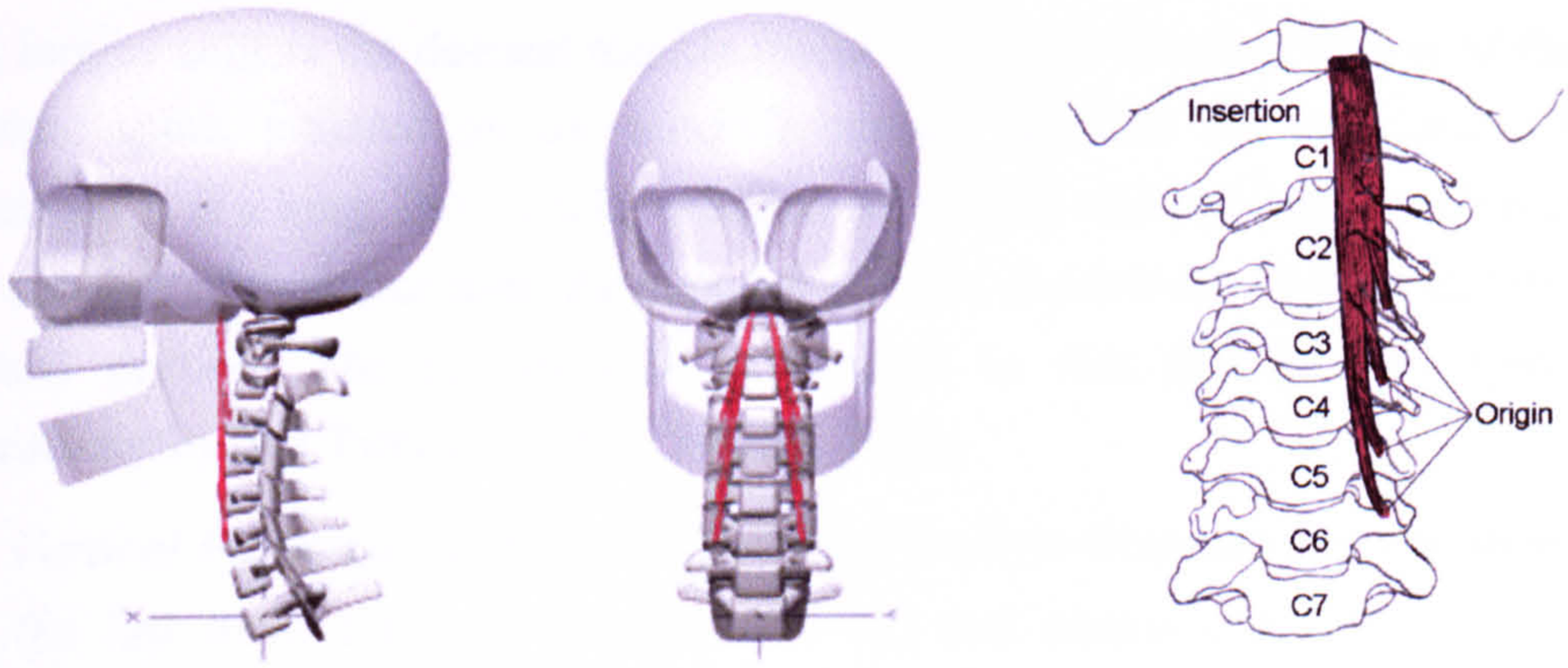


**Figure 4.21:** Positioning of the Longus Capitis muscle on the head-neck model, views of the left and front of the model. Also shown is an anatomical drawing describing the position and origins and insertions of the muscle on the cervical spine.

In the model the Longus Capitis muscle is split into four segments on each side of the neck; mid-sagittal symmetry is assumed. Morphometric parameters for the Longus Capitis have been reported by Kamibayashi and Richmond (1998). The overall mass of the muscle is divided amongst the individual

elements in proportion to the average fascicle length of each segment. Figure 4.21 shows the positioning of the muscle elements on the head-neck model along with an anatomical representation of the muscle showing the origins and insertion of the muscle on the cervical spine (adapted from Warfel, 1985). Table 4.7 shows the morphometric parameters of each muscle element of the Longus Capitis.

**Table 4.7:** Morphometric parameters of the Longus Capitis.

| **Muscle Name** | **Muscle mass (g)** | **OptFascicle Length (cm)** | **Muscle PCSA ($cm^2$)** | **Tendon $L_O^T$ (cm)** | **Whole muscle $L_{max}$ (cm)** | **Origin** | **Insertion** |
|---|---|---|---|---|---|---|---|
| **Longus capitis** | | | | | | | |
| A | 0.36 | 1.5 | 0.23 | 3.82 | 5.6 | C3 | C0 |
| B | 0.82 | 3.4 | 0.23 | 3.75 | 8.0 | C4 | C0 |
| C | 1.16 | 4.8 | 0.23 | 4.15 | 10.2 | C5 | C0 |
| D | 1.32 | 5.6 | 0.23 | 5.16 | 12.2 | C6 | C0 |
| **TOTAL** | **3.66** | | **0.92** | | | | |

## Longus Colli

The longus colli is the deepest muscle found in the pre-vertebral region of the cervical spine, situated on the anterior surface between the atlas and T3 vertebrae. It is a long, flat muscle, broad in the middle and pointed at each end and consists of three portions, the superior oblique, the inferior oblique and the vertical portion. The longus colli is thought to flex the cervical spine (Gurumoorthy and Twomey, 2000; Warfel, 1985)

The *Vertical Portion* arises from the bodies of the first three thoracic vertebrae and the last three cervical vertebrae (C5-T3) and inserts onto the anterior aspect of the body of C2, C3 and C4 vertebrae.

The *Superior Oblique* part of the muscle lies close to the longus capitis muscle with origin on the anterior tubercles of the transverse processes of the third, forth and fifth cervical vertebrae. It inserts into the tubercle on the anterior arch of the atlas.

The *Inferior Oblique* portion is attached to the anterior aspect of the first two or three thoracic vertebrae (T1-T3) and ascends to insert onto the anterior tubercles of the transverse processes of the fifth and sixth cervical vertebrae.

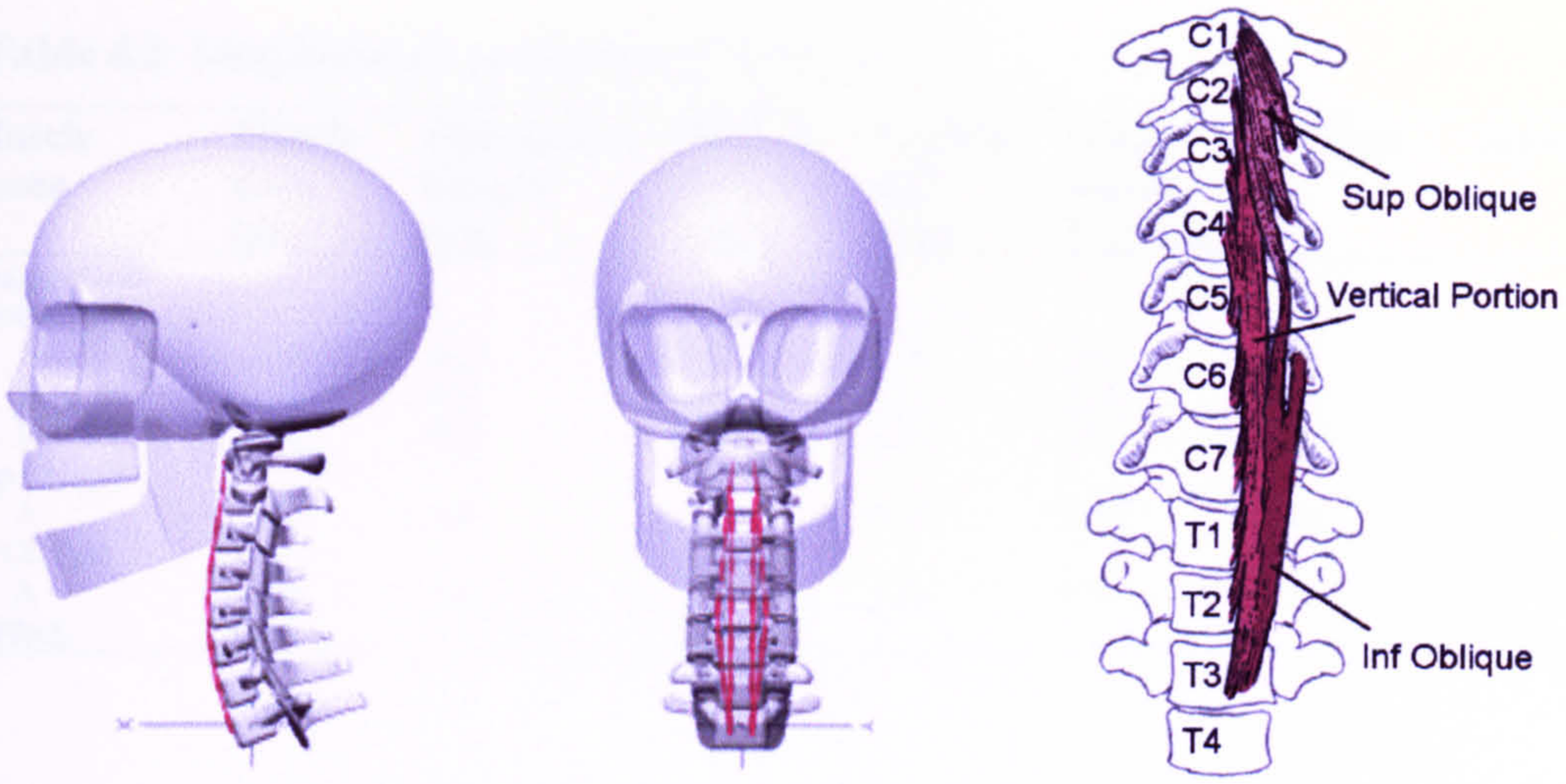


**Figure 4.22**: Positioning of the Longus Colli with respect to the head-neck model. Shown on the right: anatomical drawing showing the three sections of the muscle and their positioning on the spine.

In the model the longus colli is divided into a total of 5 individual muscle elements, 3 to represent the vertical portion and one each to represent the superior and inferior oblique portions. The vertical portion has a single origin on T1 (centre vertebrae between C5 and T3) with the three elements inserting onto C2, C3 and C4 respectively. The inferior oblique part takes the same origin position as the vertical portion on T1 and inserts at the position of the anterior tubercles of the transverse process of C5. From here arises the origin of the superior oblique portion, which inserts onto the anterior tubercle of the atlas. Figure 4.22 shows the approximated origins and insertions of the longus colli on the head-neck model and an anatomical drawing of the muscle adapted from Warfel (1985). No measured morphometric data for the longus colli could be obtained from the literature so the values were estimated based on other researches decisions (Vasavada et al., 1998; van der Horst, 2002) and on the morphometry of other muscles of the neck.

**Table 4.8**: Morphometric parameters of Longus Colli.

| Muscle Name | Muscle mass (g) | OptFascicle Length (cm) | Muscle PCSA ($cm^2$) | Tendon $L_O^T$ (cm) | Whole muscle $L_{max}$ (cm) | Origin | Insertion |
|---|---|---|---|---|---|---|---|
| **Longus Colli** | | | | | | | |
| Vertical | | | | | | | |
| A | 2.76 | 6.5 | 0.4 | 1.00 | 9.42 | T1 | C4 |
| B | 2.76 | 6.5 | 0.4 | 2.92 | 11.3 | T1 | C3 |
| C | 2.76 | 6.5 | 0.4 | 4.80 | 13.1 | T1 | C2 |
| Sup Oblique | | | | | | | |
| A | 1.53 | 3.6 | 0.4 | 3.72 | 8.24 | C5 | C1 |
| Inf Oblique | | | | | | | |
| A | 1.53 | 3.6 | 0.4 | 2.11 | 6.70 | T1 | C5 |
| **TOTAL** | **11.34** | | **2.0** | | | | |

## Scalenus: Anterior, Medius and Posterior

The three Scalenus muscles lie on either side of the anterior aspect of the cervical spine connecting the transverse processes of the middle and lower vertebrae to the first and second ribs.

The *Scalenus Anterior* takes its origin on the scalene tubercle of the first rib and inserts onto the transverse processes of C3 through C6.

The *Scalenus Medius*, arises from the posterior aspect of the first rib behind the subclavian artery inserting onto the transverse processes of C2 through C7.

The *Scalenus Posterior* arises from the superior border and lateral aspect of the second rib. It inserts via three tendinous slips onto the transverse processes of C4-C6.

Anatomical drawings of the Scalenus muscles are shown in figure 4.24 depicting the origins and insertions as described above.
The Scalenus muscles serve to flex the cervical column when contracted symmetrically. If contracted on just one side the Scalenus muscles produce lateral flexion and rotation towards the side of contraction.

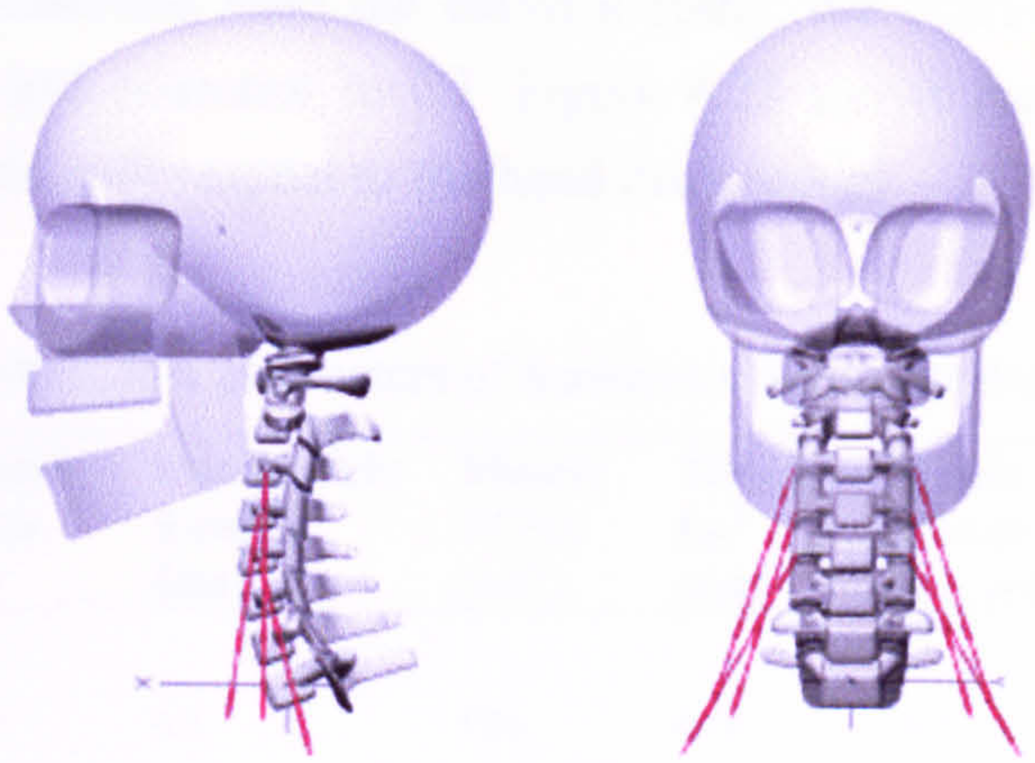

**Figure 4.23:** Positioning of the Scalenus Anterior, Medius, and Posterior muscle elements on the head-neck model.

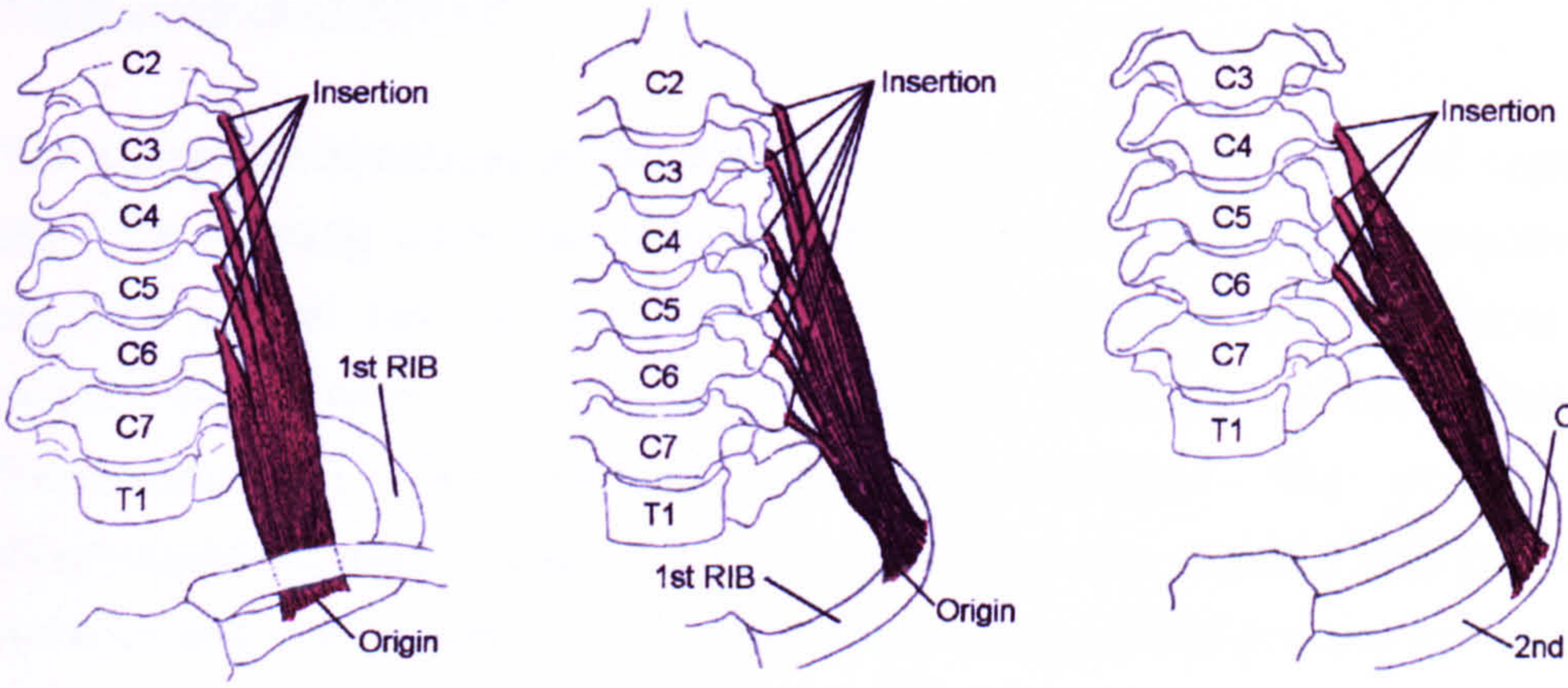


**Figure 4.24:** Anatomical drawings of the Scalenus muscles showing points of attachment to the ribs and cervical vertebra. From left to right, Scalenus Anterior, Scalenus Medius, Scalenus Posterior.

In the model each Scalenus muscle is represented by a single muscle element on each side of the neck. Kamibayashi and Richmond (1998) have reported the mass of each of the three muscles along with fascicle length and PCSA, these were used to define the morphometric parameters of the muscle elements (see table 4.9). The origins on the ribs are based on the above descriptions, anatomical drawings (Warfel, 1985; Gray, 1980) and decisions made by other

researchers (de Jager, 1996). It was decided that each Scalenus muscle would take just one insertion onto the cervical spine: the Scalenus anterior to C4, medius to C3 and posterior to C5. Figure 4.23 shows the positioning of the muscle elements with respect to the head neck model

**Table 4.9:** Morphometric parameters of Scalenus anterior, medius and posterior

| Muscle Name | Muscle mass (g) | OptFascicle Length (cm) | Muscle PCSA ($cm^2$) | Tendon $L_O^T$ (cm) | Whole muscle $L_{max}$ (cm) | Origin | Insertion |
|---|---|---|---|---|---|---|---|
| **Scalenus** | | | | | | | |
| **Anterior** | | | | | | | |
| A | 5.6 | 4.2 | 1.26 | 4.78 | 10.1 | 1st Rib | C4 |
| **Medius** | | | | | | | |
| A | 10.6 | 5.0 | 2.00 | 5.87 | 12.2 | 1st Rib | C3 |
| **Posterior** | | | | | | | |
| A | 10.6 | 6.2 | 1.61 | 3.54 | 11.5 | 2nd Rib | C5 |

## Sternocleidomastoid

The sternocleidomastoid is the strongest muscle in the pre-vertebral region of the neck running from the clavicle and sternum to the mastoid process and superior nuchal line on the skull. The sternocleidomastoid comprises four distinct bands with varying attachment points; these are the Sternomastoid, Sterno-occipital, Cleidomastoid and Cleido-occipital. The sternal head (Sternomastoid and Sterno-occipital) arises from the superior margin of the sternum and inserts onto the lateral surface of the mastoid process and onto the superior nuchal line. The clavicular head (Cleidomastoid and Cleido-occipital) has a much broader origin and insertion arising from the superior surface of the medial third of the clavicle and inserting onto the lateral surface of the mastoid process and along the superior nuchal line of the occiput. The anatomical drawing shown in figure 4.25 (adapted from Kapandji, 1974) depicts the four sub-volumes of the Sternocleidomastoid and its attachments to the sternum, clavicle and skull.

Contraction of the Sternocleidomastoid on both sides of the neck produces flexion in the cervical spine. Also these muscles can be used to produce flexion in the atlanto-occipital joints without flexion of the neck. Unilateral

contraction produces a triple movement of the head combining contralateral rotation, ipsilateral lateral bending and extension.

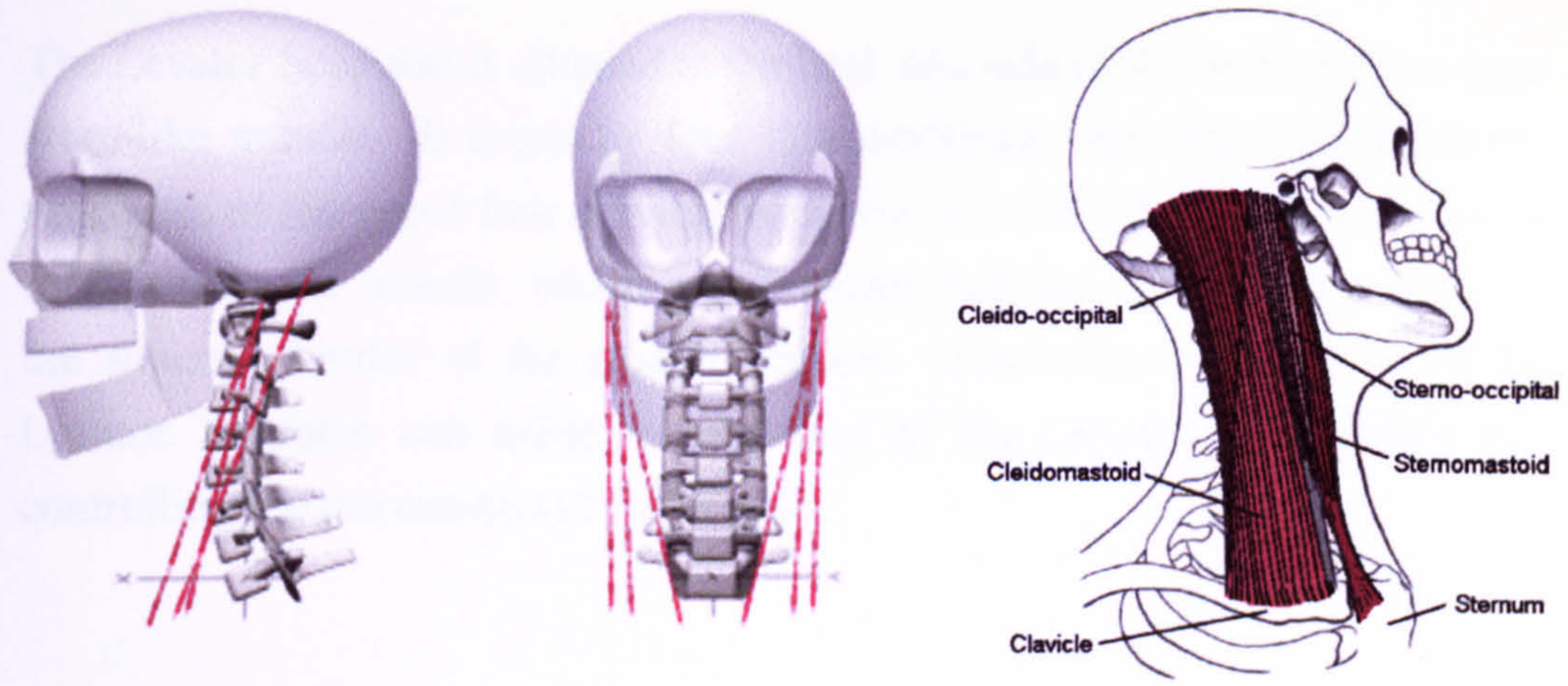


**Figure 4.25:** Positioning of the Sternocleidomastoid with respect to the head and neck model. Also shown is an anatomical drawing showing the four sub-volumes of the muscle and their attachments to the clavicle, sternum and skull.

In the model the Sternocleidomastoid is represented by three muscle elements on each side of the neck. The Sternomastoid and Sterno-occipital are represented by a single element due to their single origin on the sternum and close proximity on insertion (see figure 4.25). The Cleidomastoid and Cleido-occipital are represented individually each by a single muscle element, having origin and insertion as described above. Kamibayashi and Richmond (1998) reported total muscle mass for the Sternocleidomastoid and optimal fascicle lengths of the individual sub-volumes (table 4.10).

**Table 4.10:** Morphometric parameters of the Sternocleidomastoid.

| Muscle Name | Muscle mass (g) | OptFascicle Length (cm) | Muscle PCSA ($cm^2$) | Tendon $L_O^T$ (cm) | Whole muscle $L_{max}$ (cm) | Origin | Insertion |
|---|---|---|---|---|---|---|---|
| **Sterno-mastoid and occipital** | | | | | | | |
| A | 26.05 | 12.2 | 2.02 | 5.19 | 20.9 | Sternum | C0 |
| **Cleidomastoid** | | | | | | | |
| A | 7.18 | 12.0 | 0.56 | 3.71 | 19.3 | Clavicle | C0 |
| **Cleido-occipital** | | | | | | | |
| A | 7.18 | 11.0 | 0.62 | 7.32 | 21.4 | Clavicle | C0 |
| **TOTAL** | **40.41** | | **3.20** | | | | |

## 4.5.2.2 Extensors

### Levator Scapulae

The Levator Scapulae is situated at the back and side of the neck and is a large strap-like muscle. It arises by four thin tendinous slips from the transverse processes of the upper four cervical vertebrae, C1-C4. These four slips fuse to form a long flat muscle, which passes downward and outward to insert onto the superior border of the medial scapula. Symmetrical contraction of the Levator Scapulae can assist in extension of the cervical spine while also controlling the movements of the scapula.

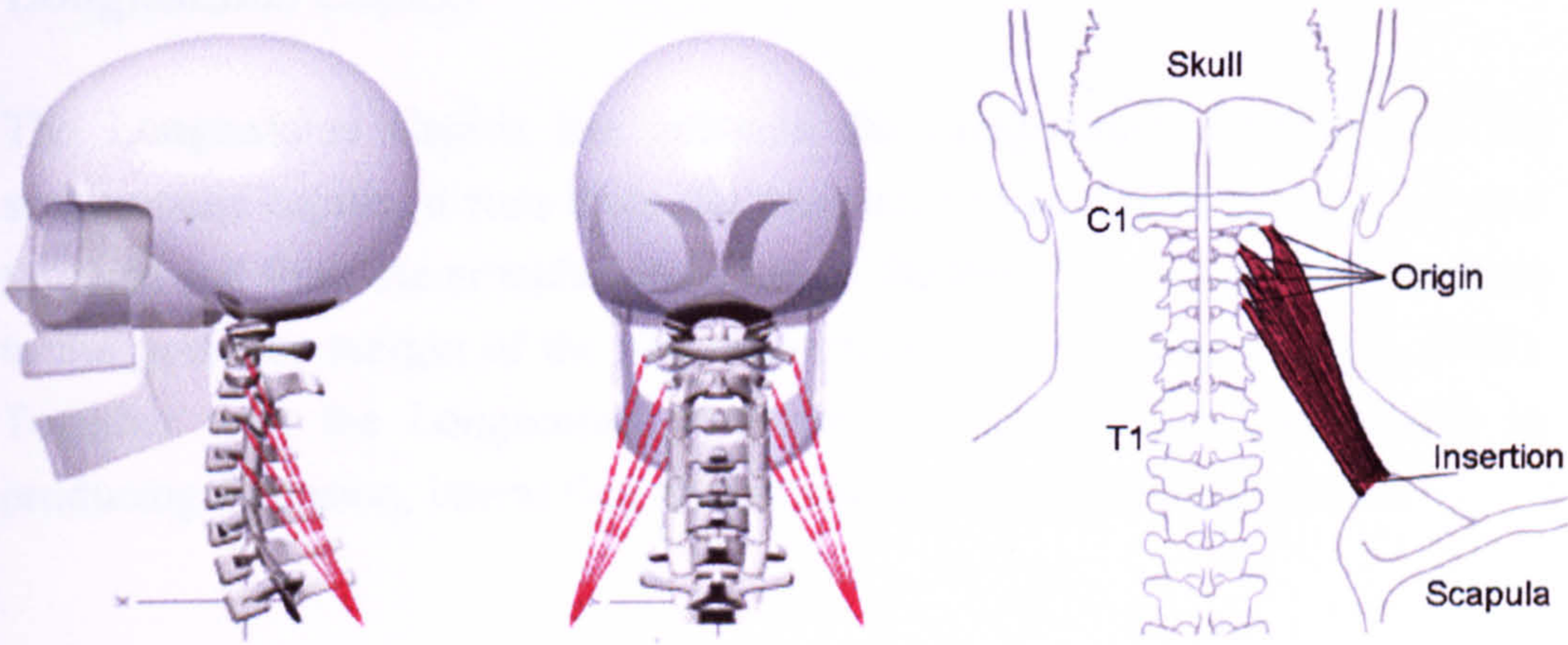


**Figure 4.26:** Positioning of the muscle elements representing the Levator Scapulae with respect to the head-neck model.

In the model the Levator Scapulae is represented by four muscle elements on each side of the neck. They have a single insertion positioned relative to T1 at the approximate location of the superior angle of the spine of the scapula (see figure 4.26), estimated from anatomical drawings and descriptions (Adams-Rouilly, 1992; Gray, 1980). The four muscle elements originate from the tips of the transverse processes of C1 through C4. Kamibayashi and Richmond (1998) reported the total mass of the Levator Scapulae along with the average optimal fascicle length for the muscle. The total mass was divided equally

between the four muscle elements with the same average fascicle length used for each, see table 4.11.

**Table 4.11:** Morphometric parameters of the Levator Scapulae.

| Muscle Name | Muscle mass (g) | OptFascicle Length (cm) | Muscle PCSA ($cm^2$) | Tendon $L_O^T$ (cm) | Whole muscle $L_{max}$ (cm) | Origin | Insertion |
|---|---|---|---|---|---|---|---|
| **Levator Scapulae** | | | | | | | |
| A | 6.15 | 10.3 | 0.56 | 4.68 | 17.9 | C1 | Scapula |
| B | 6.15 | 10.3 | 0.56 | 3.62 | 16.9 | C2 | Scapula |
| C | 6.15 | 10.3 | 0.56 | 2.40 | 15.7 | C3 | Scapula |
| D | 6.15 | 10.3 | 0.56 | 1.22 | 14.6 | C4 | Scapula |
| **TOTAL** | **24.60** | | **2.24** | | | | |

## Longissimus Capitis

The Longissimus Capitis lies between the Longissimus Cervicis and the semispinalis capitis, it runs from the transverse processes of the upper 4 or 5 thoracic and from the articular processes of the lower 3 or 4 cervical vertebrae to the posterior margin of the mastoid processes on the skull (Warfel, 1985). Together with the Longissimus Cervicis the Longissimus Capitis aids in producing extension, lateral flexion and rotation of the cervical column.

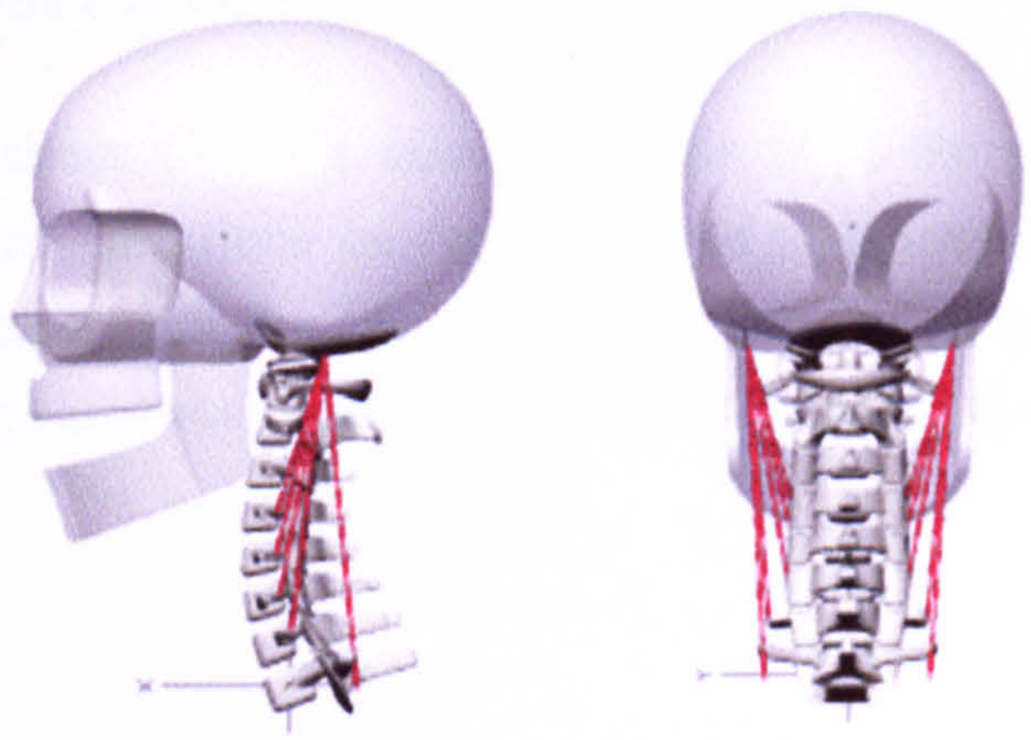

**Figure 4.27:** Positioning of the muscle elements representing the Longissimus Capitis.

In the model the Longissimus Capitis is represented by 5 individual muscle elements on each side of the neck. The first four elements have origins on the transverse processes of C4-C7 respectively, the final element having an origin positioned relative to T1 at the approximate location of the transverse process of T2. All five muscle elements share the same insertion point positioned on the skull (C0) at the location of the mastoid process (see figure 4.27). Very little data is available on the morphometric parameters of the Longissimus muscles so here they have been estimated based on other similar muscles of the neck (table 4.13). An optimal fascicle length of 6cm was chosen based on the initial length of the muscle elements and on the fascicle length chosen by Vasavada et al. (1998).

**Table 4.12**: Morphometric parameters of Longissimus Capitis

| Muscle Name | Muscle mass (g) | OptFascicle Length (cm) | Muscle PCSA ($cm^2$) | Tendon $L_O^T$ (cm) | Whole muscle $L_{max}$ (cm) | Origin | Insertion |
|---|---|---|---|---|---|---|---|
| **Longissimus Capitis** | | | | | | | |
| A | 1.04 | 6.0 | 0.16 | 1.09 | 8.85 | C4 | C0 |
| B | 1.04 | 6.0 | 0.16 | 2.71 | 10.40 | C5 | C0 |
| C | 1.04 | 6.0 | 0.16 | 4.26 | 11.90 | C6 | C0 |
| D | 1.04 | 6.0 | 0.16 | 5.64 | 13.20 | C7 | C0 |
| E | 1.04 | 6.0 | 0.16 | 7.97 | 15.43 | T2 | C0 |
| **TOTAL** | **5.20** | | **0.82** | | | | |

## Longissimus Cervicis

The Longissimus Cervicis takes its origin from the upper 4 or 5 thoracic vertebrae with insertions on the transverse processes of C2 to C6 (Warfel, 1985). Together with the Longissimus Capitis the Longissimus Cervicis aids in producing extension, lateral flexion and rotation of the cervical column.

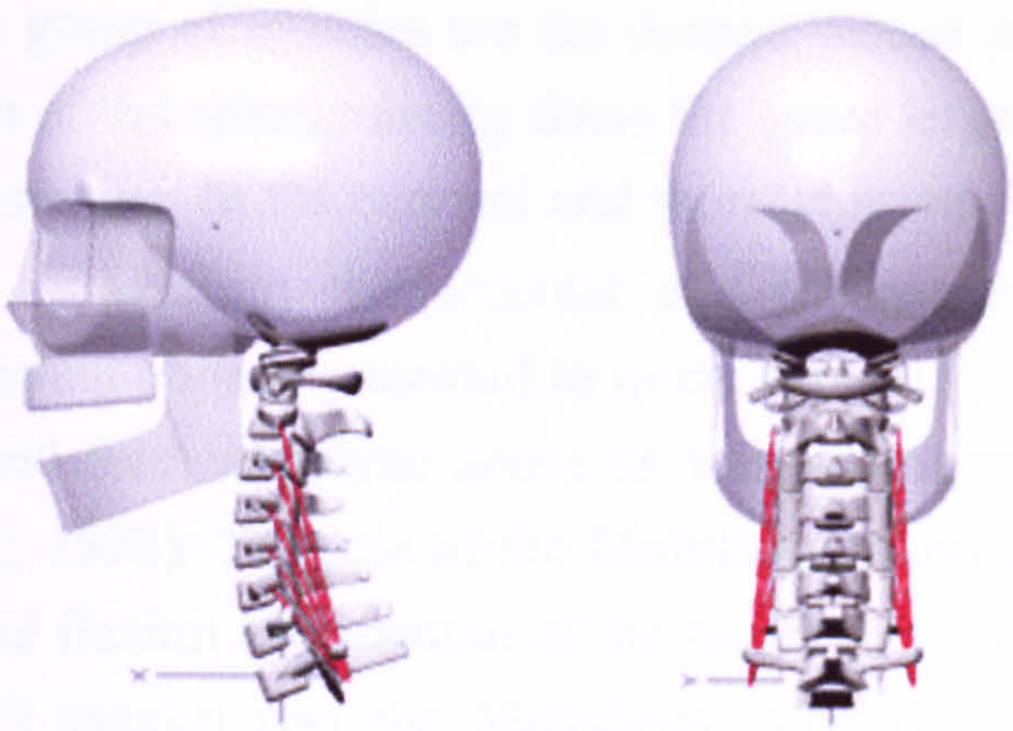

**Figure 4.28**: Positioning of the muscle elements representing the Longissimus Cervicis.

In the model the Longissimus Cervicis is represented by five muscle elements on each side of the neck originating from a point connected to T1 at the approximate position of the transverse process of T2 (see figure 4.28). The five elements insert into the transverse processes of C2 to C6. As was the case with the Longissimus Capitis very little data could be found on the morphometric parameters of the Longissimus Cervicis so here they have been estimated based on other similar muscles of the neck (table 4.13). An optimal fascicle length of 4.4cm was chosen based on the initial length of the muscle elements.

**Table 4.13**: Morphometric parameters of Longissimus Cervicis

| Muscle Name | Muscle mass (g) | OptFascicle Length (cm) | Muscle PCSA ($cm^2$) | Tendon $L_O^T$ (cm) | Whole muscle $L_{max}$ (cm) | Origin | Insertion |
|---|---|---|---|---|---|---|---|
| **Longissimus Cervicis** | | | | | | | |
| A | 1.16 | 4.4 | 0.25 | 6.76 | 12.20 | T2 | C2 |
| B | 1.16 | 4.4 | 0.25 | 5.26 | 10.76 | T2 | C3 |
| C | 1.16 | 4.4 | 0.25 | 3.75 | 9.31 | T2 | C4 |
| D | 1.16 | 4.4 | 0.25 | 2.28 | 7.91 | T2 | C5 |
| E | 1.16 | 4.4 | 0.25 | 0.79 | 6.50 | T2 | C6 |
| **TOTAL** | **5.80** | | **1.24** | | | | |

## Multifidus

The Multifidus group of muscles are the deepest placed muscles in the post-vertebral region of the spine, running down the entire length of the spine from the axis to the sacrum. In the cervical and thoracic region muscle fasciculi of varying length arise from the articular and transverse processes of the vertebrae, ascending obliquely upward to insert into the spinous process of the second, third and forth vertebrae above as well as connecting two adjacent vertebrae (Gray, 1970). The role of the Multifidus is thought to be in aiding extension, lateral flexion and rotation of the spinal column. Gurumoorthy and Twomey (2000) suggest that the Multifidus also helps control translatory movements of the facet joints.

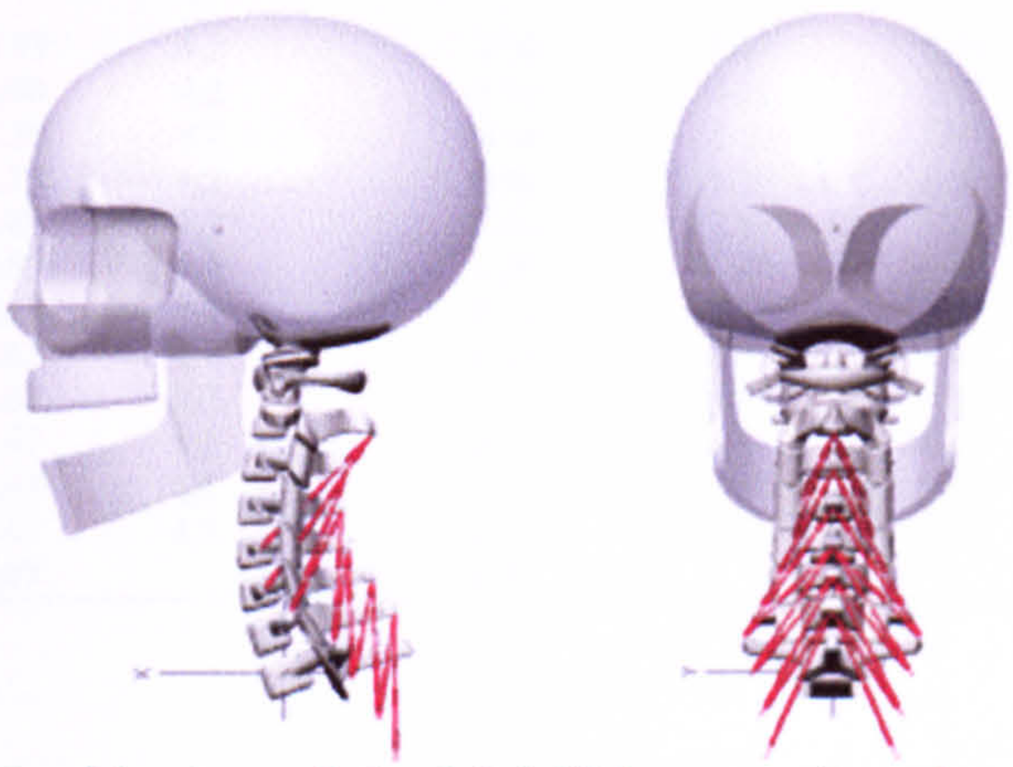

**Figure 4.29:** Positioning of the Multifidus muscles elements with respect to the head and cervical spine model.

In the model only the section of the Multifidus that has attachments to the cervical region of the neck are included. Also only the longer sections of the muscle which connect every third and forth vertebrae are included (see figure 4.29). So the first segment that makes attachment to the cervical spine has its origin on the transverse processes of T4 and inserts into the spinous process of C7. The next takes its origin on the transverse processes of T3 and splits to insert onto the spinous processes of C7 and C6; this is represented by two muscle elements in the model. From T2 transverse process two elements insert into C6 and C5 spinous processes. This pattern continues as far as C5 where

one element with origin on the articular process ascends obliquely inwards and upward to insert onto the spinous process of C2. In total there are 12 muscle elements representing the Multifidus muscle group on each side of the neck, the origin and insertion of each can be seen in table 4.14. There was no morphometric data available for the Multifidus muscle so the values were estimated based on other similar sized muscles in the neck and on other researches decisions. The optimal fascicle length was estimated to be 4.2 cm based on the lengths of the suboccipital muscles, which span similar distances as the elements of the Multifidus. The muscle mass of each element was then estimated so as to give PCSA's to match those used by van der Horst (2002).

**Table 4.14:** Morphometric parameters of Multifidus

| Muscle Name | Muscle mass (g) | OptFascicle Length (cm) | Muscle PCSA ($cm^2$) | Tendon $L_O^T$ (cm) | Whole muscle $L_{max}$ (cm) | Origin | Insertion |
|---|---|---|---|---|---|---|---|
| **Multifidus** | | | | | | | |
| A | 5.79 | 4.2 | 1 30 | 2.84 | 8 20 | T4 | C7 |
| B | 4 90 | 4.2 | 1 10 | 1.32 | 6 73 | T3 | C7 |
| C | 1.79 | 4.2 | 0.40 | 2.50 | 7 87 | T3 | C6 |
| D | 1.79 | 4.2 | 0.40 | 1.34 | 6 75 | T2 | C6 |
| E | 0.89 | 4.2 | 0.20 | 2.28 | 7 65 | T2 | C5 |
| F | 0.89 | 4.2 | 0 20 | 1.19 | 6 60 | T1 | C5 |
| G | 0.67 | 4.2 | 0 15 | 2.45 | 7.81 | T1 | C4 |
| H | 0 67 | 4.2 | 0.15 | 2 04 | 7 42 | C7 | C4 |
| I | 0.67 | 4.2 | 0.15 | 3.31 | 8 64 | C7 | C3 |
| J | 0.67 | 4 2 | 0.15 | 2.31 | 7.68 | C6 | C3 |
| K | 0.67 | 4.2 | 0.15 | 4 07 | 9 36 | C6 | C2 |
| L | 0 67 | 4 2 | 0.15 | 2.80 | 8 15 | C5 | C2 |
| **TOTAL** | **20.07** | | **4.50** | | | | |

## Semispinalis Capitis

The semispinalis capitis is a complex muscle with a broad insertion onto the occipital bone between the superior and inferior nuchal lines. The size and length of the muscle make it one of the strongest among the post-vertebral group of neck muscles. It has origins on the articular processes of the $4^{th}$ to $6^{th}$ cervical vertebrae as well as to the transverse processes of the upper 6 thoracic vertebrae and the $7^{th}$ cervical vertebra. Acting together the semispinalis capitis muscles produces extension in the atlanto-occipital joints while individual contraction extends the head with some degree of coupled rotation to the same side.

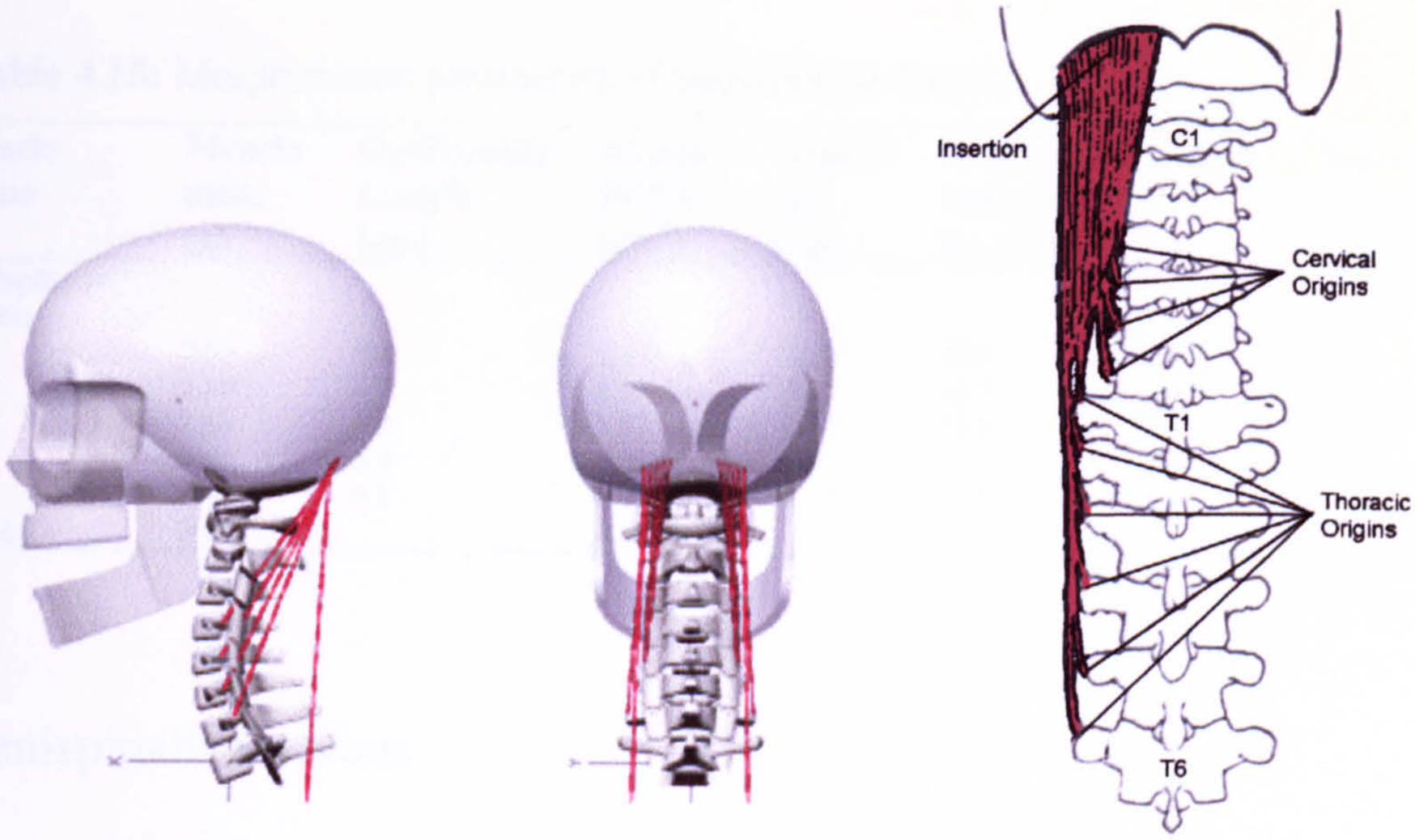


**Figure 4.30:** Positioning of the muscle elements representing the Semispinalis Capitis with respect to the head-neck model. Shown on the right: anatomical drawing showing actual origins and insertions of the muscle.

In the head-neck model the Semispinalis Capitis is represented by 5 muscle elements on each side of the neck. The section of muscle that has origins on the upper 6 thoracic vertebrae is represented by a single element with an origin at the estimated position of the transverse process of T3. The remaining part of the muscle is divided up into four elements one for each of the origins onto the transverse processes of C4-C7. All five muscle elements insert onto the occipital bone. Kamibayashi and Richmond (1998) report the total mass of the muscle to be 38.5g with the average fascicle length being 6.8cm. It was decided to evenly distribute the mass between the 5 muscle elements each having the same optimum fascicle length as no information on the proportioning of muscle mass across the muscle could be found. The morphometric parameters of the semispinalis capitis muscle elements are shown in table 4.15. Figure 4.30 shows the positioning of the muscle with respect to the head-neck model.

**Table 4.15:** Morphometric parameters of Semispinalis Capitis

| Muscle Name | Muscle mass (g) | OptFascicle Length (cm) | Muscle PCSA ($cm^2$) | Tendon $L_O^T$ (cm) | Whole muscle $L_{max}$ (cm) | Origin | Insertion |
|---|---|---|---|---|---|---|---|
| **Semispinalis Capitis** | | | | | | | |
| A | 7.68 | 6.8 | 1.07 | 3.72 | 12.4 | C4 | C0 |
| B | 7.68 | 6.8 | 1.07 | 5.05 | 13.7 | C5 | C0 |
| C | 7.68 | 6.8 | 1.07 | 6.30 | 14.9 | C6 | C0 |
| D | 7.68 | 6.8 | 1.07 | 7.43 | 16.0 | C7 | C0 |
| E | 7.68 | 6.8 | 1.07 | 10.43 | 18.8 | T3 | C0 |
| **TOTAL** | **38.4** | | **5.32** | | | | |

## Semispinalis Cervicis

The semispinalis cervicis arises from the transverse processes of the upper 5 thoracic vertebrae and inserts onto the spinous processes of C2 through C6. Branches of the upper section of the semispinalis thoracis also make attachments to the cervical vertebrae and so are included in the model. The semispinalis thoracis has origins on the transverse processes on the lower thoracic vertebrae and insert onto the spinous processes of the first 4 thoracic vertebrae and onto the last 2 cervical vertebrae (see figure 4.32), only the upper section which makes attachments to the cervical vertebrae are included in the model.

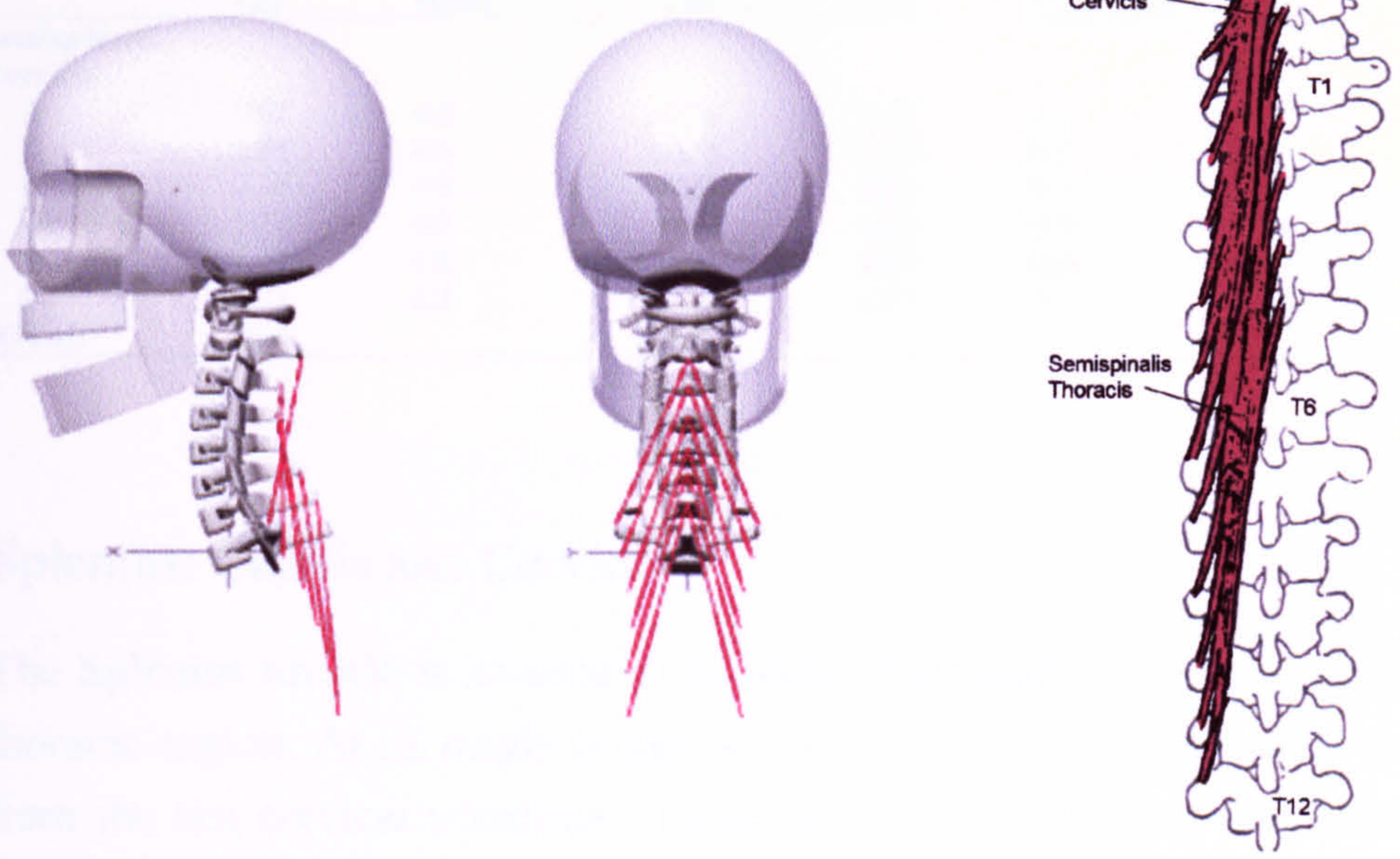


**Figure 4.31:** Positioning of the Semispinalis Cervicis muscle elements with respect to the head-neck model. Shown on the right is an anatomical drawing of the Semispinalis Cervicis and Thoracis.

In the model this muscle group is divided into 6 muscle elements on each side of the neck. The first element has its origin on the transverse process of T1 and ascends to insert onto the spinous process of C2, the remaining elements each have origin on the transverse processes of the next thoracic vertebrae down inserting on the spinous process of the 5$^{th}$ vertebrae superior to the vertebrae of origin, i.e. T1 goes to C2, T2 goes to C3, T3 goes to C4 and so on (see figure 4.31). The position of the transverse processes of the thoracic vertebrae below the level of T1 are estimated from anatomical drawings and quantitative data found in the literature (Adam-Rouilly, 1992; Panjabi et al., 1991). Kamibayashi and Richmond (1998) failed to include the semispinalis cervicis in their study of neck muscle morphometry so the values used here are based on other researches decisions (van der Horst, 1997). The same optimal fascicle length as that of the semispinalis capitis was used and the mass of the individual elements was estimated to give PCSA's similar to those used by van der Horst (2002). The resulting morphometric values used for the muscle elements can be seen in table 4.16.

**Table 4.16:** Morphometric parameters of Semispinalis Cervicis

| Muscle Name | Muscle mass (g) | OptFascicle Length (cm) | Muscle PCSA ($cm^2$) | Tendon $L_O^T$ (cm) | Whole muscle $L_{max}$ (cm) | Origin | Insertion |
|---|---|---|---|---|---|---|---|
| **Semispinalis Cervicis** | | | | | | | |
| A | 0.92 | 6.8 | 0.13 | 2.76 | 11.5 | T1 | C2 |
| B | 1.84 | 6.8 | 0.26 | 2.76 | 11.5 | T2 | C3 |
| C | 2.76 | 6.8 | 0.38 | 2.86 | 11.6 | T3 | C4 |
| D | 5.77 | 6.8 | 0.80 | 3.10 | 11.8 | T4 | C5 |
| E | 7.21 | 6.8 | 1.00 | 4.45 | 12.8 | T5 | C6 |
| F | 7.93 | 6.8 | 1.10 | 4.97 | 13.6 | T6 | C7 |
| **TOTAL** | **26.4** | | **3.67** | | | | |

## Splenius: Capitis and Cervicis

The Splenius muscle is situated at he back of the neck and upper part of the thoracic region. At its origin it can be considered as a single muscle arising from the last cervical vertebrae C7 and the upper six thoracic vertebrae (T1-T6). From this origin the muscle precedes obliquely upward and outwards dividing into two sections, the Splenius capitis and the Splenius cervicis.

The ***Splenius Capitis*** inserts into the superior nuchal line and mastoid process.

The ***Splenius Cervicis*** inserts into the posterior tubercles of the transverse processes of the upper three cervical vertebrae (C1-C3).

The muscle is thought to work in conjunction with the semispinalis capitis to extend the head and with part of the sternocleidomastoid to rotate the head (Gurumoorthy and Twomey, 2000).

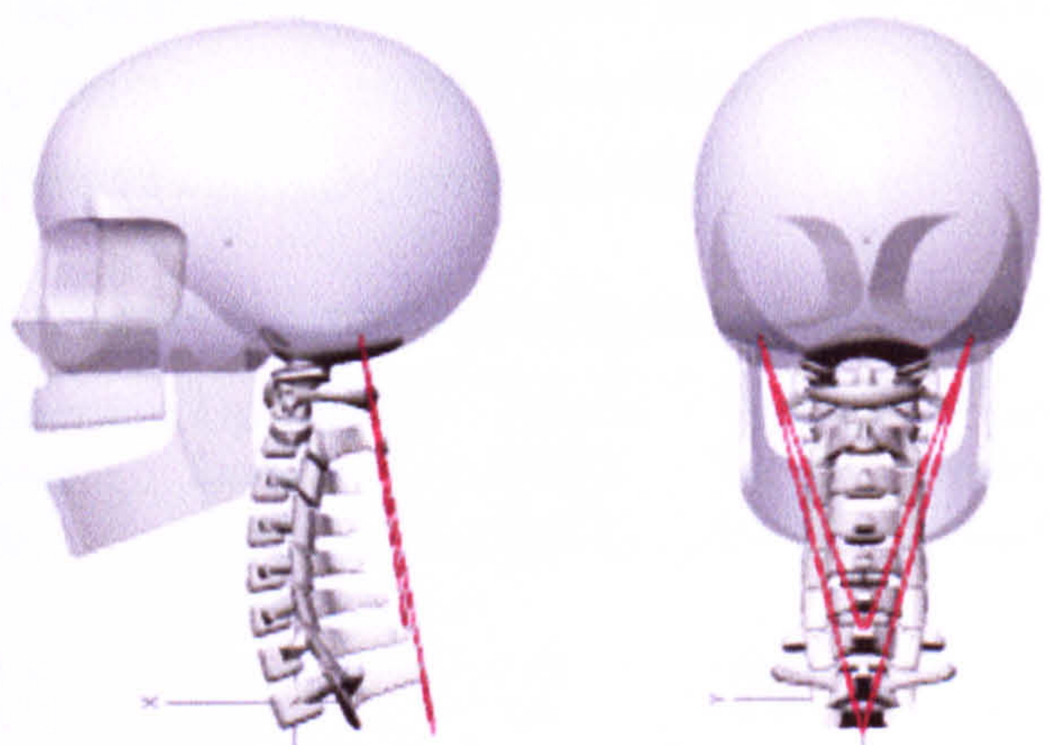

**Figure 4.32**: Positioning of the Splenius Capitis with respect to the head-neck model.

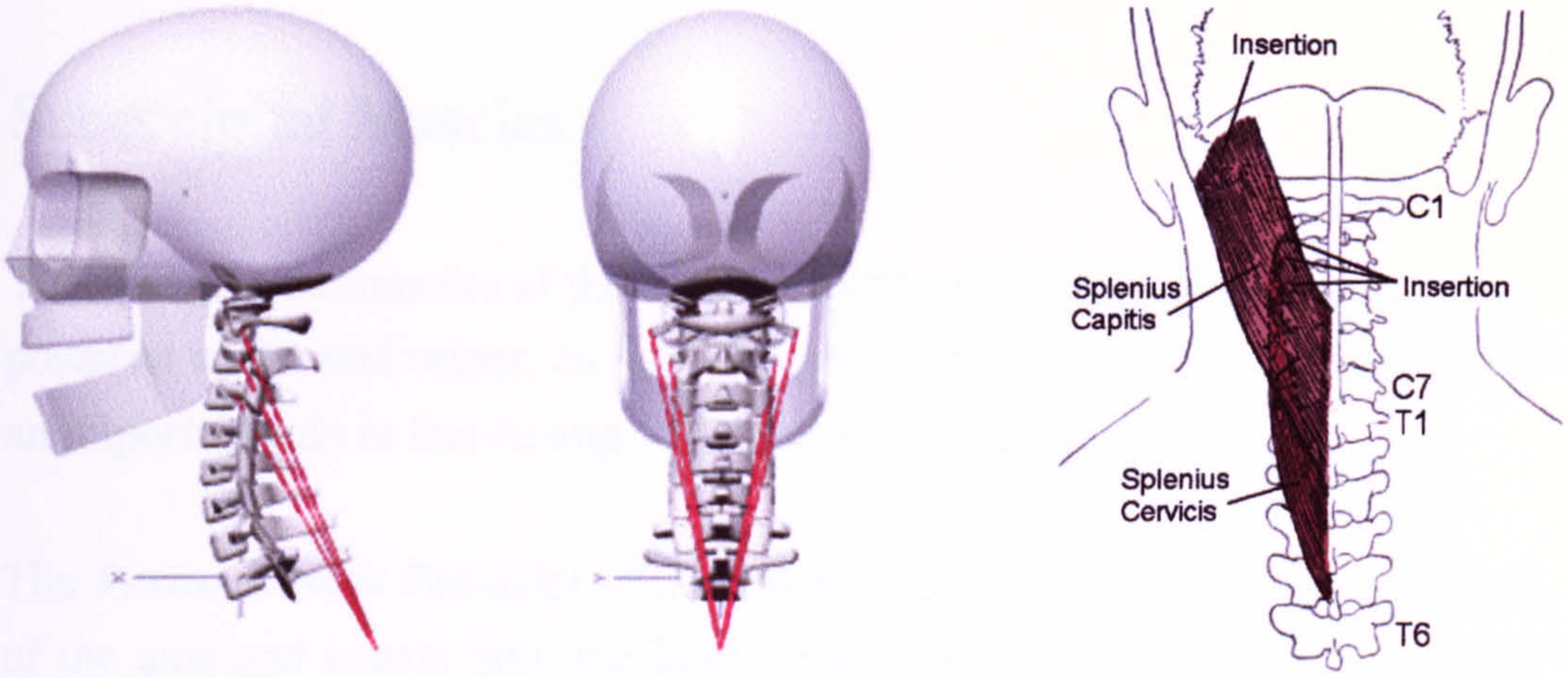


**Figure 4.33**: Positioning of the Splenius Cervicis with repect to the head-neck model. Also shown is an anatomical drawing of the Splenius capitis and cervicis showing the points of attachment to the head and spine.

In the model the Splenius muscle is represented by 5 muscle elements on each side of the neck, two for the Splenius capitis and three for the Splenius cervicis (see figures 4.32 and 4.33). The Splenius capitis elements have origins on the spinous processes of C7 and T2 and insert onto the skull positioned between the mastoid process and the lateral part of the superior nuchal line. The Splenius cervicis elements have a single origin positioned on the spinous process of T3 with insertions on the transverse processes of C1, C2 and C3. Kamibayashi and Richmond (1998) report a single weight of 42.9g for the entire Splenius muscle but give the optimal fascicle lengths for the Splenius and Cervicis separately. It was decided (based on Vasavada et al., 1998) to proportion the mass of the muscle two-thirds to the Splenius capitis and one-third to the Splenius cervicis (see table 4.17).

**Table 4.17**: Morphometric parameters of Splenius Capitis and Cervicis

| Muscle Name | Muscle mass (g) | OptFascicle Length (cm) | Muscle PCSA ($cm^2$) | Tendon $L_O^T$ (cm) | Whole muscle $L_{max}$ (cm) | Origin | Insertion |
|---|---|---|---|---|---|---|---|
| **Splenius Capitis** | | | | | | | |
| A | 14.30 | 8.6 | 1.57 | 8.40 | 19.3 | T2 | C0 |
| B | 14.30 | 8.6 | 1.57 | 4.45 | 15.5 | C7 | C0 |
| **Splenius Cervicis** | | | | | | | |
| A | 4.77 | 9.3 | 0.48 | 8.04 | 19.8 | T3 | C1 |
| B | 4.77 | 9.3 | 0.48 | 6.47 | 18.3 | T3 | C2 |
| C | 4.77 | 9.3 | 0.48 | 5.09 | 17.0 | T3 | C3 |
| **TOTAL** | **42.91** | | **4.58** | | | | |

## Suboccipital Muscles

The suboccipital muscles of the cervical spine, comprising of the rectus capitis posterior major and minor, and the obliquus capitis superior and inferior, play an important role in fine-tuning the movements of the head

The ***Rectus Capitis Posterior Major*** takes its origin from the spinous process of the axis and inserts onto the lateral part of the inferior nuchal line of the occipital bone. Contraction of both muscles produces extension of the atlanto-occipital joint, with unilateral contraction producing ipsilateral rotation of the head.

The ***Rectus Capitis Posterior Minor*** is smaller than the major lying closer to the midline of the spine and attaching to the medial third of the inferior nuchal line between the rectus Capitis posterior major muscles. Its origin is to the tubercle on the posterior arch of the atlas.

The ***Obliquus Capitis Inferior*** connects the spinous process of the axis to the transverse process of the atlas. This muscle is considered to produce ipsilateral rotation of the atlas. When acting together these muscles aid in stabilizing the atlas by bringing together the atlanto-axial joints in order to allow movements in the atlanto-occipital joints (Gurumoorthy and Twomey, 2000).

The ***Obliquus Capitis Superior*** arises from the superior aspect of the transverse process of the atlas running superiorly and posteriorly to attach to the lateral third of the inferior nuchal line. Contraction of these muscles is thought to produce extension of the atlanto-occipital joints.

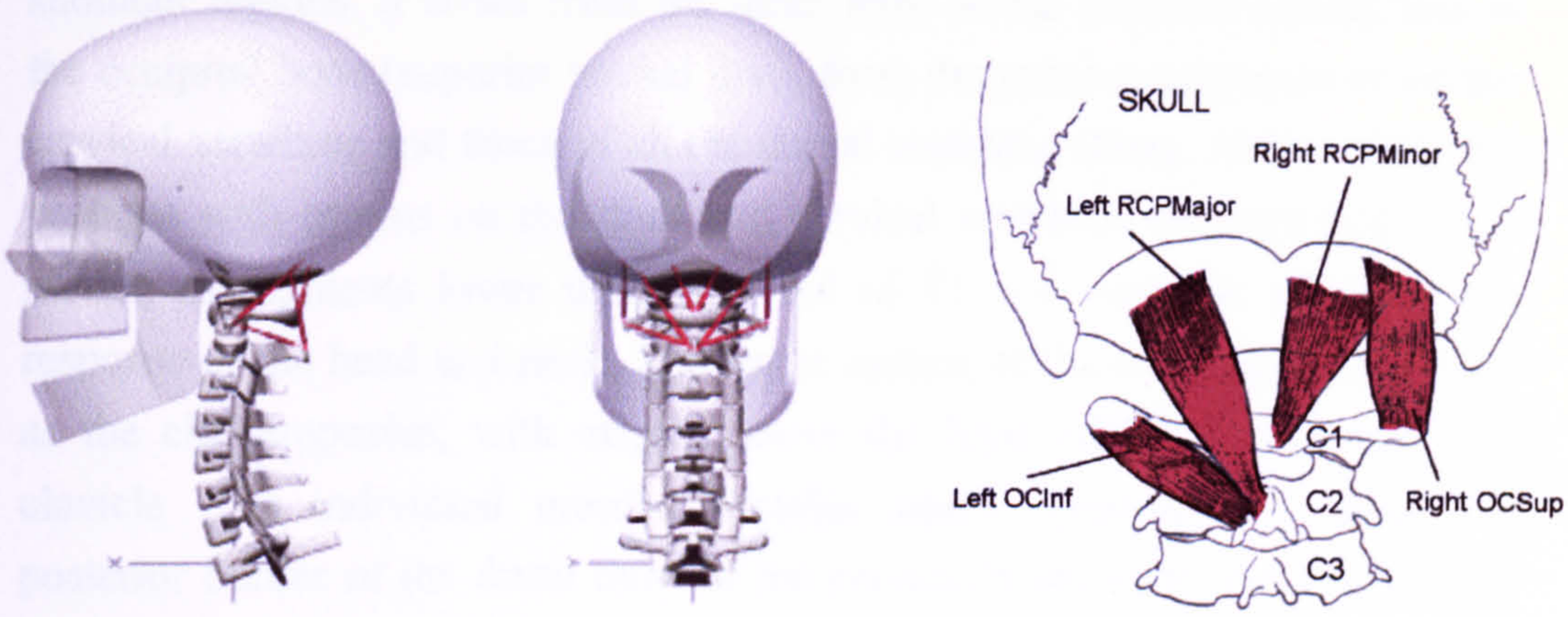


**Figure 4.34:** Positioning of the suboccipital muscles on the head-neck model. Shown on the right is an anatomical drawing of the suboccipital muscles and their attachments to the skull and vertebrae (each muscle will appear twice, one on each side of the mid-line of the spine, however each is only shown once here for clarity).

In the head-neck model each of the suboccipital muscles is represented by a single individual muscle element due to their short lengths and close proximity to the bony anatomy of the spine. The morphometric parameters shown in table 4.18 were taken from Kamibayashi and Richmond (1998). The origins and insertions of each of the muscles are as described above and are shown in figure 4.34.

**Table 4.18**: Morphometric parameters of the Suboccipital muscles.

| Muscle Name | Muscle mass (g) | OptFascicle Length (cm) | Muscle PCSA ($cm^2$) | Tendon $L_O^T$ (cm) | Whole muscle $L_{max}$ (cm) | Origin | Insertion |
|---|---|---|---|---|---|---|---|
| **RCPMajor** | | | | | | | |
| A | 3.5 | 3.7 | 0.89 | 1.01 | 5.8 | C2 | C0 |
| **RCPMinor** | | | | | | | |
| A | 1.0 | 1.9 | 0.49 | 0.80 | 3.25 | C1 | C0 |
| **OCSup** | | | | | | | |
| A | 2.5 | 2.5 | 0.94 | 2.25 | 5.1 | C1 | C0 |
| **OCInf** | | | | | | | |
| A | 5.1 | 3.8 | 1.23 | 1.21 | 6.11 | C2 | C1 |

## Trapezius

The trapezius muscle is a large prominent muscle in the cervical, thoracic and shoulder regions. It arises from the inner third of the superior curved line of the occipital bone (superior nuchal line), from the spinous processes of all the cervical vertebrae and those of all the dorsal vertebrae (Gray, 1980) . Only the portions with origins on the skull and cervical vertebrae are included in the model, as segments lower than the level of T1 will have no effect on the response of the head and neck. The upper section of the trapezius also known as the clavotrapezius, with origins above the level of C7, inserts onto the clavicle. The individual muscle fascicles attach systematically along the posterior border of the distal third of the clavicle bone, such that the fascicle from the superior nuchal line assumes the most anterior and medial attachment, followed in sequence by the fascicle from the spinous processes of the descending vertebrae, with the fibres from C6 inserting into the distal corner of the clavicle as far as the acromioclavicular joint (Johnson et al. (1994). The middle part of the trapezius (lower part in model), also known as the acromiotapezius, with origin on the C7 spinous process inserts on to the scapula on the inner border of the acromion.

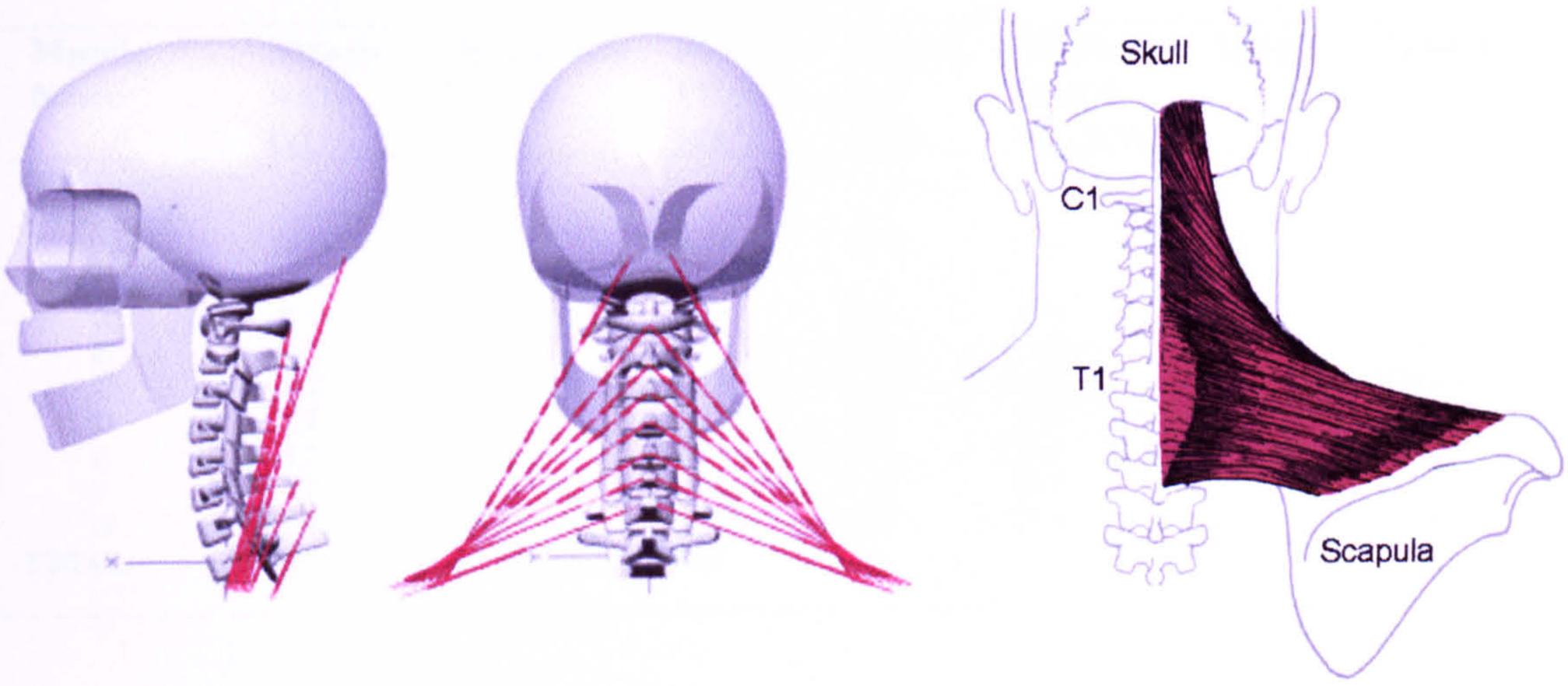


**Figure 4.35**: Positioning of the trapezius muscle showing origins on the head and spine and insertions relative to T1 at the approximate location of the clavicle and scapula. Also shown is an anatomical drawing of the upper section of the Trapezius muscle, showing attachments to the spine, skull and scapula.

The trapezius is a very powerful muscle that aids in stabilising the head and cervical column. When the trapezius muscles on both sides of the neck contract simultaneously they extend the cervical spine. When this extension is counterbalanced by the anterior muscles of the neck, it creates a bracing effect throughout the entire cervical spine. When the trapezius muscle on only one side of the neck contracts the cervical spine extends along with a contralateral rotation of the head along with a lateral bending of the neck in the direction of the contracting muscle (Kapandji, 1974).

In the model the trapezius muscle is split into 8 separate muscle elements with origins and insertions as described above (see figure 4.35). Positions of insertions onto the clavicle and scapular are based on anatomical drawings and descriptions in the literature, positioned relative to the T1 coordinate system. Johnson et al. (1994) in a detailed study of the trapezius muscle have reported fascicle length, PCSA and maximum force of each section of the muscle. Values for muscle mass were estimated so as to give the correct PCSA for each segment. The morphometric parameters used for the trapezius are shown in table 4.19.

**Table 4.19:** Morphometric parameters of Trapezius.

| Muscle Name | Muscle mass (g) | OptFascicle Length (cm) | Muscle PCSA ($cm^2$) | Tendon $L_O^T$ (cm) | Whole muscle $L_{max}$ (cm) | Origin | Insertion |
|---|---|---|---|---|---|---|---|
| **Trapezius** | | | | | | | |
| Acromiotrap | | | | | | | |
| A | 19.6 | 8.4 | 2.20 | 5.64 | 16.4 | C7 | Scapula |
| Clavotrap | | | | | | | |
| A | 6.9 | 8.4 | 0.77 | 6.95 | 17.6 | C6 | Clavicle |
| B | 6.9 | 8.4 | 0.77 | 6.92 | 17.6 | C5 | Clavicle |
| C | 6.9 | 8.4 | 0.77 | 7.30 | 17.9 | C4 | Clavicle |
| D | 2.7 | 11.0 | 0.23 | 5.25 | 19.4 | C3 | Clavicle |
| E | 2.7 | 11.0 | 0.23 | 5.97 | 20.1 | C2 | Clavicle |
| F | 2.7 | 11.0 | 0.23 | 7.12 | 21.2 | C1 | Clavicle |
| G | 3.5 | 11.0 | 0.30 | 9.89 | 23.8 | C0 | Clavicle |
| **TOTAL** | **51.9** | | **5.50** | | | | |

## 4.5.3 Muscle Curving and Force Application

Individual muscle elements that span more than one of the cervical vertebrae are represented by a chain of connected actuators leading from the point of origin to insertion to allow curving of the muscle around the vertebrae. In the initial upright head-neck position each muscle element is straight, connecting origin to insertion, a series of intermediate points are positioned on the local x-y plane of each successive vertebrae that the muscle spans (see figure 4.36a). Actuators connect adjacent points to form the muscle; it is the combined length of this chain of actuators that gives the overall length of the muscle that is used to calculate muscle force. As the neck bends the intermediate points stay fixed to their respective vertebrae and so force the chain of actuators to bend around the vertebrae (see figure 4.36b) resulting in the new overall length of the muscle. The resulting muscle force is applied at both the origin and insertion of the muscle element in the direction of the first and last actuators, effectively at a tangent to the curve of the muscle (see figure 4.36b). Figure 4.37 shows the final head and neck model with all the muscle elements in place.

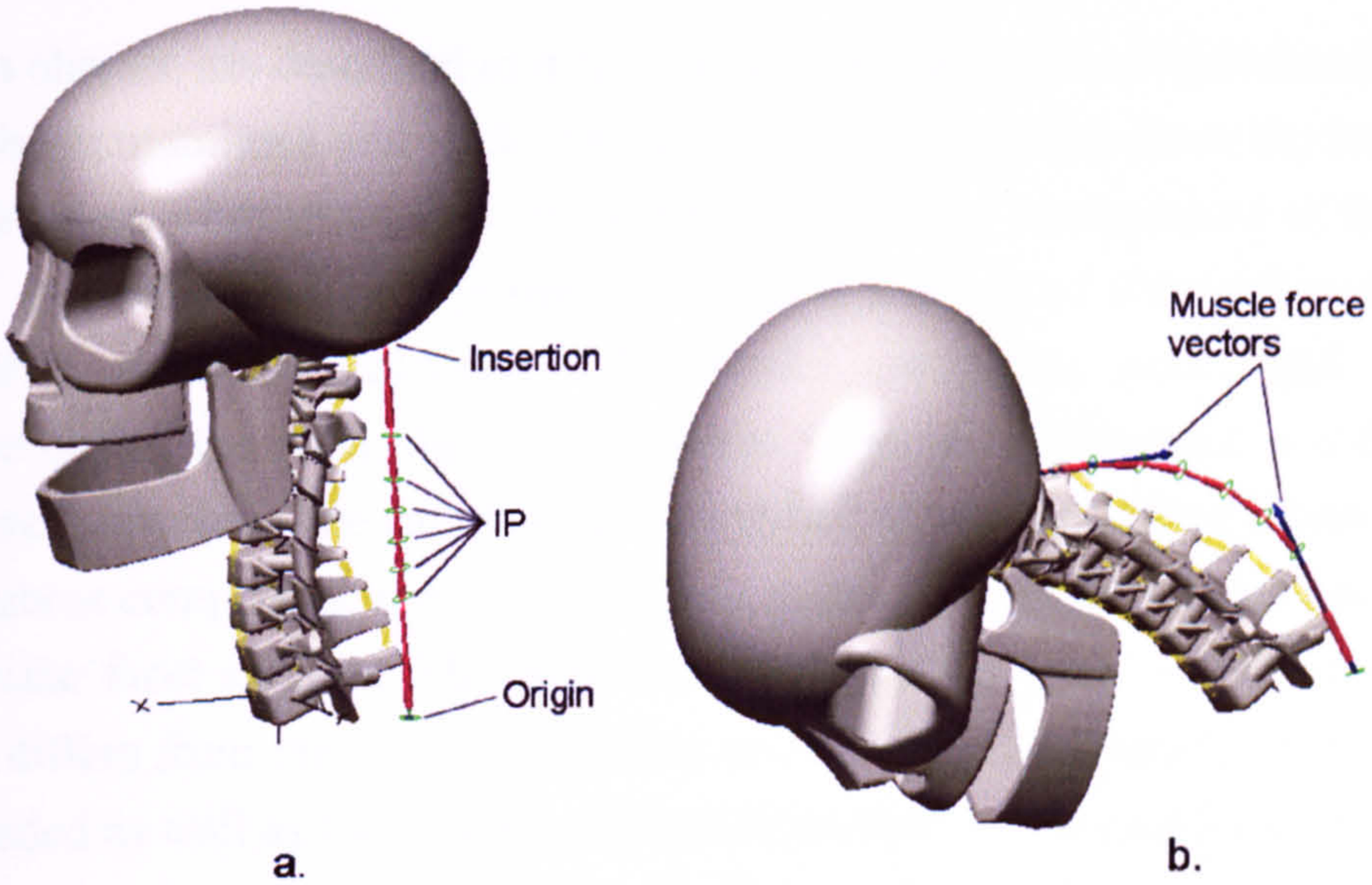


**Figure 4.36:** Muscle curving, a: muscle element in initial position showing the chain of actuators from origin to insertion with intermediate points (IP) .b: head and neck in flexed position demonstrating the curving of the muscle and showing the direction of the applied muscle force.

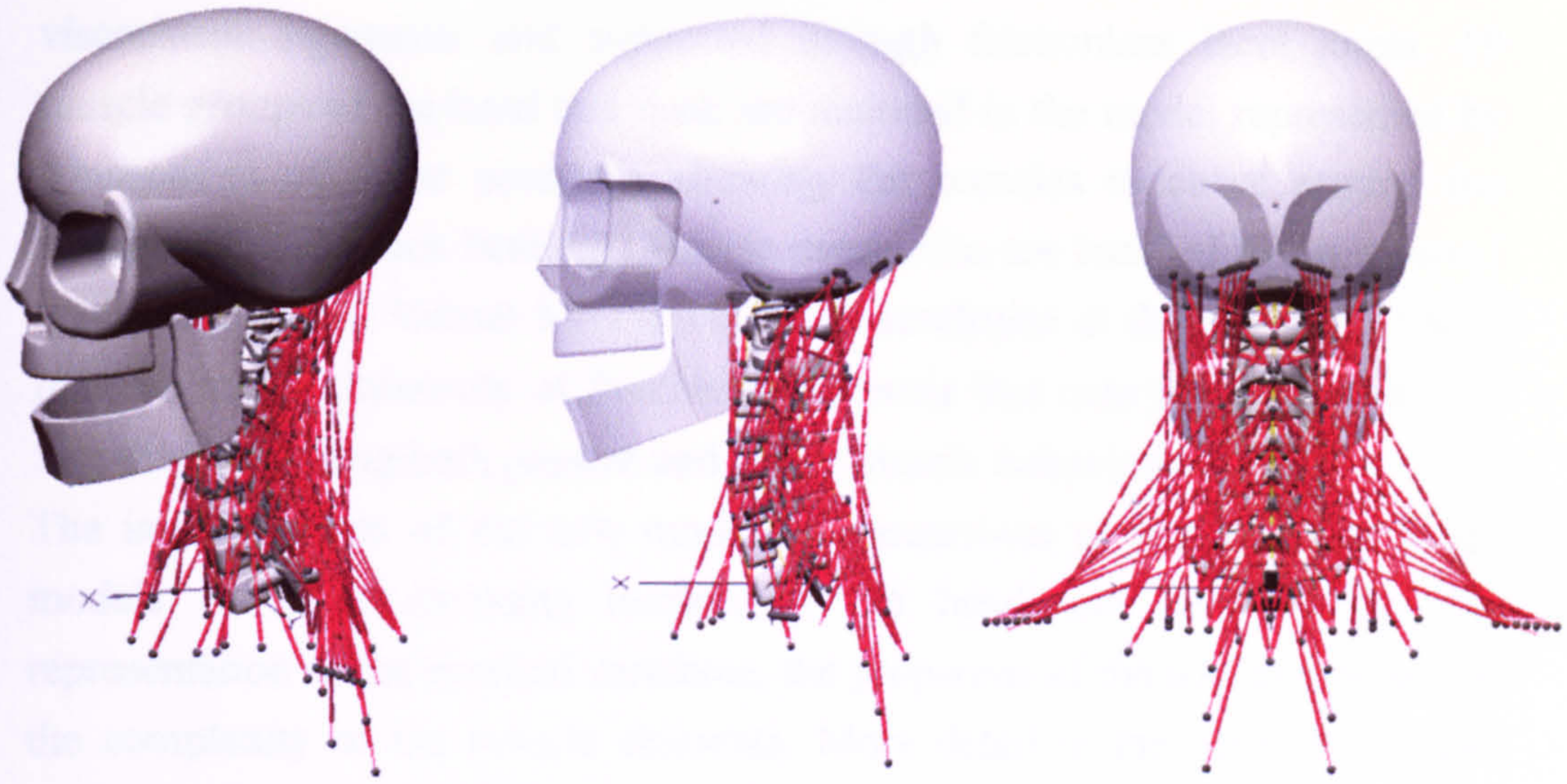

**Figure 4.37:** Isometric, lateral and rear view of the final head/neck model with all muscle elements in place. The skull shown transparent in lateral and rear view to show attachments points of muscle elements.

## 4.6 Discussion

This chapter has described in detail the development of a computational model of the human head and neck. The model developed reproduces the head and neck of an adult in an upright sitting position. The arrangement of the head and cervical vertebrae represent the natural lordosis of the neck with mid-sagittal symmetry assumed. The model comprises nine rigid bodies representing the head, the seven cervical vertebrae of the neck and the first thoracic vertebra. The vertebrae are simplified representations of actual human vertebrae comprising of a vertebral body, spinous and transverse processes and articular facet surfaces. The depiction of the upper cervical vertebrae (C1 and C2) differs from the middle and lower bodies. The dens process of the axis is included as well as the concave-convex interaction of the atlanto-odontoid and atlanto-occipital joints. The rigid bodies of the head and vertebrae were modelled using Solid Edge 3D modelling software before being imported into the dynamic simulation software VisualNastran 4D where their initial configuration, centre of gravities, mass, and inertial properties were defined according to experimental data found in the literature. The rigid vertebrae are

connected by (non)-linear viscoelastic intervertebral disc elements, non-linear viscoelastic ligaments and supported through frictionless facet joints. 19 muscle groups of the head and neck are included in the model represented by connections of linear actuators allowing the muscles to curve around the vertebrae during neck bending. Muscle mechanics are handled by an external application called Virtual Muscle vs. 3.1.5 developed at the Alfred E. Mann Institute at the University of Southern California that runs within Matlab and Simulink providing both passive and active muscle behaviour.

The improvements of the new model in comparison to previous multibody models or finite elements models of the head and neck are in the representation of the cervical vertebrae, the properties of the soft tissues and in the complexity of the muscle elements. More detail in the geometry of the vertebrae has been included in this model than seen in other multi-body models allowing for more accurate location of muscle and ligament attachment sites. Also the geometry is based on mean data from experimental measurements of human vertebrae as opposed to direct measurements from a single spine specimen, it is hoped that this method will give a more general representation of an average adult human neck. Where available, recent experimental data has been used for the mechanical properties of the discs and ligaments. Data is still lacking to fully define the non-linear characteristics of the intervertebral discs for all directions of loading; if and when this data becomes available the model can be updated easily. One of the major developments of this model is the representation of the muscles of the neck. All major muscle groups of the neck have been included in the model with the ability to curve around the neck during bending. Muscles with broad areas of attachments have been subdivided into a number of muscle elements with more accurate origins and insertions. Muscle parameters are based on a detailed study of neck muscle morphometry (Kaminayashi and Richmond, 1998) and for the first time fibre type composition of each of the muscles groups have been included in the mechanical characteristics of the muscle elements.

The main limitations of the model are the rigid representation of the head and vertebrae, the rigid contact between facet joints and the linear response of the intervertebral discs.

As stated previously one of the main advantages of multibody models over finite element models is their computational efficiency allowing for fast simulation and evaluation. In particular the software package, visualNastran 4D, used here provides an extensive analytical tool-set to evaluate designs and models allowing for pre- and post-processing visualization of the model. Once validated, the advantage of having a head-neck model within a more general engineering package such as visualNastran is its versatility, the model can be placed into any environment to study the effects on the head and neck and so be used to develop new safety features within automobiles.

In theory the model is capable of simulating both the global and local kinematics of the head with respect to the torso and of the individual vertebrae and soft tissue elements. With so many components built into the model it would be difficult to validate the system as a whole so it is important to validate the model at various stages of completion to verify the response of the individual elements and as they are brought together to form the complete model of the head and neck. The following chapter presents validation of the isolated motion segments, the completed ligamentous spine and the moment generating capacity of the neck muscles.

CHAPTER 5

# Evaluation and Verification of the Head-Neck Model and its Components

Before the head-neck model is used for impact simulation it is essential to validate the individual motion segment response with experimental data. The objective is to show the model's biofidelity at each stage of construction to give confidence in the response of the individual model components. The lower and upper cervical spine motion segment models are validated for every loading direction by comparing the segment response to published experimental data on the load-displacement behaviour of cervical spine motion segments for both small and large static loads. The response of the entire ligamentous spine model to quasi-static flexion and extension loading is also compared to experimental data to validate the head neck model before the effect of muscle stiffening is included.

## 5.1 Motion Segment Response to Small Loads

The response of the motion segments of the lower cervical spine are compared to the experimental results reported by Moroney et al. (1988). Moroney et al. tested 'intact segments'; anatomically complete segments comprising the two adjacent vertebrae, disc, facet joints and ligaments, and 'disc segments', where just the vertebral bodies and intervertebral disc are left. The disc segment response has already been used to define the model's intervertebral disc response in some but not all directions; here the 'intact segment' response is used to validate the response of a complete model motion segment for all loading directions. For load-displacement testing, each motion segment was

mounted so that the inferior vertebra was rigidly fixed while the superior vertebra was free to move in response to the applied loads. The motion segments were subjected to small static loads of 20N and 1.8 Nm in all loading directions; the resulting three-dimensional displacements were measured at the geometric centre of the upper vertebra. For simulating the segment tests the model motion segments are set up in an identical manner, the lower of the two vertebrae being anchored while leaving the upper vertebra free to move in all directions. Loads are applied to the model via an external torque or force applied at the centre of the intervertebral disc element. In the experimental tests the load was applied in effect at the centre of the intervertebral disc, such that the direction of the load did not change relative to the lower vertebra. The resulting main and coupled displacements were measured at the centre of the local body coordinate system of the upper vertebra and compared with the reported displacements. The dynamic stiffening factor for the disc and ligaments was set to 1 for all static tests.The model of the upper cervical spine, atlas, axis and occiput, is validated against the experimental results reported by Panjabi and co-workers who subjected upper cervical spine specimens to static moments of 1.5Nm and measured the main and coupled rotations. In these experiments C2 was fixed while moments were applied to the occiput and the corresponding rotations, both main and coupled, were measured at the centres of C1 and C0. Coupled translations have been reported by Oda et al. (1991) measured at two specific mid-sagittal points on C0 and C1. One point was located at the anterior edge of the foramen magnum of the occiput and another at the anterior ring of the atlas. Experimental data on the translational loading response of the upper cervical spine motion segments is not available in the literature and so validation is not possible.

The simulation set-up is the same as for the experiments; C2 is anchored while C1 and C0 are left free to move in all directions. Loads are applied via an external torque (1.5Nm) or force (20N) to the centre of the occiput and corresponding main and coupled displacements measured.

For all simulations an acceleration field of -9.81m/s$^2$ in the z-axis was included to simulate the effect of gravity.

### 5.1.1 Lower Cervical Spine

Motion segment models C5-C6 and C3-C4 were chosen as representative segments of the lower cervical spine. These two spinal units have very different facet orientations: the facets of C5-C6 point backwards and outwards where as the facets of C3-C4 point backwards and inwards. The segments also have different ligament stiffness' and different flexion-extension disc properties, it is therefore expected that the response of these two motion segments to small loads will vary slightly.

Figure 5.1 shows the main and coupled displacements of C5-C6 and C3-C4 in response to 1.8Nm for flexion, extension, right lateral bending and CCW axial rotation. Figure 5.2 shows the segments response to translational loading of 20N for anterior shear, posterior shear, right lateral shear and compression. Each graph shows the main (in bold) and coupled translations and rotations in response to the specific loading direction. Translational displacements are shown on the left side of the graph and rotation on the right. The segment responses are plotted against the mean ± 1 SD response reported by Moroney et al. (1988), no data was available for the motion segment response in tension.

All main displacements and rotations are within 1 SD of the mean reported value except for axial rotation where both segments appear slightly too flexible. Generally the coupled displacements and rotations are in good agreement with Moroney's data but a couple of responses differ significantly to the experimental data. In flexion loading both segment models exhibit little anterior shear in comparison to the reported mean, this is due to the facet positioning and orientation. The facets of the lower segments face backward at approximately 45° and because they have been positioned so they are just touching in the initial position they appear prevent the coupled anterior translation in response to flexion. Both models appear slightly too flexible in axial rotation and subsequently their coupled response in lateral bending exceeds the reported mean and SD. In response to posterior shear the C5-C6 model exhibits a relatively large amount of coupled extension, something that is not seen in the C3-C4 segment. This is thought to be due to the difference in

facet orientation. Both segments exceed the mean and SD for coupled flx/ext in response to compression loading again this is thought to be due to facet positioning in the initial position.
Generally there is very little difference in response between the two segment models when subjected to small loads.

## 5.1.2 Upper cervical Spine

Figure 5.3 shows the main and coupled displacements of C0-C1 and C1-C2 respectively in response to rotational loading. The model results are plotted against the experimental results of Panjabi and co-workers (average ± SD). In both figures the response to each rotational loading direction, flexion, extension, lateral bending and axial rotation, are shown on a separate graph (a-d). The responses in all directions, main and coupled are shown along the horizontal axis, the labels representing the positive direction of the response, left lateral shear (LLS), anterior shear (AS), tension (TNS), right lateral bending (RLB), flexion (FLX) and left axial rotation (LAR), negative values represent the opposite direction of loading ie RLS, PS, CMP, EXT and RAR. The magnitudes of the translation (left side) or rotation (right side) are plotted on the vertical axis. The main displacements for each loading direction are shown in bold.
The main displacements of C0-C1 are all with 1 SD of the reported experimental values and lie close to the average for flexion, extension and lateral bending. Coupled responses are also in good agreement with the experimental data for most directions. In axial rotation the segment exhibits little to no coupled lateral bending in contrast to the reported average, this is thought to be due to the representation of the atlanto-occipital joints and their orientation. The main displacements of the C1-C2 segment are in reasonable to good agreement for flexion and extension loading compared with experimental data. The segment appears to be too stiff in axial rotation and lateral bending and again the coupling between lateral bending and axial rotation and visa versa is weak. Also no coupled lateral shear is seen in response to lateral bending.

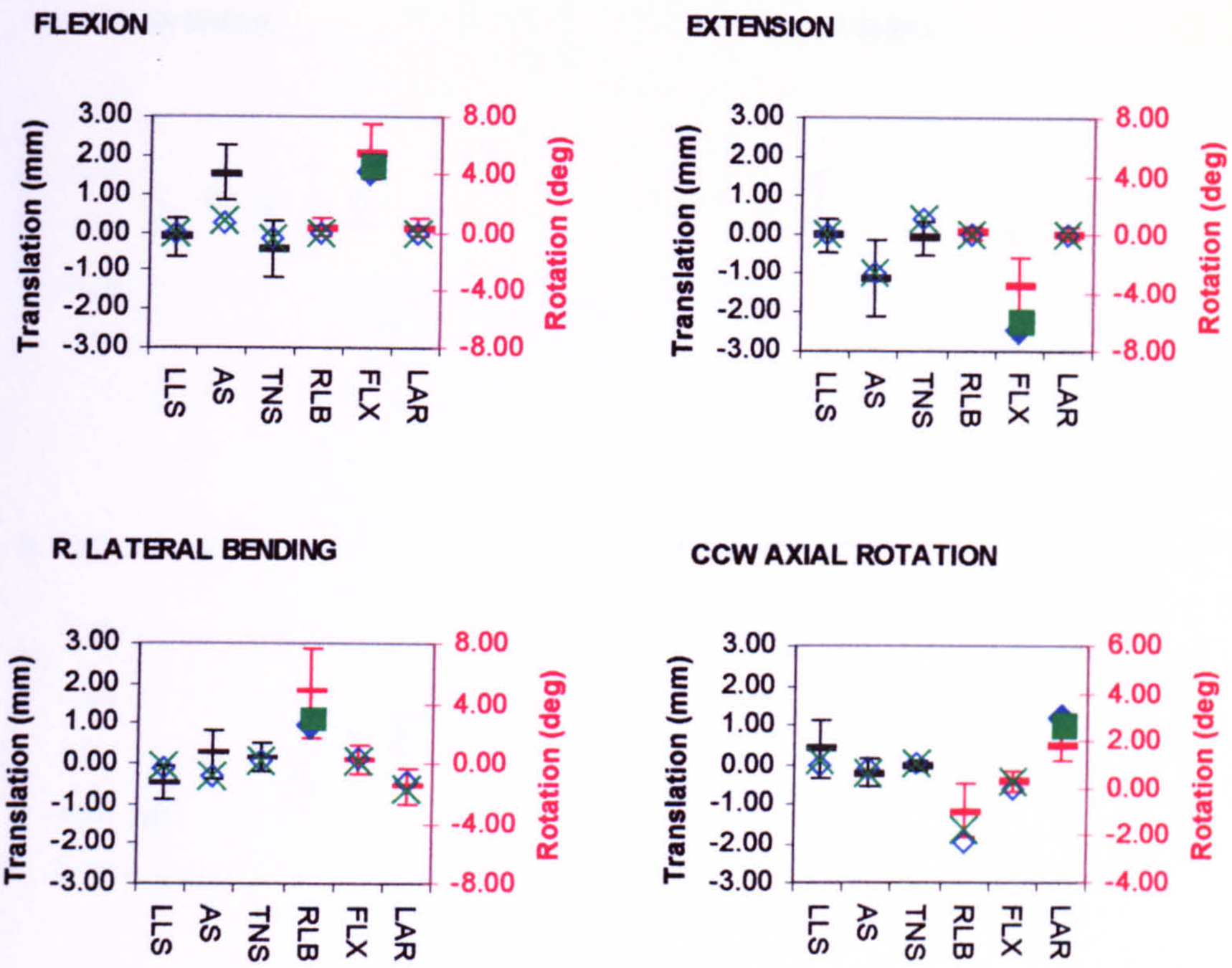


**Figure 5.1:** Main and coupled displacements of model motion segments C3-C4 (x) and C5-C6 (◇) in response to applied rotational loads of 20 Nm shown against the experimental results (average ± SD) of Moroney et al. (1988). Resulting displacements shown along the vertical axis, translations on the left, rotations on the right, main rotations are shown as a solid square (C3-C4,■) and solid diamond (C5-C6,♦). Anterior shear (+AS), posterior shear (-AS), left lateral shear (+LLS), right lateral shear (-LLS), tension (+TNS), compression (-TNS), right lateral bending (+RLB), left lateral bending (-RLB), flexion (+FLX), extension (-FLX), left axial rotation (+LAR) and right axial rotation (-LAR).

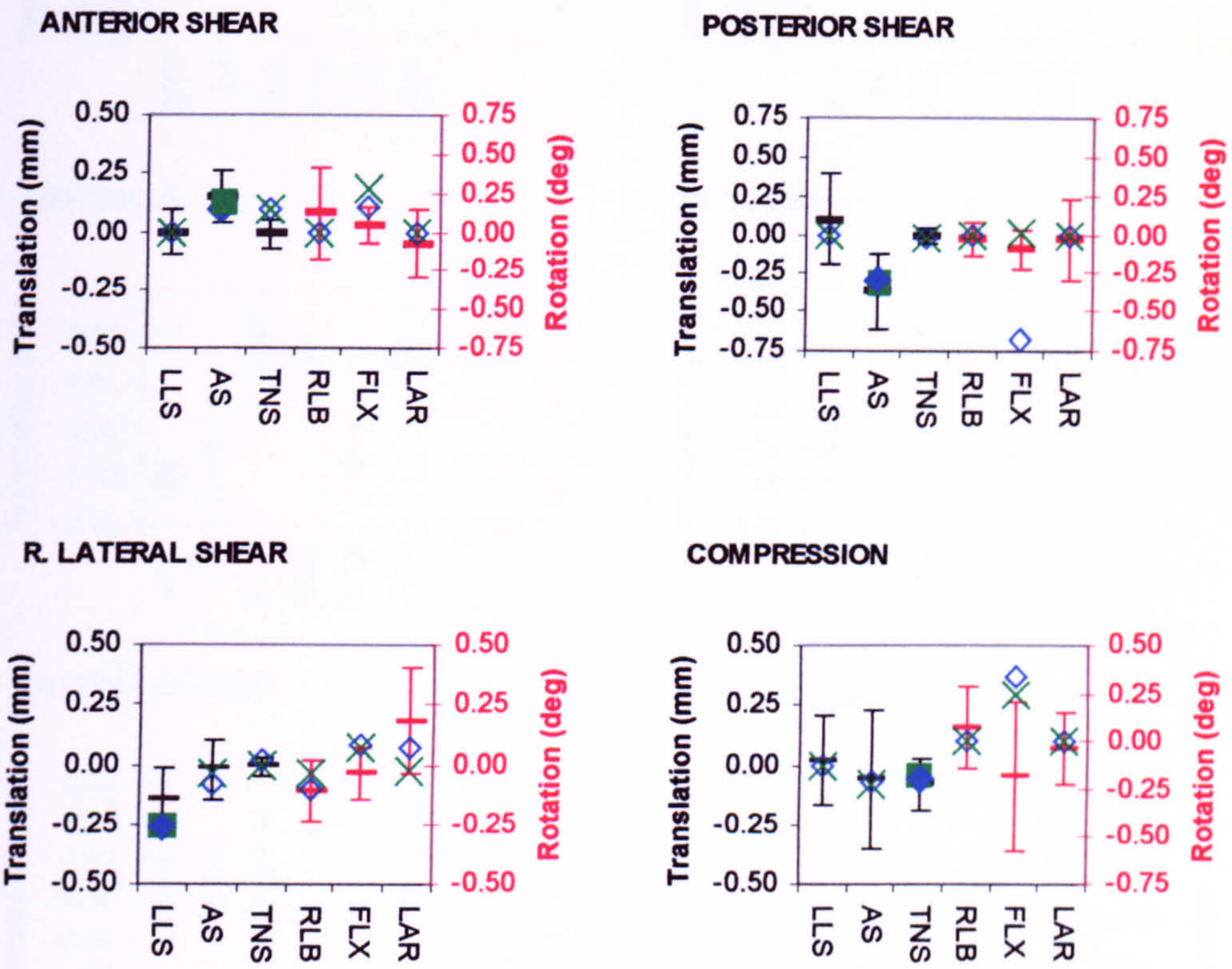


**Figure 5.2:** Main and coupled displacements of model motion segments C3-C4 (x) and C5-C6 (◇) in response to applied translational loads of 500 N shown against the experimental results (average ± SD) of Moroney et al. (1988). No experimental data was available for tension. Resulting displacements shown along the vertical axis, translations on the left, rotations on the right, main rotations are shown as a solid square (C3-C4,■) and solid diamond (C5-C6,♦). Anterior shear (+AS), posterior shear (-AS), left lateral shear (+LLS), right lateral shear (-LLS), tension (+TNS), compression (-TNS), right lateral bending (+RLB), left lateral bending (-RLB), flexion (+FLX), extension (-FLX), left axial rotation (+LAR) and right axial rotation (-LAR).

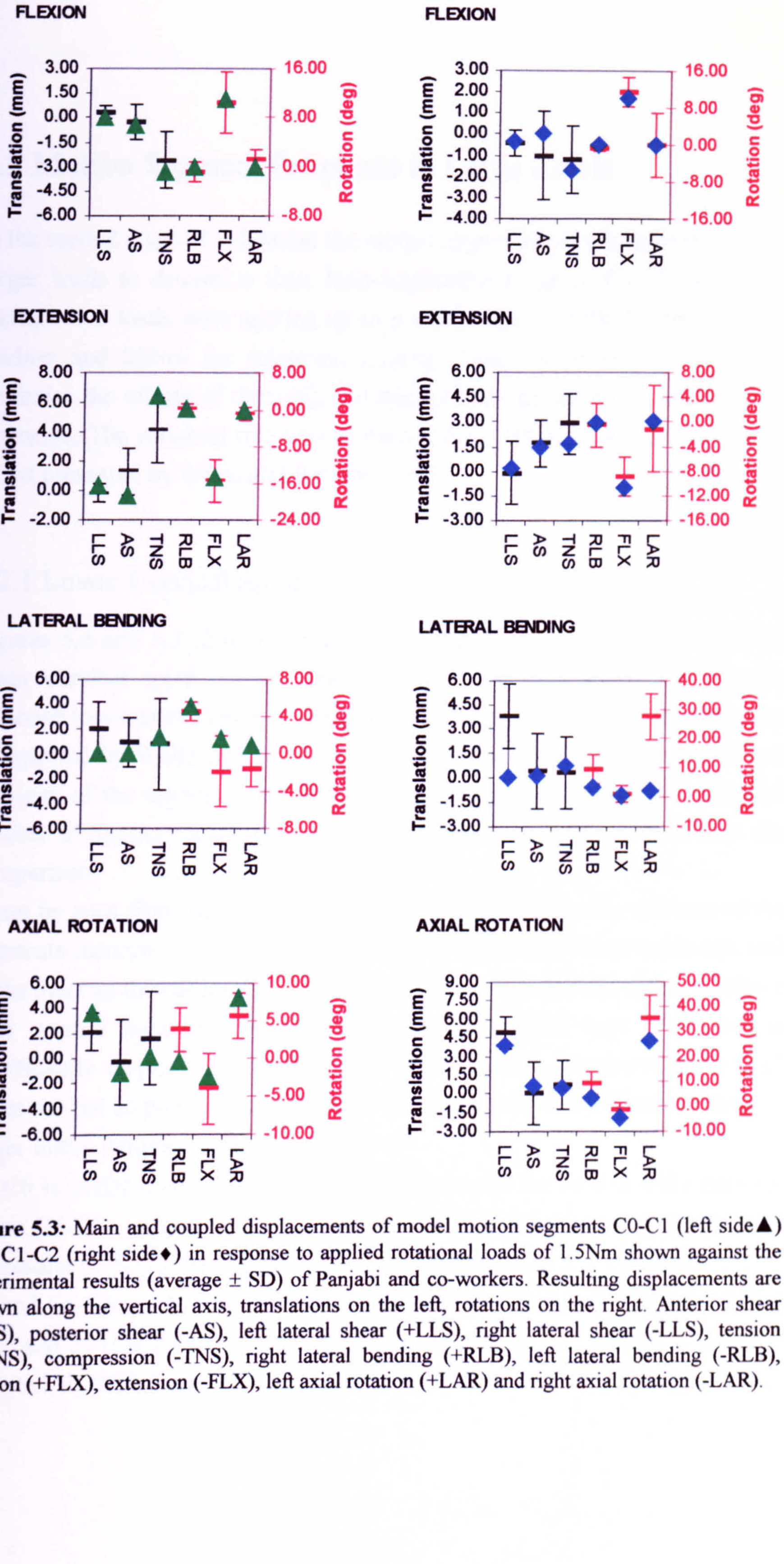


**Figure 5.3:** Main and coupled displacements of model motion segments C0-C1 (left side▲) and C1-C2 (right side♦) in response to applied rotational loads of 1.5Nm shown against the experimental results (average ± SD) of Panjabi and co-workers. Resulting displacements are shown along the vertical axis, translations on the left, rotations on the right. Anterior shear (+AS), posterior shear (-AS), left lateral shear (+LLS), right lateral shear (-LLS), tension (+TNS), compression (-TNS), right lateral bending (+RLB), left lateral bending (-RLB), flexion (+FLX), extension (-FLX), left axial rotation (+LAR) and right axial rotation (-LAR).

## 5.2 Motion Segment Response to Large Loads

In the second stage of validation the motion segments were subjected to much larger loads to determine their load-displacement curves for all directions. Incremented loads were applied up to a maximum of 500N for translational loading and 20Nm for rotational loading. Loads were applied slowly to minimise the effects of damping and thus provide the elastic response of the segments. The vertebral rotations of the segments are compared to the in vivo ROM presented by White and Panjabi (1990).

### 5.2.1 Lower Cervical Spine

Figures 5.4 and 5.5 show the response to large loads of the segments of the lower cervical spine (C3-C4 and C5-C6). Figure 5.4 shows the segment response to rotational loading along with the range of motion of the segments as reported by White and Panjabi (1990). Figure 5.5 shows the translational response of the segments, no experimental data on the translational range of motion of motion segments of the lower cervical spine is available for comparison.

It can be seen from the graphs that, for larger displacements, stiffness of the segments increases due to the resistive forces of the non-linear ligaments and of the discs as they become more and more strained. In flexion and extension a clear neutral zone can be seen where only a small load is needed to significantly displace the segment. For other loading directions the neutral zones are not so pronounced due to the linear stiffness of the discs resulting in larger initial stiffness of the segments.

C5-C6 is stiffer than C3-C4 in all directions except for flexion and extension where C5-C6 is slightly more flexible than C3-C4, which is in agreement with the results of White and Panjabi. The combined flexion and extension of C3-C4 and C5-C6 are 17 and 19 deg respectively compared to the reported ROM of 15 and 20 deg. In lateral bending the segments responses are larger than the reported ROM by around 50 and 60% for C3-C4 and C5-C6 respectively.

Again in axial rotation the displacements exceed ROM by around 35 and 40% for C5-C6 and C3-C4 respectively.

C5-C6 is slightly stiffer than C3-C4 in all shearing directions; the linearity of the discs clearly dominates the response in anterior shear, tension and compression where no neutral zones are observed.

To give insight to how the forces are distributed among the various components in a motion segment table 5.1 shows the loads in the intervertebral disc, ligaments and facet joints of C5-C6 when subjected to maximum loads of 500N and 20 Nm. The forces and moments in the disc and facet joints are expressed in the local body coordinates system of C6 while the tension in the ligaments are expressed in the direction of their orientation.

In anterior shear all elements are loaded, with symmetrical loading of the facet joints. Facet joints are unloaded for posterior shear, tension, and flexion. In posterior shear the load is shared mainly between the disc and the capsular ligaments. Uneven loading of the facet joints can be seen in lateral shear, lateral bending and axial rotation. Interestingly both capsular ligaments are heavily loaded in lateral bending and this was found to be due to the coupling of axial rotation pulling the ligaments in opposite directions. In tension all ligaments except for the ISL are loaded together with the disc, the ISL is only loaded in anterior shear, flexion and axial rotation. For compression loading the force is mainly resisted by the disc with some contribution from the facet joints. The intervertebral disc plays a large role in resisting rotational loading of the segment in all directions, in extension loading the moment exerted by the disc is around 90% of the applied load. In axial rotation all elements are loaded except for the facet joints on the left side, large forces in the right facet joint and both capsular ligaments significantly contribute in resisting the applied load.

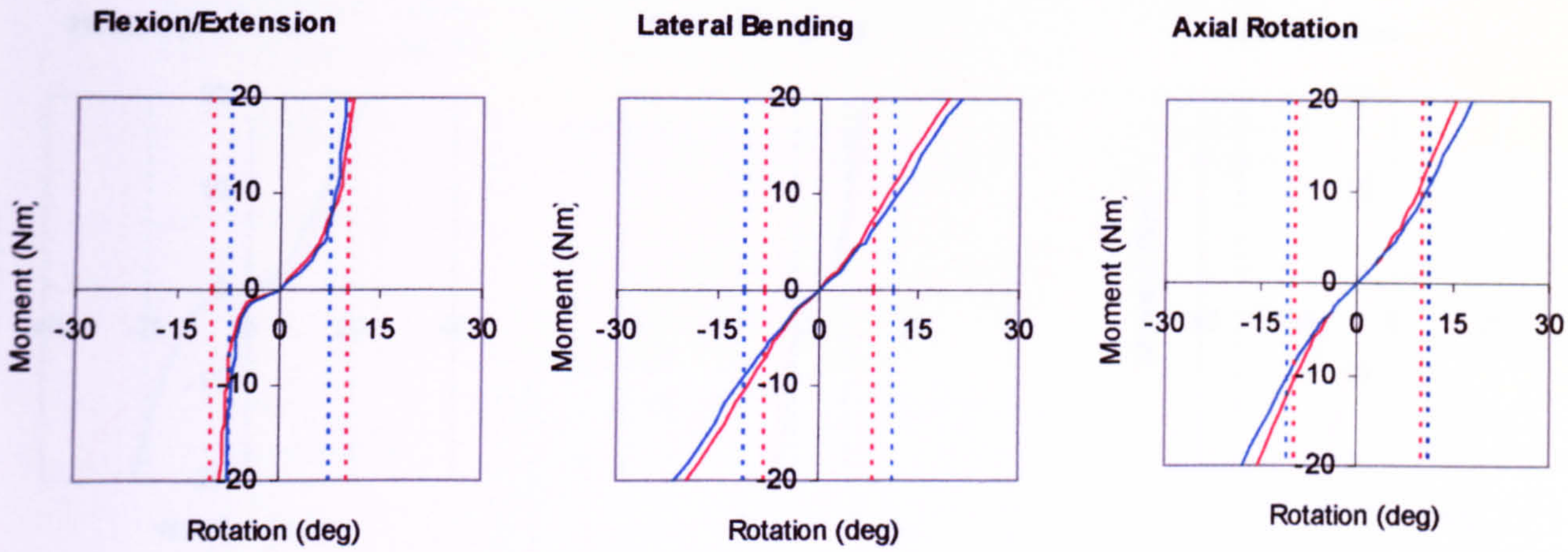


**Figure 5.4:** Response of model motion segments C3-C4 (blue) and C5-C6 (red) to applied rotational loads of 20 Nm. The vertical dotted lines shows the ROM for the corresponding motion segment as reported by White and Panjabi (1990).

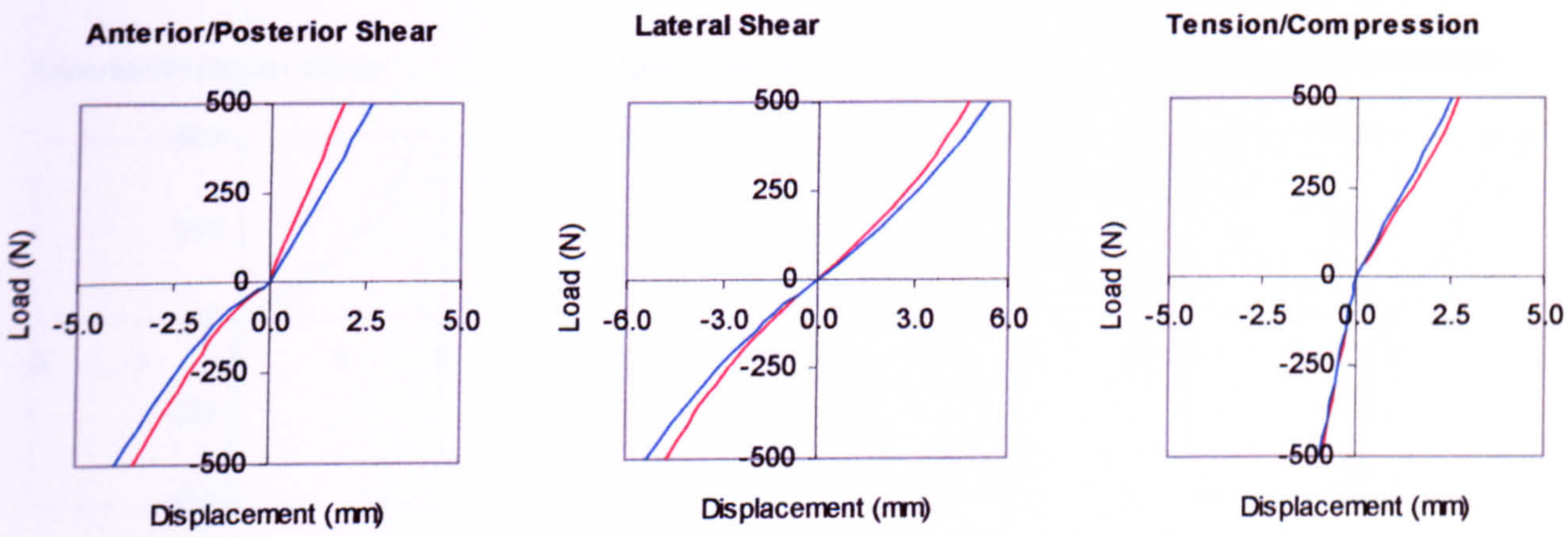


**Figure 5.5:** Response of model motion segments C3-C4 (blue) and C5-C6 (red) to applied translational loads of 500N.

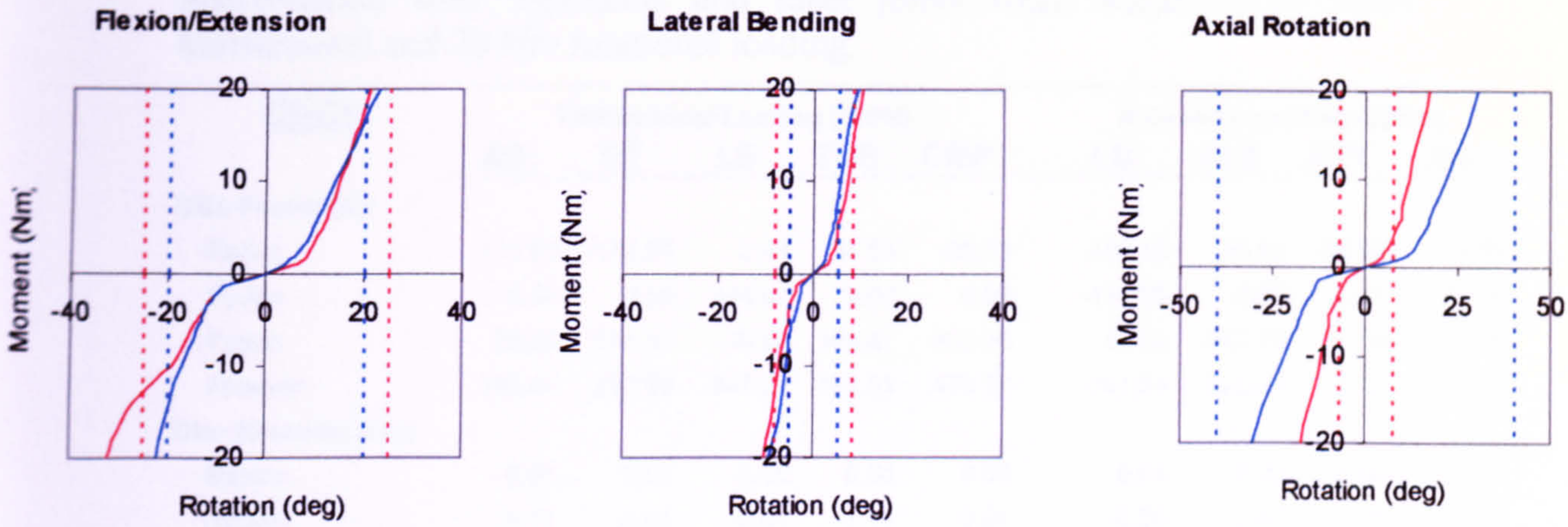


**Figure 5.6:** Response of model motion segments C0-C1 (red) and C1-C2 (blue) to applied rotational loads of 20 Nm. The vertical dotted lines shows the ROM for the corresponding motion segment as reported by White and Panjabi (1990).

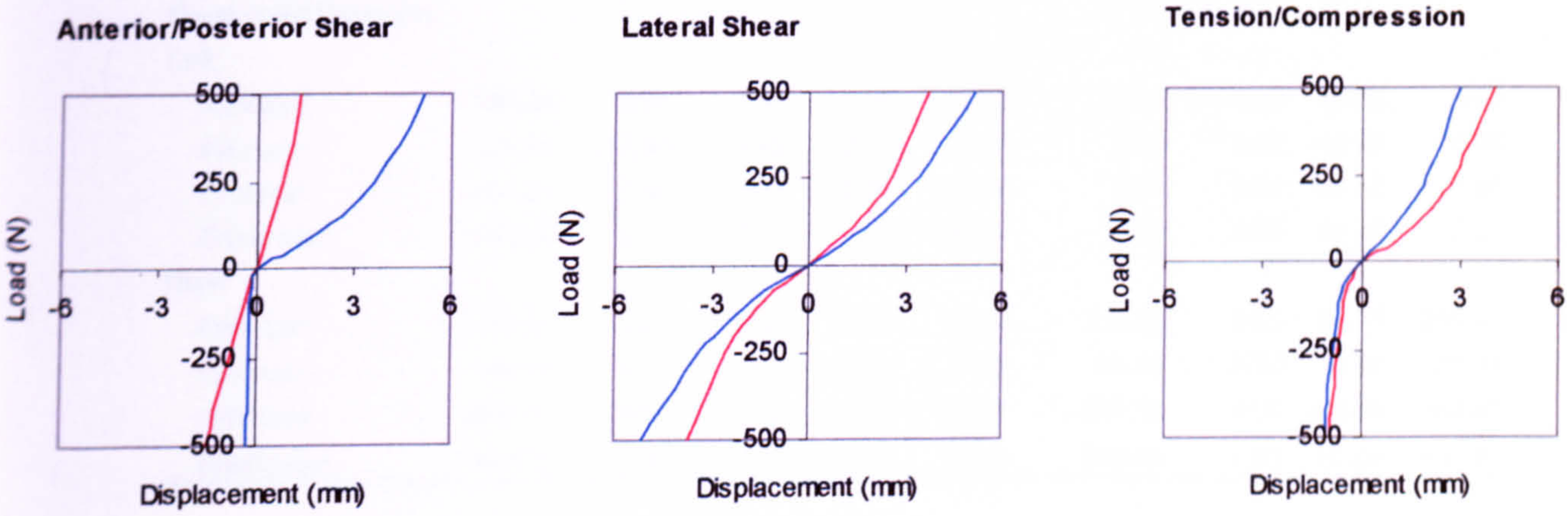


**Figure 5.7:** Response of model motion segments C0-C1 (red) and C1-C2 (blue) to applied translational loads of 500N.

**Table 5.1:** Component loading of model motion segment C5-C6. Loads in intervertebral disc, ligaments and facet joints when subjected to 500N translational and 20 Nm rotational loading.

| C5-C6 | Translational Loading (500N) | | | | | Rotational Loading (20Nm) | | | |
|---|---|---|---|---|---|---|---|---|---|
| | AS | PS | LS | TNS | CMP | LB | FLX | EXT | AR |
| **Disc Forces (N)** | | | | | | | | | |
| FxDISC | 117.59 | -174.08 | 3.44 | 51.83 | -35.13 | -109.10 | 55.10 | -70.10 | 5.66 |
| FyDISC | -0.04 | 0.00 | 344.97 | 0.00 | 0.00 | -110.99 | 0.00 | -0.01 | 73.19 |
| FzDISC | 98.58 | -154.40 | -39.34 | 184.67 | -468.96 | 42.55 | -317.79 | 28.10 | 17.01 |
| FresDISC | 153.44 | 232.69 | -347.22 | 191.81 | 470.27 | 161.34 | 322.53 | 75.52 | 75.35 |
| **Disc Moments (Nm)** | | | | | | | | | |
| MxDISC | 0.00 | 0.00 | -1.09 | 0.00 | 0.00 | 6.64 | 0.00 | 0.00 | -3.47 |
| MyDISC | 0.11 | -0.91 | -0.01 | -1.16 | 0.05 | -0.50 | 12.62 | -18.26 | 0.11 |
| MzDISC | 0.00 | 0.00 | 0.05 | 0.00 | 0.00 | -4.54 | 0.00 | 0.00 | 6.54 |
| MresDISC | 0.11 | 0.91 | 1.09 | 1.16 | 0.05 | 8.06 | 12.62 | 18.26 | 7.40 |
| **Ligament Forces (N)** | | | | | | | | | |
| ALL | 39.70 | 36.08 | 19.79 | 132.75 | 0.00 | 56.55 | 0.00 | 64.42 | 7.29 |
| PLL | 63.92 | 0.00 | 12.27 | 73.33 | 0.00 | 0.00 | 22.00 | 0.00 | 10.97 |
| FL | 86.50 | 0.00 | 3.73 | 8.73 | 0.00 | 0.00 | 135.92 | 0.00 | 54.09 |
| ISL | 45.93 | 0.00 | 0.00 | 0.00 | 0.00 | 0.00 | 74.28 | 0.00 | 49.70 |
| CL left | 44.88 | 169.55 | 85.89 | 56.67 | 6.62 | 308.42 | 51.48 | 29.12 | 290.34 |
| CL right | 45.02 | 169.55 | 143.74 | 56.67 | 6.64 | 338.23 | 51.48 | 29.16 | 222.75 |
| **Facet Joint Force (N)** | | | | | | | | | |
| Left | | | | | | | | | |
| FxLFACET | 194.94 | 0.00 | 2.71 | 0.00 | 23.22 | 0.00 | 0.00 | 63.06 | 0.00 |
| FyLFACET | -45.74 | 0.00 | -1.06 | 0.00 | -4.96 | 0.00 | 0.00 | -14.05 | 0 00 |
| FzLFACET | -208.23 | 0.00 | -2.47 | 0.00 | -20.39 | 0.00 | 0.00 | -60.86 | 0.00 |
| FresLFACET | 288.88 | 0.00 | 3.81 | 0.00 | 31.30 | 0.00 | 0.00 | 88.76 | 0.00 |
| Right | | | | | | | | | |
| FxRFACET | 195.10 | 0.00 | 122.00 | 0.00 | 23.22 | 519.82 | 0.00 | 63.10 | 259.37 |
| FyRFACET | 45.78 | 0.00 | 6.99 | 0.00 | -4.96 | 85.08 | 0.00 | 14.06 | 95.22 |
| FzRFACET | -208.40 | 0.00 | -121.39 | 0.00 | -20.39 | -287.12 | 0.00 | -60.90 | -339.66 |
| FresRFACET | -289.12 | 0.00 | 172.24 | 0.00 | 31.30 | 599.90 | 0 00 | 88.82 | 437.85 |

**Table 5.2:** Component loading of upper cervical spine model C0-C1-C2. Loads in ligaments and facet joints when subjected to 500N translational and 20 Nm rotational loading.

| ***C0-C1-C2*** | | Translational Loading (500N) | | | | | Rotational Loading (20Nm) | | | |
|---|---|---|---|---|---|---|---|---|---|---|
| | | **AS** | **PS** | **LS** | **TNS** | **CMP** | **LB** | **FLX** | **EXT** | **AR** |
| **Ligament Forces (N)** | | | | | | | | | | |
| **C0-C1** | AM | 0.00 | 70.07 | 1.47 | 40.04 | 0.00 | 17.58 | 0.00 | 96.77 | 11.28 |
| | PM | 25.80 | 0.00 | 13.15 | 9.64 | 0.00 | 19.95 | 227.19 | 0.00 | 43.11 |
| | CL L1 | 1.96 | 84.05 | 4.37 | 33.87 | 0.00 | 104.67 | 51.66 | 154.60 | 128.25 |
| | CL L2 | 12.56 | 70.72 | 5.82 | 20.80 | 0.00 | 140.33 | 138.80 | 44.73 | 207.40 |
| | CL R1 | 1.96 | 84.05 | 2.48 | 33.87 | 0.00 | 12.80 | 51.66 | 154.60 | 134.18 |
| | CL R2 | 12.56 | 70.72 | 10.48 | 20.80 | 0.00 | 7.52 | 138.80 | 44.73 | 236.49 |
| **C1-C2** | AM | 0.00 | 134.26 | 6.15 | 49.91 | 0.00 | 38.73 | 0.00 | 371.85 | 11.47 |
| | PM | 125.21 | 0.00 | 0.00 | 21.32 | 0.00 | 6.93 | 389.11 | 0.00 | 205.52 |
| | CL L1 | 3.67 | 39.93 | 0.41 | 14.63 | 0.00 | 69.03 | 0.00 | 111.34 | 102.02 |
| | CL L2 | 5.61 | 20.33 | 0.00 | 13.21 | 0.00 | 100.68 | 2.69 | 72.06 | 139.88 |
| | CL L3 | 36.57 | 1.45 | 1.81 | 11.79 | 0.00 | 63.40 | 40.60 | 11.47 | 75.86 |
| | CL L4 | 24.41 | 1.79 | 7.33 | 13.11 | 0.00 | 36.55 | 4.28 | 13.73 | 0.93 |
| | CL R1 | 3.67 | 39.93 | 26.97 | 14.63 | 0.00 | 0.00 | 0.00 | 111.34 | 139.15 |
| | CL R2 | 5.61 | 20.33 | 46.46 | 13.21 | 0.00 | 0.00 | 2.69 | 72.06 | 218.93 |
| | CL R3 | 36.57 | 1.45 | 31.45 | 11.79 | 0.00 | 0.00 | 40.60 | 11.47 | 138.61 |
| | CL R4 | 24.41 | 1.79 | 18.25 | 13.11 | 0.00 | 7.75 | 4.28 | 13.73 | 20.04 |
| APICAL | | 244.87 | 10.23 | 34.85 | 135.37 | 0.00 | 148.13 | 134.59 | 122.96 | -0.04 |
| ALAR LEFT | | 153.15 | 111.62 | 364.93 | 85.73 | 0.00 | 49.11 | 34.30 | 250.51 | 159.99 |
| ALAR RIGHT | | 153.15 | 111.62 | 0.00 | 85.73 | 0.00 | 154.17 | 34.30 | 250.51 | 0.00 |
| TL LEFT | | 56.07 | 2.09 | 180.56 | 3.14 | 6.30 | 0.00 | 19.92 | 7.07 | 0.00 |
| TL RIGHT | | 56.07 | 2.09 | 0.00 | 3.33 | 6.33 | 113.21 | 19.92 | 7.07 | 36.55 |
| TM | | 8.22 | 0.00 | 1.88 | 48.30 | 0.00 | 34.10 | 4.69 | 35.12 | -0.04 |
| **Facet Joint Force (N)** | | | | | | | | | | |
| **C0-C1** | Left | | | | | | | | | |
| | $Fres_{LFACET}$ | 205.88 | 226.87 | 199.87 | 0.00 | 271.33 | 0.00 | 222.56 | 426.83 | 323.77 |
| | Right | | | | | | | | | |
| | $Fres_{RFACET}$ | 205.88 | 226.87 | 12.63 | 0.00 | 271.33 | 702.29 | 222.56 | 426.83 | 359.79 |
| **C1-C2** | Left | | | | | | | | | |
| | $Fres_{LFACET}$ | 249.28 | 67.31 | 263.16 | 0.00 | 302.63 | 0.00 | 328 69 | 502.61 | 258.15 |
| | Right | | | | | | | | | |
| | $Fres_{RFACET}$ | 249.28 | 67.31 | 122.59 | 0.00 | 302.63 | 721.54 | 328.69 | 502.61 | 452.18 |
| **Dens Facet force (N)** | | | | | | | | | | |
| | $Fres_{FACET}$ | 0.00 | 654.89 | 93.34 | 39.37 | 0.00 | 122.97 | 0 00 | 280 52 | 58.27 |

## 5.2.2 Upper Cervical Spine

Figures 5.6 and 5.7 show the response to large loads of the segments of the upper cervical spine (C0-C1 and C1-C2). Figure 5.6 shows the segment response to rotational loading along with the range of motion of the segments as reported by White and Panjabi (1990). Figure 5.7 shows the translational response of the segments, again no experimental data on the translational range of motion segments of the upper cervical spine is available for comparison.

There is no disc present between C0-C1 or C1-C2 so all resistance to load comes from the ligaments and facet joints. Clear neutral zones in which little load is needed to deform the structure are present for all directions of rotational loading due to the non-linear response of the ligaments.

In posterior shear the motion of C1 with respect to C2 is limited by the contact between the facet on the anterior ring of C1 and the dens process of C2 while the concave-convex interaction between the atlanto-occipital joints limits both anterior and posterior shear between the occiput and C1. Anterior shear of the C1-C2 segment is limited only by the ligaments as can be seen by the progressive increase in load with displacement. Both segments have similar response to lateral bending, flexion and compression. C1-C2 shows nearly 50% greater flexibility in axial rotation than C0-C1, which is in agreement with reported ROM experiments however C1-C2 is still too stiff and C0-C1 too flexible compared with the reported ROM of White and Panjabi (1990).

Table 5.2 shows the loads present in the various components of the upper cervical spine when loaded at C0 with maximum load of 20 Nm and 500 N.

Note the symmetrical loading of the capsular, alar, and transverse ligaments along with the left and right articular facets for anterior/posterior shear, tension, compression, flexion and extension due to the mid-sagittal symmetry of the C0-C1-C2 unit. In anterior shear the articular facet of the dens is unloaded as is the anterior membrane at both levels. Large forces can be seen in the apical and alar ligaments. In posterior shear it can be seen how the majority of the applied load is taken up by the articular facet of the dens at the C1-C2 level while at C0-C1 large forces are seen in the alar ligaments and the

atlanto-occipital joints. Large forces are observed in the left alar and transverse ligaments and in the facets on the left hand side in lateral shear with significant tension in the right hand side capsular ligaments. In tension the articular facets are unloaded with the applied force been distributed across the ligaments with particularly large forces in the apical and alar ligaments. In compression the opposite is seen with practically all ligaments unloaded and the applied load being taken up by the lateral articular facets.

In rotational loading it can be seen how the apical ligament plays an important role in resisting the applied load in lateral bending, flexion and extension while it is unloaded in axial rotation. In lateral bending the right lateral facets are heavily loaded as would be expected and the left side capsular ligaments are heavily tensioned. Interestingly the articular facet of the dens process is significantly loaded in lateral bending and in extension. In axial rotation the majority of the components between C1-C2 are significantly loaded perhaps explaining why it is difficult to achieve the degree of axial rotation observed in ROM experiments.

## 5.3 Response of the Ligamentous Spine Model to Flexion/Extension Loads

The next step was to validate the entire ligamentous spine model before any musculature was included. Camacho et al. (1997) published quasi-static flexion-extension characteristics of ten human cadaveric ligamentous cervical spine specimens (the skull was also left attached during testing). For testing the specimens were turned upside down and fixed in a loading frame. The skull was fixed while pure moments were applied to T1 up to 1.5 Nm for both flexion and extension in 0.1Nm increments. The vertebral displacements were measured at each load step to produce detailed load-displacements curve for each level of the cervical spine. Due to difficulties in visualising C1 during the tests, the upper cervical spine complex was treated as a single motion segment. To simulate these tests with the cervical spine model the gravitational field was inverted and the skull of the model was rigidly anchored in space. An external torque was applied to the geometric centre of T1 and incremented in

0.1Nm steps up to a maximum value of 1.5Nm for both flexion and extension. The sagittal plane rotational displacements were measured at each load increment to produce a directly comparable load-displacement curve for each level of the ligamentous cervical spine model.

Figure 5.8 shows the simulation results for flexion and extension loading of the entire ligamentous cervical spine model. The graphs show the moment rotation curves for each level of the spine up to a maximum of ± 10Nm. Also shown on each graph are the moment rotation functions for each cervical level as defined by Camacho et al. (1997) up to ± 2Nm and the average ± SD rotation at 1.8Nm as reported by Moroney et al. (1988). Due to difficulties in visualizing C1 during testing Camacho et al. treated the C0-C1-C2 complex as a single motion segment C0-C2, this is shown in figure 5.8 against the combined model flexion/extension results of C0-C1 and C1-C2. Also shown on the C0-C2 graph is the mean (±SD) rotation at 1.5Nm as reported by Panjabi et al. (1991).

The results of Camacho are in agreement with those reported by Moroney for the lower cervical spine expect for C2-C3 in extension where Camacho predicts a slightly more flexible response. At every level the model is in good agreement with the results of Camacho et al. in extension but appear to be too stiff in flexion, this is thought to be due to the greater contribution of the ligaments in flexion as five out of the six ligaments (left & right CL, PLL, FL and ISL) at each level are tensioned while just three (ALL and left & right CL) are loaded in extension (see table 2.1). The model is in reasonable agreement with the results of Moroney although appearing to be too stiff in flexion at C6-C7 and C7-T1 and too flexible in extension at C2-C3. For the upper cervical spine segment C0-C2 the models response is in good agreement with the experimental results.

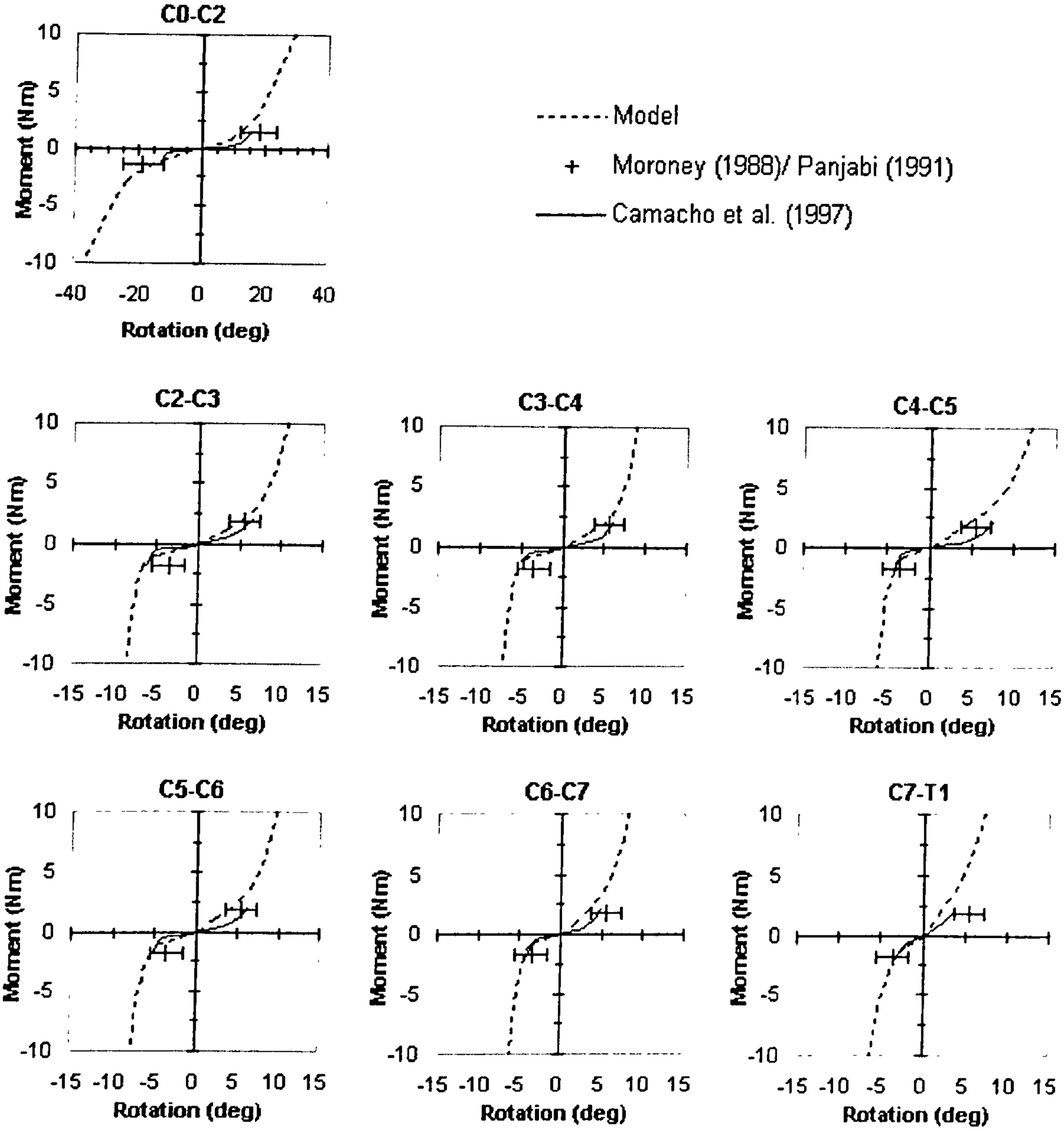


**Figure 5.8:** Flexion (+Rotation) and extension (-Rotation) response of each level of the ligamentous cervical spine model compared against the torque-rotation functions of Camacho et al. (1997) and the static small load displacements reported by Moroney et al. (1988) (C2-C7) and Panjabi et al. (1991) (C0-C2).

## 5.4 Coupling Characteristics of the Head-Neck Model

In the lower cervical spine there are two characteristic coupling motions present due to the orientation of the facet joints. Firstly flexion is coupled with anterior shear and extension with posterior shear. Secondly lateral bending is coupled with axial rotation and visa versa (White and Panjabi, 1990; Milne, 1991; and Bogduk et al., 2000).

From the results of the small load simulations (figure 5.1) it can be seen that the lower cervical spine segments exhibit the characteristic coupling of anterior shear with flexion and posterior shear with extension. In flexion however the amount of coupled anterior shear is small compared to the results of Moroney.

It can be seen form the small load simulations that axial rotation is coupled with lateral bending and also that lateral bending is coupled with axial rotation for both lower cervical spine motion segments tested. For segment C3-C4 there are 1.76 degrees of coupled right axial rotation with 3.04 degrees of right lateral bending, a ratio of 0.58. This is in agreement with White and Panjabi (1990) who state a ratio of 0.67. At C5-C6 the ratio reduces to 0.48 which is in agreement with the theory that there is a gradual decrease in the amount of axial rotation that is associated with lateral bending the further down the cervical spine you go (White and Panjabi 1990).

Similarly for coupled lateral bending with axial rotation the ratios are 0.64 and 0.78 for C3-C4 and C5-C6 respectively. Moroney's results give a lower but still comparable ratio of 0.51.

Mimura et al. (1989) presented the ROM for the lower cervical spine in axial rotation along with the range of coupled lateral bending at each vertebral level determined by Biplanar radiography. The load required to produce the ROM was not reported making it difficult to reproduce the experiments however it is still useful to compare the level of coupled motion when a similar degree of axial rotation is reached in the head-neck model. It was found that an applied load of 5Nm at C0 produced a comparable amount of axial rotation at each level of the lower cervical spine. Figure 5.9 shows the simulated response at

each level compared against the results of Mimura et al. (average ±SD) for axial rotation and coupled lateral bending. The models response is in good agreement with the experimental data demonstrating that a similar level of coupled lateral bending is reached at each level of the lower cervical spine model.

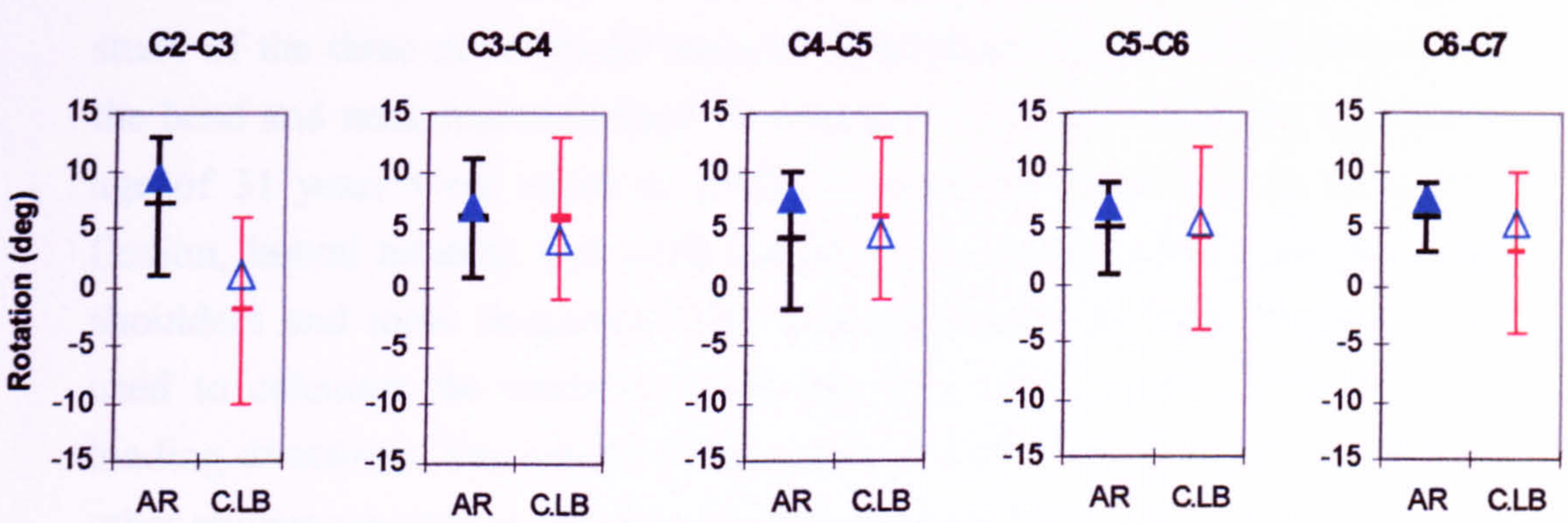


**Figure 5.9:** Normal range of motion of the lower cervical spine in axial rotation (AR) and range of coupled lateral bending (C.LB) shown against the results of Mimura et al. (average ± SD). Rotational displacement is shown on the vertical axis. The models response at each level is shown by ▲ for AR and by Δ for C.LB.

## 5.5 Moment Generating Capacity of Neck Muscles

To validate the muscles of the model the total moment generating capacity of the neck muscle elements are compared to those found experimentally using human volunteers. Vasavada et al. (2001) have presented the most complete study of the three-dimensional moment generating capacity of the muscles of the head and neck region to date. 11 men and 5 women volunteers with mean age of 31 years were asked to produce maximum head force in extension, flexion, lateral bending and axial rotation in an upright sitting position with shoulders and torso restrained. The measured forces in each direction were used to calculate the moments about the base of the neck for each of the loading directions. The results of this study as well as those from a number of other studies are used to validate the muscle elements of the head-neck model.

### 5.5.1 Method for Simulating Isometric Muscle Strength

The isometric strength of the neck muscles was simulated by activating each muscle group maximally while anchoring the rigid bodies of the model in their initial position. Moments were then resolved about the T1 anatomical coordinate system to calculate the moment generating capacity of each muscle element about the three axes of revolution. The moments generated are in flexion and extension (force generated by muscles on both sides of the neck), and axial rotation and lateral bending (force generated on one side only).

### 5.5.2 Results for Moment Generating Capacity of the Neck Muscle Elements

With all muscles maximally activated, the model estimates a total extension moment of 47Nm with the Semispinalis Capitis and Cervicis (29%), Multifidus (25%) and Levator Scapulae (18%), having the most significant contribution. The remaining 28% of the total extension moment is generated by the Longissimus, Splenius and Trapezius muscles (Figure 5.10A). The Sternocleidomastoid produces over half the flexion moment about T1 (55%)

with the other half shared fairly evenly between the three Scalenus muscles (24%) and the Longus Colli (22%) (Figure 5.10B). The total axial rotation moment (Figure 5.10C) is predicted to be 19 Nm with the Trapezius muscle having the most significant contribution (41%). Finally for lateral bending the total moment-generating capacity is 39Nm with the Trapezius (29%) and Scalenus (27%) muscles providing over half the moment with the Levator Scapulae, Sternocleidomastoid and Multifidus also providing significant contributions (Figure 5.10D). Table 5.3 compares the moments generated about T1 with those measured in a number of studies. It is thought that these values are in close enough agreement with the experimental values presented. It should be noted that the value of specific tension used in the model simulations was 50N/cm2, thought to represent an average male with reasonably developed musculature. Clearly the choice of specific tension value will affect the total-moment generating capacity predicted by the model but will not affect the relative contributions of the muscles.

**Table 5.3:** Comparison of neck muscle moments.

| Study | No. & Gender of Subjects | Extension Moment (Nm) | Flexion Moment (Nm) | Axial Rotation Moment (Nm) | Lateral Bending Moment (Nm) |
|---|---|---|---|---|---|
| Harms-Ringdahl & Schuldt (1988) | 10F | 29 | | | |
| Jordan et al. (1999) | 50M | 55 (14) | 21 (8) | | |
| | 50F | 48 (15) | 19 (4) | | |
| Mayoux-Benhamou et al. (1993) | 5M, 10F | 53 (12) | | | |
| Queisser et al. (1994) | 12M | 60 (9) | | | |
| Vasavada et al. (2001) | 11M | 52 (11) | 30 (5) | 15 (4) | 36 (8) |
| | 5F | 21 (12) | 15 (4) | 6 (3) | 16 (8) |
| **Head-Neck Model** | - | **47** | **17** | **19** | **39** |

*Note.* Mean (and standard deviation where available). M-males, F-females.

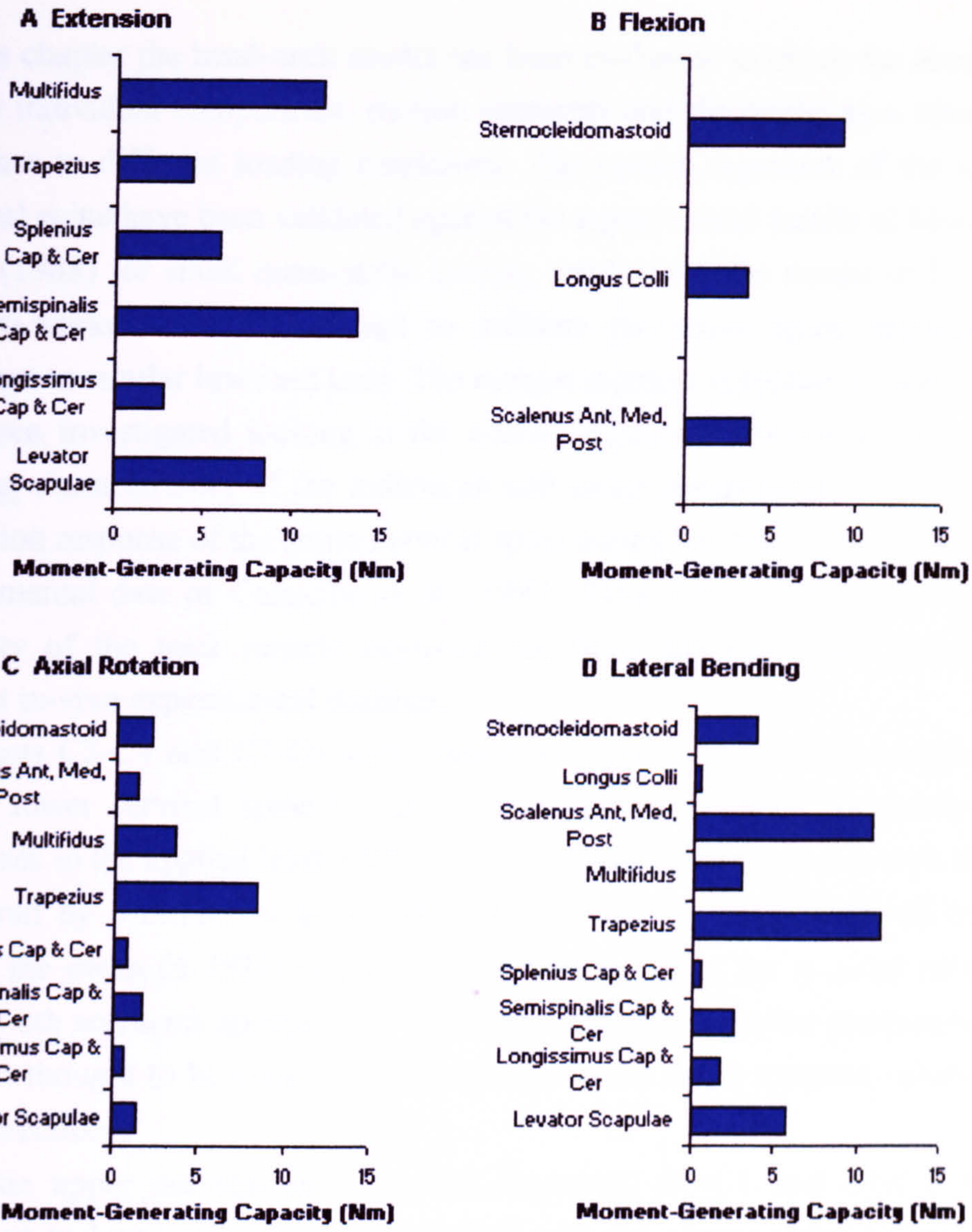


**Figure 5.10:** Moment-generating capacity of the muscle groups of the head-neck model in the initial position. Extension/Flexion; total contribution of each muscle group on both sides of the neck. Axial Rotation/Lateral Bending, total contribution of each muscle groups on one side only.

## 5.6 Discussion

In this chapter the head-neck model has been evaluated to check the accuracy of the individual components, motion segments and the model as a whole in response to different loading conditions. The motion segments of the lower cervical spine have been validated against the experimental results of Moroney et al. (1988) for small quasi-static loading conditions. The results of Panjabi and co-workers have been used to validate the upper spine segment in response to similar low load tests. The motion segment response to large loads has been investigated looking at the overall segment response and also the loading characteristics of the individual soft tissue components. The flexion-extension response of the entire cervical spine model has been compared to the experimental data of Camacho et al. (1997). Finally the moment-generating capacity of the neck muscle elements has been calculated and compared against in-vivo experimental findings.

Segments C3-C4 and C5-C6 were chosen as representative motion segments of the lower cervical spine for quasi-static low load testing. Generally the responses to the applied loads (20N, 1.8Nm) are in good agreement with those measured by Moroney et al. (1988) with the main displacements all being within the mean (± 1SD) of the reported values except for in axial rotation where both segments appear to be slightly too flexible. Coupled displacements are also thought to be reasonable being close to the mean reported values for most directions.

Both the upper cervical spine motion segments, C0-C1 and C1-C2 were subjected to low load tests and compared with the experimental findings of Panjabi and co-workers. The main displacements of C0-C1 are all with 1 SD of the reported experimental values and lie close to the average for flexion, extension and lateral bending. The main displacements of the C1-C2 segment are in reasonable to good agreement for flexion and extension loading but appear slightly too stiff in axial rotational and lateral bending compared with experimental data. Coupling between lateral bending and axial rotation for both upper spine segments is weak compared to those measured experimentally.

The next stage of validation was to subject the same motion segments to larger loads of 500N and 20 Nm in all directions of loading. The responses to rotational loading are compared to the in-vivo range of motions as reported by White and Panjabi (1990). The loads used to produce these in-vivo ranges are not known so the fact that the model segments exceed these values for some directions of loading does not invalidate the results. The responses to translation loading are also presented but no experimental data is available for comparison. A realistic response is seen for all directions of loading for both upper and lower cervical spine segments. Due to the non-linear properties of the discs in the lower segments for flexion and extension a clear neutral zone can be seen where only a small load is needed to significantly displace the segment. For other loading directions the neutral zones are not so pronounced due to the linear stiffness of the discs resulting in larger initial stiffness of the segments. Due to there being no disc present between C0-C1 and C1-C2 all resistance to load comes from the ligaments and facet joints. Clear neutral zones are observed for all directions of rotational loading due to the non-linear response of the ligaments.

A break down of all the forces present in the individual components of the C5-C6 and both upper cervical spine motion segments when subjected to the large quasi–static loads is presented. The load distribution of the components of the upper cervical spine when subjected to large loads shows the important role of the alar ligaments in limiting axial rotation and lateral bending in the C0-C1 joint.

The entire ligamentous cervical spine model was tested in flexion-extension loading and displacements at each level compared against the results of Camacho et al. (1997) and Moroney et al. (1988). The model shows good agreement for extension but appears to be too stiff in flexion; this is thought to be due to the greater contribution of the ligaments in flexion. The model is in reasonable agreement with the results of Moroney although appearing to be too stiff in flexion at C6-C7 and C7-T1 and too flexible in extension at C2-C3. For the upper cervical spine segment C0-C2 the models response is in good agreement with the experimental results.

Coupling characteristics of the model have been demonstrated and shown to be in good agreement with those observed experimentally. A qualitative comparison has been made with the experimental results of Mimura et al. (1989) showing that a reasonable level of coupled lateral bending is produced at each level of the cervical spine when subjected to axial rotation. The other significant coupling characteristic of the lower cervical spine, where extension is coupled with anterior shear and flexion with posterior shear, has been demonstrated in the small load simulations.

In the final section of this chapter the moment-generating capacity of the muscle elements has been compared with those calculated in-vivo on human volunteers. Reasonable levels of moment about T1 are reached in each direction of rotational loading in comparison with those found experimentally. In conclusion, this chapter has presented the evaluation and validation of the cervical spine model showing it to be in good agreement with experimental findings from actual human cervical spine specimens. The model segments have been tested in all directions of loading showing main and coupled motions to be accurate and realistic. It has been shown that the model can predict the loads and deformations of the individual soft-tissue elements making the model suitable for injury analysis. The validation of the muscle elements shows the morphometric values, origins and insertions selected in the previous chapter to be reasonable. The following chapter looks at the dynamic simulation of frontal and lateral impacts to further validate the completed head-neck model.

# CHAPTER 6

# Model Response to Frontal and Lateral Impacts

This chapter compares the head and neck model response to frontal and lateral impacts against human volunteer response data. To further validate the model it is important to check its ability to predict the dynamic response of the head and neck when subjected to acceleration pulses representing frontal and lateral automobile impacts. Response corridors based on sled acceleration tests with human volunteers are used to evaluate the model and investigate the effect of muscle activation on the head-neck motion. The response corridors used here have also been used by other researchers to validate mathematical and mechanical models of the head and neck (De Jager, 1996; van der Horst, 1997, 2002; THOR, 2001; and Thunnissen et al., 1995). The corridors specify the response that a valid model of the human head and neck should meet. Firstly the impacts are simulated with both passive and active muscle behaviour. Secondly the local loads in the soft-tissue elements are analysed and finally the effects of muscle specific tension, reflex time and level of activation on the kinematic response of the model are investigated.

## 6.1 NBDL Volunteer Data

The response corridors used to validate the model were produced from sled acceleration tests with human volunteers performed at the Naval Biodynamics Laboratory (NBDL). In the experiments conducted at the NBDL male human volunteers were seated in an upright position on a sled driven HYGE accelerator and exposed to short duration accelerations simulating 15g frontal and 7g lateral impacts. The resulting three-dimensional motions of the head

and first thoracic vertebral body (T1) were monitored by anatomically mounted accelerometers and photographic targets. In the frontal impact experiments the test subjects were restrained with shoulder straps, a lap belt and a pelvic strap to prevent movement of the torso during testing. Arm and wrist restraints were also used to prevent flailing. An additional chest strap was used in the lateral impacts to minimise loading of the right shoulder and a lightly padded wooden board was placed against the right shoulder to limit torso motion further (Wismans et al., 1986).

Wismans et al. (1986) presented results of the NBDL tests for frontal and lateral impacts while a new analysis of the most severe frontal impacts was made later by Thunnissen et al. (1995). The original data are used to validate the models response to lateral impact while the response corridors presented by Thunnissen et al. (1995) are used to validate the models response to frontal impact.

### 6.1.1 Frontal Impact Response Corridors

Thunnissen et al. (1995) analysed frontal tests that had a peak sled acceleration of 14.5g or higher; this resulted in 9 tests with 5 volunteers (all but one were tested twice). The average volunteer height was 169.1cm and the average weight 67.9kg. The tests were analysed using a two-pivot head-neck linkage mechanism. Three links represent the head, neck and torso connected by two pivots allowing rotation in the plane of impact. The upper pivot is located at the occipital condyles and the lower pivot at the T1 anatomical coordinate system, which was defined as being at the anterior superior corner of the vertebral body of T1, the x, y and z axis been forward, to the right, and upward. The neck link is flexible in the axial direction. It was found that the peak acceleration of T1 was twice as high as the applied sled acceleration due to deformation of the thorax/restraint system. Therefore to simulate the frontal impact the acceleration time history of T1 has been used as input to the head and neck model to avoid having to model the thorax and restraint system. Vertical acceleration during the sled tests was small enough to be ignored. The average acceleration and rotation time histories of T1 for the 15g frontal impacts are shown in figure 6.1.

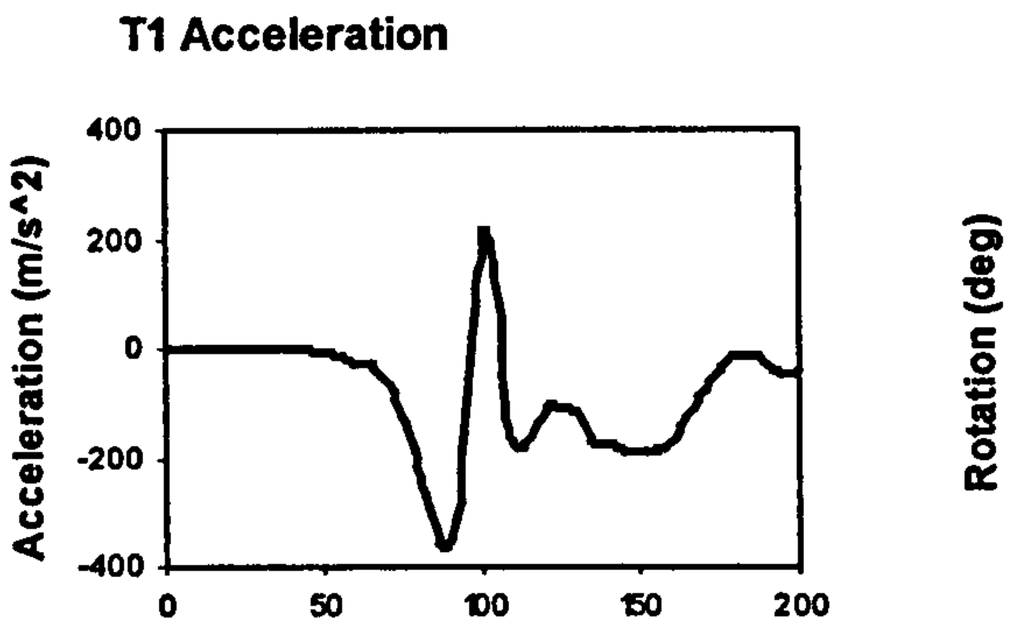


**Figure 6.1:** Average T1 acceleration and rotation used as input to the head-neck model to simulate frontal impact. Acceleration in x-axis, rotation about y-axis.

Thunnissen et al. (1995) have presented a series of response corridors defined as the response at plus and minus one standard deviation of the averaged response for the nine tests analysed. The corridors used to validate the head-neck model response are shown in figures 6.2-6.8.

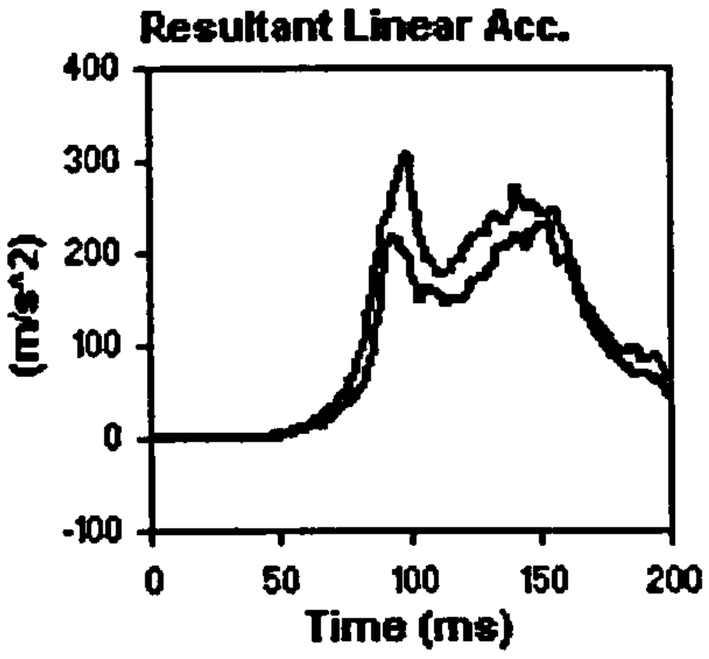


**Figure 6.2:** The resultant linear acceleration of the centre of gravity of the head relative to the laboratory coordinate system.

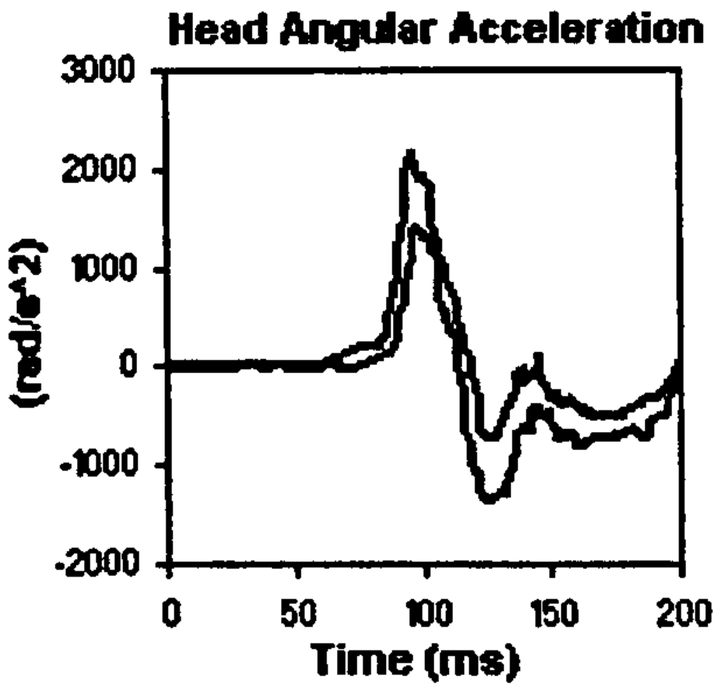


**Figure 6.3:** The mid-sagittal angular acceleration of the head, y-component relative to the laboratory coordinate system

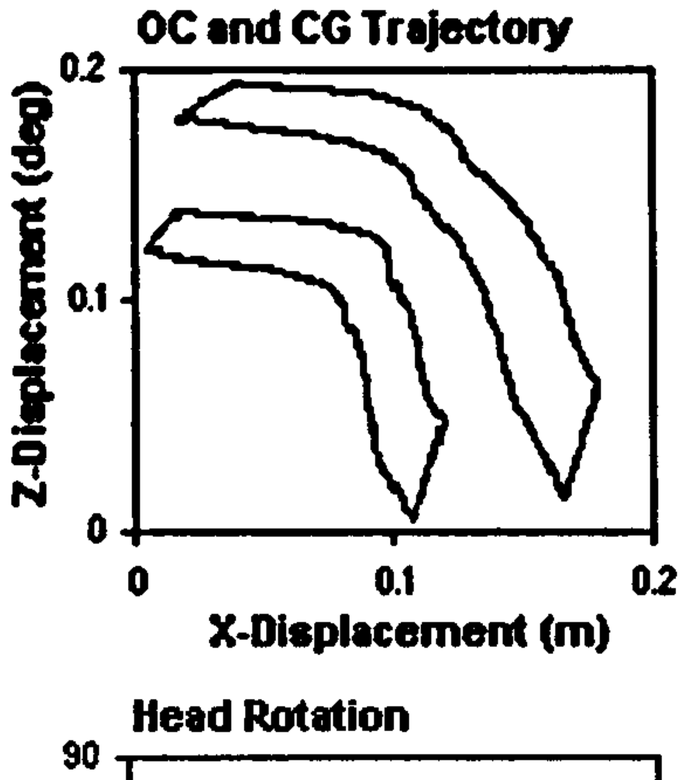


**Figure 6.4:** The trajectories of the head centre of gravity and of the occipital condyles in the mid-sagittal plane relative to the T1 coordinate system, the corridor shows the trajectory for the loading phase of the impact until the head reaches maximum flexion at around 175ms.

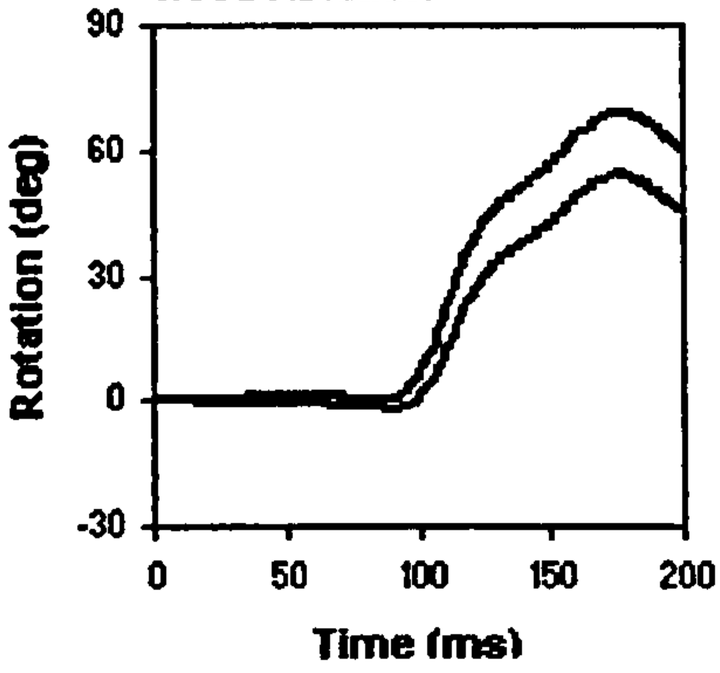


**Figure 6.5:** The rotation of the head in the y-axis.

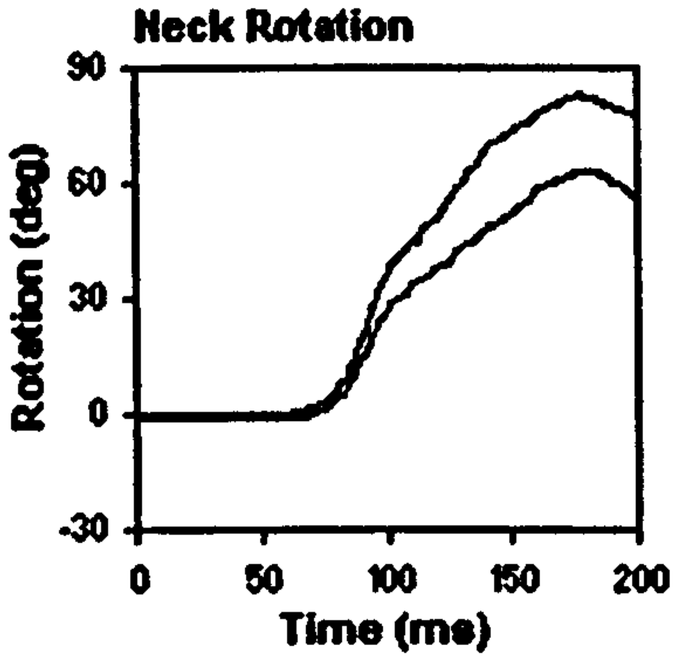


**Figure 6.6:** The rotation of the neck link in the y-axis, the neck link was defined as a point-to-point connection between the T1 anatomical origin and the origin of the occipital condyles.

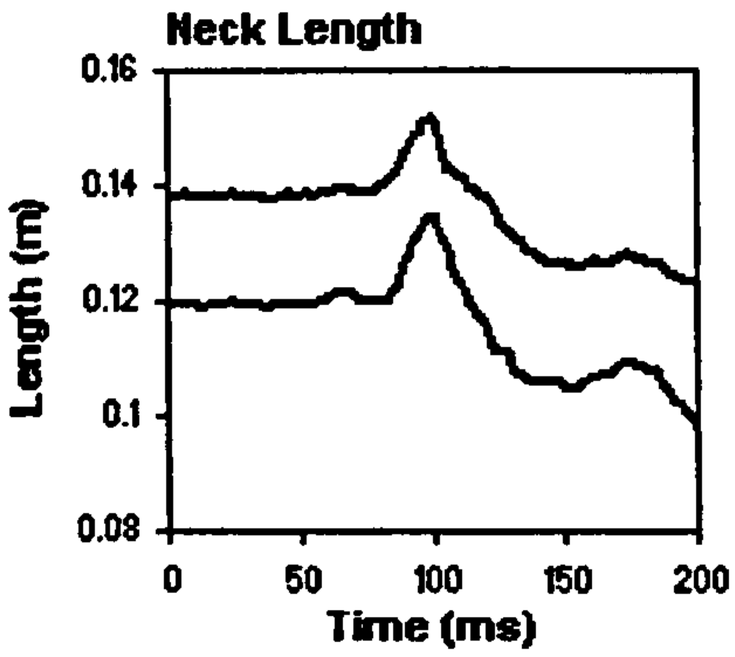


**Figure 6.7:** Neck link length with time.

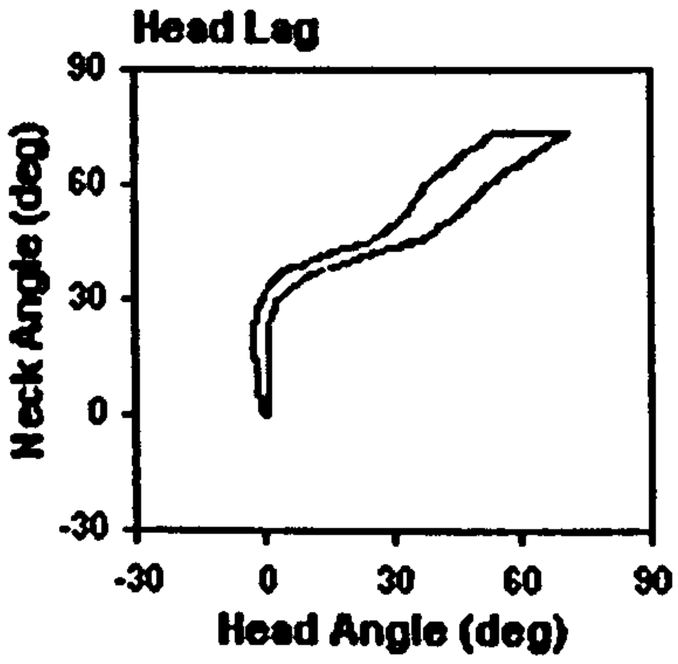


**Figure 6.8:** Head lag; a cross plot of the head and neck link angle.

## 6.1.2 Lateral Impact Response Corridors

A similar set of response corridors has been produced from lateral impact sled tests on human volunteers at the NBDL. These tests were analysed by Wismans et al. (1986) and the corridors derived using a similar two-pivot model as used for the frontal impact corridors. The lateral impacts performed were less severe then the frontal impacts with a peak acceleration of 7g. 9 volunteers were tested with a mean height of 177cm and weight 76kg. The measured acceleration at T1 is used as the model input this time in the y-direction to simulate the impact with prescribed rotation of T1 about the x-axis. T1 acceleration and rotation inputs are shown in figure 6.9 and the response corridors used to validate the head-neck response to lateral impacts are shown in figures 6.10-6.13.

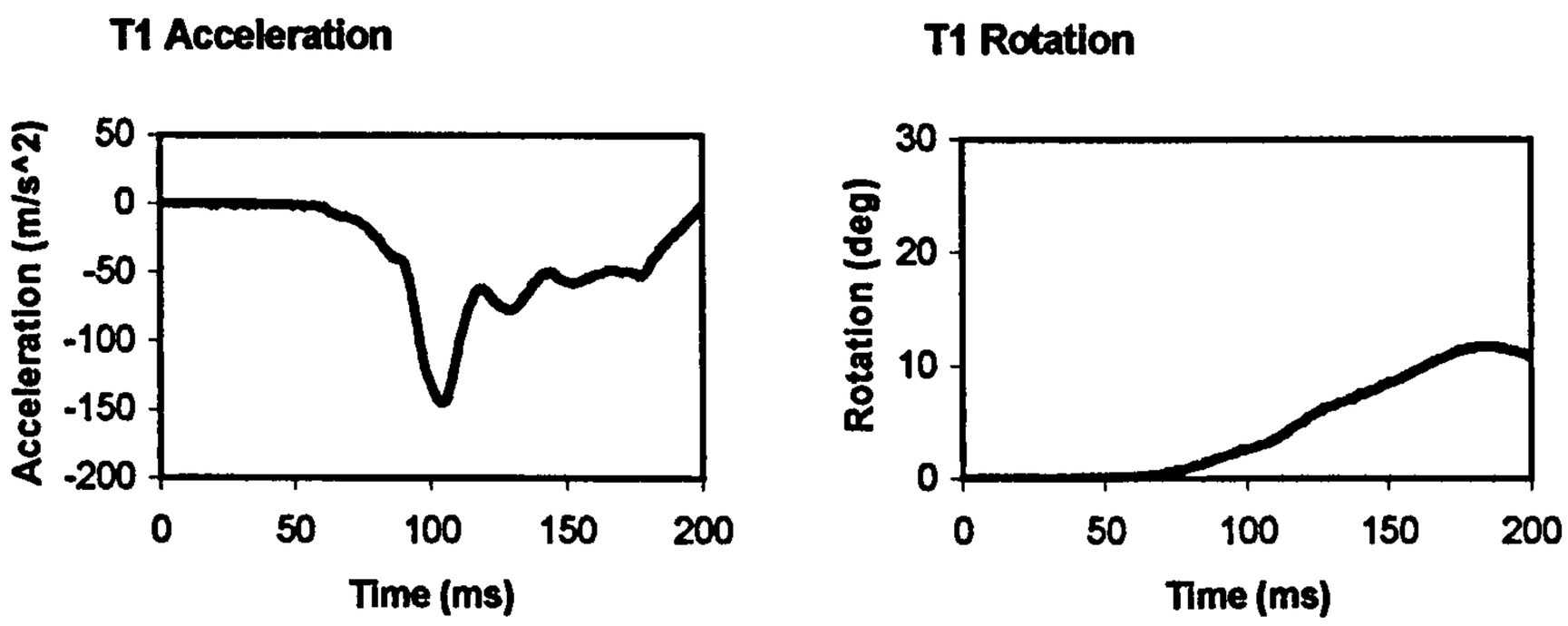


**Figure 6.9:** Average T1 input acceleration and rotation for 7g lateral impact simulation. Acceleration in y-axis, rotation about x-axis.

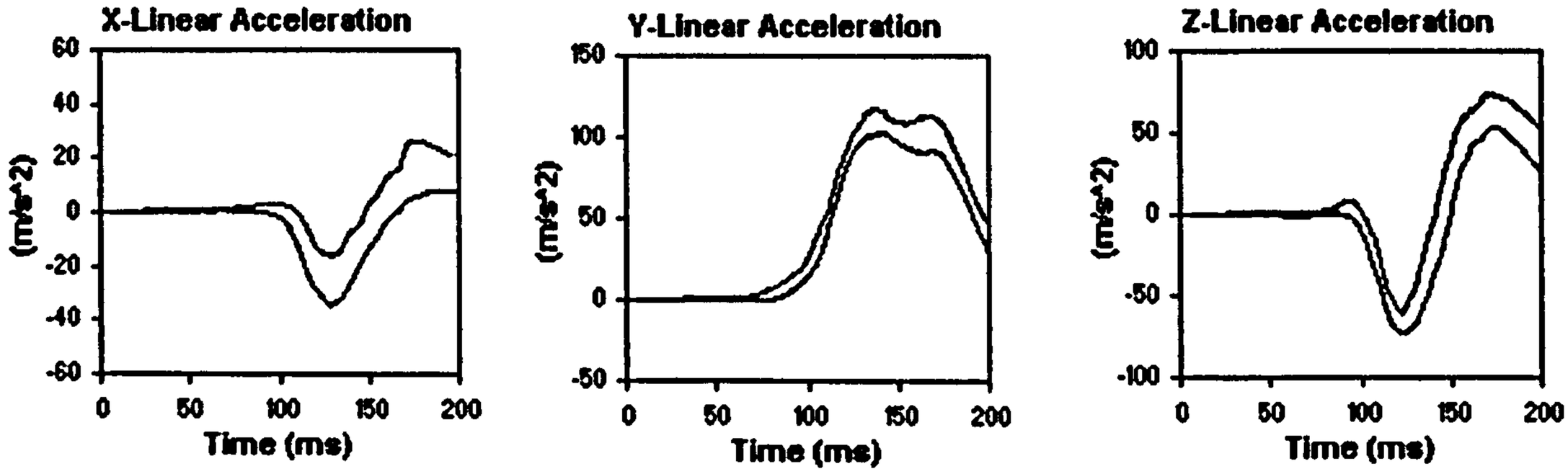


**Figure 6.10:** The x, y, and z- components of the linear acceleration of the head centre of gravity relative to the laboratory coordinate system.

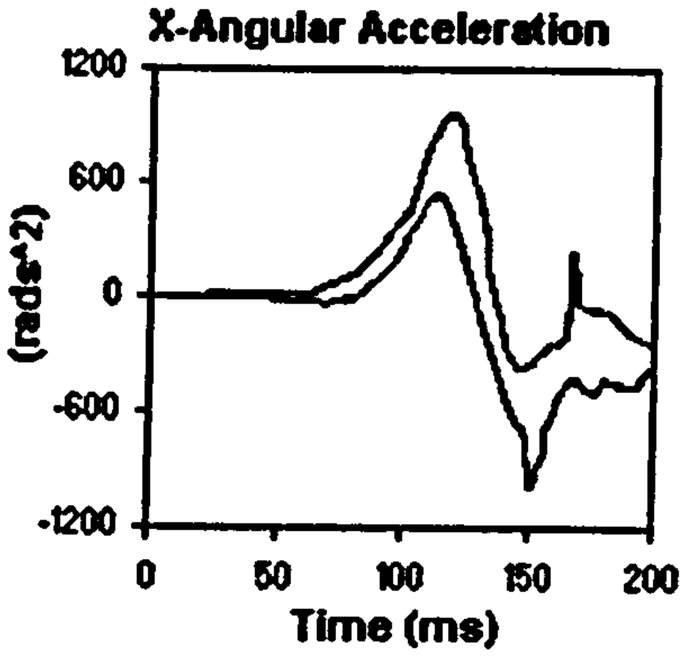


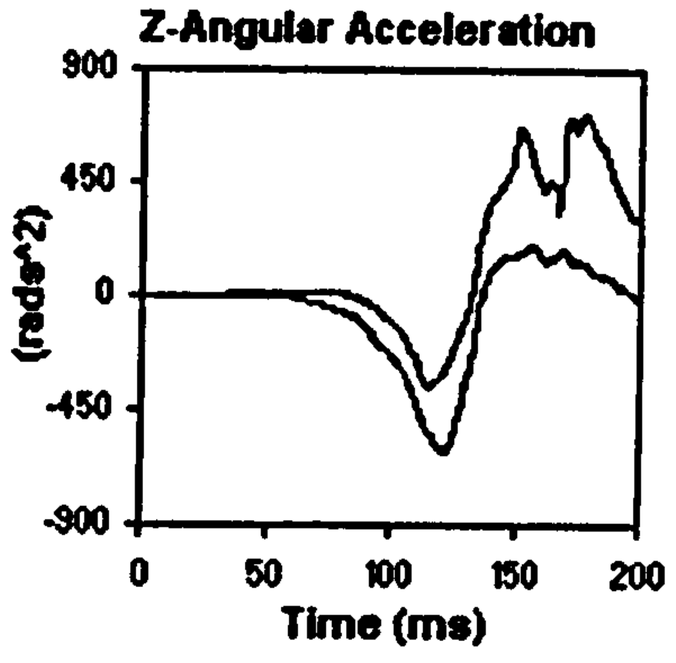


**Figure 6.11:** The x (lateral) and z (axial) angular acceleration of the head centre of gravity relative to the laboratory coordinate system.

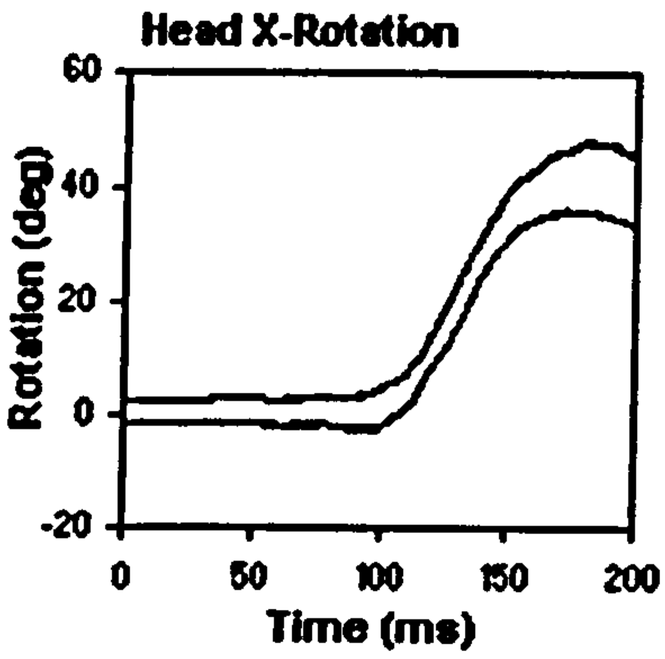


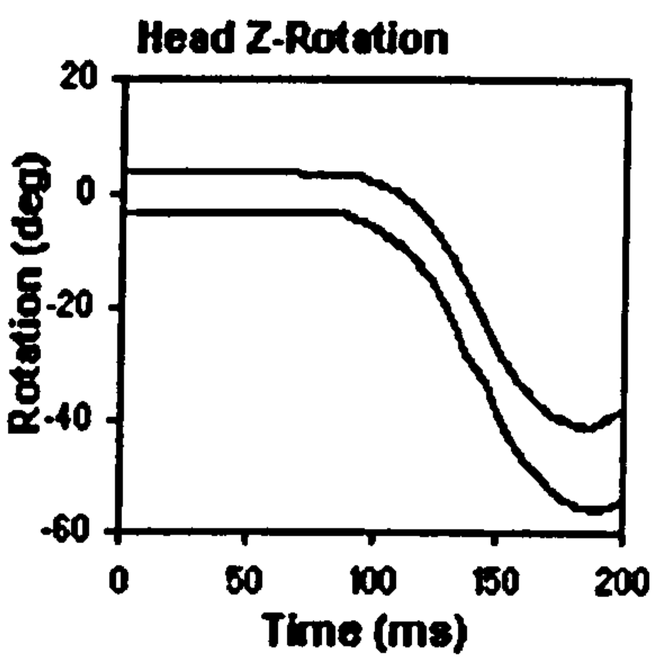


**Figure 6.12:** Rotation of the head in the x (lateral) and z (axial) axis.

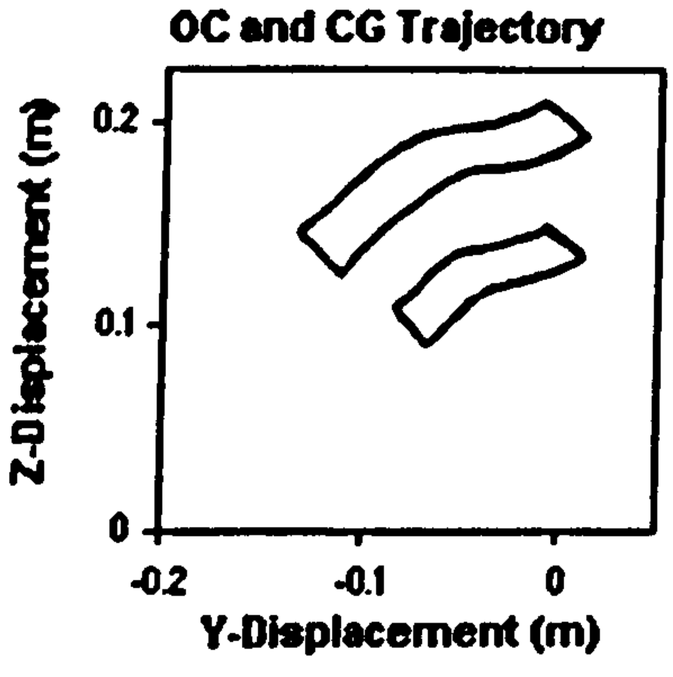


**Figure 6.13:** The trajectories of the head centre of gravity and of the occipital condyles in the lateral plane relative to the T1 coordinate system; the corridor shows the trajectory for the loading phase of the impact until the head reaches maximum lateral flexion at around 175ms.

## 6.2 Model Set-up and Simulation

In both impact simulations, frontal and lateral, the average T1 acceleration and rotation (see figures 6.1 and 6.9) from the human volunteer tests are used as inputs to the head-neck model. Motion of the T1 vertebrae was limited to the direction of impact while the rest of the model was left free to move in all directions. For frontal impact simulation T1 was accelerated in the x-axis and rotated about the y-axis while for lateral impact T1 was accelerated along the y-axis and rotated about the x-axis. For all other directions motion was found to be negligible in the analysis of the volunteer results (Wisman et al., 1986 and Thunnissen et al., 1995).

Contrary to the popular opinion that the muscles of the neck are unable to respond fast enough when exposed to high speed trauma recent research indicates that the role of the muscles in limiting head-neck motion during impact may be significant. Siegmund and Brault (2000) state that the cervical muscles can be activated early enough and are capable of altering the head and neck kinematics during impact trauma. It is conceivable that muscle contraction may have taken place in the experiments on the human volunteers at the NBDL and so experiments with active and passive musculature are simulated and compared with the response corridors. Cervical muscle contraction during trauma is thought to be a reflex response but the pathways mediating the response are unclear. There are a number of possible ways that the muscles may be triggered; during an impact there is a rapid sequence of events that may lead to the muscle reflex such as a loud noise on impact, vehicle motion and vibration and induced whole-body motion. The reflex time, the time between stimulus and muscle activation, has been shown to be anywhere between 60 and 175 ms for cervical spine muscles (Siegmund and Brault, 2000). An initial reflex response time of 75ms has been used in the frontal and lateral impact simulations. All muscles are activated together after the 75ms reflex time. The effect of reflex time is explored further in section 6.6.

All simulations were conducted on a standard desktop pc with AMD Athlon XP 2400 CPU, and 1GB PC2700 DDR RAM, 200ms of simulation taking approximately 11,000 cpu seconds.

## 6.3 Frontal Impact Simulation Results

Figure 6.14 depicts the overall head–neck model response with active musculature over the first 200 ms of the 15g frontal impact. Muscle reflex time was set to 75 ms. Over the initial stages of impact (<100ms) as the neck is rotating forward the head translates forwards with respect to T1 with very little rotation. Following 100 ms up to around 160ms, where maximum forward flexion is reached, the head and neck rotate together. After the point of maximum flexion the head and neck begin to rebound towards the initial position. Muscle force vectors are shown in blue and it can be seen how force is developed in the extensor muscles as the head is thrown forward then on rebound the flexor muscles of the neck try to resist the return motion of the head.

The model is compared to the NBDL volunteer response corridors for both active and passive muscle behaviour to see the effect muscles forces have on the overall response of the model. The resultant accelerations of the head are shown in figure 6.15a-d along with the trajectories of the occiput and centre of gravity of the head. The linear and angular accelerations of the head with active muscles differ only slightly from the passive response and both are in reasonable agreement with response corridors. The drop in linear acceleration at round 110ms is too great in the model compared to that experienced by the human volunteers and the peak angular accelerations of the head appear slightly too weak. The trajectories of the occipital condyles and the head centre of gravity fall well within the corridors for active muscle response; with passive properties the head displacement is greater in the horizontal direction. Figure 6.16a-d shows the head and neck rotation, neck length and head lag of the model compared to the response corridors of the NBDL volunteers. Neck rotation agrees well with the corridor for the first 110ms, after which rotation becomes too large and exceeds the corridors slightly, maximum rotation of the neck is reached at 160ms around 15ms earlier than the volunteers. Muscle activation plays only a small role in reducing the maximum rotation of the neck. Head rotation of the model with active and passive muscle behaviour agrees well with the corridor for the first 140 ms after which head rotation of the passive model becomes too great, the resistive force developed by the

active muscles prevent the head rotation from exceeding the corridors. The effect of active muscle contraction can also be clearly seen in the graph showing change of neck length with time (figure 6.16c). With passive muscles the length of the neck increases beyond the corridor but with the stiffening effect of the active muscles the model response falls well within the corridor. The length of the neck starts to return towards its starting length sooner than was seen with the volunteers. Figure 6.16d shows the neck angle versus the head angle showing how the flexion of the head lags behind the rotation of the neck link for both passive and active muscle simulation during the initial stages of impact. Practically no head rotation was experienced by the volunteers for the first 100ms of impact whereas the model shows around 5° of forward flexion. After the neck link reaches around 35° both the head and neck rotate together and follow the volunteer corridor closely. Towards the end of the impact, head rotation of the passive model begins to exceed the rotation of the neck link as the model begins to rebound.

Figure 6.17 shows the rotation about the y-axis between each vertebral pair of the active and passive neck model compared against the static in-vivo ranges of motion reported by White and Panjabi (1990) for flexion-extension. The affect of muscle stiffening is most noticeable and significant in the upper two joints. With passive properties the upper cervical segments are forced into some degree of extension as the head rotation lags behind the rotation of the lower neck. All other joints are forced into flexion as the neck rotates forward. The muscle forces developed hold the C0-C1 joint in extension between 100 and 150 ms, effectively locking the joint, and prevent this joint every going into flexion and thus reducing the overall rotation of the head significantly. The level of flexion reached in the C1-C2 joint is also greatly reduced by the active muscle forces. The joints of the lower cervical spine are all affected to a lesser degree by the active muscle forces, reducing the level of flexion reached in each joint. The joint rotations agree reasonably well with the in-vivo ranges of motion except for C7-T1 and C2-C3, which significantly exceed the boundaries.

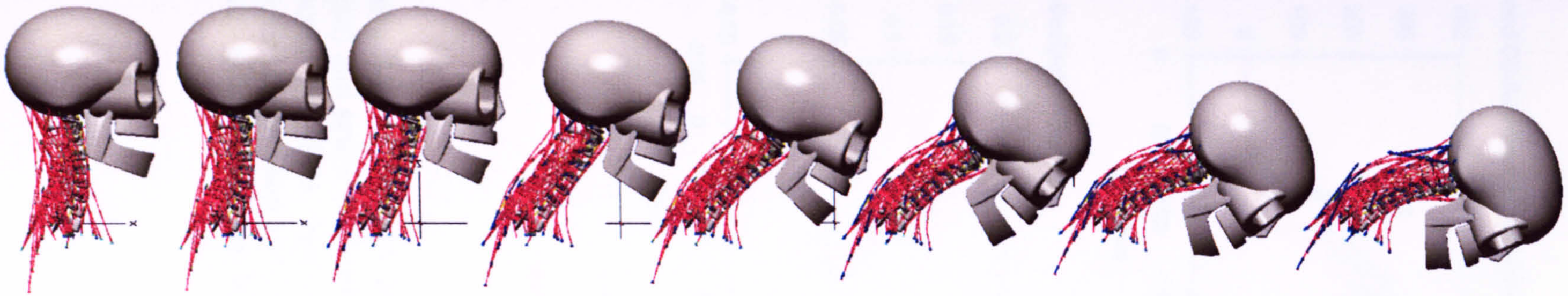


**Figure 6.14:** Time history of head-neck model response to 15g frontal impact with 100% active musculature. Muscle force vectors are shown in blue.

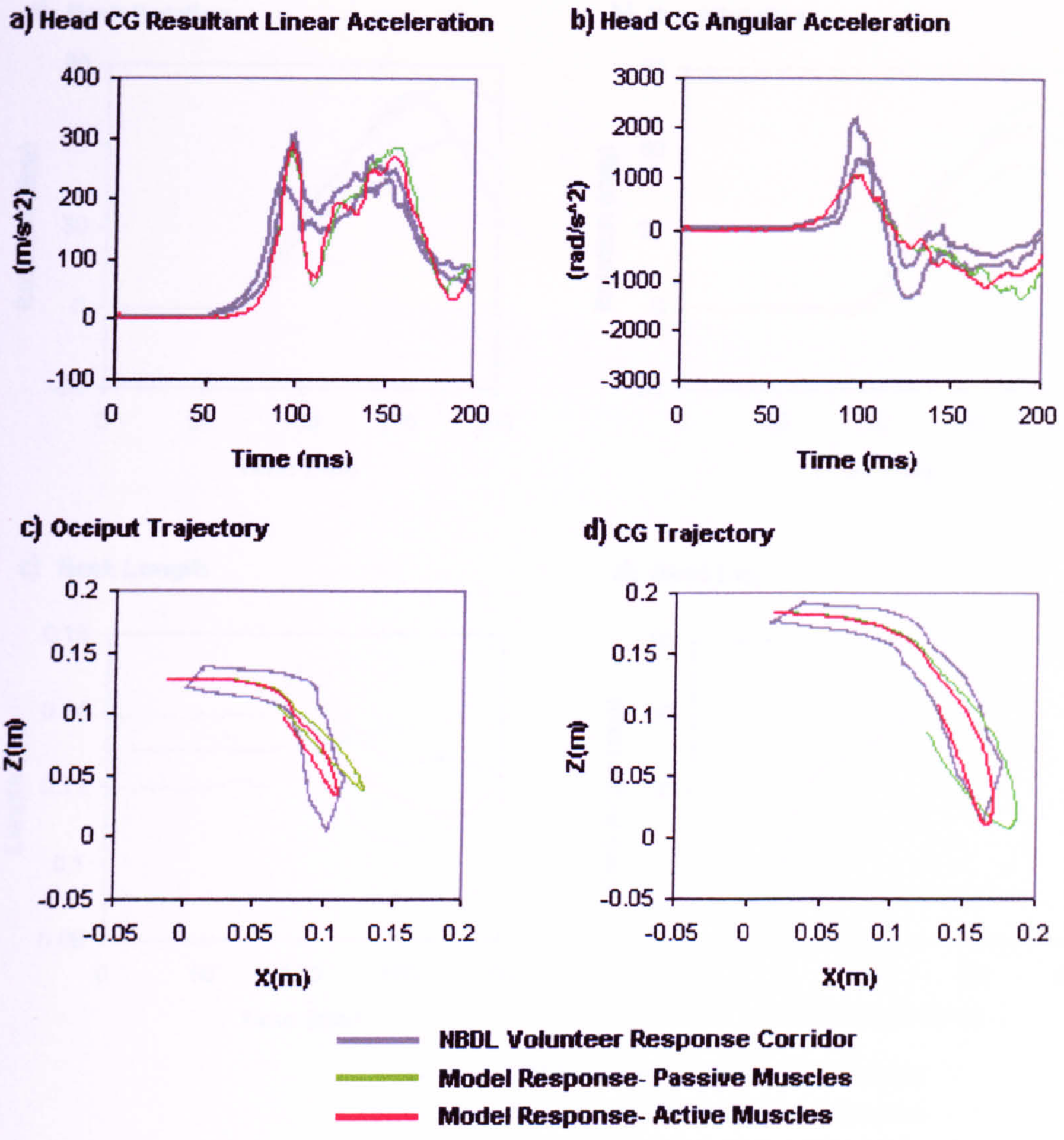


**Figure 6.15:** Head-neck model response to 15g frontal impact with passive (green) and active (red) muscle behaviour compared against NBDL volunteer response corridors. Top row: resultant head centre of gravity linear and angular acceleration versus time. Bottom row: occiput and head centre of gravity trajectories in the horizontal (X) and vertical (Z) planes.

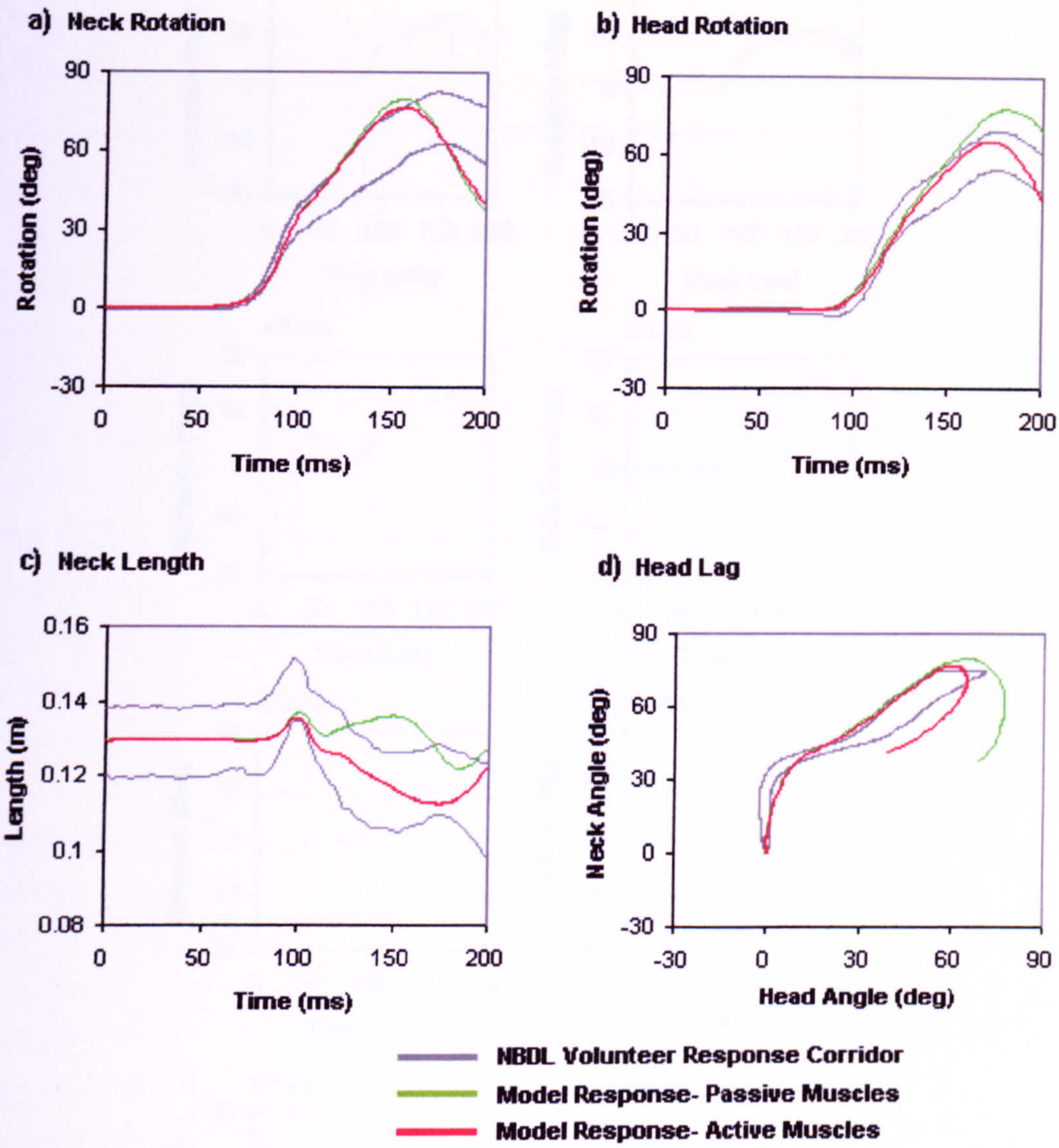


**Figure 6.16:** Head-neck model response to 15g frontal impact with passive (green) and active (red) muscle behaviour compared against NBDL volunteer response corridors. Top row: neck link and head rotation versus time. Bottom row: Neck link length versus time and head lag; cross plot of neck link angle and head angle.

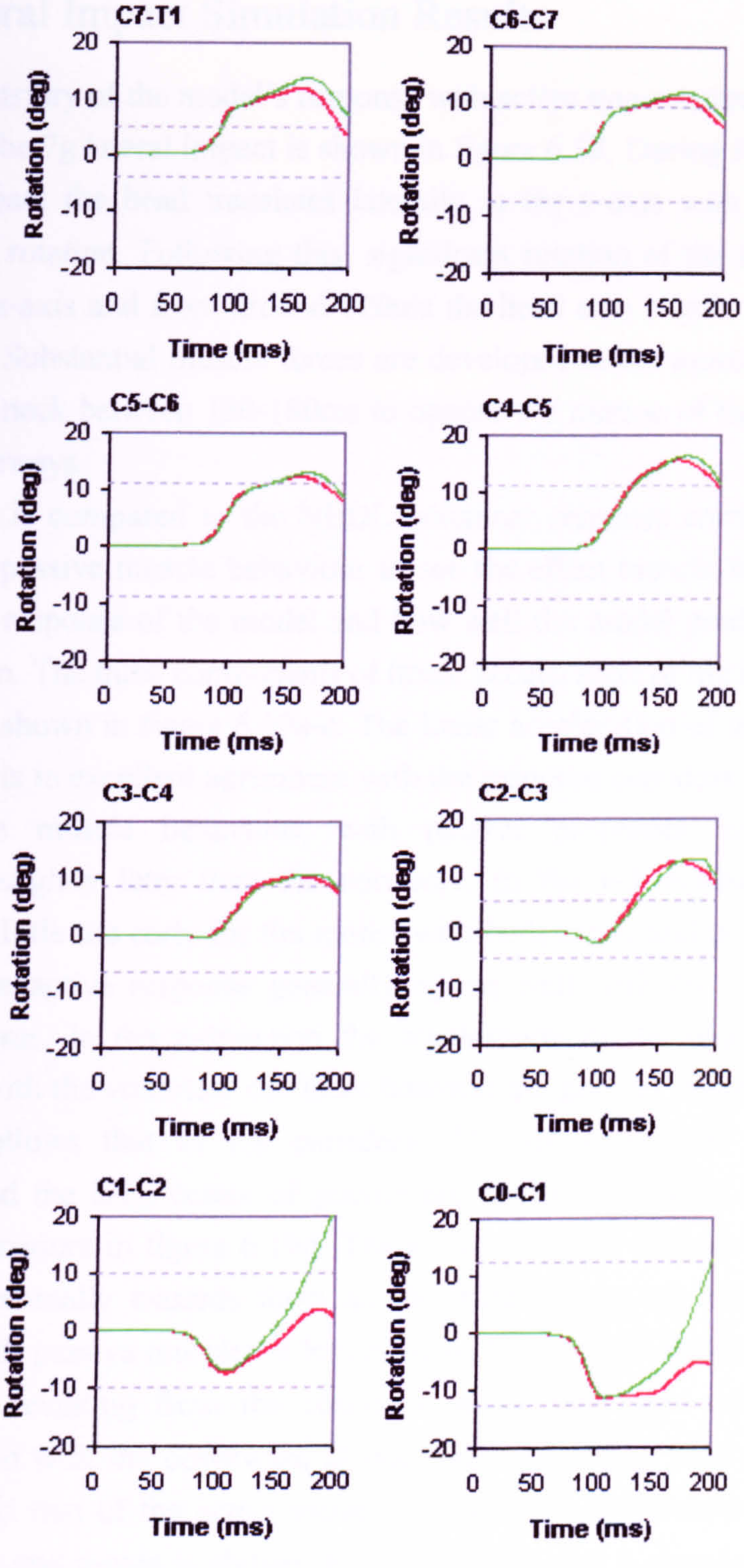


**Figure 6.17:** Intervertebral joint rotations about the y-axis for the 15g frontal impact. Shown are the active (red) and passive (green) model response compared against the static in-vivo ranges of motion (grey dotted lines, Tables 2.1 and 2.2, Chapter 2).

## 6.4 Lateral Impact Simulation Results

The time history of the model's response with active musculature over the first 200ms of the 7g lateral impact is shown in figure 6.18. During the first 110ms of the impact the head translates laterally in the y-axis with only a small amount of rotation. Following this, significant rotation of the head develops about the x-axis and from around 120ms the head also begins to twist about the z-axis. Substantial muscle forces are developed in the muscles on the left side of the neck between 130-180ms to oppose the motion of the head as it is thrown sideways.

The model is compared to the NBDL volunteer response corridors for both active and passive muscle behaviour to see the effect muscle forces have on the overall response of the model and how well the model predicts the head-neck motion. The three components of linear acceleration of the head centre of gravity are shown in figure 6.19a-c. The linear acceleration of the head in the x-direction is in excellent agreement with the response corridors for the model with active muscle behaviour, with passive properties acceleration is developed slightly later than the corridors. In the y-direction acceleration increases a little too early for the model with both active and passive muscles however the active response generally agrees well with the corridors after around 120ms. In the z-direction the acceleration of the model is smaller compared with the volunteer corridors however the general shape of the active response follows that of the corridors. The trajectories of the occipital condyles and the head centre of gravity are compared against the volunteer response corridors in figure 6.19d. The active response follows the corridors well but eventually exceeds them as the head rotates too far. The model response with passive muscles is less good with too much displacement in the y-direction, deviating from the corridors earlier than seen with the active response, and with the downward displacement exceeding both the volunteer corridors and that of the active model. The angular acceleration of the head about the x- and z-axis is shown in figures 6.20a and b showing reasonable agreement between the active model and the response corridors.

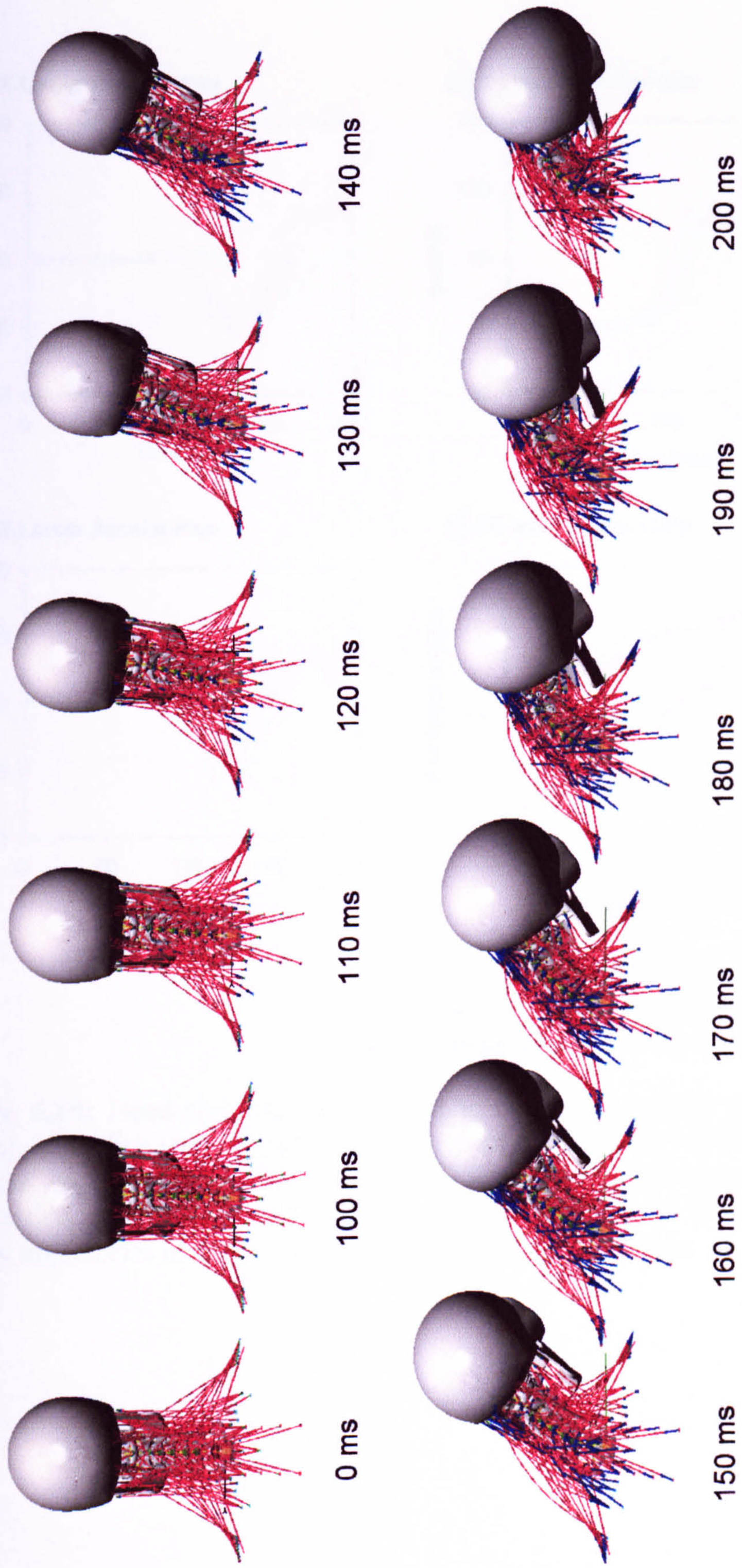


**Figure 6.18:** Time history of head-neck model response to 7g lateral impact with 100% active musculature. Muscle force vectors are shown in blue.

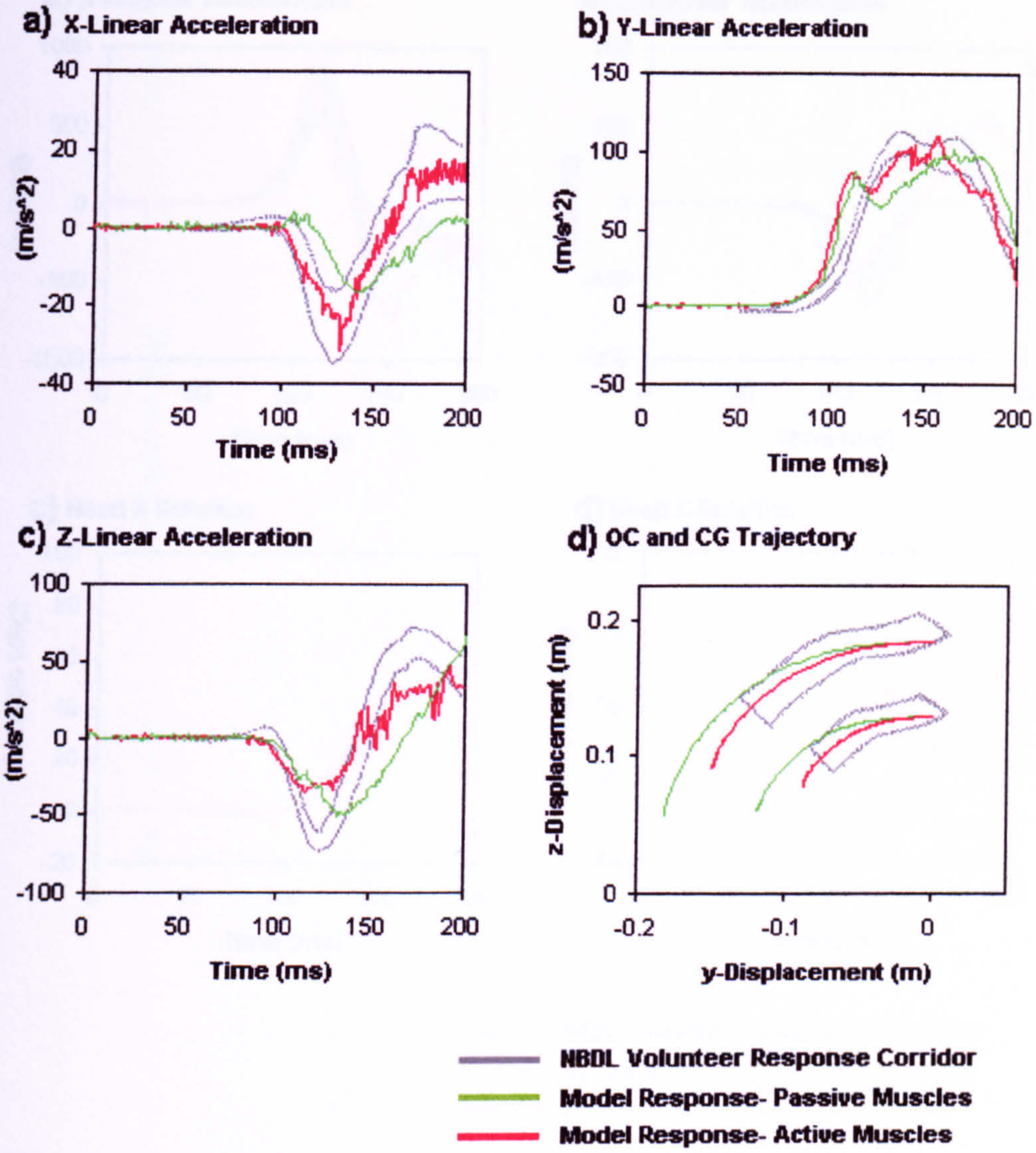


**Figure 6.19:** Head-neck model response to 7g lateral impact with passive (green) and active (red) muscle behaviour compared against NBDL volunteer response corridors. a), b) and c): x, y, and z linear components of the acceleration of the head centre of gravity. d): occiput and head centre of gravity trajectories in the horizontal (X) and vertical (Z) planes.

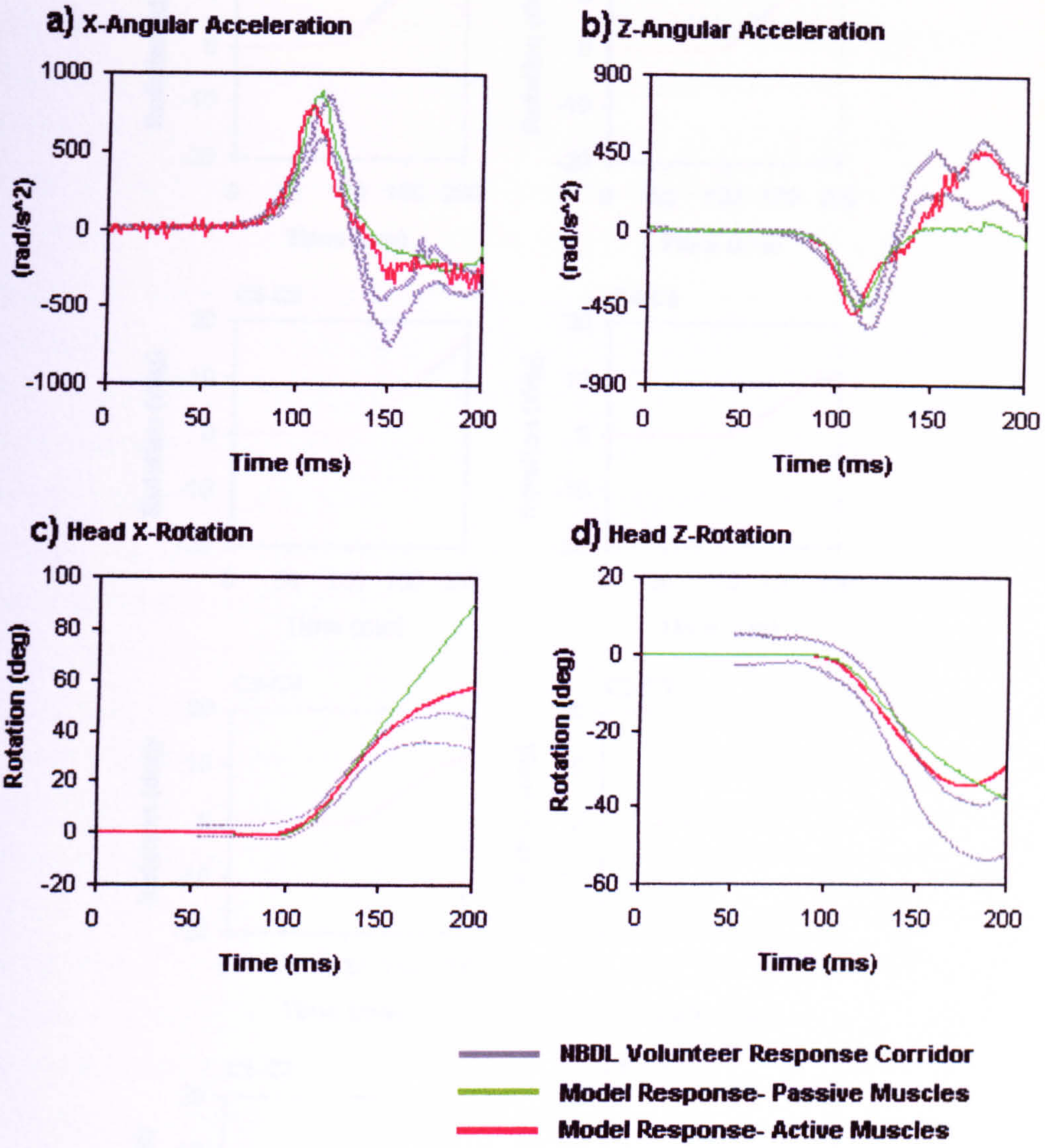


**Figure 6.20:** Head-neck model response to 7g lateral impact with passive (green) and active (red) muscle behaviour compared against NBDL volunteer response corridors. a) and b): x and z components of angular acceleration of the head centre of gravity with time. c) and d) rotation of the head about the x and z axis versus time.

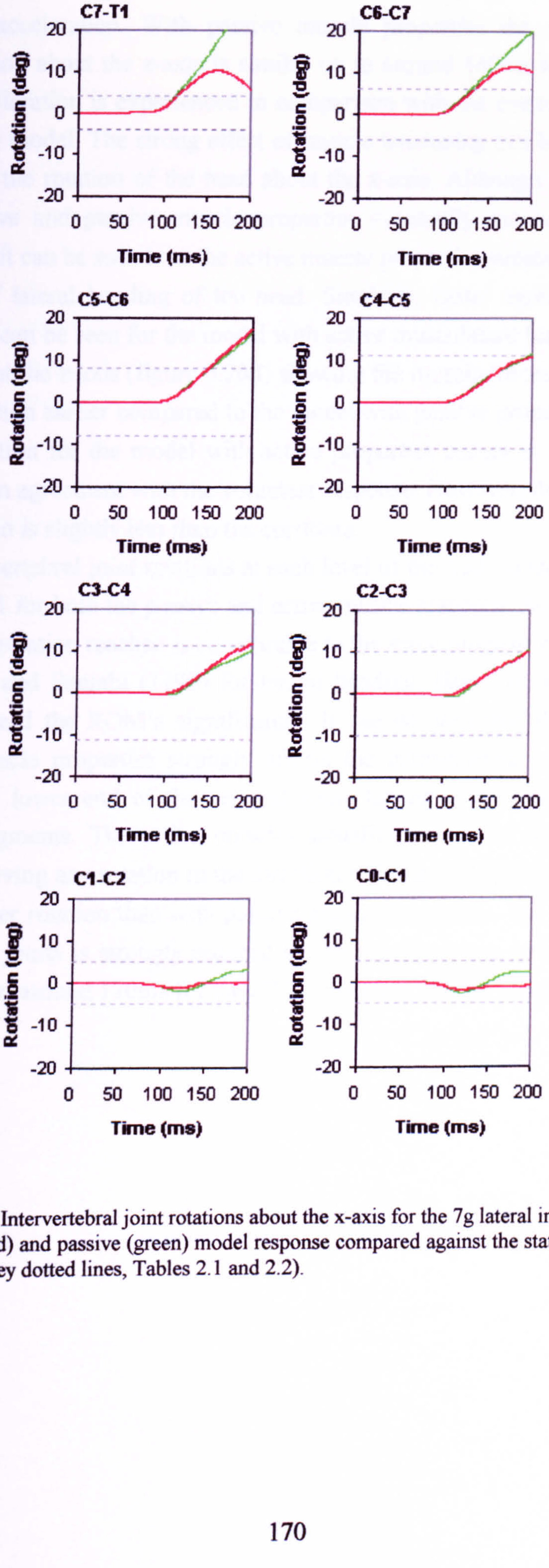


**Figure 6.21:** Intervertebral joint rotations about the x-axis for the 7g lateral impact. Shown are the active (red) and passive (green) model response compared against the static in-vivo ranges of motion (grey dotted lines, Tables 2.1 and 2.2).

A fairly similar response is seen between active and passive model for the x-angular acceleration. With passive muscle properties the models angular acceleration about the z-axis is similar up to around 140ms following which little acceleration is experienced in comparison with the corridors and that of the active model. The strong effect of muscle tensioning can be seen in figure 6.20c on the rotation of the head about the x-axis. Although the model with both active and passive muscle properties eventually exceed the volunteer corridors it can be seen how the active muscle properties substantially limit the degree of lateral bending of the head. Similarly, better agreement with the corridors can be seen for the model with active musculature for rotation of the head about the z-axis (figure 6.20d) showing the muscle forces to increase the axial rotation earlier compared to the model with passive properties. The peak axial rotation for the model with active properties occurs at around 180ms, which is in agreement with the volunteer response. However, the magnitude of the rotation is slightly less than the corridors.

The intervertebral joint rotations at each level of the neck model are shown in figure 6.21 for both the passive and active muscle response. At most levels the degree of rotation reached is comparable to the static range of motion reported by White and Panjabi (1990) for lateral bending. However, the lower three joints exceed the ROM's significantly. It can be seen that the inclusion of active muscle properties strongly affects the intervertebral response of the upper and lower end of the cervical spine having less of an affect on the middle segments. The active muscles actually prevent the upper two joints from achieving any rotation in the direction of impact while C2-C3 and C3-C4 have greater rotation than with passive muscle properties. The rotation of the lower two joints is strongly reduced by the muscle forces with peak rotation occurring at around 170ms for the C7-T1 joint and about 185ms for C6-C7.

## 6.5 Component Loading for Frontal Impact

To demonstrate the head-neck model's ability to predict the local loading of the soft-tissue components a detailed analysis of the individual component loads over the 200ms frontal impact has been performed. The case with muscle activation has been used as this was shown to give best agreement with the volunteer response corridors. Firstly the loads in the ligaments of the upper and lower cervical spine are presented, followed by the force and moments in the intervertebral discs. The maximum loads experienced over the 200ms are presented along with a comparison with the failure forces of the corresponding soft-tissue where available. Finally the forces developed in the active muscle elements are studied.

### 6.5.1 Ligament Forces

Figure 6.22 shows the forces developed in the ligaments of the lower cervical spine, for clarity the ligaments are split further into mid- (C2-C5) and lower- (C5-T1) cervical spine levels. It can be seen how for the majority of the ligaments maximum force occurs at around 100ms, corresponding to the time of maximum head acceleration and maximum neck excursion. Significant forces are developed in the majority of ligaments of the mid-cervical level due to the tensile loading of the neck as the head is thrown forward. Little force is developed in the anterior longitudinal ligaments of the lower levels, as flexion of the lower vertebrae is dominant early in the impact (see figure 6.17). Consequently all the posterior ligaments of the lower levels develop large loads, in most cases larger than their equivalent ligaments of the mid-levels. The loads in the posterior ligaments (FL, CL, ISL) of C2-C3 are small in the early stages of impact due to this segment been forced into extension (see figure 6.17). As the neck rotates further and flexion is developed at all levels of the lower cervical spine the tension in the anterior longitudinal ligaments is relieved while the posterior ligaments become more and more strained. A second general peak in ligament force can be seen around 150-160ms as maximum forward flexion of the neck is reached.

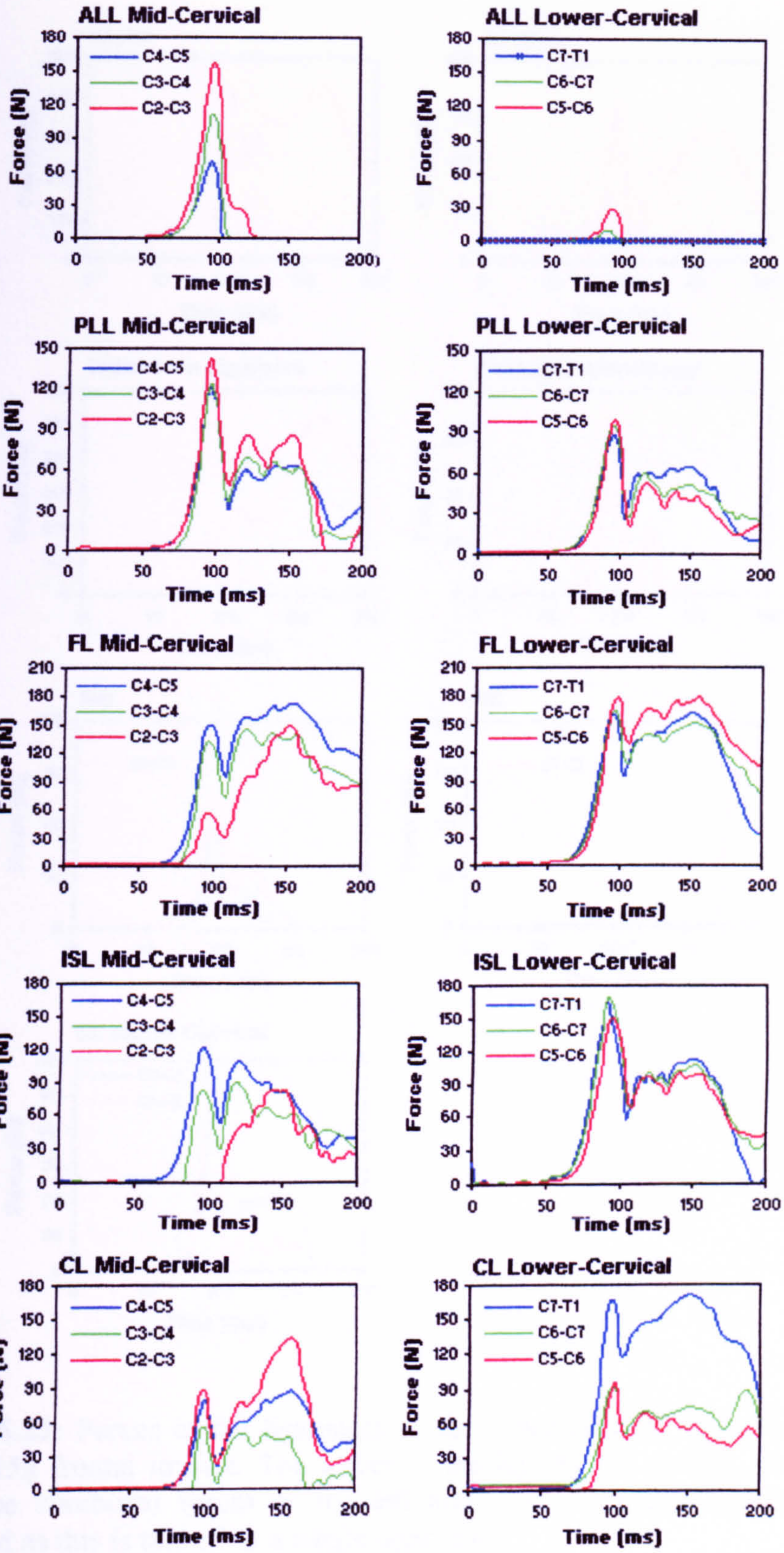


**Figure 6.22:** Forces in the ligaments of the lower cervical spine during the 200ms 15g frontal impact. The forces in the left CL ligaments are shown.

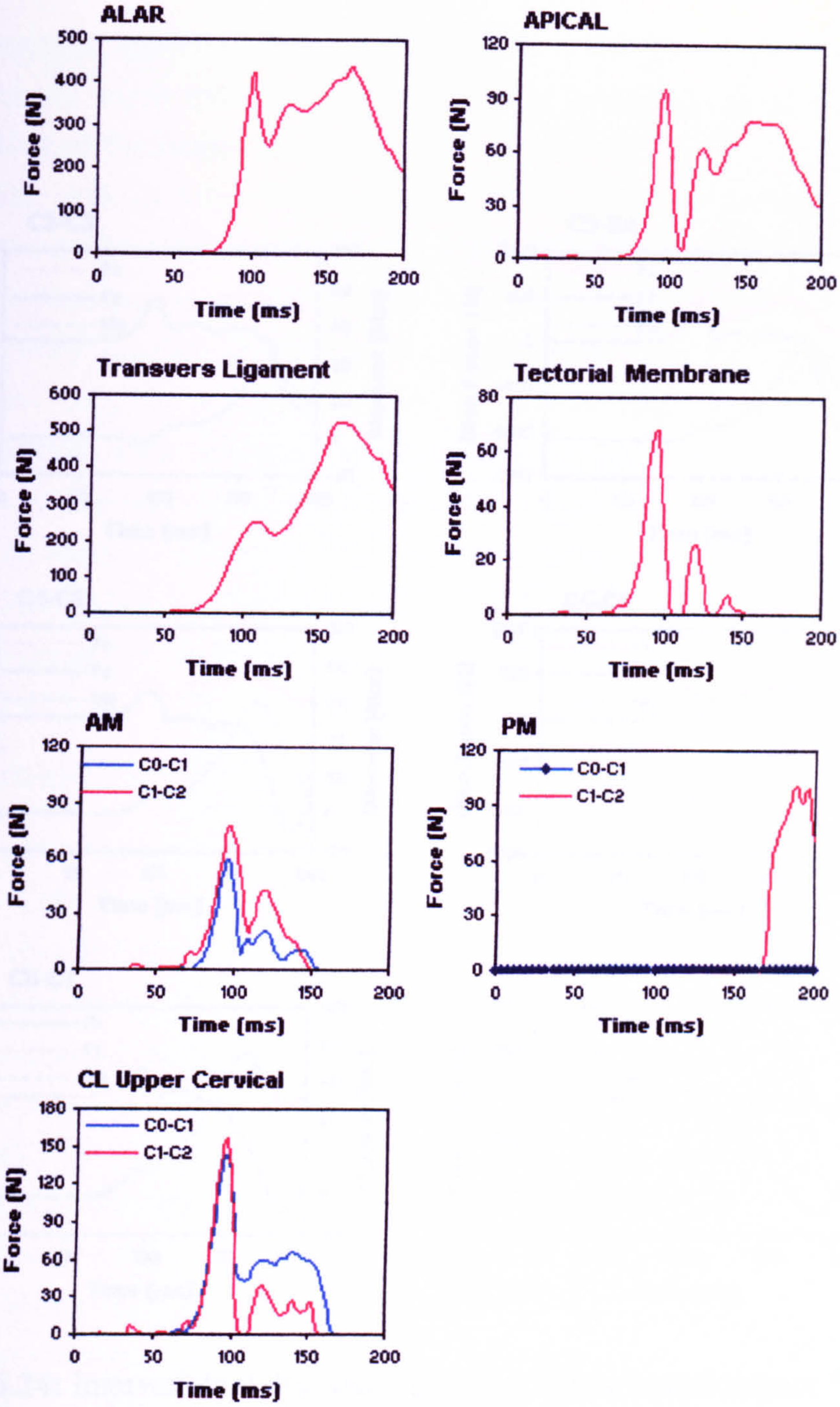


**Figure 6.23:** Forces in the ligaments of the upper cervical spine during the 200ms 15g frontal impact. The forces in the left ALAR and CL are shown while the combined forces of the left and right transverse ligaments are presented as this is treated as a single ligament.

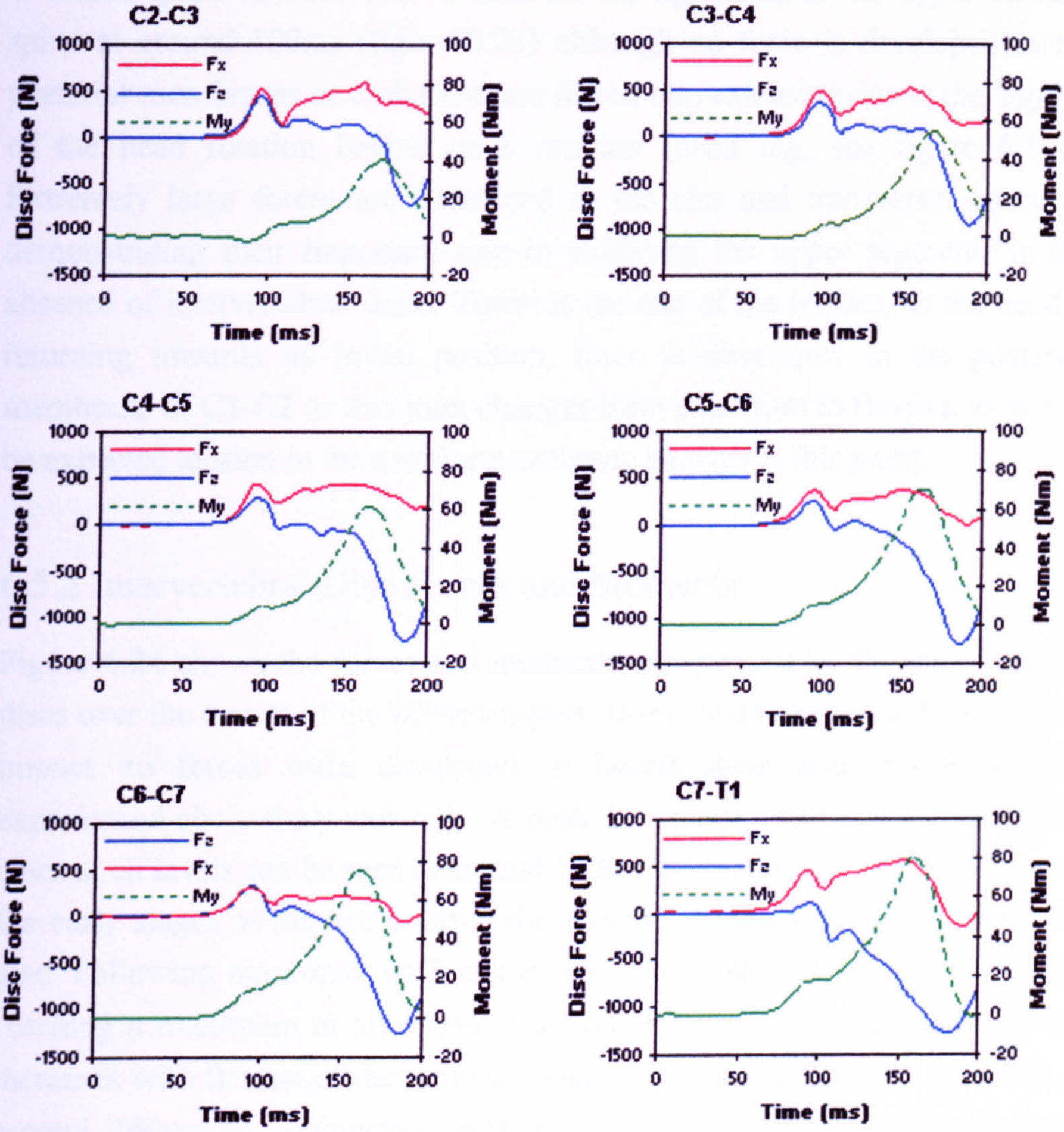


**Figure 6.24:** Intervertebral disc loads over the 200ms frontal impact. The disc forces Fx and Fz are shown on the left axis and moment My on the right axis.

The capsular ligaments of the lowest segment C7-T1 appear to be loaded significantly more than at other levels; this is thought to be due to the orientation of the facets at this level.

A similar peak in force can be seen for the ligaments of the upper cervical spine at around 100ms (figure 6.23) although no force is developed in the posterior membranes as both joints are forced into extension due to the lagging of the head rotation behind neck rotation (head lag, see figure 6.16d). Extremely large forces are developed in the alar and transverse ligaments demonstrating their important role in stiffening the upper segments in the absence of intervertebral discs. Towards the end of the impact, as the head is returning towards its initial position, force is developed in the posterior membrane of C1-C2 as this joint changes from extension to flexion, as would be expected tension in the anterior membrane tails off at this point.

## 6.5.2 Intervertebral Disc Forces and Moments

Figure 6.24 shows the forces and moments experienced by the intervertebral discs over the course of the 200ms impact. Due to the nature of a direct frontal impact no forces were developed in lateral shear and moments were experienced about the y-axis only. A peak in anterior shear and tension of the discs at all levels can be seen at around 100ms at maximum neck excursion. In the early stages of impact anterior shear is the dominant force of the C7-T1 disc. Following maximum neck excursion compression in the discs develops reaching a maximum at all levels at around 180-190ms. Torque in the discs increases with flexion of the vertebrae and reaches a maximum at all levels at around 160ms in conjunction with maximum neck rotation. Successively greater moments are placed on the discs with each level of the cervical spine down to C7-T1 experiencing the greatest torque.

### 6.5.3 Muscle Forces

Figure 6.25 shows the maximum force developed in each of the muscle elements on the left side of the neck during the 15g frontal impact. Due to the mid-sagittal symmetry of the neck model and the direction of the frontal impact being solely in the x-z plane the forces in the left and right muscle elements are identical. All the muscles play a role in resisting the forward flexion of the head with the Semispinalis Capitis and Cervicis, Splenius Capitis, Trapezius, Levator Scapulae, and the sub-occipital muscle providing the most resistance to the forward motion of the head and neck. The large forces in the Scalenus and Sternocleidomastoid muscles are developed following the maximum rotation of the neck as the head and neck begin to rebound. The total combined muscle force acting on the head and cervical spine over the duration of the 200ms impact is shown in figure 6.26. It can be seen that significant muscle force is built up following the 75ms onset delay reaching an initial peak at the point of maximum neck excursion (~100ms), the force then drops off as the majority of muscles are rapidly shortened as the head is pulled back by the shortening of the neck due to the large initial tension in the discs and ligaments (see 'Neck Length' in figure 6.16c and ligament and disc forces in figures 6.22-6.24). Muscle force then increases as the head and neck flex forward lengthening the muscles, a second peak where maximum muscle force is reached is seen at around 160ms at the point of maximum neck flexion. As the head and neck begin to rebound the muscle force tails off slightly as the majority of muscles on the posterior of the neck begin to shorten, however at this point forces begin to develop in the Sternocleidomastoid and Scalenus muscles as they try to resist the return motion of the head and neck.

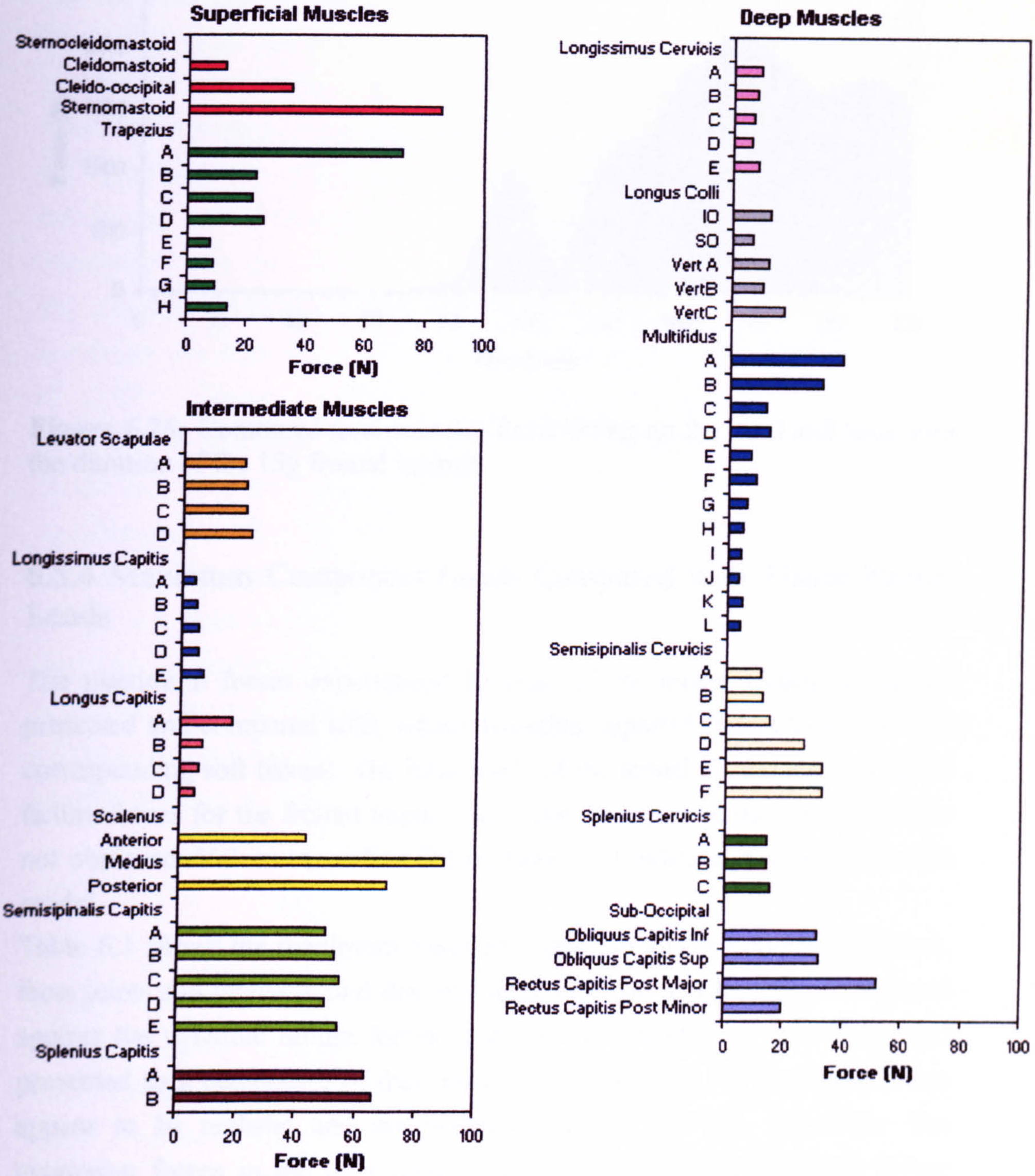


**Figure 6.25:** Maximum muscle force developed in each of the muscle elements on the left side of the neck for active response to 15g frontal impact.

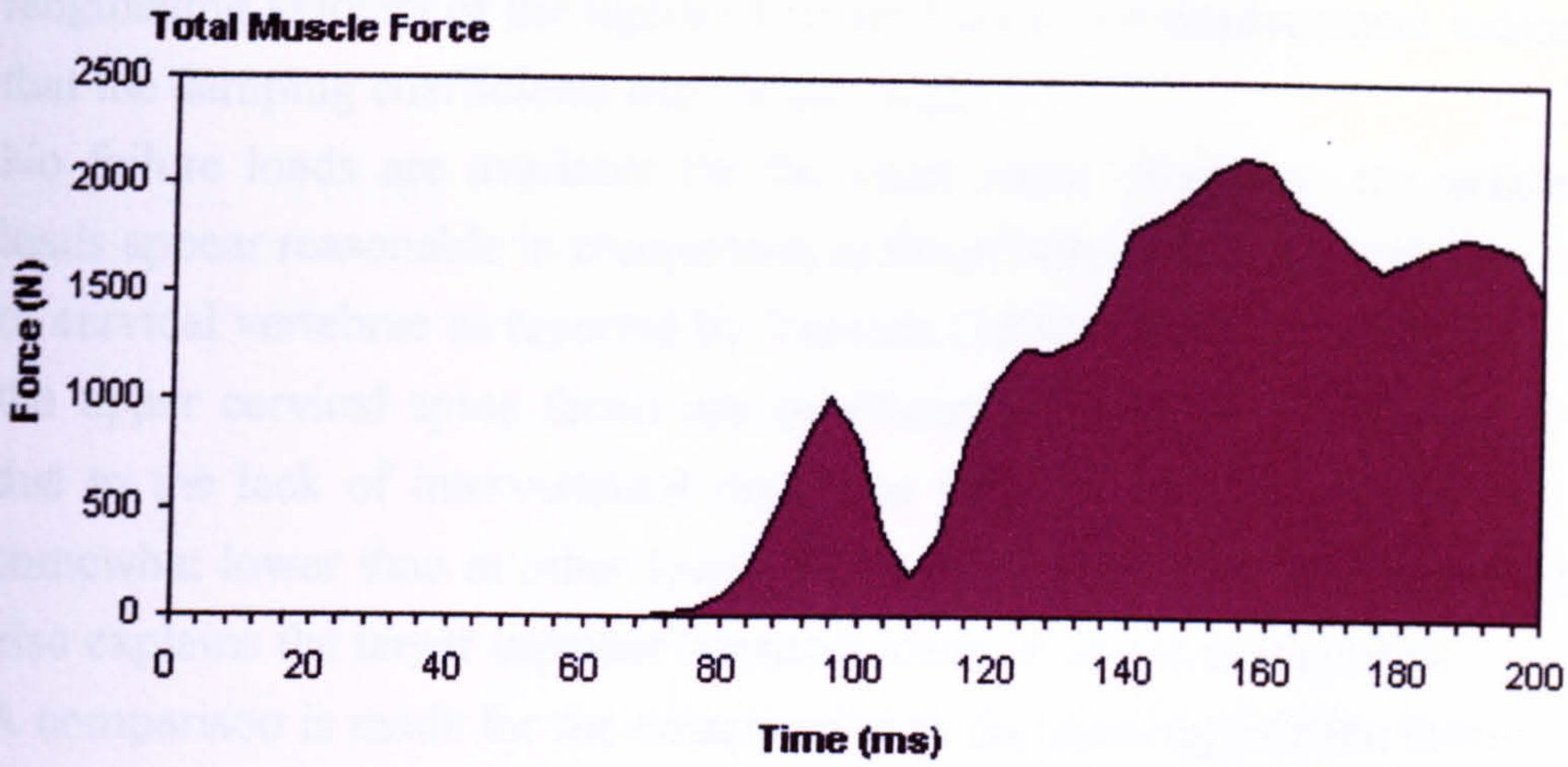


**Figure 6.26:** Combined total muscles force acting on the head and neck over the duration of the 15g frontal impact.

## 6.5.4 Maximum Component Loads Compared with Tissue Failure Loads

The maximum forces experienced by each of the model's components are presented and compared with, where available, reported failure loads for their corresponding soft tissues. The local loads of the model should not exceed the failure forces for the frontal impact simulated, as injury to the volunteers was not observed. Values exceeding failure loads will indicate inaccuracies in the model.

Table 6.1 shows the maximum loads developed in all the cervical ligaments, facet joints and intervertebral disc elements. All ligament forces are compared against the dynamic failure forces calculated in Chapter 2 (Table 2.12) and presented as a percentage of that failure force (% Fail). All ligaments forces appear to be realistic and acceptable except for the ISL ligaments. The maximum forces in the inter-spinous ligaments exceed the dynamic failure loads at levels C4 through T1 indicating that perhaps the position of these ligaments is inaccurate (spanning adjacent spinous process tips) or the material properties are too stiff. The maximum loads of the ISL at these levels occur at around 100ms, a long time before maximum rotation between these joints is experienced. Therefore the large loads developed appear due to the

lengthening velocity of the ligament rather than to the displacement indicating that the damping coefficients may be too high.

No failure loads are available for the facet joints. However, the maximum loads appear reasonable in comparison to the 3100N compression failure force of cervical vertebrae as reported by Yamada (1970). As expected the loads on the upper cervical spine facets are significantly larger than the lower levels due to the lack of intervertebral disc. The force on the facets of C7-T1 are somewhat lower than at other levels, likely due to the facet orientation which also explains the larger capsular ligament loads observed at this level.

A comparison is made for the compression in the discs against the failure load of 3140N (Yamada, 1970). The maximum compression reached appears acceptable at all levels, never exceeding 50% of the predicted failure load. No failure force of discs in anterior shear could be found but the loads reached are significantly less than the compression forces so would appear to be tolerable. Moments in the discs seem high in comparison to the static failure load of 3.5Nm for isolated discs segments as reported by Moroney et al. (1988). However, the dynamic failure loads have not been reported and it is reasonable to assume, due to the structure of the intervertebral discs, that they are able to withstand significant loads under dynamic conditions. Maximum moment reached increases at each level down of the cervical spine.

## 6.6 Effect of Muscle Parameters on Head-Neck Response

An investigation into the effect of muscle parameters on the overall head-neck response to frontal impact was performed. The same 15g frontal impact acceleration pulse as used in the model validation was used with an identical model set-up. The three parameters thought to have the most influence on the effect of the head-neck muscles were:

- The onset/reflex delay of muscle activation,
- The value of specific tension of muscle,
- The percentage of maximum activation reached.

**Table 6.1:** Maximum resulting loads and percent of failure force for the individual soft tissues during the 200ms frontal impact simulation with active musculature (forces exceeding 100% of failure load are underlined).

| | Upper-Cervical Spine | | | | | | Mid-Cervical Spine | | | | | | Lower-Cervical Spine | | | | | |
|---|---|---|---|---|---|---|---|---|---|---|---|---|---|---|---|---|---|---|
| | C0-C2 | | C0-C1 | | C1-C2 | | C2-C3 | | C3-C4 | | C4-C5 | | C5-C6 | | C6-C7 | | C7-T1 | |
| | Max. | % Fail | Max. | % Fail | Max. | % Fail | Max. | % Fail | Max. | % Fail | Max. | % Fail | Max. | % Fail | Max. | % Fail | Max. | % Fail |
| **Ligament Force (N) *** | | | | | | | | | | | | | | | | | | |
| ALL | | | | | | | 157 | 61.1 | 114 | 44.4 | 67 | 26.1 | 32 | 8.6 | 8 | 2.2 | 0 | 0 |
| PLL | | | | | | | 143 | 66.5 | 124 | 57.7 | 120 | 55.8 | 100 | 27.0 | 96 | 25.9 | 87 | 23.5 |
| FL | | | | | | | 148 | 58.7 | 146 | 57.9 | 173 | 68.7 | 184 | 48.3 | 167 | 43.8 | 161 | 42.3 |
| ISL | | | | | | | 81 | 85.3 | 85 | 89.5 | 122 | **128** | 155 | **154** | 169 | **167** | 164 | **162** |
| CL | | | 142 | 16.7 | 156 | 18.3 | 144 | 23.4 | 58 | 9.4 | 88 | 14.3 | 92 | 11.8 | 96 | 12.3 | 176 | 22.6 |
| ALAR | 419 | 43.5 | | | | | | | | | | | | | | | | |
| APICAL | 96 | 16.6 | | | | | | | | | | | | | | | | |
| AM | | | 60 | 9.5 | 76 | 10.0 | | | | | | | | | | | | |
| PM | | | 0 | 0 | 100 | 32.8 | | | | | | | | | | | | |
| TL | | | | | 518 | 54.2 | | | | | | | | | | | | |
| TM | 70 | 34.1 | | | | | | | | | | | | | | | | |
| **Facet Joint Force (N) **** | | | | | | | | | | | | | | | | | | |
| FresFACET | | | 609 | - | 620 | - | 293 | - | 305 | - | 277 | - | 246 | - | 374 | - | 145 | - |
| **Disc Force (N) ***** | | | | | | | | | | | | | | | | | | |
| Fx | | | | | | | 608 | - | 483 | - | 439 | - | 357 | - | 308 | - | 557 | - |
| Fz | | | | | | | -741 | 23.6 | -973 | 31.0 | -1263 | 40.2 | -1298 | 41.4 | -1252 | 39.9 | -1280 | 40.8 |
| **Disc Moment (Nm)** | | | | | | | | | | | | | | | | | | |
| My | | | | | | | 40 | - | 54 | - | 62 | - | 70 | - | 76 | - | 80 | - |

* % Fail for ligaments = Percentage of dynamic failure force (Table 2.12, Chapter 2)

** % Fail for facet joints = no data available

*** % Fail for Discs = Percentage of failure in compression only ( 3139N, Yamada, 1970)

The time delay before the onset of muscle activation is likely to significantly affect the overall response of the head and neck to impact. The range of reflex response times simulated was 25-100ms in 25ms steps. For all four simulations 100% muscle activation was used with a specific tension of $50N/cm^2$.

The specific tension of muscle is defined as the maximal isometric force produced at the optimal length per unit cross-sectional area. As stated previously this value has been estimated to be anywhere between 20 and 100 $N/cm^2$ and this variation is likely due to gender differences and different levels of muscular development. Three different values of specific tension are explored from 30-$70N/cm^2$, for all tests muscle activation was kept at 100% with an onset delay of 75ms.

Finally the effect of muscle activation level is studied. The level of activation of all the neck muscles was set to a percentage of maximum activation, five levels were explored from 0-100% in 25% steps. For all five tests muscle onset time was set at 75ms with a specific tension value of $50N/cm^2$.

To evaluate the affect of altering the above muscle parameters the change in the overall head and neck rotation was compared.

**Results:** From the comparisons with the volunteer response corridors it was seen that muscle tensioning has the greatest influence over head and neck rotation but little to no effect on the head accelerations. Figure 6.27 shows the effect of changing the various muscle parameters on the head and neck rotation during the 15g frontal impact. It can be seen that delaying the onset of muscle activation results in a significantly increased head and neck rotation. Interestingly the time to peak head and neck rotation is reduced as the delay is increased. As expected, reducing the value of specific tension results in increased head and neck rotation with the peak value of head rotation occurring slightly later with smaller values. The time to peak neck rotation does not appear to be affected by the value of specific tension. Finally decreasing the percentage of muscle activation leads to increases in head rotation with the most pronounced increase being with 0% active which is the same as the passive muscle case already seen. The effect of activation level on neck rotation is small.

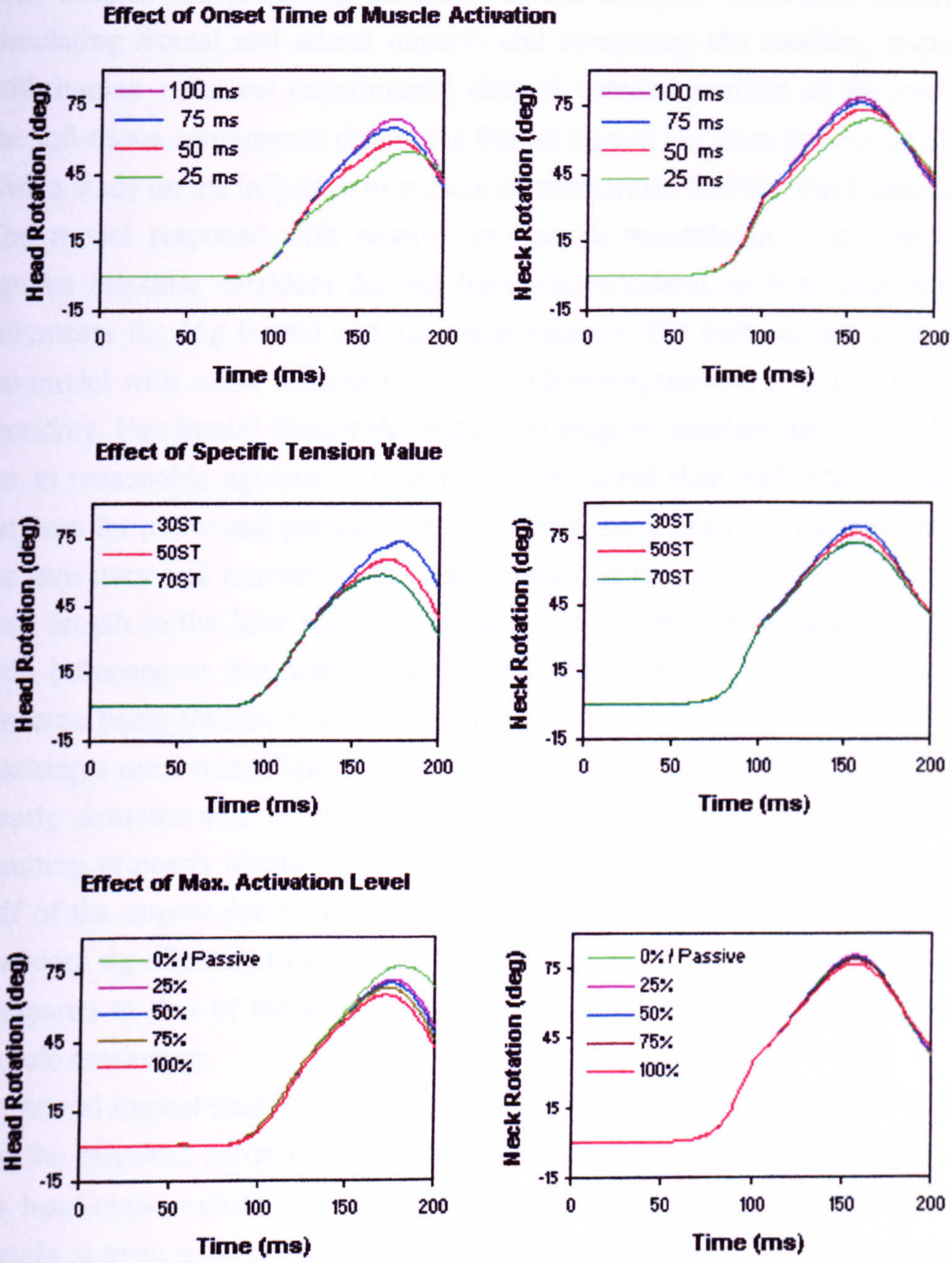


**Figure 6.27:** Change of head and neck rotation with varying muscle parameters.

## 6.7 Discussion

This chapter has presented validation of the complete head-neck model by simulating frontal and lateral impacts and comparing the resulting response with human volunteer experimental data. A detailed analysis of the loads in the soft-tissue components during the frontal impact has been performed along with a study on the influence of muscle parameters on the head-neck motion.

The model response with passive and active musculature was compared against response corridors derived from sled acceleration tests with human volunteers for 15g frontal and 7g lateral impacts. For both impact directions the model with active musculature shows closest agreement with the response corridors. For frontal impact the linear and angular accelerations of the head are in reasonable agreement with the experimental data with little variation between the active and passive response. The passive muscle properties lead to the trajectory and rotation of the head exceeding the corridors as well as the neck length in the later stages of impact. Muscle tensioning appears to have little influence on the rotation of the neck with both the passive and active response being similar, both resulting in reasonable levels of neck rotation, but reaching a maximum slightly earlier than seen with the volunteers. Head lag is clearly demonstrated by the model with both passive and active behaviour resulting in nearly identical rotation between the head and neck over the first half of the impact duration. However, the passive response deviates from the corridors significantly towards the end of the impact as head rotation increases compared to that of the active model where head rotation is reduced due to muscle tensioning.

For lateral impact satisfactory agreement is observed between the active model and the response corridors, with muscle tensioning having a greater effect on the head-neck motion than seen with the frontal impact. The influence of muscle activation leads to significantly reduced head rotation in the impact direction as well as reduced head and occipital condyle trajectories, although they still exceed the response corridors towards the end of the impact. The linear and angular accelerations of the head are also improved due to muscle tensioning. In comparison with the volunteer data the model appears to be too flexible in lateral bending, this is likely due to the linear stiffness of the

intervertebral discs in this direction, resulting in too large displacements at high loads.

The intervertebral joint rotations for both impact directions clearly show the strong effect muscle tensioning has on the upper cervical spine segments. In the frontal impact the developed muscle forces prevent the atlanto-occipital joint from ever going into flexion and significantly reduce the level of flexion reached in the atlanto-axial joint; together accounting for the majority of the overall reduction in head rotation. Similarly in lateral impacts the muscle tensioning reduces the rotation of the upper joints but also has a strong influence on the rotation of the lower two joints of the cervical spine. In comparison with the in-vivo ranges of motion, the rotations of the joints are acceptable.

From the analysis of frontal and lateral impact it would appear that that the inclusion of active muscle behaviour is essential in accurately predicting the head-neck response to impact. The passive response is more likely to represent the response of cadaveric specimens where the influence of active musculature is absent. Indeed Wismans et al. (1987) in a comparison between the NBDL human volunteer response and cadaver head-neck response to similar frontal impacts observed greater head rotations in the cadaver tests resulting in 'overtipping' of the head as head rotation exceeded neck rotation. This characteristic of cadaver response was clearly seen in the model response with passive muscles.

The analysis of local loads in the soft-tissue components of the model demonstrates the model's ability to predict injury to the cervical spine. The ligament forces show a clear peak in force quite early in the impact in conjunction with the peak head acceleration. For the majority of the cervical ligaments this peak also corresponds to the maximum load experienced over the course of the 200ms acceleration pulse. Although for the severity of impact simulated no injury is expected, as none was seen in the volunteers it is reasonable to assume that in impacts of greater severity it will be at this initial peak in force where injury would occur. The intervertebral discs experience a similar peak in force at around 100ms as the neck reaches maximum excursion under a combination of tension and axial shear. In the later stages of the

impact significant compressive forces and torque around the y-axis are developed in the discs.

Maximum loads developed in all the cervical ligaments have been shown to be below the predicted failure forces for the 15g frontal impact except for the inter-spinous ligament. The ISL of the lower four joints experience forces beyond the maximum dynamic failure loads indicating an inaccuracy in the model. As stated previously, no injuries were sustained by the human volunteers during the frontal sled impact tests so the forces in all components of the spine should be within tolerable limits. The maximum loads of the ISL occur early in the impact, a long time before maximum rotation between these joints is experienced. Therefore the large loads developed appear to be due to the lengthening velocity of the ligament rather than to the displacement indicating that the damping coefficients may be too high. No data on the viscous behaviour of the ligaments is available and so the damping coefficients used were based on those used by de Jager (1996). Experimental studies on spinal ligaments need to be performed to define their viscous characteristics. The loads on the cervical articular facets appear reasonable in comparison to vertebral failure loads although no data was available for the tolerance levels of these joints. The compressive loads developed in the intervertebral discs never exceed 50% of the reported failure forces in this mode of loading. However, it is unclear if the combination of anterior shear and compression would cause damage. Disc moments appear large in comparison to the reported static failure torques for forward flexion however dynamic failure loads have not been reported. Dynamic properties of the intervertebral discs characterising the response to large loads and failure limits in all directions of loading need to be established for both modelling and validation purposes.

Having established the need for muscle activation to properly define the head-neck response the role of certain muscle parameters was investigated. It has been shown that delaying the onset of muscle activation beyond the original 75ms results in an increased head and neck rotation, which would have exceeded the volunteer response corridors. An earlier onset time of around 50ms would have decreased rotations while still remaining within the defined corridors while a very fast response time of 25ms would decrease head

rotations below the corridors. Based on reported muscle reflex times (Siegmund and Brault, 2000), a response time of less than 75ms would require some form of pre-impact warning to be physically possible. Altering the value of specific tension of the muscles has a significant effect on the resulting head and neck rotations, increasing values resulting in reduced rotations. The subjects from the NBDL tests were young males recruited from the U.S. Navy and screened for good health (Thunnissen et al., 1995) so it can be assumed that the a relatively high value of specific tension would give the most accurate results. For a general population a lower value may be more suitable. The value of 50N/cm$^2$ used in the original simulations appears acceptable. Varying the degree of muscle activation lead to changes in overall head rotation but appears to have little effect on neck rotation, 100% activation gives best correspondence with the response corridors. In the simulations all muscles were inactive for the first 75ms at which point they became maximally activated. In reality some level of muscle activation will be present throughout the duration of the impact, initially to maintain head and neck posture. Simulating this complex neural activation is beyond the scope of this research and appears unnecessary to predict the head-neck response to dynamic impacts. However, the nature of the muscle model used means the inclusion of such a control scheme would be possible if desired.

In summary, the complete head-neck model has been used to simulate frontal and lateral impacts in an effort to dynamically validate its response. Reasonable to good agreement with human volunteer response corridors has been demonstrated for the model with active musculature, highlighting the important role the muscles of the neck play in the head-neck response. The model has been shown to be able to predict the loads and deformations of the cervical spine components making it suitable for injury analysis.

# CHAPTER 7

# Simulation of Whiplash Trauma

The aim of this chapter is to validate the ligamentous cervical spine model with experiments using a bench-top trauma sled and isolated cervical spine specimens. These studies used cadaveric cervical spine specimens stripped of all non-ligamentous soft tissues mounted to a bench top sled device where an acceleration pulse is applied to the base of the specimen to reproduce whiplash trauma. These tests are an alternative to experiments using volunteers, whole body cadavers or anthropometrical crash dummies and have been shown to effectively simulate whiplash trauma and have provided valuable insights into the complex events and interactions that cause injuries to the cervical spine. In the resulting head-neck motion a characteristic S-shaped curvature of the neck with lower level hyperextension and upper level flexion has been observed followed by subsequent C-shaped curvature with extension at all levels of the entire cervical spine.

This chapter first presents simulations of these rear-end impact sled tests using the ligamentous cervical spine model. The model is used without musculature with an acceleration pulse applied to T1. Varying levels of impact severity are simulated. A qualitative comparison of the resulting head-neck motion to that described in the literature is presented as well as a quantitative comparison of head motion and maximum vertebral rotations. An analysis of the internal loads of the soft-tissue components for the most severe impact simulated has been completed to identify possible areas of injury. Finally the muscles are added back to the model to study their effect on the head-neck motion and on the internal forces developed in the neck. The effects of both passive and active musculature are investigated.

## 7.1 Experimental Set-up

Panjabi and co-workers (1997, 1998a, 1998b) used a bench-top trauma sled to simulate whiplash trauma on human cadaveric cervical spine specimens. The general arrangement of the sled apparatus is shown in figure 7.1. The spine specimens tested were cleaned of all muscle tissue and mounted to the sled at T1. The trauma sled ran on horizontal linear bearings and was accelerated by a pneumatic piston, power springs and an electromagnet release. A steel head surrogate representing a $50^{th}$ percentile human head was attached to the occiput with the centre of gravity positioned analogous to that of a real head. The weight of the surrogate head was fully balanced by a pneumatic suspension system effectively negating gravitational pull, but the inertial components of the head were effective. A head stop set at a 45° angle was positioned so that the natural extension of the head led to a perpendicular contact of the head and head stop. The exact positioning and purpose of this stop is not explained and how much of an effect the stop has on the overall displacement of the head and on the maximum rotations of the vertebrae is unclear. However, it is assumed that for the initial loading phase the stop will not be contacted by the head. Trauma acceleration was applied to the specimen by an impactor mounted on the linear bearings. Head motion was monitored with two translational and one rotational potentiometer. Each vertebra was fitted with a motion monitoring flag to measure vertebral rotations using high-speed video. The profile of the sled acceleration-time curve inputted to the base of the specimen represented the whiplash trauma input. The acceleration input was a triangular pulse with duration of 105ms. Peak accelerations of 2.5g, 4.5g. 6.5g and 8.5g ($1g = 9.8m/s^2$) were studied (Grauer et al., 1997). The resulting rotation, vertical and horizontal translation of the head with time for the 8.5g trauma are presented along with the maximum vertebral rotations reached at each level of the cervical spine for each trauma class. A detailed description of the response of the head and neck motion are also presented.

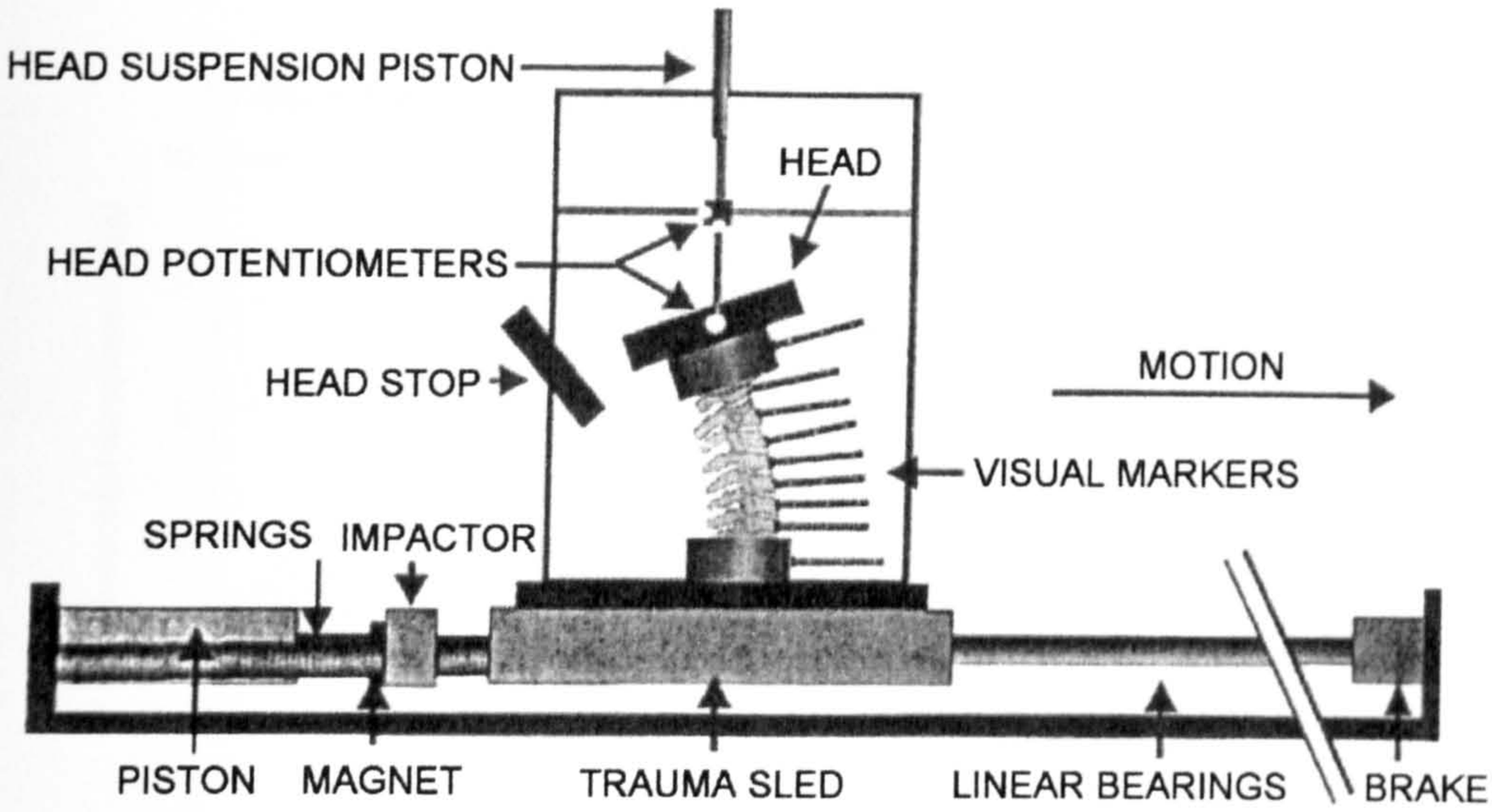


**Figure 7.1**: Experimental set-up of the bench-top trauma sled (adapted from Grauer et al, 1997).

## 7.2 Simulation Set-up

To simulate the bench-top sled tests all muscles were removed from the head-neck model. The motion of T1 was constrained so only translation along the x-axis was possible. The skull model as described in chapter 3 was used as this is based on a $50^{th}$ percentile human head and so is comparable to the surrogate head used in the experiments. No gravitational effects are simulated at this stage. Unfortunately the actual acceleration profiles used in the experiments are not presented so idealized acceleration profiles are used as input to the model as described by Raynak and Ching (2000). The profiles are triangular with the same 105ms duration and corresponding peak accelerations (figure 7.2). The resulting head rotations and translations are compared against the results for the 8.5g trauma class and the maximum vertebral rotations are compared at all levels. No head stop is included in the simulation as the exact position and function of the head stop are unclear from the experimental results, this may lead to inaccuracies in the simulation results.

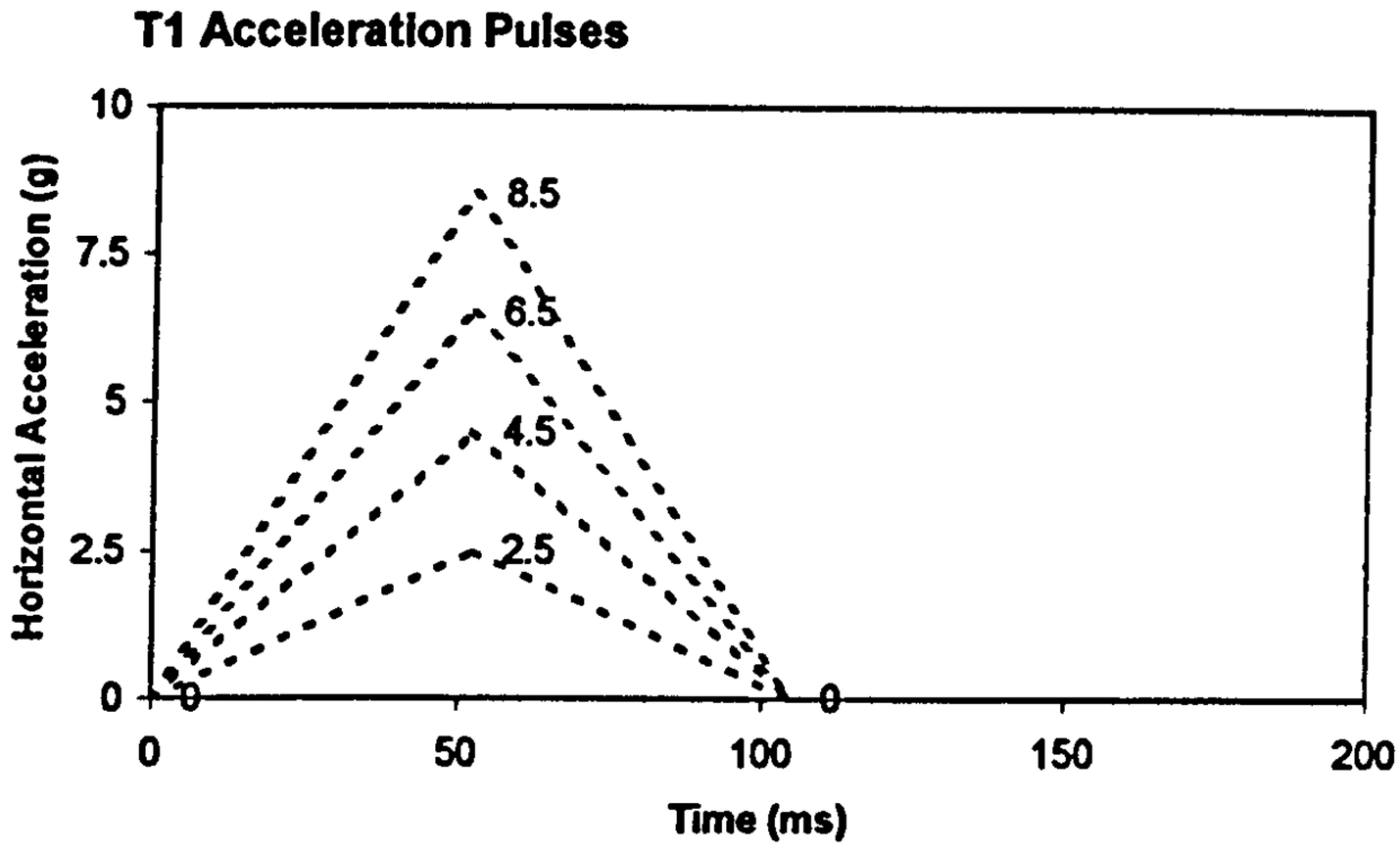


**Figure 7.2:** Horizontal T1 acceleration profiles used as input to the head-neck model for the four classes of impact trauma, 2.5-8.5g.

## 7.3 Simulation Results

The overall response of the ligamentous spine model to the 8.5g trauma class is shown schematically in figure 7.3. Figure 7.4 shows the head rotation and head vertical and horizontal translation for the 8.5g trauma class compared to the experimental results of Grauer et al. (1997). The model shows a similar response to the cadaveric spine specimen but the maximum rotation of the head is around 10° greater in the model. Following the maximum rotation and maximum posterior translation of the head the model rebounds slightly slower than is seen with the spine specimen. The vertical displacement of the head with respect to the torso is in good agreement with the experimental results reaching a peak of around 5cm below the initial height.

During the acceleration portion of the whiplash the head translates posteriorly and inferiorly with respect to T1 and the spine extends. Over the 50-75ms time period the development of the characteristic S-shaped curvature of the cervical spine is observed. It can be seen from the vertebral rotation graphs shown in figure 6.5 that during this time period the upper levels of the spine (C0-C3) are flexed while the lower levels (C5-T1) are extended as was seen in the experimental results. The 75-100ms time period sees the upper vertebrae of

the model change from flexion to extension as the whole model becomes more and more extended into a C-shaped curvature as also observed in the isolated spine experiments. Maximum extension of the head and neck is reached at approximately 125ms, slightly later than the experimental results. In the later stages of trauma the head returns towards its initial starting configuration.

Figures 7.6 and 7.7 compare the maximum intervertebral rotations of the model for the four trauma classes simulated with those reported for the spine specimens. Figure 7.6 shows the maximum flexion and extension of the upper three levels of the cervical spine. The graphs show that although the upper levels are initially forced into flexion in the model, the levels of flexion experienced are noticeably smaller than the isolated spine specimens indicating that perhaps the model is too stiff in flexion in these areas. The levels of extension experienced in the later stages of impact agree more favourably with the experimental data. Figure 7.7 shows the maximum intervertebral extension rotations experienced by the lower five levels of the spine model. Although small levels of flexion were experienced (less than 0.3° at all levels) for some of the lower segments in the early stages of impact they are not presented here as they are thought small enough to be insignificant to the overall response. Comparable levels of extension are seen at each level for each trauma class; noticeable differences can be seen at C3-C4 for 6.5g and at C6-C7 for both 4.5g and 8.5g impacts (no data was reported for C7-T1 at 4.5g). Generally level C6-C7 appears to be too stiff when compared to the experimental results. As would be expected the response of the model shows increasing levels of maximum flexion and extension for the increasing severity of impact, this pattern however is not clear in the experimental results of the cadaveric ligamentous spine specimens.

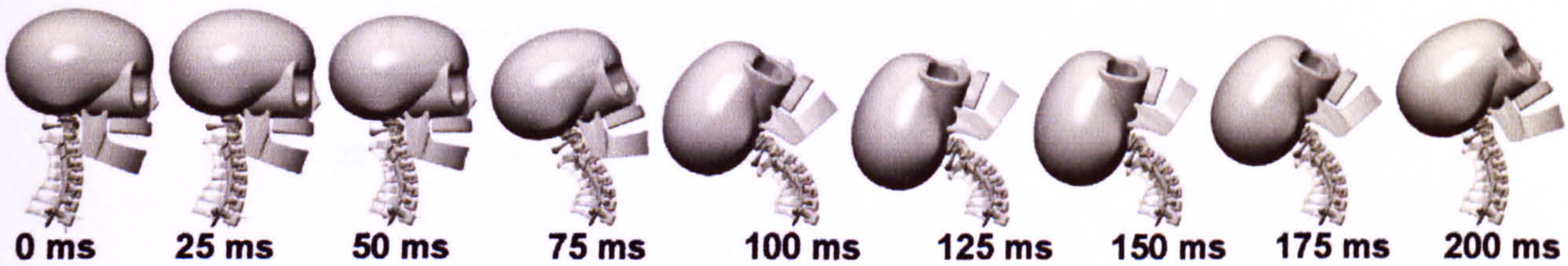


**Figure 7.3:** Kinematics of ligamentous head-neck model for 8.5g rear-end impact trauma at 25ms time intervals.

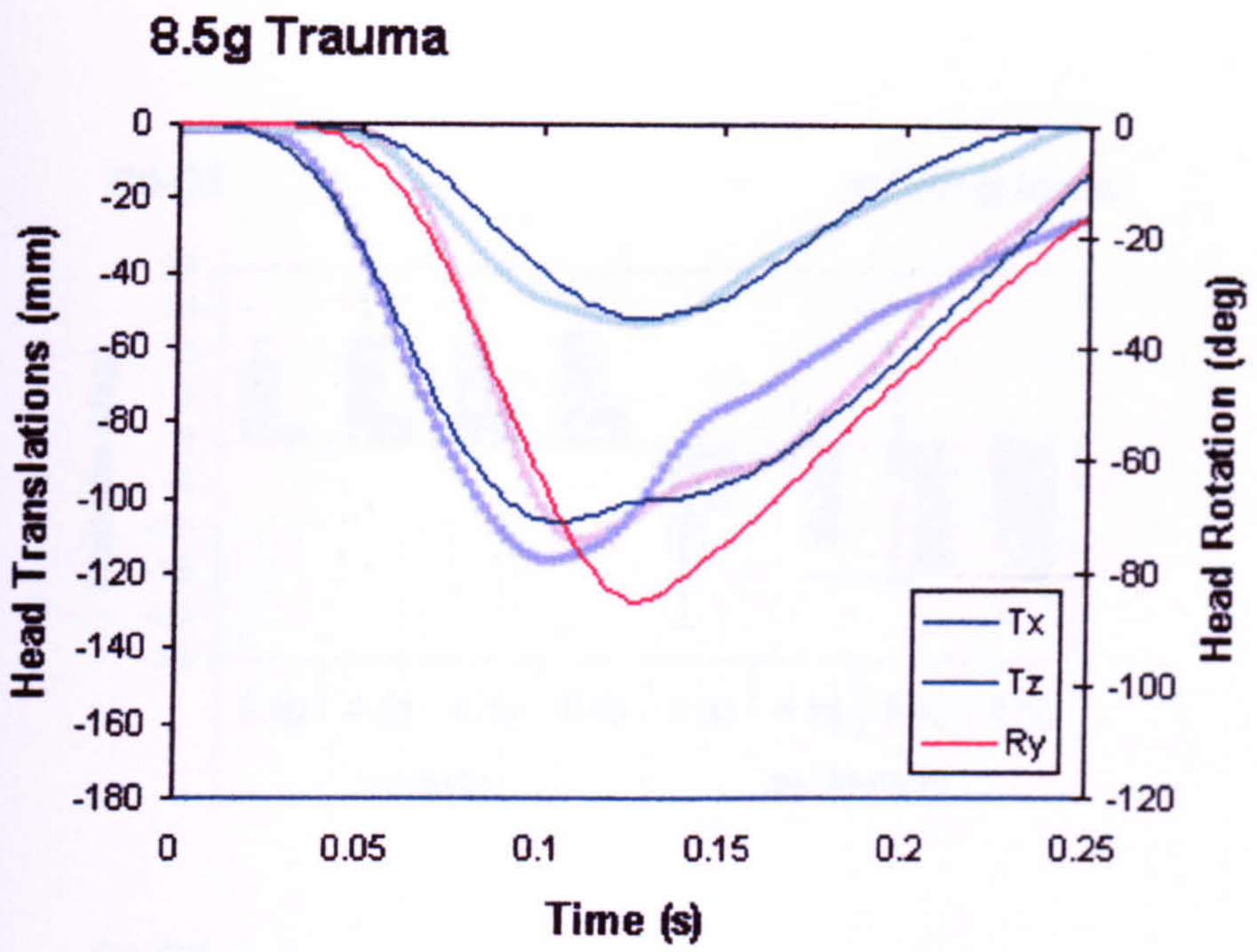


**Figure 7.4:** Head rotation, and translations with respect to T1 versus time. Simulation of 8.5g bench-top trauma test using the ligamentous head-neck model compared with experimental results (shown in respective faded colours). Negative values indicate posterior (-x) and inferior (-z) translations and extension (-y) rotations.

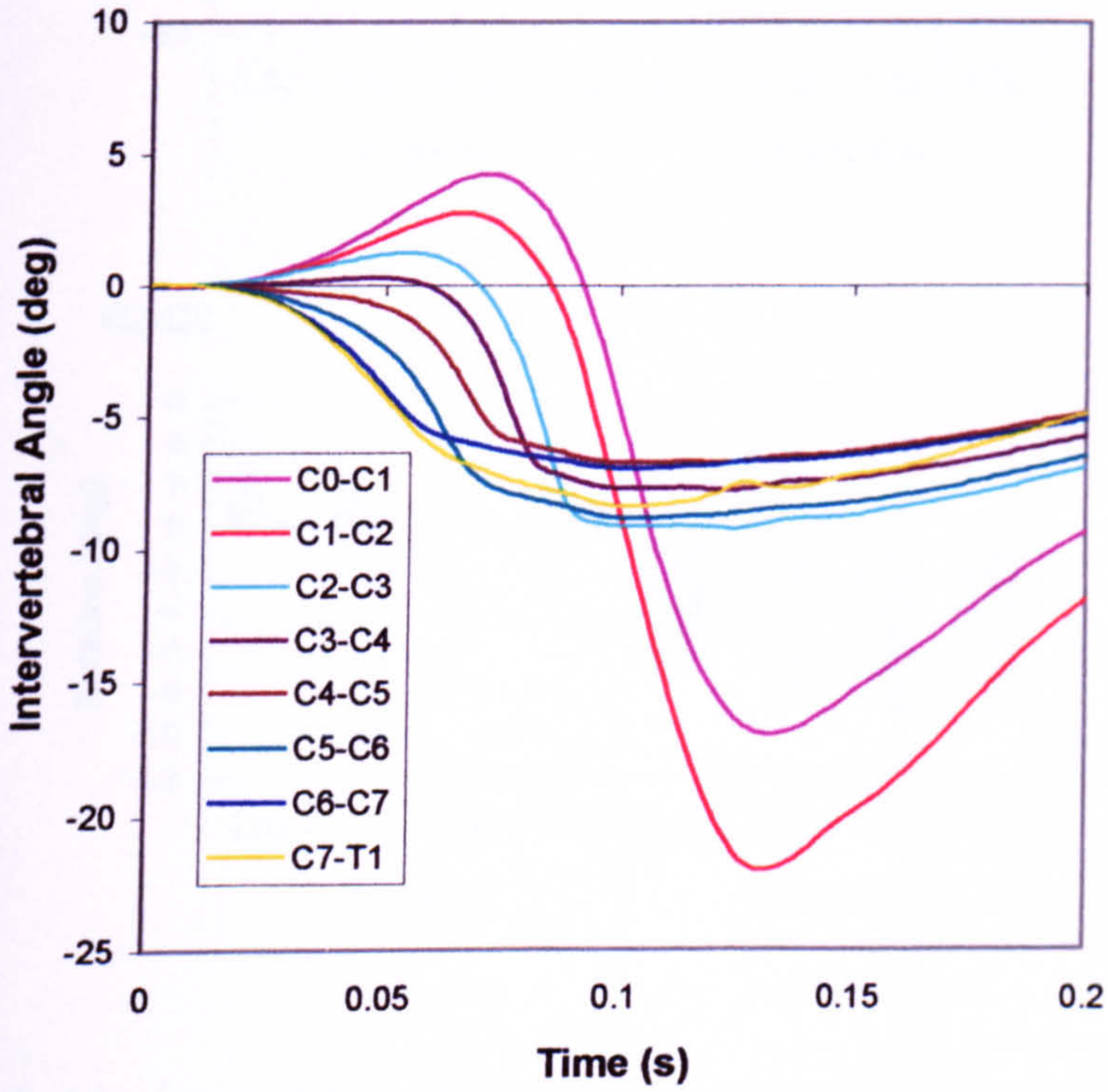


**Figure 7.5:** Intervertebral rotations at each level of the head-neck model in response to the applied 8.5g acceleration pulse at T1. Positive rotations indicate flexion response while negative values indicate extension.

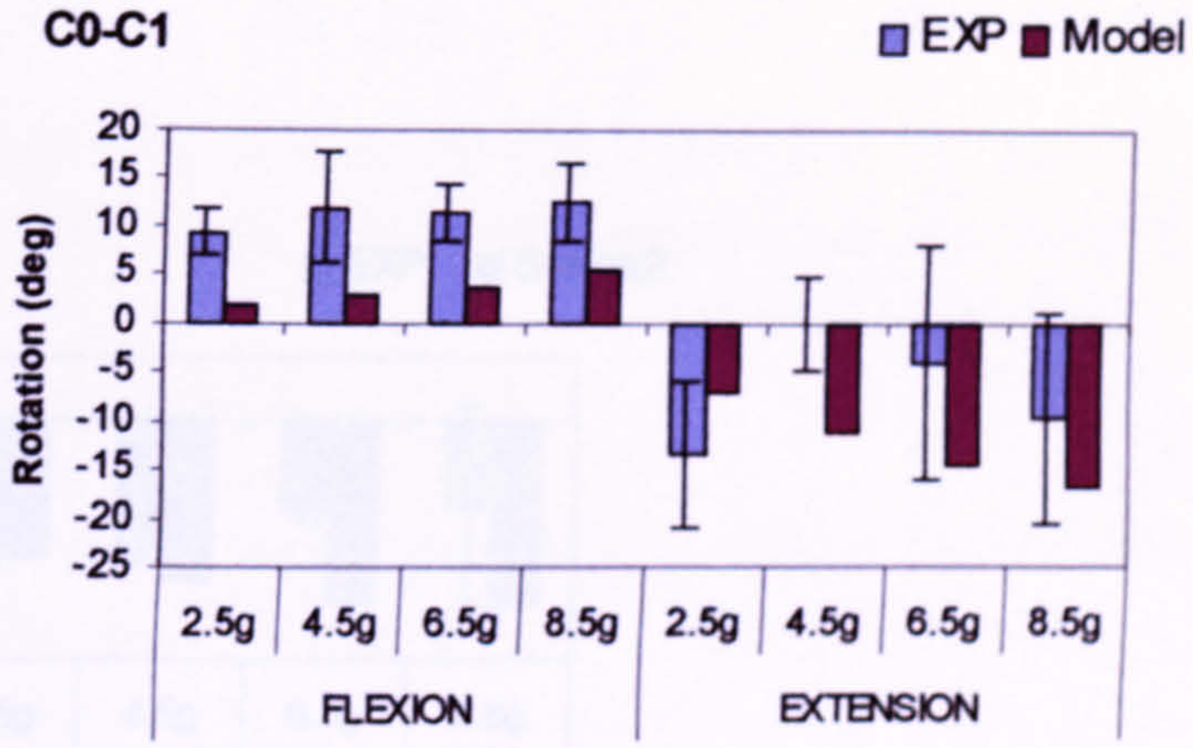





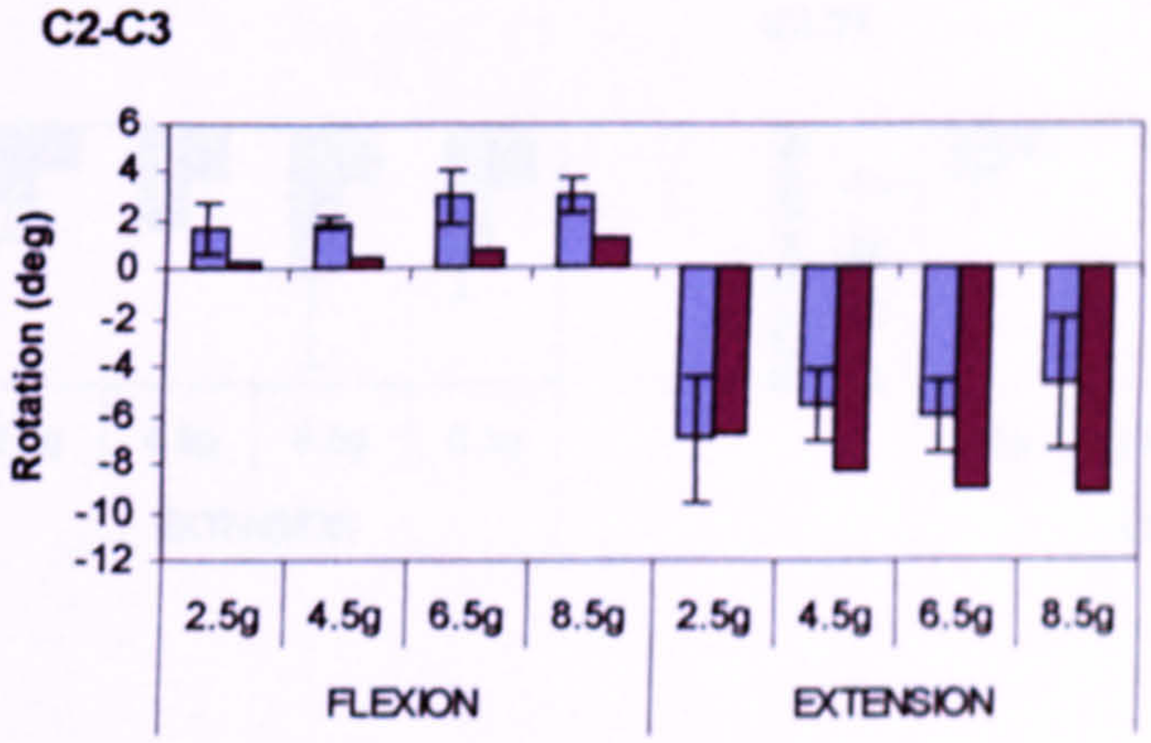


**Figure 7.6:** Maximum intervertebral angles achieved during the four whiplash trauma classes for the upper three motion segments of the ligamentous cervical spine model, shown against the average ±SD of the experimental data.

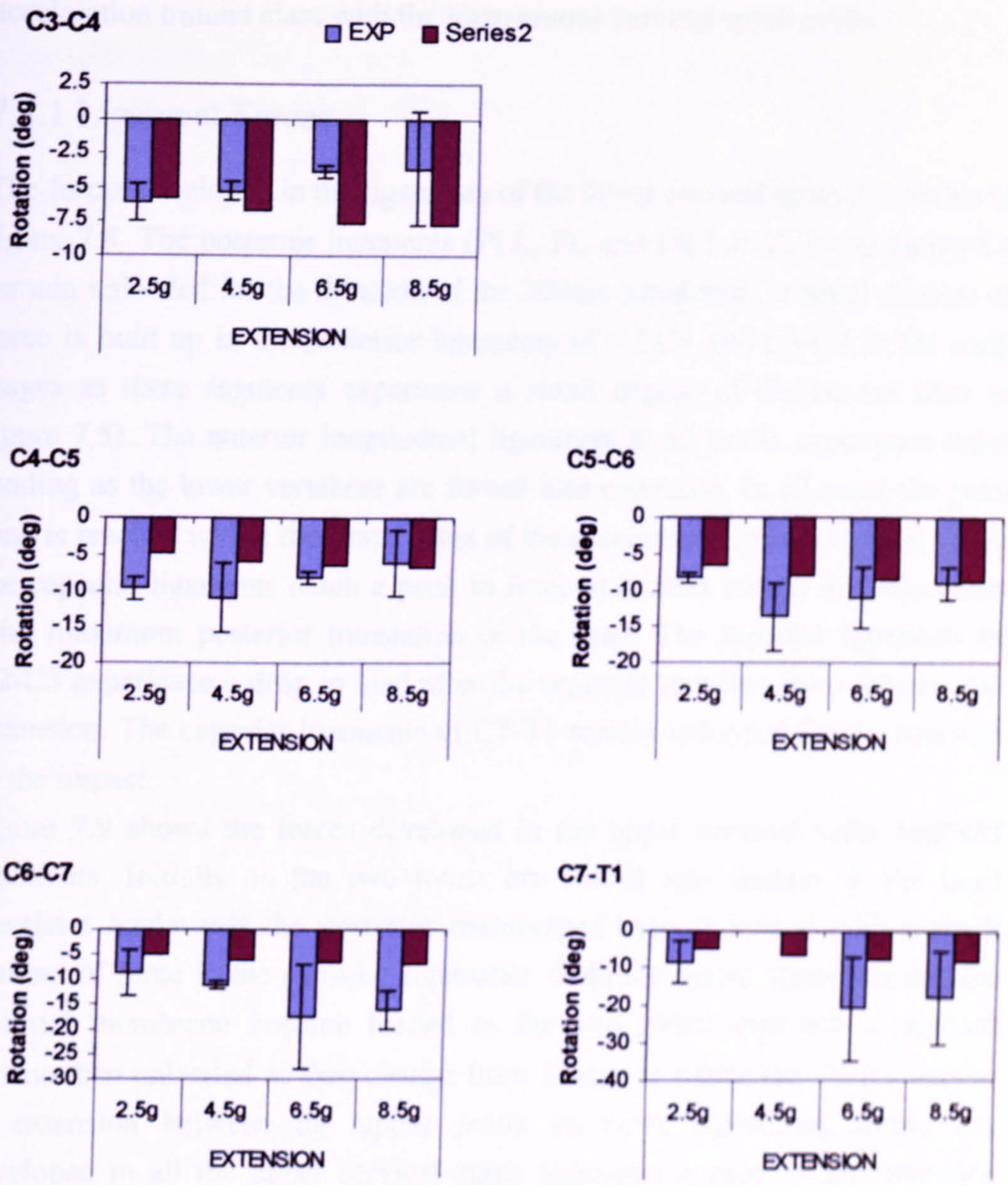


**Figure 7.7:** Maximum intervertebral angles achieved during the four whiplash trauma classes for the lower five motion segments of the ligamentous cervical spine model, shown against the average ±SD of the experimental data. The lower segments of the model did not experience significant levels of flexion during any of the trauma classes so only maximum extension is shown.

## 7.4 Component Loading During Whiplash Trauma

The local loads developed in the soft-tissue elements are studied for the 8.5g acceleration trauma class with the ligamentous cervical spine model.

### 7.4.1 Ligament Forces

The forces developed in the ligaments of the lower cervical spine are shown in figure 7.8. The posterior ligaments (PLL, FL and ISL) at all levels below C4 remain unloaded for the duration of the 200ms simulation, a small amount of force is built up in the posterior ligaments of C2-C3 and C3-C4 in the early stages as these segments experience a small degree of flexion (as seen in figure 7.5). The anterior longitudinal ligaments at all levels experience rapid loading as the lower vertebrae are forced into extension, in all cases the peak load is reached within the first 100ms of the acceleration pulse. At most levels the capsular ligaments reach a peak in force at around 100ms in conjunction with maximum posterior translation of the head. The capsular ligaments of C2-C3 experience a drop in load after the segment transfers from flexion into extension. The capsular ligaments of C7-T1 remain unloaded for the majority of the impact.

Figure 7.9 shows the forces developed in the upper cervical spine segment ligaments. Initially as the two joints are forced into flexion as the head translates backwards the posterior membranes become tensed with a small amount of force in the capsular ligaments. Both the apical ligaments and the tectorial membrane become loaded as the two joints approach maximum flexion then unloaded as they change from flexion to extension. As the degree of extension between the upper joints increases significant forces are developed in all the upper cervical spine ligaments except for the posterior membranes, which become totally unloaded. A peak in force is seen at the point of maximum head rotation at around 125ms with the ALAR ligaments reaching a maximum load of around 85% of their predicted dynamic failure force (see Chapter 2, Table 2.12). Large forces are also seen in the C1-C2 anterior membrane, apical ligament and in the capsular ligaments at both levels.

## 7.4.2 Intervertebral Disc Forces and Moments

Figure 7.10 shows the forces and moments experienced by the intervertebral discs over the course of the 200ms impact. As was the case with the frontal impact, no forces were developed in lateral shear and moments were experienced about the y-axis only. The discs experience increasing levels of posterior shear up to around 100ms followed by a sharp decrease after the T1 acceleration ends and the facet joints become loaded as the head and neck start to return towards their initial position. Axially the discs experience a small compressive force at the start of the acceleration pulse before being pulled in tension as the head and neck extend, however the C7-T1 disc remains in compression for the first 100ms. Peak tensile force is reached just prior to the end of the acceleration pulse following which the discs are compressed as the head continues to displace vertically. Maximum compression in the neck is seen at around 125ms in conjunction with the maximum rearward rotation of the head and consequently maximum torque in the discs. The maximum moment in the lower two discs peaks slightly earlier at around 100ms.

## 7.4.3 Facet Force

The loads exerted by the facet joints over the 200ms simulation are shown in figure 7.11. The facets of the lower cervical spine are unloaded for the extension phase of the 'whiplash' motion, coming into contact as the head reaches its maximum rotation and the neck begins to rebound back towards its initial position. At this point some of the shear force in the discs is transferred to the facet joints with a peak in force as they are first brought into contact at around 125ms. Similarly the lateral articular facets of the upper segments remain largely unloaded for the first 100ms than force is developed rapidly as the upper joints become extended as the head reaches maximum rearward rotation corresponding to a peak in force in the facet joints at 125ms. The facets remain loaded as head rotation reverses. The forces on the upper cervical facets are significantly greater than those seen in the lower joints with peak values of around 900N in each side. Also shown in figure 7.11 is the load on the facet of the dens showing the force exerted between the anterior ring of the atlas and odontoid process of the axis. The dens facet is loaded from the onset of the T1 acceleration reaching a maximum at around 120ms.

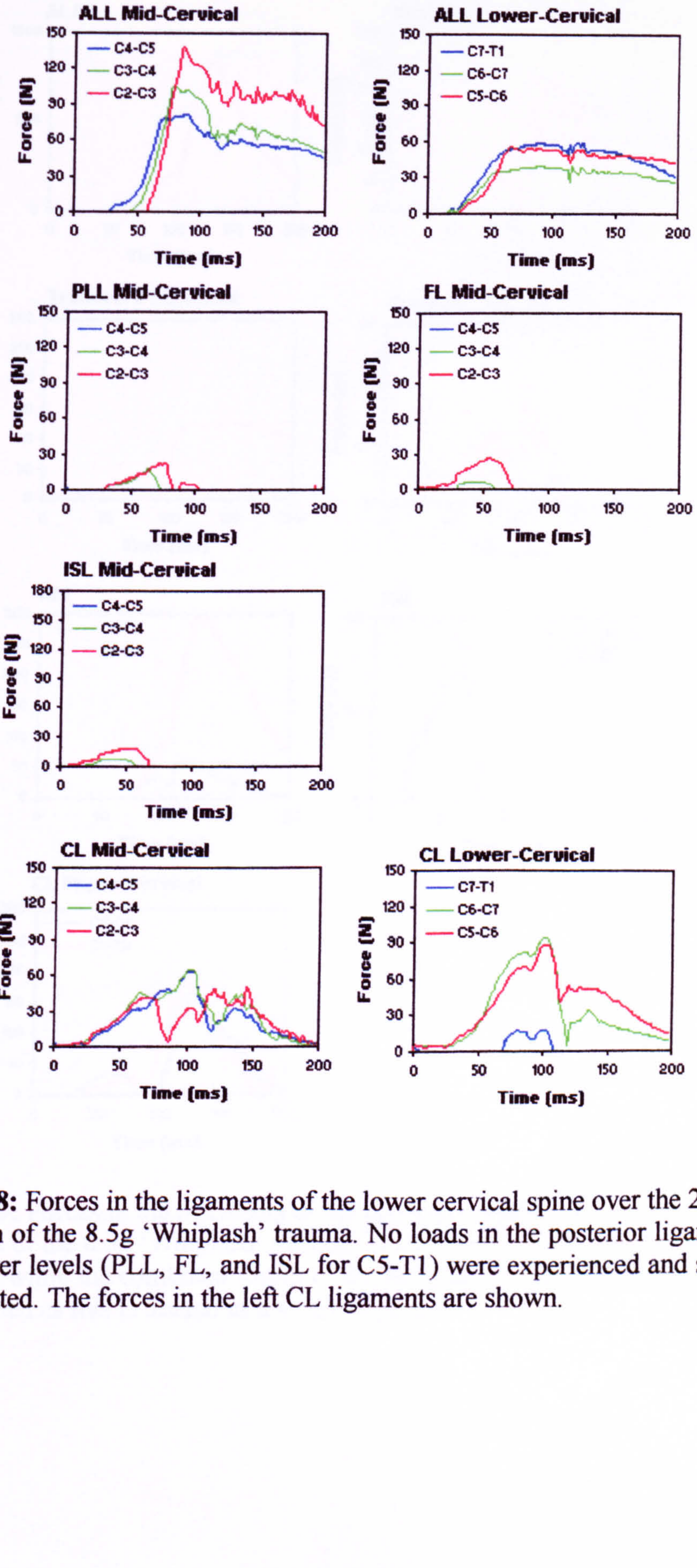


**Figure 7.8:** Forces in the ligaments of the lower cervical spine over the 200ms simulation of the 8.5g 'Whiplash' trauma. No loads in the posterior ligaments of the lower levels (PLL, FL, and ISL for C5-T1) were experienced and so are not presented. The forces in the left CL ligaments are shown.

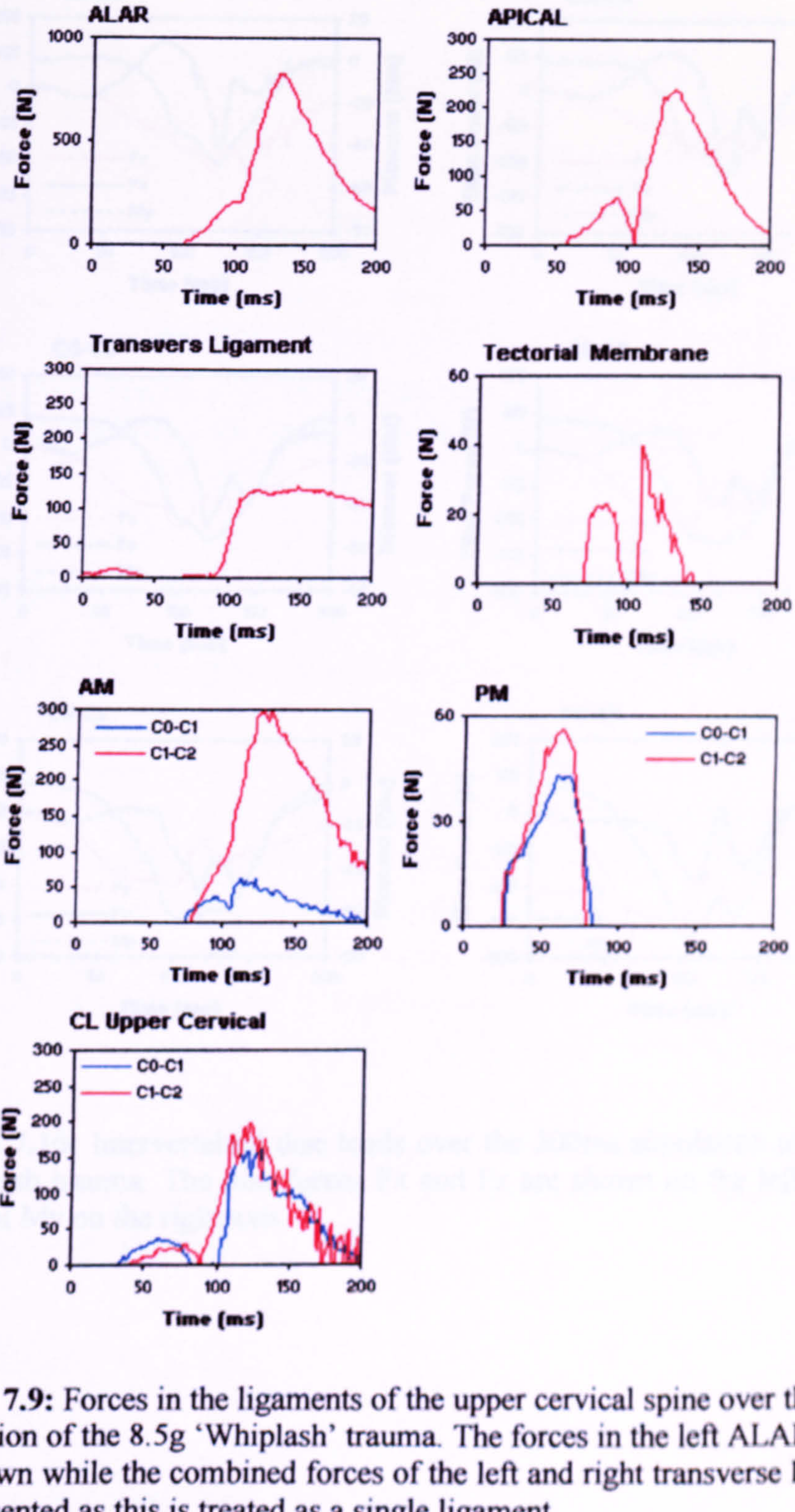


**Figure 7.9:** Forces in the ligaments of the upper cervical spine over the 200ms simulation of the 8.5g 'Whiplash' trauma. The forces in the left ALAR and CL are shown while the combined forces of the left and right transverse ligaments are presented as this is treated as a single ligament.

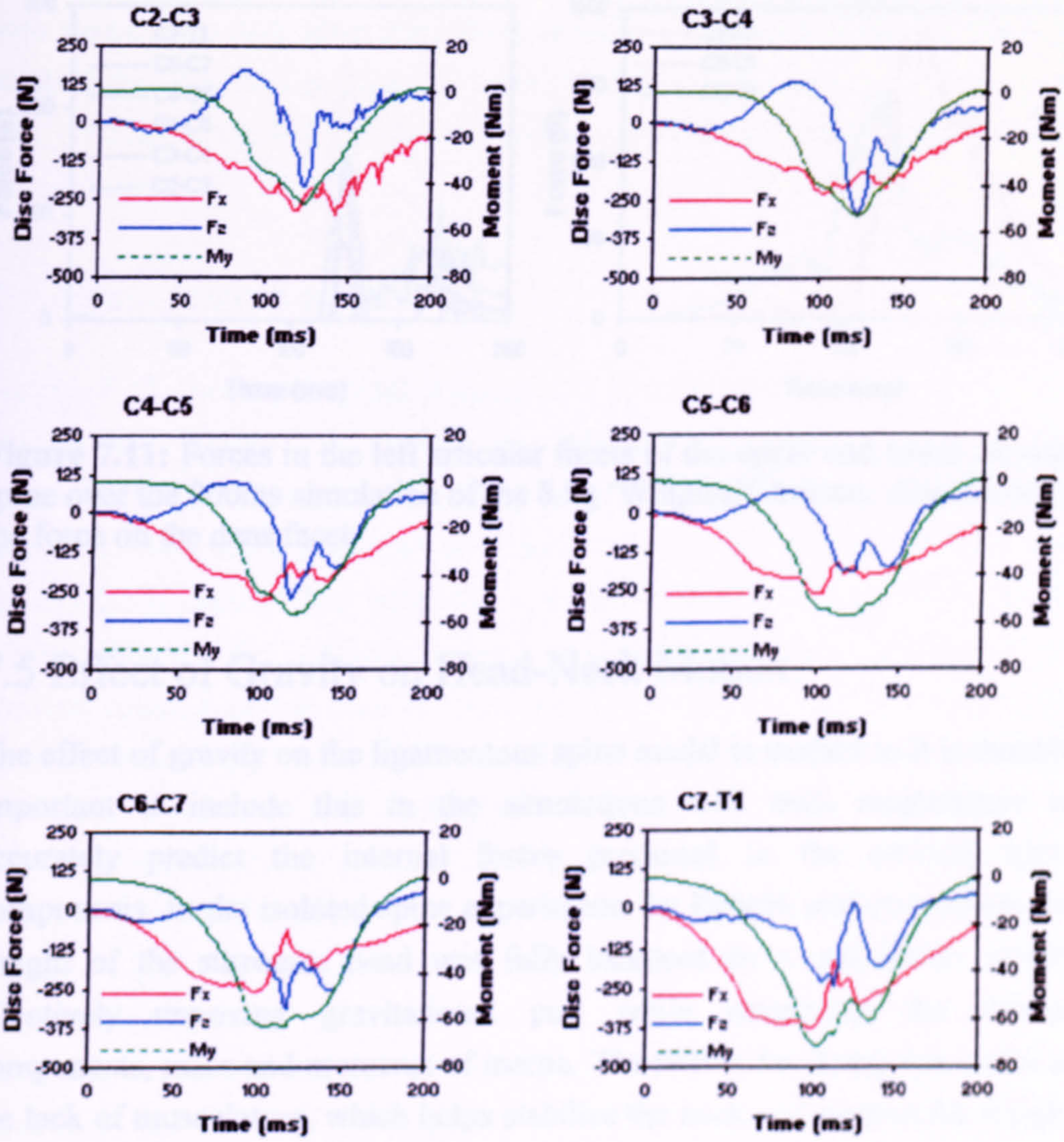


**Figure 7.10:** Intervertebral disc loads over the 200ms simulation of the 8.5g 'Whiplash trauma. The disc forces Fx and Fz are shown on the left axis and moment My on the right axis.

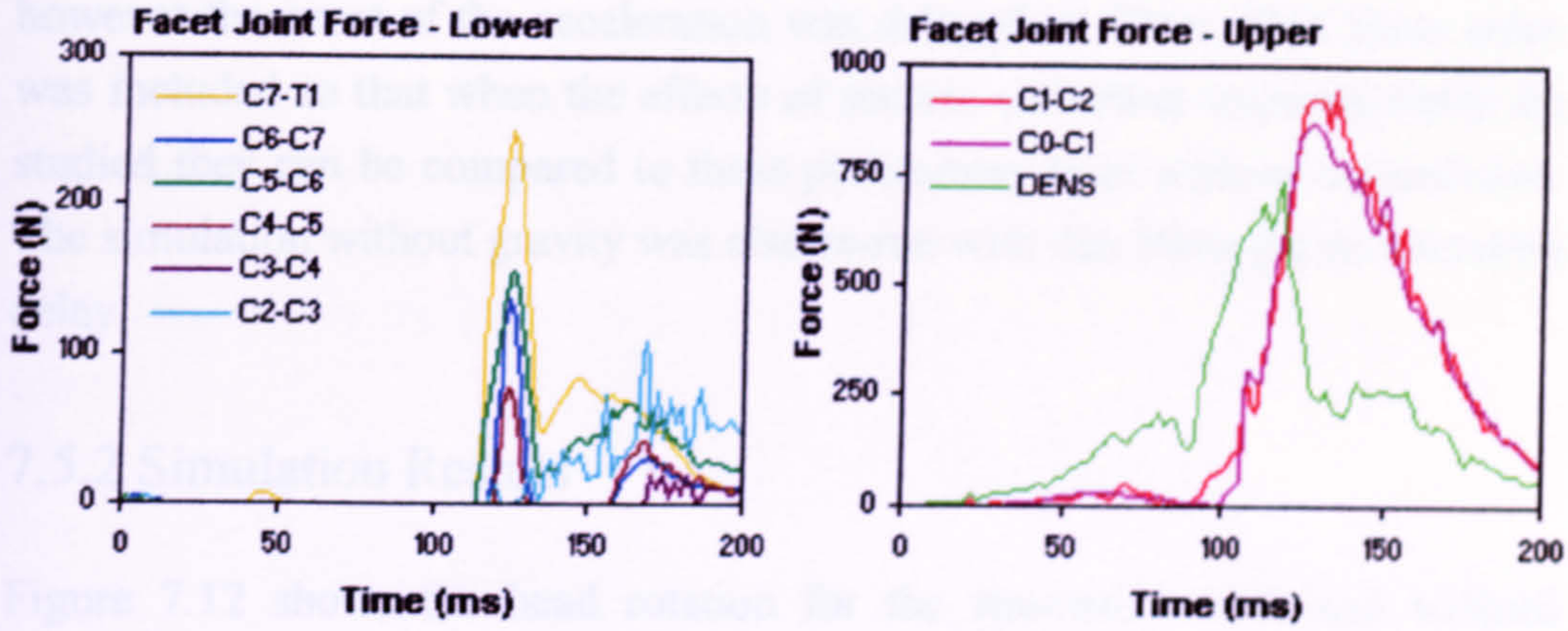


**Figure 7.11:** Forces in the left articular facets of the upper and lower cervical spine over the 200ms simulation of the 8.5g 'Whiplash' trauma. Also shown is the force on the dens facet.

## 7.5 Effect of Gravity on Head-Neck Motion.

The effect of gravity on the ligamentous spine model is studied as it is thought important to include this in the simulations with neck musculature to accurately predict the internal forces produced in the cervical spine components. In the isolated spine experiments by Panjabi and co-workers the weight of the surrogate head was fully balanced by a suspension system effectively removing gravitational pull while preserving the inertial components, mass and moments of inertia. The reason for doing this is due to the lack of musculature, which helps stabilize the neck and support the weight of the head. In reality the weight of the head will place the neck in some degree of compression and will affect the forces developed in the soft-tissue, in this section gravity is added to the simulation with the ligamentous cervical spine model to compare the resulting head and vertebral rotations and internal forces to the results without gravity.

### 7.5.1 Simulation Set-up.

The same model set-up as described in the first section of this chapter was used. A gravitational acceleration was applied to the model environment equal to the earth's gravitational force of $-9.81 m/s^2$ in the z-axis. The same

acceleration pulse was used as input to T1 to simulate the 8.5g sled test however the onset of the acceleration was delayed by 50ms. This 50ms delay was included so that when the effects of muscle activation response times are studied they can be compared to these preliminary tests without musculature. The simulation without gravity was also re-run with this 50ms pre-acceleration delay.

## 7.5.2 Simulation Results

Figure 7.12 shows the head rotation for the simulation with and without gravity and figure 7.13 depicts the intervertebral rotations for the two simulations. The effect of gravity only has a small influence on the maximum rearward rotation of the head and neck reducing the overall extension by around 2.5% around 5ms after the maximum extension is reached without gravity. Due too the eccentric position of the heads centre of gravity a small forward rotation of the head is seen therefore increasing the level of flexion reached in the upper two neck joints as the 'S' shaped curvature of the neck is developed. The rotations of the lower vertebrae are unaffected by gravity.

The maximum forces and moments experienced by the intervertebral discs with and without the effects of gravity are shown in figure 7.14. With gravity on, the weight of the head places the neck in compression from the start of the simulation; this has a noticeable effect on the overall response of the discs. The peak tensile force developed in the discs at the end of the acceleration pulse is greatly reduced when gravity is included with the lower three levels (C5-T1) experiencing practically no tensile forces throughout the simulation. In conjunction with maximum head extension the peak disc compression and torque are reduced with the inclusion of gravity, the moment placed on the upper levels in particular being reduced by around 10%. Posterior shear is only slightly affected by gravity, in general reducing the peak value by 0-5% depending on cervical level.

Analysis of the ligament forces revealed small differences in peak force for the majority of the upper and lower cervical spine ligaments. Worthy of note are the alar and apical ligaments, which had a 12 and 14% reduction in peak force respectively with the inclusion of gravity, and the posterior membranes, which had an increase in peak force of 27 and 67% for the C0-C1 and C1-C2

segments. The large increase in tension of the posterior membranes is due to the increased level of flexion reached in the upper joints.

The peak facet joint forces of the lower cervical spine remain fairly similar with the inclusion of gravity with less than 5% variation at each level. The upper facet joints C0-C1 and C1-C2 both have a reduced peak force of 10 and 17% respectively while the dens facet has an increase of 8% to maximum load.

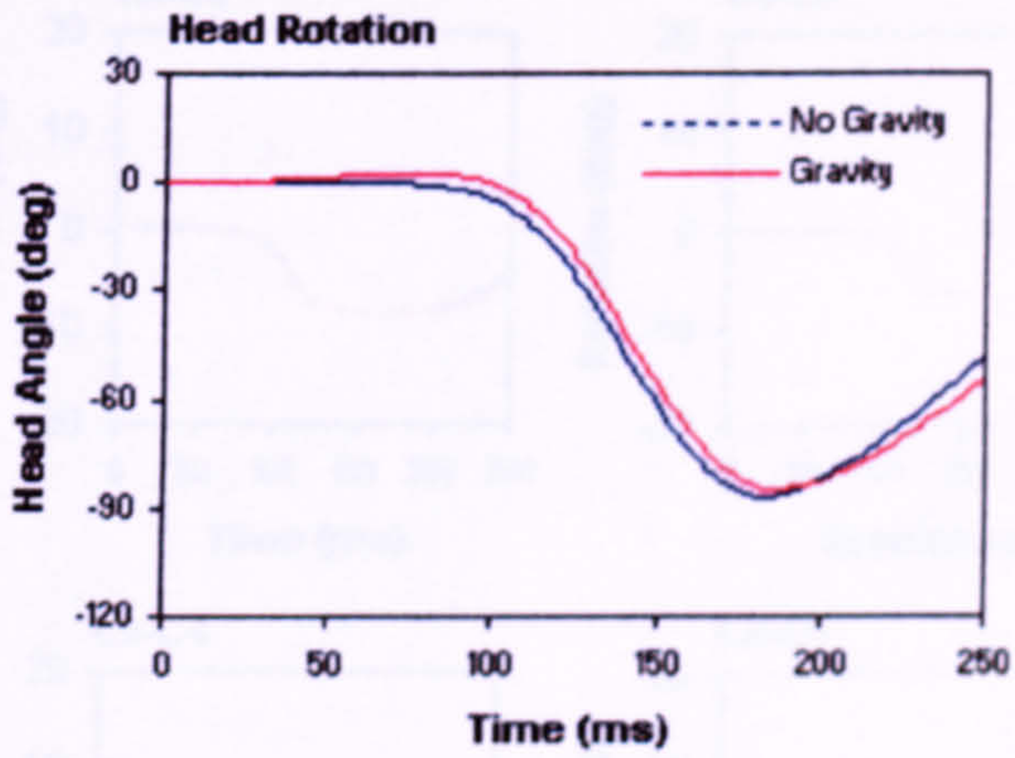


**Figure 7.12:** Resulting head rotation for the ligamentous spine model in response to 8.5g acceleration impact with and without the effects of gravity.

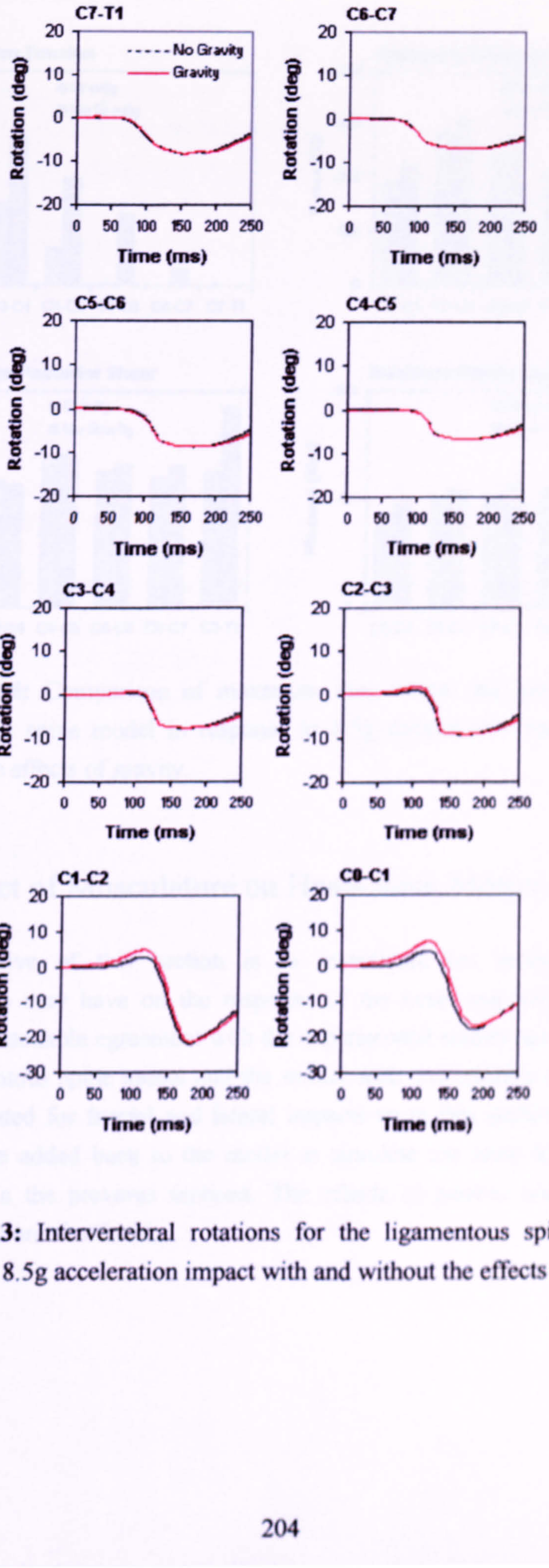


**Figure 7.13:** Intervertebral rotations for the ligamentous spine model in response to 8.5g acceleration impact with and without the effects of gravity.

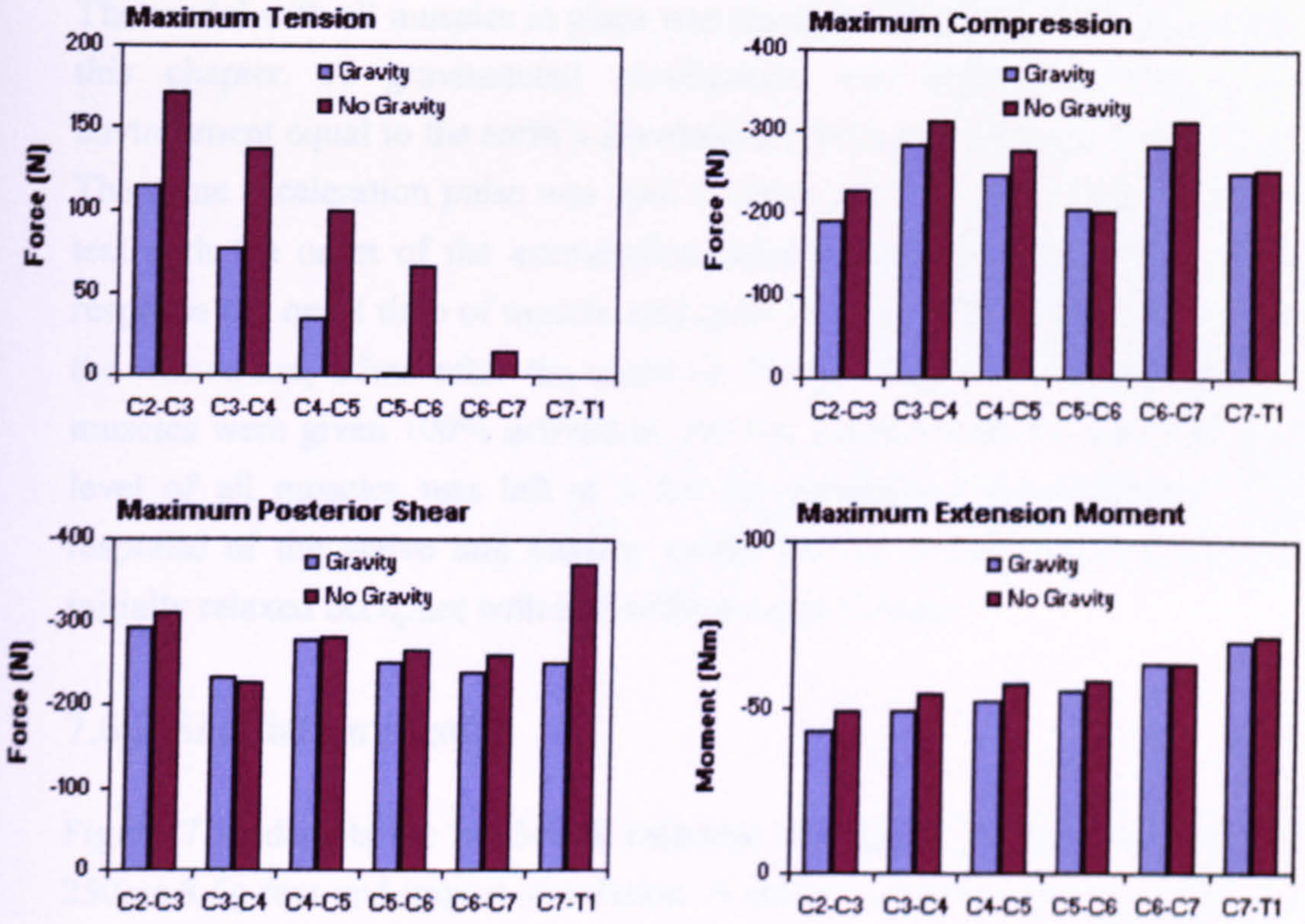


**Figure 7.14:** Comparison of maximum disc forces and moments for the ligamentous spine model in response to 8.5g acceleration impact with and without the effects of gravity.

## 7.6 Effect of Musculature on Head-Neck Motion

The objective of this section is to investigate the possible influence musculature may have on the response of the head and neck to rear-end impact. Reasonable agreement with the experimental results has been seen for the ligamentous spine model and the model with musculature has previously been validated for frontal and lateral impacts so in this section all the neck muscles are added back to the model to simulate the same 8.5g impact as described in the previous sections. The effects of passive and fully active musculature are simulated.

### 7.6.1 Simulation Set-up

The model with all muscles in place was set-up as described in the first part of this chapter. A gravitational acceleration was applied to the model environment equal to the earth's gravitational force of $-9.81 m/s^2$ in the z-axis. The same acceleration pulse was used as input to T1 to simulate the 8.5g sled test with the onset of the acceleration delayed by 50ms. For active muscle response the onset time of muscle activation was set at 75ms after the start of the simulation, 25ms after the onset of T1 acceleration, at which point all muscles were given 100% activation. For the passive response, the activation level of all muscles was left at 0 for the duration of the simulation. The response of the active and passive model can be assumed to represent an initially relaxed occupant with and without muscle response.

### 7.6.2 Simulation Results

Figure 7.15 depicts the head-neck response with active musculature over the 250ms 8.5g rear-end impact simulation. A similar overall response is obtained as was seen for the ligamentous cervical spine model. It can be seen from the blue force vectors how muscle force is developed in the anterior muscle groups of the neck in response to the initial retraction motion of the head with respect to T1 and continues to increase as the head and neck extend. Forces are developed in the posterior muscle groups following the rebound of the head. Figure 7.16 compares the head and neck rotation of the passive and active spine model. Very little difference is seen between the two responses, both reaching the same level of head extension at the same time. Peak neck rotation is reduced slightly with quicker rebound of the neck observed with muscle tensioning.

Figure 7.17 compares the peak forces and moments developed in the intervertebral discs for the passive, active and ligamentous cervical spine model. With active musculature the level of compression in the discs is significantly increased at all levels except for C7-T1. For the upper four intervertebral discs the peak compressive force is over double that seen for the ligamentous model. The peak tensile forces in the lower cervical spine are increased with passive muscle properties, with active musculature only the C2-

C3 disc experiences any level of tension with a peak value similar to the ligamentous spine model. Shear forces in the disc are generally decreased with active muscles while the passive model shows increases in peak posterior shear at all levels. The peak extension moment on the discs is fairly similar for the upper four levels for the active and passive model, both being around 30% higher than with the ligamentous model. For the lower two levels, C6-T1, the maximum torque on the discs with active musculature is about the same as experienced by the ligamentous model while the passive model remains around 15% higher.

Due to the increased compressive forces in the neck generated by the active muscle response the peak forces experienced by the facet joints are significantly increased. Figure 7.18 shows the maximum facet force on the left articular facets and also the peak force on the dens facet. The passive response of muscles has little affect on the peak loads of the lower cervical spine facets showing similar values to those seen with the ligamentous model. The upper cervical spine facets have greatly increased maximum load with the inclusion of muscles to the model both with active and passive response.

Small variations were seen in peak ligament forces with the inclusion of active and passive musculature. Table 7.1 presents the maximum ligament forces for the active muscle simulation as percentages of dynamic failure load. It can be seen that the Alar ligaments reach 100% of their predicted dynamic failure load indicating their vulnerability in rear-end impact. The anterior longitudinal ligaments also reach relatively high loads with the ALL of C2-C3 being over 50% the dynamic failure force.

## 7.6.3 Muscle Forces

Figures 7.19-7.21 show the change in length and force generation of each of the muscle elements of the head-neck model. The lengths and forces shown are for the muscle elements on the left side of the neck, due to the mid-sagittal symmetry of the model the forces developed are the same for the muscle elements on the right of the neck. The flexor muscle groups, figure 7.19, develop force as the head and neck extend backwards lengthening the muscle elements. Significant force is developed in the Sternomastoid (S-M) and in the Scalenus muscles as the neck forms the 'S' shaped curvature around 100-

130ms (see figure 7.15). The Scalenus muscles continue to develop force throughout the simulation duration as they experience only small length changes due to their attachment sites and orientation to the neck. The Longus Capitis elements reach a peak in force and length in conjunction with maximum head extension at around 180ms (figure 7.16) after which force drops off as the muscles are shortened upon rebound of the head.

Of the extensor muscles only the Semispinalis Capitis (figure 7.20) and sub-occipital (figure 7.21) muscle groups offer any significant resistance to the early translatory motion between the head and torso. The sub-occipital muscles are lengthened as the upper cervical segments are forced into flexion in the early stages of impact, this results in force generation peaking at around 120 ms in conjunction with peak flexion of the upper two joints. The Semispinalis Capitis muscle elements are also lengthened early on as the upper neck flexors while the lower neck extends. As the neck reaches peak extension ~155-190ms (figure 7.16) the majority of extensor muscles begin to develop force which increases as the muscle elements are lengthened as the head and neck rebound. The Trapezius muscle elements (figure 7.21) with insertions onto the lower cervical vertebrae (A-D) experience only small changes in length due to their oblique orientation with respect to the neck and so experience almost isometric force development following the initial onset delay of activation. Although large forces are developed by these Trapezius muscle elements, due to their low attachment sites and lines of action they offer little resistance to the overall motion of the head.

**Table 7.1:** Peak ligament forces as percentage of dynamic failure force for 8.5g rear-end impact simulation with active musculature.

| | C0-C2 | C0-C1 | C1-C2 | C2-C3 | C3-C4 | C4-C5 | C5-C6 | C6-C7 | C7-T1 |
|---|---|---|---|---|---|---|---|---|---|
| **Ligament** | | | | | | | | | |
| ALL | | | | 56 | 30 | 23 | 14 | 10 | 15 |
| PLL | | | | 6 | 3 | 1 | 1 | 1 | 1 |
| FL | | | | 15 | 7 | 4 | 3 | 3 | 3 |
| ISL | | | | 25 | 16 | 8 | 11 | 15 | 16 |
| CL | | 21 | 28 | 6 | 7 | 5 | 7 | 4 | 1 |
| ALAR | 100 | | | | | | | | |
| APICAL | 43 | | | | | | | | |
| AM | | | 10 | 42 | | | | | |
| PM | | | 16 | 21 | | | | | |
| TL | | | | 6 | | | | | |
| TM | 20 | | | | | | | | |

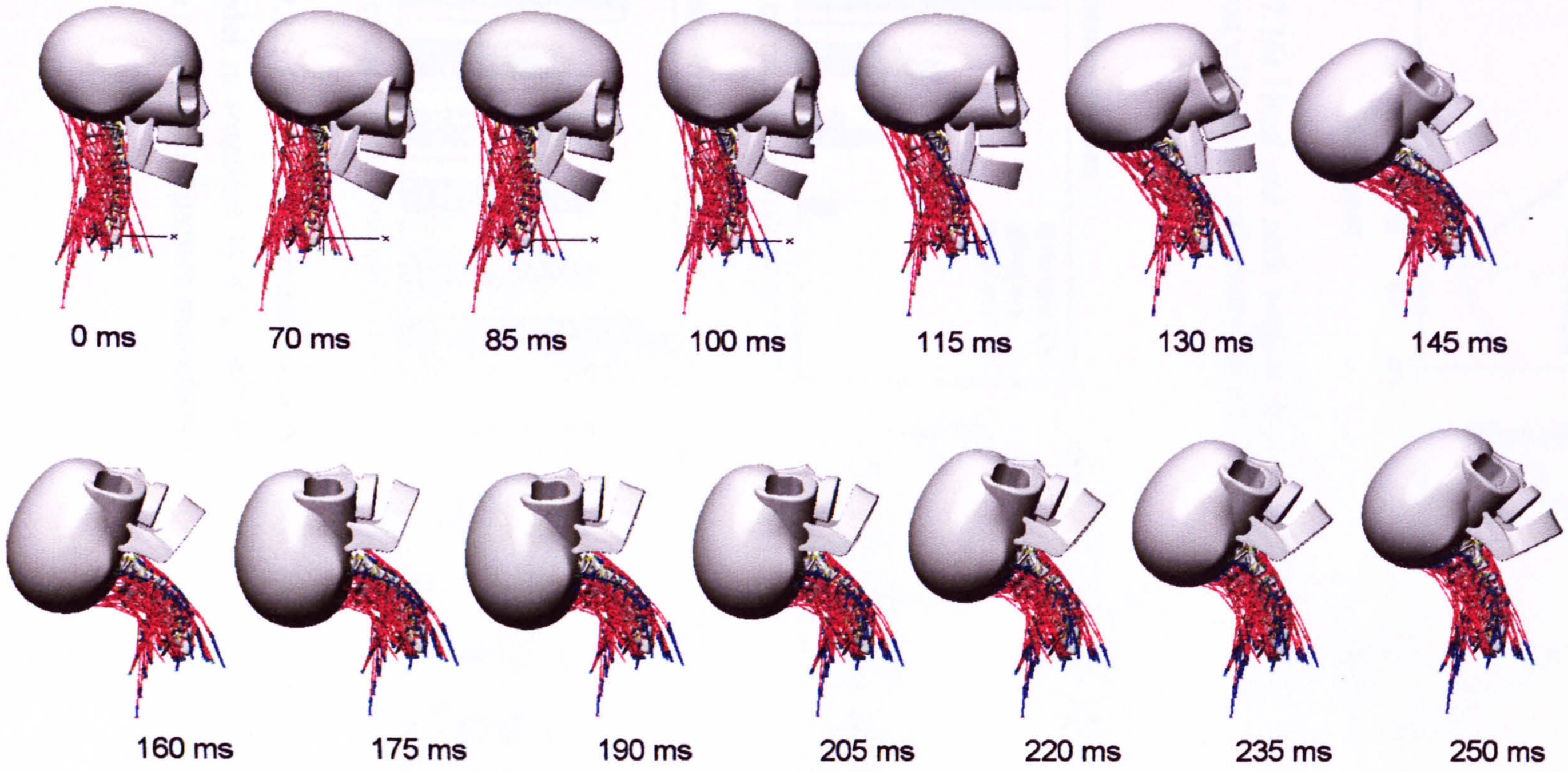


**Figure 7.15:** Time history of head-neck response to 8.5g rear-end impact with 100% active musculature. Muscle force vectors are shown in blue.

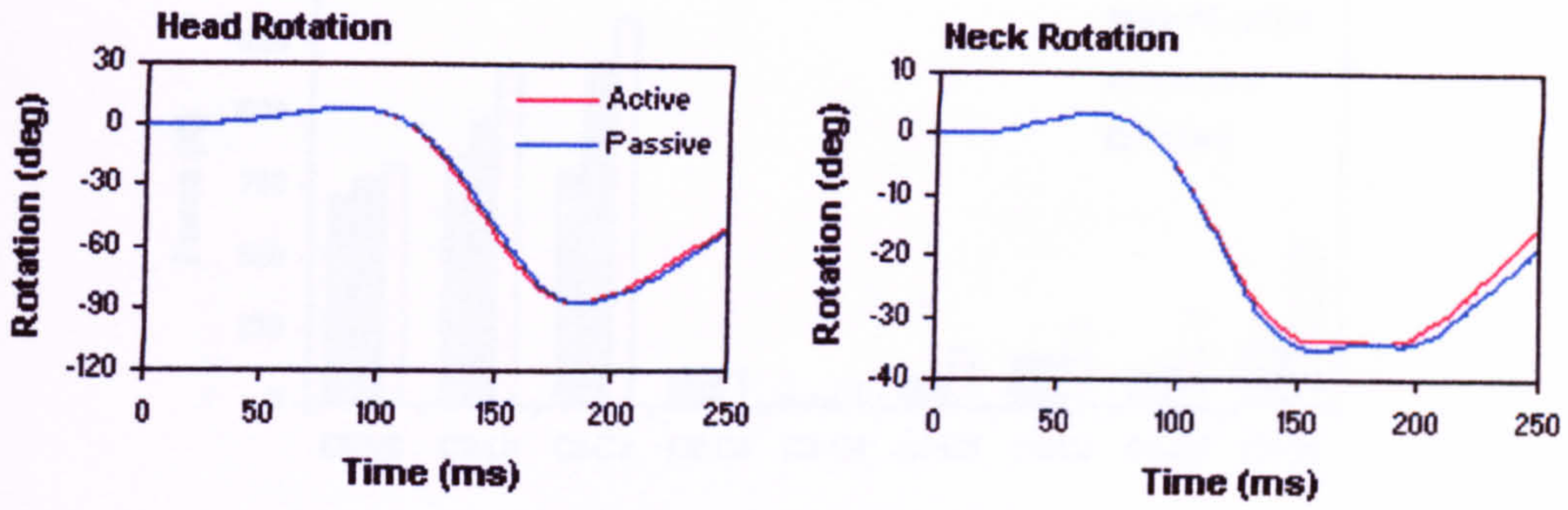


**Figure 7.16:** Head and neck rotation in response to the 8.5g rear-end impact simulation with active and passive muscle behaviour.

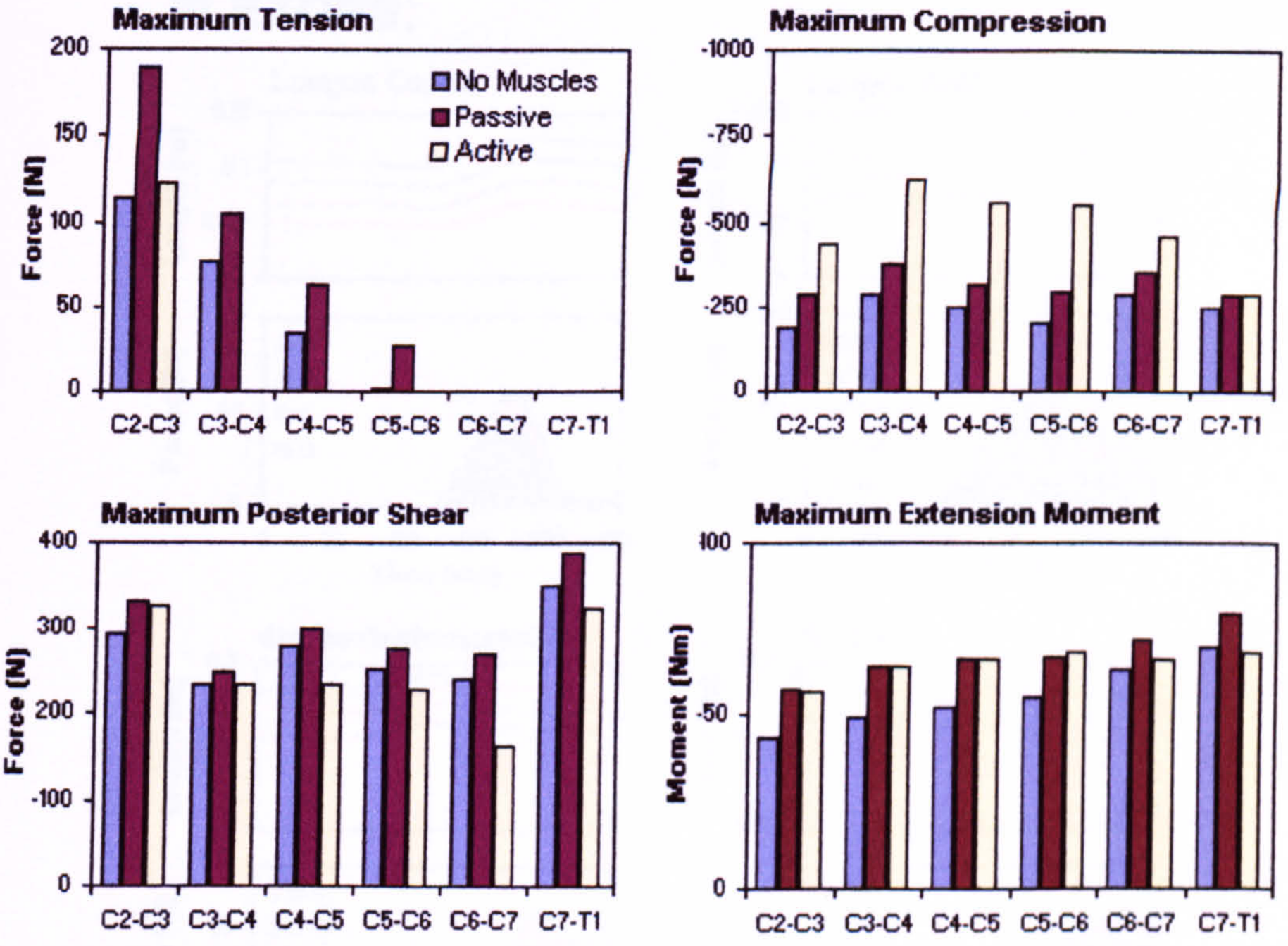


**Figure 7.17:** Comparison of maximum disc forces and moments for the head-neck model in response to 8.5g acceleration impact with and without the influence of active and passive musculature.

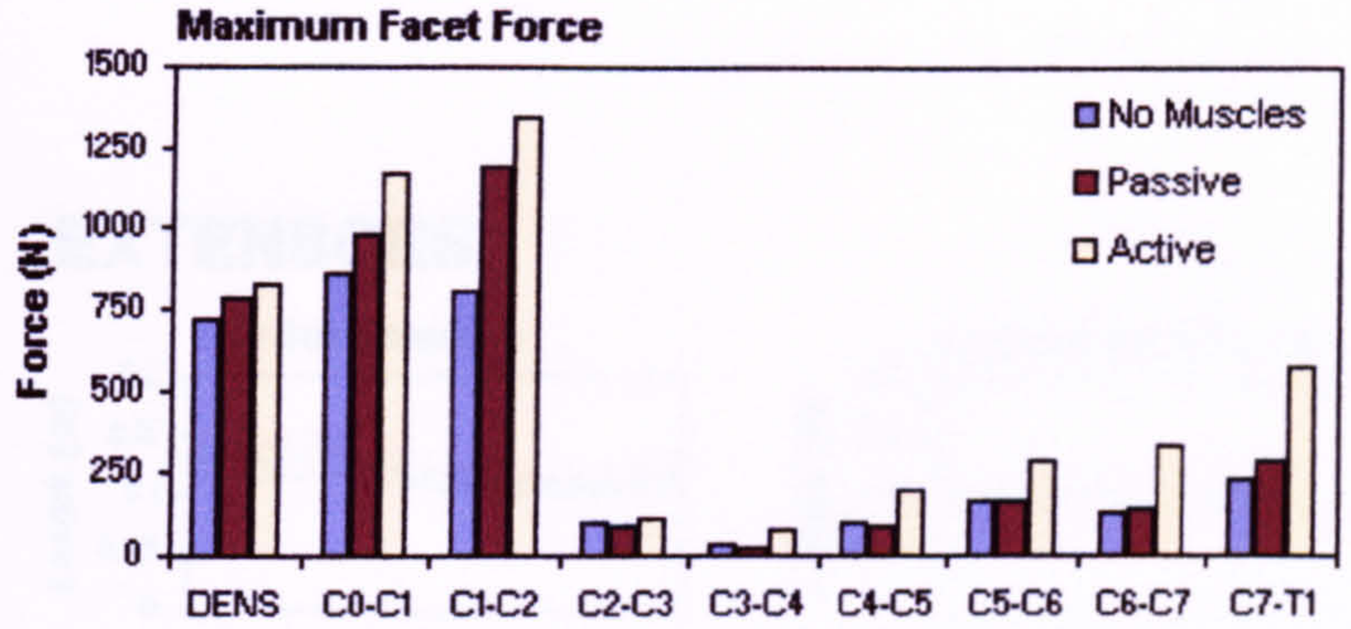


**Figure 7.18:** Comparison of maximum facet forces for the head-neck model in response to 8.5g acceleration impact with and without the influence of active and passive musculature.

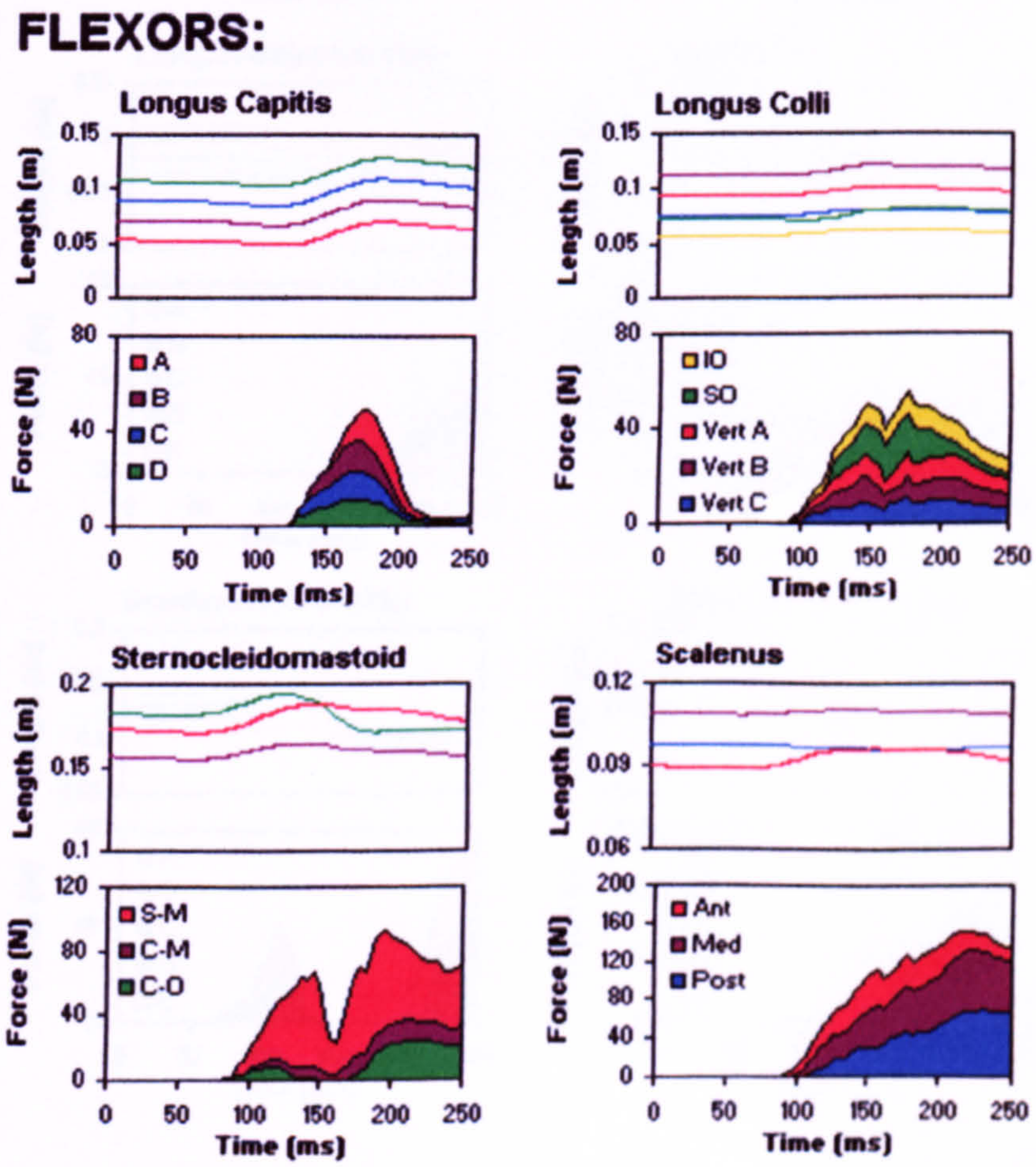


**Figure 7.19:** Length and force of the flexor muscle groups with time for the 250ms 8.5g rear-end impact simulation with active muscles (75ms onset time with 100% activation)

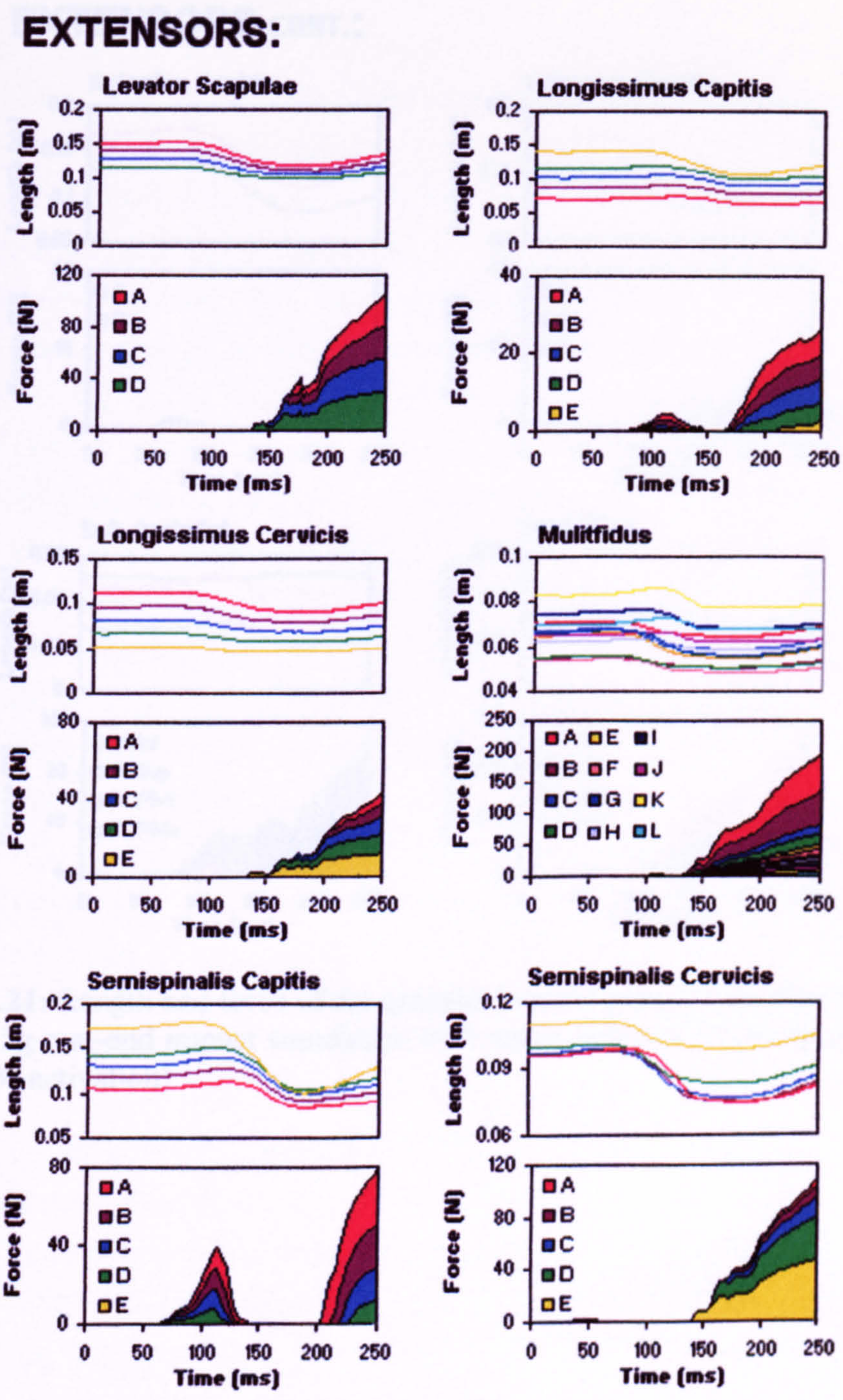


**Figure 7.20:** Length and force of the extensor muscle groups with time for the 250ms 8.5g rear-end impact simulation with active muscles (75ms onset time with 100% activation)

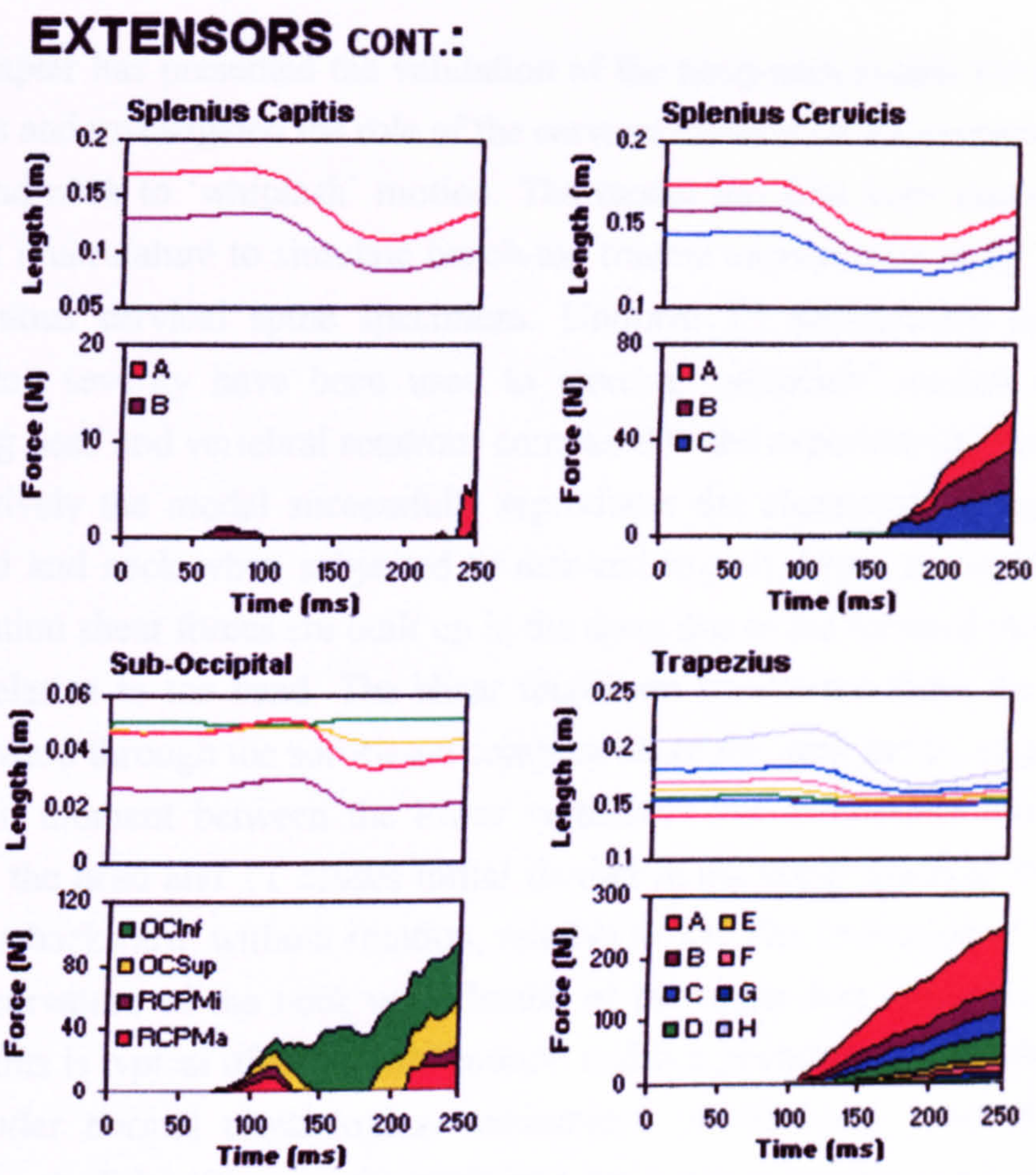


**Figure 7.21:** Length and force of the extensor muscle groups with time for the 250ms 8.5g rear-end impact simulation with active muscles (75ms onset time with 100% activation)

## 7.7 Discussion

The chapter has presented the validation of the head-neck model for rear-end impacts and investigated the role of the cervical muscles on the response of the head and neck to 'whiplash' motion. The model has first been implemented without musculature to simulate bench-top trauma experiments using isolated ligamentous cervical spine specimens. Uniform T1 acceleration pulses of increasing severity have been used to recreate 'whiplash' motion and the resulting head and vertebral rotations compared to the experimental findings.

Qualitatively the model successfully reproduces the characteristic motion of the head and neck when subjected to rear-end impact. From the onset of T1 acceleration shear forces are built up in the discs due to the forward movement of T1 relative to the head. The shear forces are transferred from the lowest level upward through the soft-tissue components of the neck model creating an extension moment between the lower vertebrae. The differential movement between the head and T1 causes initial flexion in the upper joints as the head translates backward, without rotation, relative to T1. The formation of this 'S' shaped curvature of the neck with flexion of the upper and extension of the lower joints is typical of 'whiplash' motion and is a phenomenon that does not occur under normal physiological movements of the head. Following the development of the 'S' curve the neck then goes into extension at all levels as the head rotates rearward to a point of maximum extension before rebounding towards its initial position.

For the most severe impact simulated the resulting head rotation and displacement agree reasonably well with the experimental results however the maximum extension of the head is greater than seen with the spine specimens. The maximum intervertebral rotations are shown to increase with increasing impact severity and agree reasonably well with reported values. Analysis of the load on the soft-tissue components has revealed significant forces developed in the anterior longitudinal ligaments of the lower cervical spine with a peak in force occurring as early as 70ms after the onset of T1 acceleration. The upper cervical spine ligaments experience large forces in conjunction with maximum extension of the head. The intervertebral discs

experience combinations of posterior shear, tension/compression and extension moments throughout the 'whiplash' motion. The articular facets of the lower cervical spine are unloaded for the extension phase of the motion only coming into contact as the head reaches maximum extension and the neck begins to rebound.

The effect of gravity was shown to have only a small influence on the head and neck rotation, slightly increasing the level of flexion of the upper joints in the early stages of impact. Of the soft-tissue components the intervertebral discs seemed most affected by gravity, with a reduction in the levels of tension developed in the discs at all levels. Although the discs became compressed early in the simulation due to the weight of the head the maximum compressive forces experienced were reduced, as were the peak extension moments on the discs.

Following the validation of the ligamentous spine model the cervical musculature was added back to the model to study the effects of active and passive muscle response on the head-neck motion and internal loads when subjected to the most severe 'whiplash' acceleration. Little difference was observed between the active and passive response in terms of head and neck rotation. However, muscle tensioning significantly altered the internal loads in the soft-tissue components for the activation scenario simulated. It would appear that although the anterior (flexors) muscle groups of the neck are able to generate significant force in reaction to the retraction phase of the head relative to the torso their attachments to the head and neck and subsequent lines of action make them not well suited to resisting this translatory motion, instead generating increasing levels of compression in the neck. Peak disc compression forces and peak facet forces are dramatically increased with the inclusion of muscle tensioning while the levels of posterior shear in the discs are reduced.

Only one activation state has been simulated which represents an initially unaware occupant with a muscle reflex delay of 75ms after which all cervical muscles become maximally activated. Further simulations exploring different levels of activation, reflex delay and co-contraction schemes need to be investigated to properly determine the possible influence of active musculature. Also the affect of pre-tensed muscles should be studied.

Analysis of peak ligament forces shows the Alar ligaments to be at risk of injury in the 8.5g rear-end impact however this peak in force occurs in conjunction with maximum extension of the head and so would most likely be prevented by the use of a head restraint as would the peak forces for the majority of the upper cervical spine ligaments. In the lower cervical spine the anterior longitudinal ligaments reach a peak in force prior to the development of maximum head and neck extension due to the local extension of the lower vertebrae in the formation of the 'S' shaped curvature of the neck. The inclusion of a head restraint to the model simulation would identify if these ligament forces can be prevented and would help determine the required positioning of a head restraint to best prevent excessive loads developing in the soft-tissue components.

In conclusion the ligamentous spine model has been validated with reasonable success against experimental results using human cervical spine specimens for simulated rear-end impact. The characteristics of 'whiplash' motion have been accurately reproduced in terms of head and vertebral kinematics. The soft-tissue loads have been investigated and the effects of gravity studied. Finally all the muscle elements were added back to the model to study the effects of active and passive muscle behaviour. The model results with active musculature suggest that the influence of active muscle response is unable to significantly alter the head and neck kinematics of an initially unaware occupant but will affect the forces developed in the cervical soft-tissues.

# CHAPTER 8

# Conclusions and Recommendations

The rationale behind the research described in this thesis was that a computational model of the human head and neck, capable of simulating the dynamic response to automobile impacts, could help explain neck injury mechanisms. The objective of the research has been to develop a model that could accurately predict the resulting head-neck motion in response to acceleration impacts of various directions and severities. As well as being able to define the motion of the head with respect to the torso the model should also be able to predict the local kinematics of the individual vertebrae as well as the loads and deformations of the surrounding soft tissues.
This chapter summarises the development and validation of the head-neck model described in this thesis and reviews the findings of this research.

## 8.1 Model Development

The computational model described in this thesis represents the human head and cervical spine of an adult in an upright sitting position. Implemented in visualNastran 4D dynamic simulation and analysis software the model comprises nine rigid bodies with detailed geometry representing the head, seven cervical vertebrae of the neck and the first thoracic vertebra. The arrangement of the head and cervical vertebrae in their initial position describes the natural lordosis of the neck with mid-sagittal symmetry assumed. The rigid bodies are interconnected by spring and damper constraints

representing the soft-tissues of the neck. (Non)-linear viscoelastic 'bushing' constraints connect adjacent vertebrae representing the cervical intervertebral discs, non-linear viscoelastic spring-damper elements are used to describe the cervical ligaments and frictionless rigid-body contact idealizes facet joint behaviour. 19 muscle groups of the head and neck are included in the model represented by connections of linear actuators allowing the muscles to curve around the vertebrae during neck bending. Muscle mechanics are handled by an external application that runs within Matlab and Simulink providing both passive and active muscle behaviour.

## 8.2 Validation

The individual motion segments of the upper and lower cervical spine model have been validated for quasi-static loading in all six degrees of freedom. Resulting main and coupled displacements of the lower joints have shown good agreement with experimental results using isolated cadaveric cervical motion segments, generally being within one standard deviation of the reported values. Good agreement was also seen for the main rotational displacements of the upper two joints however the atlanto-axial joint appeared to be slightly too stiff in axial rotation and lateral bending.

In the next stage of validation the individual motion segments were subjected to large loads and compared against in-vivo ranges of motion determined from measurements on human volunteers, realistic responses were seen for all directions of loading. An analysis of the internal forces in the soft-tissue components when subjected to large static loads revealed the load distribution across the segment joints highlighting the role of each element in response to different loading directions.

The entire neck model without musculature was subjected to flexion and extension loads and the resulting displacements at each level compared with experimental values. In general a good response was seen at all levels. Coupling characteristics of the model have been demonstrated and shown to be in good agreement with those observed experimentally.

The moment-generating capacity of the neck muscles was calculated and found to be in good agreement with those determined from human volunteers

thus giving confidence in the choices made on the muscle morphometry and on the origins and insertions of the individual muscle elements.

The complete head-neck model has been used to simulate frontal and lateral impacts with the resulting response compared against response corridors derived from sled acceleration tests using human volunteers. The effect of passive and fully active muscle behaviour was simulated and it was found that for both impact directions the inclusion of active muscle tensioning gave closest agreement with the experimental data. Good agreement was seen for both impact directions however for lateral impact, in comparison with the volunteer corridors, the model appears to be too flexible in lateral bending. Maximum loads developed in the soft-tissues components were compared to reported tissue failure loads where available showing reasonable levels of force development throughout the model.

Additional validation of the ligamentous spine model showed the response to rear-end impact accelerations to be in reasonable agreement with experimental results. The model was implemented without musculature to simulate bench-top trauma experiments using cadaveric isolated cervical spine specimens. The model successfully reproduced the characteristic 'whiplash' motion and resulting head and vertebral rotations and displacements.

## 8.3 Contributions to Knowledge

From the analysis of frontal and lateral impacts it was found that the inclusion of active muscle behaviour is essential in predicting the head-neck response to impact. In both impacts the developed muscle forces limit the movement between the joints of the upper cervical spine significantly reducing the degree of rotation of the head in the plane of impact. In lateral impacts the muscle tensioning also has a strong influence on the rotation of the lower two joints of the cervical spine. With passive properties the response of the head-neck model is analogous to the response of cadaveric specimens where the influence of active musculature is absent.

Analysis of the local loads in the soft-tissue components of the model during the frontal impact with active musculature revealed a clear peak in force in the majority of ligaments and in the intervertebral discs very early in the impact

before any forward rotation of the head had occurred. It is hypothesised that, in impacts of greater severity than simulated here, injury would occur at this early phase of the head and neck response as the neck reaches maximum excursion but before the head begins to rotate.

Contrary to the findings for frontal and lateral impacts the results from the rear-end simulations suggest the role of active musculature to have little affect on the resulting head and neck kinematics. Little difference was observed between the active and passive response in terms of head and vertebral rotations however the active muscle tensing resulted in significantly altered loading of the soft-tissue components. From the results it seems that, although the anterior muscle groups of the head and neck are able to generate significant force in reaction to the retraction phase of the head relative to the torso in rear-end impacts, their attachments to the head and neck and subsequent lines of action make them not well suited to resisting this translatory motion, instead generating increasing levels of compression in the neck. Peak disc compression forces and peak facet forces were shown to be dramatically increased with the inclusion of muscle tensioning while the levels of posterior shear in the discs were reduced.

## 8.4 Critical Assessment

Although the computational model of the head and neck has shown good agreement with experimental data for both static and dynamic conditions certain assumptions and simplifications due to missing material properties and modelling restrictions have left room for improvement and future development.

Information regarding the material properties of the intervertebral discs was found to be lacking; linear stiffness characteristics derived from static testing of isolated disc segments were used to define the response of the discs in most directions while non-linear load curves derived from experiments on intact motion segments were used to define the response for flexion and extension. Further experimental work needs to be completed to determine the intervertebral disc properties in response to static and dynamic conditions in

all directions of loading for each level of the cervical spine. The dynamic behaviour of all cervical spine ligaments also needs to be assessed.
Further measurements of cervical spine muscle morphometry should be completed to be able to accurately define the properties of all neck muscles. Also the level of activation and onset times of cervical muscles in response to impacts should be investigated.
While the ligamentous cervical spine model has been validated against bench-top trauma experiments using isolated spine specimens, additional information could be provided from these tests to help improve the model's response, such as measured soft-tissue loads and response to other impact directions. Also further static testing of the entire ligamentous cervical spine should be done to characterise the vertebral rotations in response to all load directions and to determine the magnitude of coupled motions at each level of the cervical spine.

## 8.5 Further Applications

The head-neck model developed has been shown to successfully predict the response of the human head and neck to impacts of various severity and direction. In addition the model is able to simulate the effects of active and passive muscle behaviour and predict the internal loads and deformations of the various soft tissue components of the cervical spine.
In the model simulations for rear-end impact the activation scenario of the muscle elements was kept simple, idealizing the response to that of an initially unaware occupant with a muscle onset delay based on experimental findings. Following the onset delay all muscles were activated maximally in response to the acceleration impact. In reality the activation scheme for the individual muscle groups is likely to vary depending on function and strength. Also the timing and level of activation of the muscle groups is expected to vary with severity and duration of impact. The initial state of the muscles prior to impact could also affect the resulting head-neck response, and indeed it has been shown that initially pre-tensed muscles of an occupant aware of an impending collision can stiffen the neck resulting in decreased head and neck rotation (Siegmund and Brault, 2000). Although further experimental work is required

to determine the relative contributions, timings, and activation levels of the various muscle groups of the neck during such impacts, the head-neck model described in this thesis is capable of simulating any activation scenario to study the role of cervical musculature on the head-neck response to impacts.

The model's ability to predict the forces developed in the soft-tissue components has been demonstrated making it suitable for investigating injury mechanisms and together with experimental research suitable for establishing injury thresholds. Further experimental work is required to determine the tolerance limits of all the soft-tissues of the cervical spine. Once established, these can be used to assess the likelihood of injury occurring in simulated crash scenarios.

In all simulations the head-neck model has been used in isolation, looking at the head and neck kinematics without the effects of the rest of the human body and without any external contact with the head. Particularly in rear-end impacts where a large amount of interaction is seen between the torso and car seat, and head and head restraint, the inclusion of these external interactions could aid in better prediction of head response. An early attempt at modelling the rest of the human body was made towards the end of this research integrating the head-neck model (Figure 8.1), with the aim of simulating rear-end impacts with a seat, seat belt and head restraint. However, the work was considered beyond the scope of this research and was postponed for future investigation. It is believed that a complete human body model together with the head-neck model described in this thesis could be used to study the effects of seating posture, and head-restraint position on the head and neck response to rear-end impact. Such a model could also be used to evaluate car safety design features.

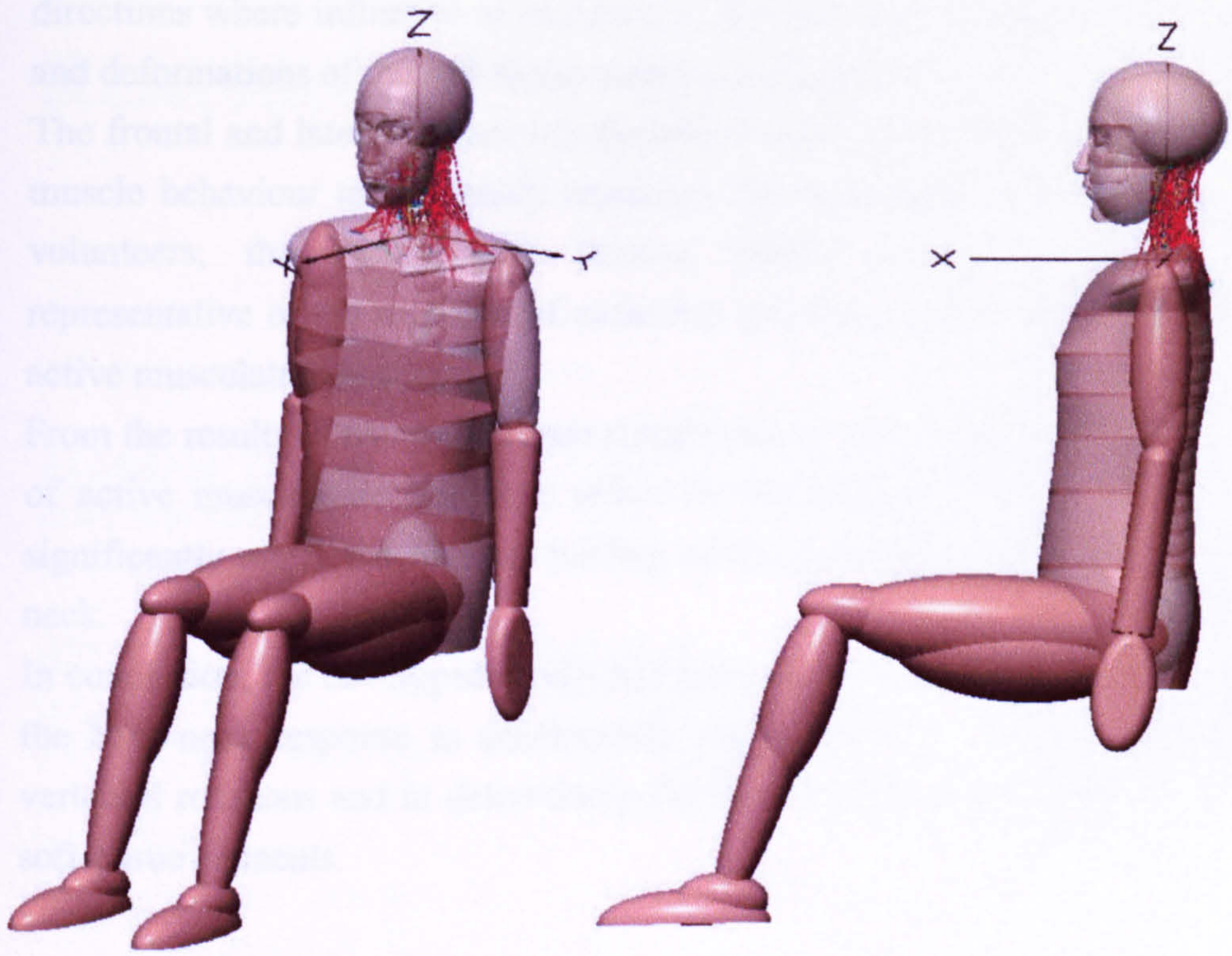


**Figure 8.1:** Integration of head-neck model with a multi-body model of the human body.

## 8.6 Final Conclusions

A computational model of the human head and cervical spine has been developed. The model consists of rigid-body representations of the head, seven vertebrae of the neck and the first thoracic vertebra interconnected by (non)-linear viscoelastic disc elements, non-linear viscoelastic ligaments, frictionless facet joints and contractile muscle elements describing both passive and active muscle behaviour and with the ability to curve around the vertebrae of the neck during bending.

The model has been validated against experimental data for small and large static loading conditions. The resulting main and coupled displacements of the individual motion segments have been shown to be accurate and the moment generating capacity of the neck muscle elements realistic. The model has been

used for the dynamic simulation of impacts in frontal, lateral and rear-end directions where influence of muscle activity have been studied and the loads and deformations of the soft-tissue components analysed.

The frontal and lateral impact simulations revealed the need to include active muscle behaviour to accurately reproduce the head-neck motions of human volunteers; the model with passive muscle properties being more representative of the response of cadaveric specimens where the influence of active musculature is absent.

From the results of rear-end impact simulations it was found that the inclusion of active musculature has little affect on the head and neck rotations but significantly alters the internal loading of the soft-tissue components of the neck.

In conclusion, the developed model has been shown to be useful in predicting the head-neck response to acceleration impacts both in terms of head and vertebral rotations and in determining the local loads and deformations of its soft-tissue elements.

# References

Adam-Rouilly, 1992. The Vertebral Column. *Anatomical Chart Co.*

ALDMAN, B., 1986. An analytical approach to the impact biomechanics of head and neck injury. In *Proceedings 30th Annual AAAM Conference*, 439-454.

BELYTSCHKO, T.B., ANDRIACCHI, T.P., SCHULTZ, A.B., AND GALANTE, J.O., 1972. Analog studies of forces in the human spine: computational techniques. *Journal of Biomechanics*, 6361-371.

BELYTSCHKO, T.B., SCHWER, L., AND SCHULTZ, A.B., 1976. A model for analytical investigation of three-dimensional head-spine dynamics. Technical Report AMRL-TR-76-10, Aerospace Medical Research Laboratory, Wright-Patterson Air Force Base, Ohio.

BOSIO, A.C. AND BOWMAN, B.M., 1986. Simulation of Head-Neck Dynamic Response in –Gx and +Gy. *30th Stapp Car Crash Conference Proceedings*, pages 345-378. Society of Automotive Engineers. SAE Paper No. 861895.

BOGDUK, N., AND MERCER, S., 2000. Biomechanics of the cervical spine. 1: Normal Kinematics. *Clinical Biomechanics*, 15:633-648.

BOGDUK, N., AND YOGANANDAN, N., 2001. Biomechanics of the cervical spine Part 3: minor injuries. *Clinical Biomechanics*, 16, 267-275.

BOYD-CLARKE, L.C., BRIGGS, C.A., AND GALEA, M.P., 2001. Comparative histochemical composition of muscle fibres in a pre- and a postvertebral muscle of the cervical spine. *Journal of Anatomy*, 199: 709-716.

BRAULT, J.R., SIEGMUND, G.P., AND WHEELER, J.B., 2000. Cervical muscle response during whiplash: evidence of a lengthening muscle contraction. *Clinical Biomechanics*, 15: 426-443.

BROWN, I.E., AND LOEB, G.E., 2000. Measured and modelled properties of mammalian skeletal muscle: IV. Dynamics of activation and deactivation. *J Muscle Res Cell Motil*, 21: 33-47.

BROWN, I.E., CHENG, E.J., AND LOEB, G.E., 1999. Measured and modelled properties of mammalian skeletal muscle: II. The effects of stimulus frequency on force-length and force-velocity relationships. *J Muscle Res Cell Motil*, 20: 627-43.

BROWN, I.E., SATODA, T., RICHMOND, F.J.R., LOEB, G.E., 1998. Feline caudofermoralis muscle. Muscle fiber properties, architecture, and motor innervation. *Exp Brain Res.*, 121: 76-91.

CAMACHO, D.L., NIGHTINGALE, R.W., ROBINETTE, J.J., VANGURI S.K., COATES D.J., AND MYERS B.S., 1997. Experimental Flexibility Measurements for the Development of a Computational Head-Neck Model Validated for Near-Vertex Head Impact. In *Proceedings of the 41st Stapp Car Crash Conference*, pages 473-486. Society of Automotive Engineers, SAE Paper No. 973345.

CHANG, H., GILBERTSON, L.G., GOEL, V.K., WINTERBOTTOM, J.M., CLARK, C.R., AND PATWARDHAN, A., 1992. Dynamic response of the occipito-atlanto-axial (C0-C1-C2) complex in right axial rotation. *Journal of Orthopaedic Research*, 10:446-453.

CHAZAL, J., TANGUY, A., BOURGES, M., GAUREL, G., ESCANDE, G., GUILLOT, M., AND VANNEUVILLE, G., 1985. Biomechanical properties of spinal ligaments and a histological study of the supraspinal ligament in traction. *Journal of Biomechanics*, 18(3):167-176.

CHENG, E.J., BROWN, I.E., AND LOEB, G.E., 2000. Virtual Muscle: A computational approach to understanding the effects of muscle properties on motor control. *Journal of Neuroscience Methods*, 101: 117-130.

CHENG E., BROWN I., AND LOEB J., 2001. Virtual Muscle 3.1.5: Muscle Model For Matlab. Users Manual, - http://ami.usc.edu/Projects/MuscluarModeling/index.asp.

CRAMER, H., LIU, Y.K., AND VON ROSENBERG, D.U., 1976. A Distributed Parameter Model of the Inertially Loaded Human Spine. *Journal of Biomechanics*, 9: 115-130

DAUVILLIERS, F., BENDJELLAL, F., WEISS, M., LAVASTE, F., AND TARRIERE, C., 1994. Development of a finite element model of the neck. In

*Proceedings of the 38th Stapp Car Crash Conference*, pages 77-91. Society of Automotive Engineers, SAE Paper No. 942210.

DENG, B., BEGEMAN, P.C., YANG, K.H., TASHMAN, S., AND KING, A.I., 2000. Kinematics of human cadaver cervical spine during low speed rear-end impacts. *Stapp Car Crash Journal*, 44, 171-188.

DENG, YC, GOLDSMITH, W., 1987. Response of a Human Head/Neck/Upper-torso Replica to Dynamic Loading-I. Physical Model. *Journal of Biomechanics*, 20, No.5, 487-497.

DENG, YC, GOLDSMITH, W., 1987. Response of a Human Head/Neck/Upper-torso Replica to Dynamic Loading-II. Analytical/Numerical Model. *Journal of Biomechanics*, 20(5): 471-486.

DE JAGER, M.K.J., 1996. Mathematical head-neck models for acceleration impacts. PhD Thesis, Technical University of Eindhoven.

DOHERTY, B.J., AND HEGGENESS, M.H., 1994. The quantitative anatomy of the atlas. *Spine*, 19(22): 2497-2500.

DOHERTY, B.J., AND HEGGENESS, M.H., 1995. Quantitative anatomy of the second cervical vertebrae. *Spine*, 20(5): 513-517.

DVORAK, J., SCHNEIDER, E., SALDINGER, P., AND RAHN, B., 1988. Biomechanics of the craniocervical region: The alar and transverse ligaments. *Journal of Orthopaedic Research*, 6:452-461.

EBRAHEIM, N.A., XU, R., CHALLGREN, E., AND YEASTING, R.A., 1997a. Quantitative anatomy of the cervical facet and the posterior projection of its inferior facet. *Journal of spinal disorders*, 10(4): 308-316.

EWING, C.L., THOMAS, D.J., AND LUSTICK, L., 1977. Dynamic response of the human head and neck to +Gy impact acceleration. In *Preceedings of the 21st Stapp Car Crash Conference*, Society of Automotive Engineers, 547-586.

FROBIN, W., LEIVSETH, G., BIGGERMANN, M., AND BRINCKMANN, P., 2002. Vertebral height, disc height, posteroanterior displacements and dens-atlas gap in the cervical spine: precision measurement protocol and normal data. *Clinical Biomechanics*, 17: 423-431.

GENTLE, C.R., GOLINSKI, W.Z., AND HEITPLATZ, F., 2001. Computational studies of 'whiplash' injuries. *Proc Instn Mech Engrs*, 215(H):181-189.

GOEL, V.K., CLARK, C.R., MCGOWAN, D., AND GOYAL, S., 1984. An in-vitro study of the kinematics of the normal, injured and stabilized cervical spine. *Journal of Biomechanics*, 17(5): 363-376.

GOEL, V.K., CLARK, C.R., GALLAES, K., AND LIU, Y.K., 1988a. Moment-rotation relationships of the ligamentous occipito-atlanto-axial complex. *Journal of Biomechanics*, 21(8): 673-680.

GOEL, V.K., CLARK, C.R., HARRIS, K.G., AND SCHULTE, K.R., 1988b. Kinematics of the cervical spine: effects of multiple total laminectomy and facet wiring. *Journal of Orthopaedic Research*, 6: 611-619.

GRAUER, J.N, PANJABI, M.M., CHOLEWICKI, J., NIBU, K., AND DVORAK, J., 1997. Whiplash produces an S-shaped curvature of the neck with hyperextension at lower levels. *Spine*, 22(21): 2489-2494.

GRAY, H., 1980. *Grays anatomy*. 36th ed. Edited by Peter L. Williams & Roger Warwick. Churchill Livingstone.

GURUMOORTHY, D., AND TWOMEY, L.T., 2000. Morhphology of cervical muscles and relevance to whiplash. In Frontiers in Whiplash Trauma. Clinical and Biomechanical, pages 60-71. Editors: Yoganandan, N., and Pintar F.A. IOS Press, Amsterdamn. ISSN 0929-6743

HALIDIN, P.H., BROLIN, K., KLEIVEN S., VON HOIST, H., JAKOBSSON, L., AND PALMERTZ, C., 2000. Investigation of conditions that affect neck compression-flexion injuries using numerical techniques. *Stapp Car Crash Journal*, 44, 127-138

HARMS-RINGDAHL, K., AND SCHULDT, K., 1988. Maximum neck extension strength and relative neck muscular load in different cervical spine positions. *Clinical Biomechanics*, 4L 17-24.

HILL, A.V., 1970. *First and Last Experiments in Muscle Mechanics*. C.U.P.

HERZOG, W., KAMAL, S., AND CLARKE, H.D., 1992. Myofilament lengths of cat skeletal muscle: theoretical considerations and functional implications. Journal of Biomechanics, 25: 945-948.

HOBBS, P.C., 1972. An anthropometric survey of 500 royal air force aircrew heads. Royal Aircraft Establishment Technical Report 73137. Procurement Executive, Ministry of Defence, Farnborough, Hants.

HUSTON, J.C., PASSERELLO, C.E., AND HUSTON, R.L., 1976. Numerical prediction of head/neck response to shock impact. *Measurement and prediction of structural and biodynamic crack-impact response*, ASME, 137-149.

JOHNSON, G., BOGDUK, N., NOWITZKE, A., AND HOUSE, D., 1994. Anatomy and actions of the trapezius muscle. *Clinical Biomechanics*, 9: 44-50.

JORDAN, A., MEHLSEN, J., AND BULOW, P.M., 1999. Maximum isometric strength of the cervical musculature in 100 healthy volunteers. *Spine*, 24: 1343-1348.

KAMIBAYASHI L.K., AND RICHMOND F.J.R., 1998. Morphometry of human neck muscles. *Spine*, 23(12): 1314-1323.

KANEOKA, K., ONO, K., INAMI, S., AND HAYASHI, K., 1999. Motion analysis of cervical vertebrae during whiplash loading. *Spine*, 24(8): 763-770.

KAPANDJI, I.A., 1974. *The Physiology of the Joints, Volume 3: The Trunk and Vertebral Column.* Churchill Livingstone, Edinburgh, Second Edition.

KLEINBERGER, M., 1993. Application of finite element techniques to the study of cervical spine mechanics. *In Proceedings of the 37th Stapp Car Crash Conference*. San Antonio, TX; 261-272.

KUMARESAN, S., YOGANANDAN, N., AND PINTAR, F.A., 1997. Methodology to quantify the uncovertebral joint in the human cervical spine. Journal of Musculoskeletal Research, 1: 1-9.

LYSELL, E., 1969. Motion in the cervical spine.. *Acta Orthop. Scand.*, 123 (Suppl.).

MACNAB, I., 1964. Acceleration injuries of the cervical spine. *Journal of Bone and Joint Surgery*, 46.

MAYOUX-BENHAMOU, M.A., REVEL, M., 1993. Influence of head position on dorsal neck muscle efficiency. *Electromyogr Clin Neurophysiol*, 33: 161-166.

MERRILL, T., GOLDSMITH, W. AND DENG, Y-C., 1984. Three Dimensional Response of a Lumped Parameter Head – Neck Model Due to Impact and Impulsive Loading. *Journal of Biomechancis*, 17(2): 81-95.

MILNE, N., 1991. The role of zygapophysial joint orientation and uncinate processes in controlling motion in the cervical spine. *Journal of Anatomy*, 178: 189-201.

MIMURA, M., MORIYA, H., WATANABE, T., TAKAHASHI, K., YAGMAGATA, M., TAMAKI, T.I., 1989. Three-dimensional motion analysis of the cervical spine with special reference to the axial rotation. *Spine*, 14:1135-1139.

MORONEY, S.P., SCHULTZ, A.B., MILLER, J.A.A., AND ANDERSSON, G.B.J., 1988. Load-displacement properties of lower cervical spine motion segments. *Journal of Biomechanics*, 21(9): 769-779.

MORRIS, A.P., AND THOMAS, P., 1996a. A study of soft tissue neck injuries in the UK. *Proceedings 15th International technical Conference on Enhanced Safety of Vehicles*, May 13-16, Melbourne, Australia, 1412-1425.

MORRIS, A.P., AND THOMAS, P., 1996b. Neck injuries in the UK co-operative crash injury study. In *Proceedings of the 40th Stapp Car Carsh Conference*. Society of Automotive Engineers, 267-329. SAE Paper No. 962433.

MYKLEBUST, J.B., PINTAR, F., YOGANANDAN, N., CUSICK, J.F., MAIMAN, D., MYERS, T.J., AND SANCES, A., 1988. Tensile strength of spinal ligaments. *Spine*, 13(5):526-531.

NIGHTINGALE, R.W., MCELHANEY, J.H., RICHARDSSON, J.H., AND MYERS, B.S., 1996. Dynamic responses of the head and cervical spine to axial impact loading. Journal of Biomechanics, 29(3): 307-318.

NIGHTINGALE, R.W., MCELHANEY, J.H., CAMACHO, D.L., KLEINBERGER, M., WINKELSTEIN, B.A., AND MYERS, B.S., 1997. The dynamic responses of the cervical spine: Buckling, end conditions and tolerance in compression impacts. In Proceedings of the 38th Stapp Car Crash Conference, SAE 973344.

NISSAN, M., AND GILAD, I., 1984. The cervical and lumbar vertebrae-and anthropometric model. *Engineering in Medicine*, 13(3): 111-114.

NITSCHE, S., KRABBEL, G., APPEL, H., AND HAUG, E., 1996 Validation of a finite-element-model of the human neck. In the *International conference of the biomechanics of impact*. Dublin. Sept. pp.107-122.

NOWITZKE, A., WESTAWAY, M., AND BOGDUK, N., 1994. Cervical zygapophysial joints: geometrical parameters and relationship to cervical kinematics. Clinical Biomechanics, 9: 342-347.

NYGREN, A., 1984. Injuries to car occupants – some aspects of the interior safety of cars. *Akta Oto-Larynologica*, S395. ISSN 0365-5237.

ODA, T., PANJABI, M.M., AND CRISCO III, J.J., 1991. Three-dimensional movements of the upper cervical spine. Journal of Spinal Disorders, 4: 411-419.

ODA, T., PANJABI, M.M., CRISCO III, J.J., BUEFF, H.U., GROB, D., AND DVORAK, J., 1992. Role of tectorial membrane in the stability of the upper cervical spine. *Clinical Biomechanics*, 7: 201-207.

OLNEY, D.B., AND MARSEN, A.K., 1986. The effect of head restraints and seat belts on the incidence of neck injury in car accidents. *Injury*, 17, 365-367.

ONO, K., AND KANNO, M., 1993. Influences of the physical parameters on the risk to neck injuries in low impact speed rear-end collisions. *Proceedings IRCOBI Conference*, September 16-18, Eindhoven, The Netherlands, 201-212.

ONO, K., KANEOKA, K., WITTEK, A., KAJZER, J., 1997. Cervical injury mechanism based on the analysis of human cervical vertebral motion and head-neck-torso kinematics during low speed rear impacts. In *Proceedings of the 41st Stapp Car Crash Conference*, 339-356. Society of Automotive Engineers, SAE Paper No. 973340.

ORNE, D., AND LIU, Y.K., 1971. A mathematical model of spinal response to impact. *Journal of Biomechanics*, 4:49-71.

PANJABI, M.M., 1972. Three-dimensional mathematical model of the human spine structure. *Journal of Biomechanics*, 6:671-680.

PANJABI, M.M., SUMMERS, D.J., PELKER, R.R., VIDEMAN, T., FRIEDLAENDER, G.E., AND SOUTHWICK, W.O., 1986. Three-dimensional load-displacement curves due to forces on the cervical spine. *Journal of Orthopaedic Research*, 4: 152-161.

PANJABI, M.M., CHOLEWICKI, J., NIBU, K., BABT, L.B., AND DVORAK, J., 1998a. Simulation of whiplash trauma using whole cervical spine specimens. Spine, 23(1): 17-24.

PANJABI, M.M., CHOLEWICKI, J., NIBU, K., GRAUER, J.N., BABT, L.B., AND DVORAK, J., 1998b. Mechanism of whiplash injury. *Clinical Biomechanics*, 13: 239-249.

PANJABI, M.M., DVORAK, J., DURANCEAU, J., YAMAMOTO, I., GEBER, M., RAUSCHING, W., AND BUEFF, H.U., 1988. Three-dimensional movements of the upper cervical spine. *Spine*, 13:726-730.

PANJABI, M.M., DVORAK J., CRISCO III, J.J., ODA, T., HILIBRAND, A., AND GROB, D., 1991a. Flexion, extension, and lateral bending of the upper cervical spine in response to alar ligament transections. *Journal of spinal disorders*, 4(2): 157-167.

PANJABI, M.M., DVORAK, J., CRISCO III, J.J., ODA, T. WANG, P., AND GROB, D., 1991b. Effects of alar ligament transection on upper cervical spine rotation. *Journal of Orthopaedic Research*, 9: 584-593.

PANJABI, M.M., TAKATA, K., GOEL, V., FEDERICO, D., OXLAND, T., DURANCEAU, J., AND KRAG, M., 1991c. Thoracic human vertebrae. Quantitative three-dimensional anatomy. *Spine*,16(8): 888-901.

PANJABI, M.M., OXLAND, T.R., AND PARKS, E.H., 1991d. Quantitative anatomy of cervical spine ligaments. Part 1. Upper cervical spine. *Journal of Spinal Disorders*, 4(3): 270-276.

PANJABI, M.M., OXLAND, T.R., AND PARKS, E.H., 1991e. Quantitative anatomy of cervical spine ligaments. Part 2. Middle and lower cervical spine. *Journal of Spinal Disorders*, 4(3): 277-285.

PANJABI, M.M. DURANCEAU, J., GOEL, V., OXLAND, T., AND TAKATA, K., 1992. Cervical human vertebrae. Quantitative three-dimensional anatomy of the middle and lower regions. Spine, 16(8): 861-869.

PANJABI, M.M., OXLAND, T., TAKATA, K., GOEL, V., DURANCEAU, J., AND KRAG, M., 1993. Articular facets of the human spine. *Spine*, 18(10): 1298-1310.

PANJABI, M.M., LYDON, C., VASAVADA, A., GROB, D., CRISCO III, J.J., AND DVORAK, J., 1994. On the understanding of clinical stability. *Spine*, 19(23): 2642-2650.

PENNING, L., 1992a. Acceleration injury of the cervical spine by hypertranslation of the head. Part 1: Effect of normal translation of the head on cervical spine motion: a radiologic study. *European Spine Journal*,1, 7-12.

PENNING, L., 1992b. Acceleration injury of the cervical spine by hypertranslation of the head. Part 2: Effect of normal translation of the head on cervical spine motion: discussion of literature data. *European Spine Journal*,1, 13-19.

PINTAR, F.A., MYKLEBUST, J.B., SANCES JR., A., AND YOGANANDAN, N., 1986. Biomechanical properties of the human intervertebral disk in tension. *In: Proceedings of the ASME*. New York, NY, p.38-39.

QUEISSER, F., BLUTHNER, R., SEIDEL, H., 1994. Control of positioning the cervical spine and its application to measuring extensor strength. *Clinical Biomechanics*, 9: 157-161.

RACK, P.M.H., AND WESTBURY, D.R., 1969. The effects of length and stimulus rate on tension in the isometric cat soleus muscle. J Physiol., 204: 443-460.

RAYNAK, G.C., AND CHING, R.P., 2000. Dynamic sled tuning for benchtop whiplash simulation. In N. Yoganandan and F.A. Pintar, editors, *Frontiers in Whiplash Trauma, Clinical and Biomechanical*, pages 186-197. IOS Press, Amsterdam. ISSN 0929-6743.

REID, S.E., AND RAVIV, G., 1981. Neck muscle resistance to head impact. Aviat Space Environ Med: 78-84.

REBER, J.G. AND GOLDSMITH, W., 1979. Analysis of large head-neck motions. *Journal of Biomechanics*, 12:211-222.

RICHTER, M., WILKE, H.J., KLUGER, P., CLAES, L., AND PUHL, W., 2000. Load-displacement properties of the normal and injured lower cervical spine in vitro. *European Spine Journal*, 9: 104-108.

RICHMOND, F.J.R., SINGH, K., AND CORNEIL, B.D., 2001. Neck muscles in the rhesus monkey. I. Muscle morphometry and histochemistry," *J. Neurosci.* 86: 1717-1728.

SCHAFFLER, M.B., ALSON, M.D., HELLER, J.G., AND GARFIN, S.R., 1992. Morphology of the dens. *Spine*, 17(7):738-742.

SCOTT, S.H., BROWN, I.E., AND LOEB, G.E., 1996. Mechanics of feline soleus: I. Effect of fascicle length and velocity on force output. J. Muscle Res Cell Motil., 17: 207-219.

SHEA, M., EDWARDS, W.T., WHITE, A.A., AND HAYES, W.C., 1991. Variations of stiffness and strength along the human cervical spine. Journal of Biomechanics, 24: 95-107.

SIEGMUND, GP., MYERS, B.S., DAVIS, M.B., BOHNET, H.K., AND WINKELSTEIN, B.A., 2001. Mechanical evidence of cervical facet capsule injury during whiplash. Spine, 26(19): 2095-2101.

SIEGMUND, G.P., AND BRAULT, J.R., 2000. Role of cervical muscles during whiplash. In N. Yoganandan and F.A. Pintar, editors, *Frontiers in Whiplash Trauma, Clinical and Biomechanical*, pages 295–320. IOS Press, Amsterdam. ISSN 0929-6743.

SNYDER, R.G., CHAFFIN, D.B., AND FOUST, D.R., 1975. Bioengineering study of basic physical measurements related to susceptibility to cervical hyperextension-hyperflexion injury. Report UM-HSRI-BI-75-6, Highway Safety Research Institute, University of Michigan, Ann Arbor, Michigan.

SVENSSON, M.Y., ALDMAN, B., HANSSON, H.A., LOVSUND, P., SEEMAN, T., SUNESON, A., AND ORTENGREN, T., 1993. Pressure effects in the spinal canal during whiplash motion – a possible cause of injury to the cervical spinal ganglia. In *International IRCOBI Conference on the Biomechanics of Impacts*, 189-200.

THATCHAM, 2001. Whiplash Research. *THATCHAM.ORG, the motor insurance repair research centre*. http://www.thatcham.org/

THOR, 2001. Biomechanical response requirements of the THOR NHTSA advanced frontal dummy (revision 2001.02). Trauma assessment device development program. http://www-nrd.nhtsa.dot.gov/departments/nrd-51/THORAdv/THORAdv.htm.

THUNNISSEN, J., WISMANS, J., EWING, C.L., AND THOMAS, D.J., 1995. Human volunteer head-neck response in frontal flexion: A new Analysis. In *Proceedings of the 39th STAPP Car Crash Confernece*, pages 439-460. Society of Automotive Engineers. SAE Paper No. 952721.

TIEN, C.S., HUSTON, R.L., 1987. Numerical Advances in Gross-Motion Simulations of Head and Neck Dynamics, *J. Biomechanical Engineering – Transactions of the ASME.*, 109, No.2, 163-168.

TOMINAGA, T., DICKMAN, C.A., SONNTAG, V.K.H., AND COONS, S., 1995. Comparative anatomy of the baboon and the human cervical spine. *Spine*, 20(2): 131-137.

TSUCHISASHI, M, 1981. Road traffic accidents and abbreviated injury scale (AIS) in Japan. *Accident Analysis and Prevention*, 13, 37-42.

VAN DER HORST M.J., THUNNSISSEN J.G.M., HAPPEE R., VAN HAASTER R.M.H.P., WISMANS J.S.H.M., 1997. The influence of muscle activity on the head-neck response during impact. *SAE conference proceedings*, 315, 487-508.

VAN DER HORST M.J., 2002.. *Human Head Neck Response in Frontal, Lateral and Rear End Impact Loading - modelling and validation.* PhD Thesis, Technical University of Eindhoven.

VAN EE, C.A., NIGHTINGALE, R.W., CAMACHO, D.L.A., CHANCEY, V.C., KNAUB, K.E., SUN, E.A., AND MYERS, B.A., 2000. Tensile Properties of the Human Muscular and Ligamentous Cervical Spine. *In proceedings of 44th Stapp Car Crash Conference*, pages 85-102. Society of Automotive Engineers.

VASAVADA, A.N., LI, S., AND DELP, S.L., 1998. Influence of muscle morphometry and moment arms on the moment-generating capacity of human neck muscles. *Spine*, 23(4): 412-422.

VASAVADA, A.N., LI, S., AND DELP, S.L., 2001. Three-dimensional isometric strength of neck muscles in humans. Spine, 26(17)L 1904-1909.

VISHTEH, A.G., CRAWFORD, N.R., MELTON, M.S., SPETZLER, R.F., SONNTAG, V.K.H., AND DICKMAN, C.A., 1999. Stability of the craniovertebral junction after unilateral occipital condyle resection: a biomechanical study. *J. Neurosurg: Spine*, 90:91-98.

Visible Human Project, 1994. *National Library of Medicine*, http://www.nlm.nih.gov/research/visible/visible_human.html

WALKER, L.B., HARRIS, E.H., AND PONTIUS, U.R., 1973. Mass, volume, centre of mass, and mass moment of inertia of head and head and neck of the human body. *17th Stapp Car Crash Conference*, pages 525-537. Society of Automotive Engineers. SAE Paper No. 730985

WARFEL, J.H., 1985. *The Head, Neck, and Trunk.* 5th Edition. Lea and Febiger, Philadelphia.

WERNE, S., 1957. Studies in spontaneous atlas dislocation. *Acta Orthop. Scand.*, 23(Suppl.), 165-173.

WHITE III, A.A., AND PANJABI, M.M., 1990. *Clinical Biomechanics of the Spine.* J.B. Lippincott Company, Philadelphia, Toronto, 2nd Edition.

WINKELSTEIN, B.A., 1997. A Biomechanical study of the role of the cervical articular facet joint in whiplash injury. PHD Proposal, Department of Biomedical Engineering, Duke University.

WINKELSTEIN, B.A., NIGHTINGALE, R.W., RICHARDSON, W.J., AND MYERS, B.S., 2000a. The cervical facet capsule and its role in whiplash injury. Spine, 23(10): 1238-1246.

WINKELSTEIN, B.A., AND MYERS, B.S., 2000b. Cervical motion segment, combined loading, muscle forces, and facet joint: A mechanical hypothesis for whiplash injury. In Frontiers in Whiplash Trauma. Clinical and Biomechanical, pages 248-262. Editors: Yoganandan, N., and Pintar F.A. IOS Press, Amsterdamn. ISSN 0929-6743.

WINTERS, J.M., AND STARK, L., 1988. Estimated mechanical properties of synergistic muscles involved in movements of a variety of human joints. Journal of Biomechanics, 21: 1027-1041.

WINTERS, J.M., AND WOO, S.L-Y., 1990. *Multiple Muscle Systems: Biomechanics and Movement Organization.* Springer-Verlag.

WILLIAMS, J.L., BELYTSCHKO, T.B., 1983. A Three Dimensional Model of the Human Cervical Spine for Impact Simulation. Jo*urnal of Biomechanics*, 105, 322-331.

WISMAN, J., VAN OORSHOT, E., AND WOLTRING, H.J., 1986. Omni-directional human head-neck response. *30th Stapp Car Crash Proceedings*, pages 313-331. Society of Automotive Engineers. SAE Paper No. 861893.

WISMAN, J., PHILIPPENS, M., VAN OORSHOT, E., KALLIERIS, D., AND MATTERN, R., 1987. Comparison of human volunteer and cadaver head-neck response in frontal flexion. *31th Stapp Car Crash Proceedings*, pages 1-11. Society of Automotive Engineers. SAE Paper No. 872194.

WITTEK, A, ONO, K., KAJZER, J., 2000. Finite element model for simulation of muscle effects on kinematic response of cervical spine in low-speed rear-end impacts. *JARI Research Journal*, 22(5) 224-227.

XU, R., NADAUD, B.A., EBRAHEIM, N.A., AND YEASTING, R.A., 1995. Morphology of the second cervical vertebra and the posterior projection of the C2 pedicle axis. *Spine*, 20(3): 259-263.

XU, R., BURGAR, A., EBRAHEIM, N.A., AND YEASTING, R.A., 1999. The quantitative anatomy of the laminas of the spine. *Spine*, 24(2): 107-113.

YAMADA, H., 1970. Strength of Biological Materials. Williams and Wilkins, Baltimore. Editor: F.G. Evans.

YANG, K.H., ZHU, F., LUAN, F., ZHAO, L., AND BEGEMAN, P.C., 1998. Development of a Finite Element Model of the Human Neck. In *Proceedings of the 42nd Stapp Car Crash Conference*, pages 195-205. Society of Automotive Engineers. SAE Paper No. 983157

YOGANANDAN, N., PINTAR, F.A., BUTLER, J., REINARTZ, J., SANCES, A., AND LARSON, S.J., 1989. Dynamic response of human cervical spine ligaments. *Spine*, 14(10):1102-1109.

YOGANANDAN, N., AND PINTAR, F.A., 1997. Inertial loading of the human cervical spine. *Journal of Biomechanical Engineering*, 119: 237-240.

YOGANANDAN, N., PINTAR, F.A., CUSICK, J.F., SUN, E., AND EPPINGER, R., 1998a. Whiplash injury mechanisms. *Whiplash '98 Symposium*, 23.

YOGANANDAN, N., PINTAR, F.A., AND KLIENBERGER, M., 1998b. Cervical spine vertebral and facet joint kinematics under whiplash. Journal of Biomechanical Engineering, 120: 305-307.

YOGANANDAN, N., PINTAR, F.A., MAIMAN, D.J., CUSICK, J.F., SANCES JR., A., AND WALSH, P.R., 1996. Human head-neck biomechanics under axial tension. *Medical Engineering and Physics*, 18(4):289-294.

YOGANANDAN, N., KUMARESAN, S., AND PINTAR, F.A., 2000. Geometric and mechanical properties of human cervical spine ligaments. *Journal of Biomechanical Engineering*, 122:623-629.

YOGANANDAN, N., KUMARESAN, S., AND PINTAR, F.A.., 2001. Biomechanics of the cervical spine part 2. Cervical spine soft tissue responses and biomechanical modelling. *Clinical Biomechanics*, 16:1-27.

ZAJAC, F.E., 1989. Muscle and tendon: Properties, models, scaling, and application to biomechanics and motor control. *Critical Reviews in Biomedical Engineering*, 17:359-411.

# Appendix A

## Equations and coefficients for 'Virtual Muscle' muscle model.

Extrapolated parameters for human skeletal muscle fiber types and associated model equations (Cheng et al., 2000).

| CURVE | Typical slow-twitch fibers | | | | Fast-twitch fibers | | |
|---|---|---|---|---|---|---|---|
| **Tendon Elasticity** | | | | | | | |
| $F_{SE}(L^T) = c^T k^T \ln\left\{\exp\left[\frac{(L^T - L_r^T)}{k^T}\right] + 1\right\}$ | $c^T$ 27.8 | $k^T$ 0.0047 | $L_r^T$ 0.964 | | $c^T$ (same as slow twitch) | $k^T$ | $L_r^T$ |
| **Parallel Elastic Element** | | | | | | | |
| $F_{PE1}(L) = c_1 k_1 \ln\left\{\exp\left[\frac{(L/L_{max} - L_{r1})}{k_1}\right] + 1\right\} + \eta V$ | $c_1$ 23.0 | $k_1$ 0.046 | $L_{r1}$ 1.17 | $\eta$ 0.001 | $c_1$ (same as slow twitch) | $k_2$ | $L_{r2}$ |
| **Thick Filament Compression** | | | | | | | |
| $F_{PE2}(L) = c_2\{\exp[k_2(L - L_{r2})] - 1\}, \quad F_{PE2} \le 0$ | $c_2$ −0.020 | $k_2$ −21.0 | $L_{r2}$ 0.70 | | $c_2$ (same as slow twitch) | $k_2$ | $L_{r2}$ |
| **Force-Length** | | | | | | | |
| $FL(L) = \exp\left(-\text{abs}\left\lvert\frac{L^\beta - 1}{\omega}\right\rvert^\rho\right)$ | $\omega$ 1.12 | $\beta$ 2.30 | $\rho$ 1.62 | | $\omega$ 0.75 | $\beta$ 1.55 | $\rho$ 2.12 |
| **Force-Velocity** | | | | | | | |
| $FV(V, L) = \begin{cases}(V_{max} - V)/(V_{max} \pm (c_{v0} + c_{v1}L)V), & V \le 0\\ (b_v - (a_{v0} + a_{v1}L + a_{v2}L^2)V)/(b_v + V), & V > 0\end{cases}$ | $V_{max}$ −7.88 | $c_{v0}$ 5.88 | $c_{v1}$ 0 | | $V_{max}$ −9.15 | $c_{v0}$ −5.70 | $c_{v1}$ 9.18 |
| **Effective Activation** | | | | | | | |
| $Af(f_{eff}, L_{eff}, Y, S) = 1 - \exp\left[-\left(\frac{YSf_{eff}}{a_f n_f}\right)^{n_f}\right], \; n_f = n_{f0} + n_{f1}\left(\frac{1}{L_{eff}} - 1\right)$ | $a_{v0}$ −4.70<br>$a_f$ 0.56 | $a_{v1}$ 8.41<br>$n_{f0}$ 2.1 | $a_{v2}$ −5.34<br>$n_{f1}$ 5 | $b_v$ 0.35 | $a_{v0}$ −1.53<br>$a_f$ 0.56 | $a_{v1}$ 0<br>$n_{f0}$ 2.1 | $a_{v2}$ 0<br>$n_{f1}$ 3.3 |
| **Activation Delay** | | | | | | | |
| $\dot{L}_{eff}(t) = \frac{[L(t) - L_{eff}(t)]^3}{T_L(1 - Af)}$ | $T_L$(ms) 0.088 | | | | $T_L$(ms) (same as slow twitch) | | |
| **Sag** | | | | | | | |
| $\dot{S}(t, f_{eff}) = \frac{a_s - S(t)}{T_s}, \quad a_s = \begin{cases}a_{S1}, f_{eff}(t) < 0.1\\ a_{S2}, f_{eff}(t) \ge 0.1\end{cases}$ | $a_{s1}$ 1.0 | $a_{s2}$ 1.0 | $T_s$(ms) – | | $a_{s1}$ 1.76 | $a_{s2}$ 0.96 | $T_s$(ms) 43 |
| **Yield** | | | | | | | |
| $\dot{Y}(t) = \frac{1 - c_Y[1 - \exp(-\text{abs}\lvert V\rvert/V_Y)] - Y(t)}{T_Y}$ | $c_Y$ 0.35 | $V_Y$ 0.1 | $T_Y$(ms) 200 | | $c_Y$ 0 | $V_Y$ – | $T_Y$(ms) – |
| **Rise and Fall Time** | | | | | | | |
| $\dot{f}_{int}(t, f_{env}, L) = \frac{f_{env}(t) - f_{int}(t)}{T_f}$, $\dot{f}_{eff}(t, f_{int}, L) = \frac{f_{int}(t) - f_{eff}(t)}{T_f}$, $T_f = \begin{cases}T_{f1}L^2 + T_{f2}f_{env}(t), & \dot{f}_{eff}(t) \ge 0\\ (T_{f3} + T_{f4}Af)/(L), & \dot{f}_{eff}(t) < 0\end{cases}$ | $T_{f1}$(ms) 24.2 | $T_{f2}$(ms) 16 | $T_{f3}$(ms) 33.2 | $T_{f4}$(ms) 17.8 | $T_{f1}$(ms) 20.6 | $T_{f2}$(ms) 13.6 | $T_{f3}$(ms) 28.2 |